FINAL REPORT

Characterization of Emissions and Air Quality Modeling for Predicting the Impacts of Prescribed Burns at DoD Lands

SERDP Project RC-1647

OCTOBER 2012

Mehmet Talat Odman
School of Civil and Environmental Engineering,
Georgia Institute of Technology

SERDP
DOD ▪ EPA ▪ DOE

Report Documentation Page

Form Approved
OMB No. 0704-0188

1. REPORT DATE	2. REPORT TYPE	3. DATES COVERED
OCT 2012		**00-00-2012 to 00-00-2012**

4. TITLE AND SUBTITLE	5a. CONTRACT NUMBER
Characterization of Emissions and Air Quality Modeling for Predicting the Impacts of Prescribed Burns at DoD Lands	5b. GRANT NUMBER
	5c. PROGRAM ELEMENT NUMBER
6. AUTHOR(S)	5d. PROJECT NUMBER
	5e. TASK NUMBER
	5f. WORK UNIT NUMBER
7. PERFORMING ORGANIZATION NAME(S) AND ADDRESS(ES) **Georgia Institute of Technology,School of Civil and Environmental Engineering,Atlanta,GA,30332**	8. PERFORMING ORGANIZATION REPORT NUMBER
9. SPONSORING/MONITORING AGENCY NAME(S) AND ADDRESS(ES)	10. SPONSOR/MONITOR'S ACRONYM(S)
	11. SPONSOR/MONITOR'S REPORT NUMBER(S)

12. DISTRIBUTION/AVAILABILITY STATEMENT
Approved for public release; distribution unlimited

13. SUPPLEMENTARY NOTES

14. ABSTRACT

Objectives: Prescribed burning (PB) is an effective and economical land management tool for maintaining fire-adapted ecosystems, reducing wildfire risk, and improving training realism at Department of Defense (DoD) facilities. Pollutants emitted from prescribed fires, however, may be transported downwind, mix with emissions from other sources, form other pollutants, and contribute to poor air quality of urban areas in the region. As a result, compliance with ambient air quality standards in urban areas proximal to DoD prescribed burning activities may require tougher restrictions on DoD?s air emissions in the future. Because the alternatives to PB are costly and may have undesired ecological impacts, it is important for DoD to be able to control the emissions from its PB operations and to minimize their air quality impacts. Therefore, it is necessary to better characterize PB emissions and to more accurately predict their air quality impacts. This project aimed to improve the characterization of PB emissions by collecting field data most relevant to the modeling of PB plumes and developing a simulation framework that can accurately predict the impacts of prescribed burns on regional air quality. The objectives were to (1) better characterize the fuel types and loads for the sites to be studied; (2) estimate accurately the emissions from the burns to be simulated; (3) develop an air quality modeling system with sufficient resolution to characterize PB plumes, track their regional transport and chemistry, and discern their impacts from other pollution sources; (4) identify the data needs for model evaluation, collect new data, and evaluate the models; (5) consider the effects of inherent uncertainties in model inputs on model results; (6) and simulate the regional air quality impacts of DoD PB operations in the Southeast and assess alternative burning strategies. Technical Approach: This project applied existing USFS tools to the characterization of fuel beds on DoD lands. PB emission factors derived from prior field measurements of particulate matter (PM), carbon monoxide (CO), and volatile organic compounds (VOC) in the Southeast were compared to laboratory and in situ emissions measurements. ?Daysmoke,? an empirical plume model designed specifically for PB, and the Community Multiscale Air Quality (CMAQ) model were coupled using the improved grid resolution provided by the Adaptive Grid (AG) technology. This enabled adequate representation of plume dynamics and chemistry at local scales as well as accurate prediction of impacts over regional scales. The coupled models were first evaluated using existing data. Additional data needs were identified and fulfilled by monitoring campaigns at Fort Benning and Eglin Air Force Base (AFB). The models were evaluated by comparing model predictions to measurements. The sources of uncertainty in

15. SUBJECT TERMS

16. SECURITY CLASSIFICATION OF:			17. LIMITATION OF ABSTRACT	18. NUMBER OF PAGES	19a. NAME OF RESPONSIBLE PERSON
a. REPORT	b. ABSTRACT	c. THIS PAGE			
unclassified	**unclassified**	**unclassified**	**Same as Report (SAR)**	**258**	

Table of Contents

List of Tables

List of Figures

List of Acronyms

AB	Army Base
AP-42	Compilation of Air Pollutant emission factors
AFB	Air Force Base
AGM	Adaptive Grid Model
AG-CMAQ	Adaptive Grid CMAQ
AGD-CMAQ	Adaptive Grid CMAQ coupled with Daysmoke
AG-MM5	Adaptive Grid MM5
ATV	All-Terrain Vehicle
AQM	Air Quality Model
CA	Cellular Automata
CALPUFF	California Air Resources Board's Gaussian puff dispersion model
CASTNet	Clean Air Status Trends Network
CDT	Central Daylight-savings Time
CFL	Courant Friedrichs Lewy
CI	Core Intensity
CMAQ	Community Multiscale Air Quality model
CMAS	Community Modeling & Analysis System
CO	Carbon monoxide
CO_2	Carbon dioxide
CONSUME	A fuel consumption model
CPS	Condensation Particle Counter
CST	Central Standard Time
DAQ	Data acquisition
DASS	Data Acquisition and Sampling System
DDM	Decoupled Direct Method
DoD	Department of Defense
DSAGA	Dynamic Solution Adaptive Grid Algorithm
EC	Elemental Carbon
EDT	Eastern Daylight-savings Time
EF	Emissions Factor
EPA	Environmental Protection Agency
EST	Eastern Standard Time
FAST	Fourier Amplitude Sensitivity Test
FCCS	Fuel Characteristic Classification System
FEPS	Fire Emission Production Simulator
FFT	Fast Fourier Transform
FRM	Federal Reference Method
FS	Forest Service
GIT	Georgia Institute of Technology
GMT	Greenwich Mean Time
IMPROVE	Interagency Monitoring of Protected Visual Environments
IPR	In-Progress Review
JFSP	Joint Fire Science Program
LES	Large Eddy Simulation

LIDAR	Light Detection and Ranging
MAQSIP	Multiscale Air Quality Simulation Platform
MFB	Mean Fractional Bias
MFE	Mean Fractional Error
MM	Meteorological Model
MM5	Fifth-Generation NCAR / Penn State Mesoscale Model
MNB	Mean Normalized Bias
MNE	Mean Normalized Error
MODIS	Moderate resolution Imaging Spectroradiometer
NASA	National Aeronautical and Space Administration
NCAR	National Center for Atmospheric Research
NCSU	North Carolina State University
NFDRS	National Fire Danger Rating System
NO	Nitric oxide
NO_2	Nitrogen dioxide
NO_x	Oxides of nitrogen
NO_y	Sum of NO_x and its oxidation products
NOAA	National Oceanic and Atmospheric Administration
O_3	Ozone
OAQPS	Office of Air Quality Planning and Standards
OC	Organic Carbon
PB	Prescribed Burning
PBL	Planetary Boundary Layer
PI	Principal Investigator
PM	Particulate Matter
$PM_{2.5}$	PM with aerodynamic diameter smaller than 2.5 microns
PM_{10}	PM with aerodynamic diameter smaller than 10 microns
RAWS	Remote Automatic Weather Station
RCW	Red-Cockaded Woodpecker
ROS	Rate of Spread, or fire spread rate
Rx-CADRE	Prescribed Fire Combustion and Atmospheric Research Experiment
SCICHEM	Second-order Closure Integrated puff model with Chemistry
SERDP	Strategic Environmental Research and Development Program
SFS	Smoke Forecasting System
SHRMC-4S	Southern High-Resolution Modeling Consortium Southern Smoke Simulation System
SMPS	Scanning Mobility Particle Sizer
SO_2	Sulfur dioxide
SOA	Secondary Organic Aerosol
SON	Statement of Need
SRS	Savannah River Site
STN	Speciated Trends Network
SVOC	Semi Volatile Organic Compounds
TAC	Technical Advisory Committee
TEOM	Tapered Element Oscillating Microbalance
TOC	Total Organic Carbon

TOT	Thermal Optical Transmittance
TSI	Thermo-Systems, Inc.
UGA	University of Georgia
UMASS	University of Massachusetts Amherst
USDA	United States Department of Agriculture
USFS	United States Forest Service
UTC	Universal Time Coordinate
UXO	Unexploded Ordnance
VARTSTEP	Variable Time-Step Algorithm
VOC	Volatile Organic Compounds
WD	Wind Direction
WRAP	Western Regional Air Partnership
WRF	Weather Research and Forecasting model
WS	Wind Speed
WSOC	Water Soluble Organic Carbon

Keywords

Adaptive grid, aerostat, ceilometer, dispersion model, emission factor, field study, fire progression, fuel consumption, fuel load, land breeze, long-range transport, model evaluation, prescribed burning, sea breeze, sensitivity analysis, sounding, subgrid model, uncertainty, wind direction, wind speed.

Acknowledgements

This research was sponsored by the Strategic Environmental Research and Development Program (SERDP). The United States Forest Service contributed significantly by sharing the cost. Two grants by Joint Fire Science Program (JFSP) leveraged certain parts of this research.

This report was made possible by inputs provided by co-PIs and other investigators. Substantial input by USFS Southern Research Station PI Dr. Gary Achtemeier deserves special acknowledgement. Other PIs who contributed to the report are Dr. Roby Greenwald of Emory University, Dr. Brian Gullett of US EPA, Dr. Luke Naeher of UGA and Dr. Armistead Russell of Georgia Tech. Contributions by Dr. Scott Goodrick and Dr. Yongqiang Liu of USFS Southern Research Station, Dr. William Stevens and Dr. Johanna Aurell of US EPA, Mr. Fernando Garcia-Menendez and Ms. Aika Yano of Georgia Tech are appreciated.

We thank Dr. Hugh Westbury and Dr. Donald Imm for their coordination at Fort Benning, Mr. Robert Larimore and Mr. James Parker for accommodating us at Fort Benning and Mr. Thomas Hutcherson for guiding our sampling teams at Fort Benning and providing burn information. Mr. Adam Gray of UGA is noted for managing the ground-smoke sampling at Fort Benning.

Special thanks are in order to the PI of Rx-CADRE Dr. Roger Ottmar of USFS Pacific Northwest for planning the study at Eglin AFB and providing fuels data. Mr. Kevin Hiers and Mr. Brett Williams hosted us at Eglin AFB and provided invaluable burn information.

We thank Dr. Xindi Bian of USFS Northern Research Station who provided weather forecasts for the burns at Eglin, and Dr. Bill Jackson of USFS who provided emissions data for the Atlanta Smoke Incident. Special thanks are extended to Dr. Yongtao Hu who provided invaluable modeling support at Georgia Tech.

We thank the members of the Technical Advisory Committee for their guidance throughout this research, especially to Dr. William Sommers of George Mason University, Dr. Michael Chang of Georgia Tech and Dr. Lindsay Boring of Jones Center.

We thank the PIs and co-PIs of SERDP projects RC-1648 and RC-1649 for their engagement in our research, namely Dr. Wayne Miller of UC Riverside, Dr. Timothy Johnson of Pacific Northwest National Laboratory, Dr. David Weise of USFS, and Dr. Robert Yokelson of University of Montana.

We appreciate the inputs by all of those who participated in our survey for identifying alternative burning scenarios, especially Dr. Di Tian of Georgia Department of Natural Resources, Mr. Daniel Chan of Georgia Forestry Commission, Dr. John Blake of USFS Savannah River Site, and Dr. Robert Mitchell of Jones Center. Some of the participants who provided valuable input are already mentioned above for their other contributions.

We thank Dr. Robert Holst and Dr. John Hall of SERDP and Mr. Kevin Hiers for reviewing this report and contributing to its improvement by their invaluable comments.

Finally, the lead Principal Investigator (PI) Dr. Talat Odman wishes to thank his family for their kind support and understanding during four years of research that led to this report.

Abstract

Objectives: Prescribed burning (PB) is an effective and economical land management tool for maintaining fire-adapted ecosystems, reducing wildfire risk, and improving training realism at Department of Defense (DoD) facilities. Pollutants emitted from prescribed fires, however, may be transported downwind, mix with emissions from other sources, form other pollutants, and contribute to poor air quality of urban areas in the region. As a result, compliance with ambient air quality standards in urban areas proximal to DoD prescribed burning activities may require tougher restrictions on DoD's air emissions in the future. Because the alternatives to PB are costly and may have undesired ecological impacts, it is important for DoD to be able to control the emissions from its PB operations and to minimize their air quality impacts. Therefore, it is necessary to better characterize PB emissions and to more accurately predict their air quality impacts.

This project aimed to improve the characterization of PB emissions by collecting field data most relevant to the modeling of PB plumes and developing a simulation framework that can accurately predict the impacts of prescribed burns on regional air quality. The objectives were to (1) better characterize the fuel types and loads for the sites to be studied; (2) estimate accurately the emissions from the burns to be simulated; (3) develop an air quality modeling system with sufficient resolution to characterize PB plumes, track their regional transport and chemistry, and discern their impacts from other pollution sources; (4) identify the data needs for model evaluation, collect new data, and evaluate the models; (5) consider the effects of inherent uncertainties in model inputs on model results; (6) and simulate the regional air quality impacts of DoD PB operations in the Southeast and assess alternative burning strategies.

Technical Approach: This project applied existing USFS tools to the characterization of fuel beds on DoD lands. PB emission factors derived from prior field measurements of particulate matter (PM), carbon monoxide (CO), and volatile organic compounds (VOC) in the Southeast were compared to laboratory and in situ emissions measurements. "Daysmoke," an empirical plume model designed specifically for PB, and the Community Multiscale Air Quality (CMAQ) model were coupled using the improved grid resolution provided by the Adaptive Grid (AG) technology. This enabled adequate representation of plume dynamics and chemistry at local scales as well as accurate prediction of impacts over regional scales. The coupled models were first evaluated using existing data. Additional data needs were identified and fulfilled by monitoring campaigns at Fort Benning and Eglin Air Force Base (AFB). The models were evaluated by comparing model predictions to measurements. The sources of uncertainty in model predictions were investigated through sensitivity analysis. Finally, various scenarios were simulated to quantify the air quality impacts of alternative PB scenarios, such as changing the burning times, frequencies, and methods.

Results: The modeling system developed for predicting the air quality impacts of prescribed burns incorporates several new elements into emission, dispersion, and transport process components, all with significant potential for improving the accuracy of the predictions. Initial evaluations of the components individually and together using field data from burns monitored at Fort Benning and observations from regional networks led to significant accuracy improvements. Daysmoke predicted plume structures and smoke concentrations generally in agreement with

observations, whereas AG-CMAQ reduced the artificial diffusion inherent to air quality models and produced better defined plumes compared to the standard CMAQ.

The data collected at Fort Benning consisted of measurements of plume height with a lidar ceilometer and short-range smoke concentrations with ground-based mobile platforms. A more comprehensive field study was conducted at Eglin AFB to collect data for final evaluation of the modeling system. As part of this study, the fuels were measured both before and after the burn. Emissions of CO_2 and $PM_{2.5}$ were measured with a platform mounted on a tethered aerostat. Comparison to measurements revealed that although both fuel loads and consumptions were overestimated, by 20% and 10% respectively, total emissions were underestimated by 15%. These results showed that the uncertainties in emission estimates are relatively small. Winds were also measured at Eglin with pilot balloon soundings before the burns and airborne (mounted on the aerostat) and ground-based sonic anemometers during the burns. Low wind speeds (WS) and varying wind directions (WD), particularly during transition from land to sea breeze, were difficult to predict with weather prediction models. For sustained and steady wind periods, typical WS errors were 10 to 30% and WD errors were 10 to 20° at altitudes most relevant to plume transport.

Predicted plume heights were in agreement with the ceilometers measurements during initial flaming stages of the burns but modeled plumes collapsed faster. Ground-level $PM_{2.5}$ also was measured at Eglin, both with fixed and mobile platforms. The agreement of predicted ground-level concentrations with observations varied; typically better agreement was obtained near the burn plot and the differences grew with downwind distance. Simulation of a historic smoke incident with the modeling system resulted in significant under-prediction of $PM_{2.5}$ concentrations observed at monitors about 80 km downwind. The reasons were investigated through a sensitivity analysis. Emission related parameters such as emission strength, timing, and vertical distribution (plume fraction penetrating into the free troposphere) proved to have little effect on the underestimation. WS and WD emerged as the most prominent factors. Sensitivity to WD was very large as ±10° rotation of the wind field would make the plume totally miss the monitors. Changing WD by 5° increased modeled peak $PM_{2.5}$ concentrations at the monitors by 20% of the under-prediction amount. More important, reducing WS by 30% compensated for 70% of the under-prediction. Both of these adjustments are well within the uncertainty bounds determined for wind fields and justified by the differences between meteorological model predictions and data from the most proximate sounding.

Benefits: This research integrated improved emissions data, important burn-front information, and advanced plume modeling techniques in regional air quality models. It enabled more accurate prediction of the air quality impacts of prescribed burns. Using the developed simulation framework, DoD land managers can plan their operations to minimize the impacts to regional air quality. The benefit to the scientific community is access to improved PB emissions and accurate models for the dispersion, transport, and chemistry of these emissions.

1 Objective

Prescribed burning (PB) is an effective and economical land management tool for improving and maintaining an ecosystem, reducing wildfire risk, and improving training realism at Department of Defense (DoD) facilities. However, pollutants emitted from prescribed fires may be transported downwind, mix with emissions from other sources, form other pollutants, and contribute to poor air quality of urban areas in the region. Compliance of those urban areas with ambient air quality standards may require tougher restrictions on DoD's air emissions in the future. Since the alternatives of PB are costly, it is important for DoD to be able to control the emissions from its PB operations and to minimize their air quality impacts. Therefore it is necessary to better characterize PB emissions and to more accurately predict their air quality impacts.

This project aims at improving the characterization of prescribed burn (PB) emissions, collecting field data most relevant to the modeling of PB plumes, and developing a simulation framework that can accurately predict the impacts of prescribed burns on regional air quality. Specific objectives are to:

1. Use existing USFS tools to characterize the fuels on sites to be studied,
2. Accurately estimate emissions from the burns to be simulated,
3. Develop a sub-grid treatment for PB plumes in regional-scale air quality models
4. Increase the grid resolution for adequate coupling of the sub-grid scale plume models with regional-scale air quality models
5. Evaluate the coupled models with prescribed fire data
6. Identify and collect the data needed for more rigorous evaluation of the models
7. Analyze the effects of uncertainties inherent in model inputs on model results
8. Simulate the regional air quality impacts of DoD PB operations in the Southeast, and
9. Assess alternative burning strategies.

2 Background

The reasons for conducting PB operations at military installations include improving and maintaining endangered species habitat, reducing the risk of wildfires, preparing sites for seeding and planting, managing understory hardwoods, controlling disease, improving forage for grazing, enhancing appearance, and improving access. For example, at Fort Benning a major objective is to convert the landscape as close to its pre-settlement condition (longleaf pine forest) to protect the endangered red-cockaded woodpecker (RCW) habitat and prescribed burning is the most economical means. Approximately 30,000 acres must be prescribed burned each year during the growing season to reduce unwanted vegetation that would compete with longleaf seedlings. Prescribed burning is an efficient and effective means for reducing the build-up of fuels that may lead to catastrophic fires. Heavy roughs can build up posing a serious threat from wildfire to lives, property, and all natural resources. A burning rotation of approximately 3 years is usually adequate to fire proof pine stands and reduce this threat. Prescribed burning also controls brown spot disease, which is a fungal infection that weakens and eventually kills longleaf seedlings. Wildlife species such as deer, turkey, quail, and doves also benefit from prescribed burning. Prescribed burning on a regular basis also serves a military need by providing a safer training environment with improved access and visibility. Lastly, growing season burns have significantly reduced the tick population on the installation.

Smoke complaints and the threat of litigation from smoke-related incidents / accidents are major concerns of the PB operations. Fort Benning follows voluntary smoke management guidelines in an effort to minimize the adverse impacts from smoke. Particulate matter (PM) emissions and the effect of PB on ozone levels in Columbus-Phenix City metropolitan areas are also of concern. Forest fires produce nitrogen oxides (NO_x) and volatile organic compounds (VOC) emissions and may form ozone (Cheng et al., 1998). PB emissions may be transported downwind, mix with emissions from other sources and contribute to poor air quality in urban areas. Recognizing the Columbus ozone problem, the majority of the burns (70-75%) were shifted to the January-April period. However the threat of PM pollution continues during this season. What is needed is an accurate forecasting system so that the PB operation can be conducted to minimize undesirable air quality impacts. Estimates of missions and models of dispersion, chemistry and long-range transport are the key components of such a system.

2.1 State of Emissions Estimates

Emission factors are estimates of the quantity of emissions of a pollutant species per amount of material burned. Wildland fire emission factors have been developed under either field or laboratory conditions. The U.S. EPA (1996) formed a table of default values (AP-42 Table) for fire emission factors of major species. Improvements were made through the EPA Office of Air Quality Planning and Standards (OAQPS) to obtain separate emission factors for flaming and smoldering and for different forest species. They are presented in Tables 38 and 39 in a report to EPA (Battye and Battye, 2002). The Forest Service (FS) conducted extensive field experiments of prescribed fires in the Southeast in 1996 (Hao et al., 2002). Emission factors were estimated for various ecosystems at a number of National Forests, Wildlife Refuges, and Air Force Bases. Georgia Institute of Technology (GIT) recently conducted measurements of prescribed burns at

Fort Benning (Baumann, 2005) and provided estimates of emission factors specific to that ecosystem.

Each set of emission factors is applied to the specific geographic, ecological and environmental circumstances of forest fuel and burn. The AP-42 Table has been widely used in developing regional and nation-wide emission inventory (Liu, 2004; WRAP, 2002), but it was developed based on studies conducted in the west during 1970s and 1980s. The FS measurements are specific for the Southeast. This region is characterized by a diverse ecosystem and environmental conditions, which leads to large variations in emission factors from one site to another. The GIT study (Baumann, 2005) is specific to Fort Benning. There are some noticeable differences in the magnitudes of emission factors from different sources. For example, in comparison with the $PM_{2.5}$ emission factor in the AP-42 Table for the Southeast, the median value of $PM_{2.5}$ emission factor from the FS measurements is about one third smaller, and the value from GIT measurements is much smaller. Thus, specific circumstance of fuel and burning needs to be taken into account when specifying a magnitude of emission factors for fire emission calculation.

2.2 State of Models

Reactive plume models, with a history dating back to early 1980s (Stewart and Liu, 1981) are probably the most reliable tools to predict plume behavior. These models are developed to track plume dispersion and chemical transport using our best understanding of atmospheric turbulence and chemistry. Most of them are designed for plumes from industrial emission sources such as large power plants. CALPUFF is one of the most popular models (EarthTech, 2000). It accounts for vertical wind shear by splitting the plume when necessary and offers a number of dispersion options under various atmospheric stability conditions. These features increase the fidelity of dispersion and downwind transport. However, its treatment of chemistry is highly simplified. SCICHEM (Karamchandani et al., 2000) has a more comprehensive treatment of plume chemistry, including some account of turbulent concentration fluctuations on chemical kinetics. But even SCICHEM is only reliable for large power plant plumes being transported steadily over rural regions with homogeneous land cover and relatively constant ambient conditions and, with no interference from other point source or urban plumes. When there is interaction between plumes, reactive plume models cannot accurately estimate the formation of secondary pollutants, such as ozone or Secondary Organic Aerosols (SOA) (Karamchandani et al., 2000). Hence, in geographic regions where emission sources are diverse and numerous, reactive plume models are not applicable in the long-range. The best use for these models is the study of local or short-range impacts of individual plumes.

A regional scale air quality model (AQM) can provide more realistic ambient concentrations to the reactive plume models. It can also account for the injection of emissions from other sources that cannot all be modeled individually due to computational limitations. There have been several attempts to couple reactive plume models with regional AQMs (Gillani and Godowitch, 1999; Kumar and Russell, 1996). Recently, SCICHEM has been coupled with CMAQ and, in an application to Central California, remarkably good agreement was obtained with NO_y and O_3 measurements up to 5-km distances downwind of the sources (Vijayaraghavan et al., 2006). Hence more accurate ambient concentrations help the plume models in the short range. The other expectation from coupling the models is to be able to transfer accurate plume information from

the sub-grid (i.e., reactive plume) model to the grid (i.e., regional air quality) model. This other side of the coin is known as the plume "hand-over" problem. Kumar and Russell (1996) proposed handing over the plume after 1-hr of tracking it with the sub-grid model. Another approach is to hand over when physical plume dimensions reach the grid scales (Karamchandani et al., 2002). Gillani and Pleim (1996) suggested that the chemical maturity of the plume should be used as a hand-over criterion. A power plant plume is considered "mature" when its NO_x-rich and O_3-poor core levels off. This is the recommended criteria for SCICHEM coupled with CMAQ (Karamchandani et al., 2002). Satisfying this criterion often requires tracking the plume with the sub-grid model for long distances (~70 km). Prolonged tracking with the sub-grid model delays the interaction of the plume with all the other plumes in its surroundings.

To our knowledge, no improvement in agreement between predictions and observations at ground monitors beyond ~10 km downwind has been reported with coupled models. This led to the general impression in modeling circles that plume-in-grid (i.e., coupled) models are unnecessary. As a result, the computationally expensive plume-in-grid capability is often turned off in regional applications (Morris et al., 2005). One of our hypotheses in this research is that, in order for model coupling to be beneficial in the mid-to-long range, the plume should be handed over as quickly as possible but only when the grid resolution can support the structure of the plume. This of course requires very fine grid resolution (~250 m). The adaptive grid technique (Khan et al., 2005) is capable of providing this resolution at reasonable computational cost.

Without the plume-in-grid treatment, the only means left to include fire plumes in regional-scale AQMs such as CMAQ (Byun and Ching, 1999) and WRF-chem (Grell et al., 2005) is to treat them as point sources (such as industrial stacks) and/or area sources (such as vehicle emissions in cities). Point source emissions go through plume rise calculations and they are distributed through the vertical layers of the models at the vertical column coinciding with the source location. Area sources are directly mixed into the surface layer. These oversimplifications of plume mixing with the environment are not adequate to simulate patterns of pollution dispersion and concentration over large multiple state areas. Prescribed burns are transient (occurring only once every few years in any particular area) and ground-level (not from elevated stacks) and thus do not qualify as point sources. Prescribed burns release considerable amounts of heat which leads to buoyant plumes capable of distributing smoke well above the ground and thus do not qualify as area sources either. Furthermore, fire intensity, hence heat production and emission rates, varies throughout the life of the burn with corresponding changes in plume dynamics.

Another problem is that none of these models includes the "human element" – how the burns are engineered by land managers. By the choice of firing method – head fire, back fire, mass ignition (where, when, and how much fire is dropped) – land managers can determine the timing of heat production and how much heat is produced over the course of the burn. Thus the human element can be a major contributor to how high smoke goes and how much gets there during a period of evolving mixing layer height within a time-dependent wind field. One exception is the Daysmoke model (Achtemeier, 2005a) which was designed considering unique characteristics of prescribed fire plumes including the human element.

In summary, there is no simple method for determining where in regional-scale AQMs wildland fire plumes should be placed or how much smoke should be placed there, thus the contribution of

emissions from wildland fire, especially to the particulate matter (PM) loads, is problematic. Given that the prescribed burn programs, for example the one in the Southeast, release large amounts of $PM_{2.5}$, carbon monoxide and NO_x, this is also a problem for the fidelity of all regional air quality simulations. Local plume models and regional AQMs have advanced our knowledge of smoke transport and dispersion to a certain level. To increase our understanding, there is now a need for a proper subgrid model for prescribed fire plumes in regional scale models and an appropriate coupling methodology.

3 Materials and Methods

The overall technical approach is summarized in Figure 1. The emissions estimation task is followed by model development and simulations. Then, model predictions are evaluated with field data. There were several cycles of these tasks including new field measurements. Finally, alternative burning strategies were simulated using the evaluated modeling system.

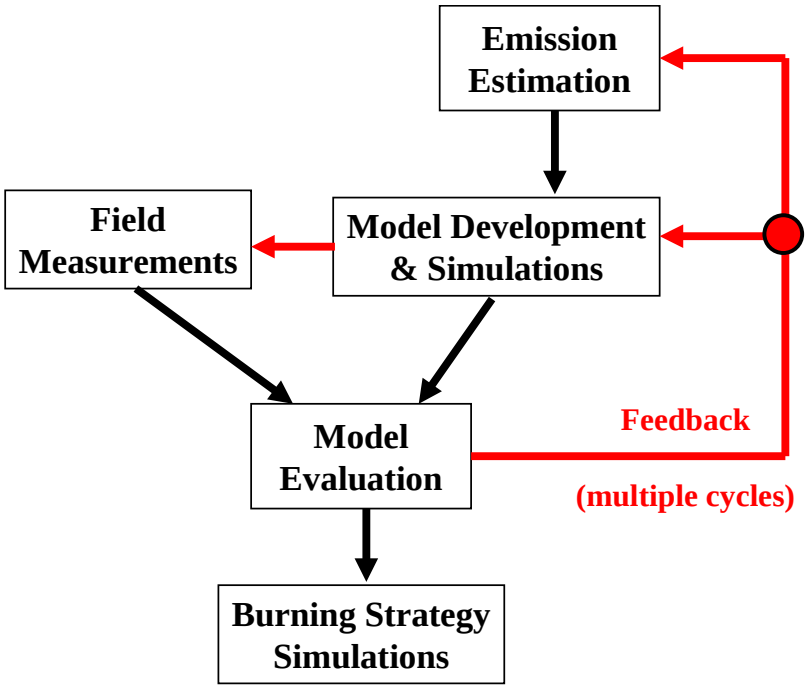

Figure 1. Technical approach.

As part of the emission estimation task a classification system developed by the Forest Service (FS) is applied to the characterization of fuel beds on DoD lands. PB emission factors are derived from prior field measurements of particulate matter, carbon monoxide, and volatile organic compounds in the Southeast. The models used in the project are "Daysmoke," an empirical plume model designed specifically for prescribed burns, and the Community Multiscale Air Quality (CMAQ) model. These two models have been coupled using the improved grid resolution provided by the Adaptive Grid Model (AGM) technology. The goal is to enable accurate representation of plume dynamics and chemistry at local scales for accurate prediction of the air quality impacts over regional scales. The models were initially evaluated using available data. Additional data needs were identified and fulfilled by a real-time downwind monitoring component that focused on the PB operation at military installations. The models were re-evaluated by reconciling the differences between model predictions and measurements.

3.1 Emission Estimation Methods

Emission estimation methods include the methods for estimating fuel loads and fuel consumptions, and the use of emission factors for emission calculations.

3.1.1 Method for Estimating Fuel Loads

An estimate of the fuel load in a burn unit is the starting point for any attempt to calculate the emissions from a wildland fire. Detailed measurements of fuel loads are time consuming to obtain and are therefore not done as part of a land manager's normal burn planning. Wildland fuel photo series (Ottmar et al., 2000; Ottmar et al., 2003; Scholl and Waldrop, 1999) represent a practical tool developed for land managers. It allows fuel loads to be estimated by comparing site conditions against a collection of photographs with known fuel loadings. A limitation of photo series is that they are not produced for every locality/ecosystem type, as is the case for Fort Benning in the Piedmont of Georgia.

This study utilizes a combination of photo series developed for nearby ecosystems (Ottmar et al., 2000; Ottmar et al., 2003; Scholl and Waldrop, 1999). For a subset of burn units available on Fort Benning representing the two major soil types (clay vs. sand) and fire return intervals from 1 to 5 years, three technicians visually surveyed each site and described the site in terms of photo series fuel types. This description was often highly qualitative (e.g., site looks like fuel type *n*, but could also be *m*). The descriptions were then translated into fuel loadings by weighted averages of the fuel bed components. If only one fuel model was specified, its weight was set to 1.0. For cases with multiple fuel models, weights were based on any qualifiers used in the description. No qualifiers provided equal weighting, while a qualifier of "more like" received a larger weight (in the case of two fuel models, if models *n* and *m* both were applicable, but the site looked more like *n*, it received a weight of 0.67 while *m* received a weight of 0.33). Every observer's fuel load estimates for a site were subsequently averaged to provide a final fuel load estimate for a burn unit.

3.1.2 Method for Estimating Fuel Consumption

Fuel consumption is estimated using CONSUME 3.0, an empirical model developed from measured consumption data (Prichard et al., 2005). CONSUME requires general burn information including the number of acres burned, and the description of the fuelbed and its environment. Site specific fuel loads can be entered or a fuel bed with predefined fuel load profile can be selected from the FCCS classification. For example, for Fort Benning, the cover type is very close to loblolly pine, which is under "Subtropical" eco-region and "Conifer Forest" vegetation form. Environment variables to be input to CONSUME include the fuel moisture content of the different layers (10-hr fuels, 1000-hr fuels, duff, etc.), duration of the flaming phase, wind speed, slope, and the number of days since it last rained.

CONSUME outputs include fuel consumption, heat release rates and emissions. The consumption estimates show how much fuel of each type (i.e., litter, woody, non-woody, shrubs, etc.) existed before the burn and how much got consumed/burned in tons/acre (Figure 2). Heat release rates are also by fuel type, essentially how much heat got released from burning each fuel type, in btu/ft^2. Emissions outputs are and the total emissions of PM, PM_{10}, $PM_{2.5}$, CO, CO_2, CH_4, and non-methane hydrocarbon from the burn. The emissions outputs from CONSUME were noted for comparison to the emissions to be calculated as described below.

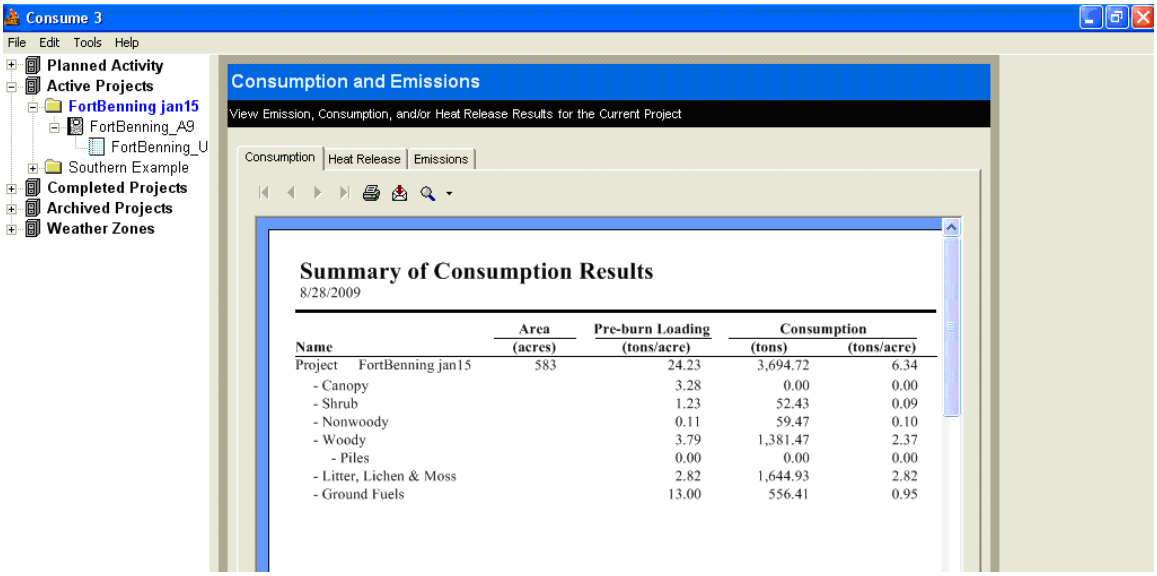

Figure 2. Consumption results from CONSUME 3.0 for the January 15, 2009 burn.

3.1.3 Method for Estimating Emissions

Total emissions are estimated using emission factors (EFs) defined as mass of pollutant emitted per unit mass of fuel consumed. Multiplying EFs by the consumption estimates from CONSUME yields total emissions estimates. The EFs used here are based on field measurements (Urbanski et al., 2009). Laboratory measurements are another source for EFs. In SERDP project RC-1649 burns were simulated in a laboratory using the fuels collected at Fort Benning and the emissions of various chemical species were measured (Burling et al., 2010). Table 1 gives a summary of the EFs used here.

Note that Table 1 contains two sets of emission factors: one for flaming and one for smoldering. Smoldering is the slow, low-temperature, flameless form of combustion that occurs when there is not enough oxygen for complete combustion of the fuel. Incomplete combustion produces carbon monoxide (CO) whereas complete combustion produces carbon dioxide (CO_2). In field and laboratory studies, it is possible to make a distinction between the flaming and smoldering phases by measuring CO and CO_2. In the flaming phase, CO_2 is the dominant combustion product (i.e., complete combustion). On the other hand, CO is the dominant combustion product of the smoldering phase. The transition from flaming phase to smoldering phase can be distinguished by the decrease in CO_2 and increase in CO emissions.

Table 1. Emission factors used in estimating emissions*.

	lbs/ton		g/kg	
	Flaming	Smoldering	Flaming	Smoldering
CO	164.0000	212.0000	82.0000	106.0000
CH4	4.6400	6.8400	2.3200	3.4200
PM25	23.0000	21.0000	11.5000	10.5000
CO2	3328.0000	3298.0000	1664.0000	1649.0000
C2H4	2.6000	2.6000	1.3000	1.3000
C2H2	1.0000	0.9600	0.5000	0.4800
C2H6	0.6400	0.9200	0.3200	0.4600
C3H6	1.0200	1.1800	0.5100	0.5900
C3H8	0.1720	0.2200	0.0860	0.1100
C3H4	0.1000	0.1000	0.0500	0.0500
NMHC	5.5400	6.0000	2.7700	3.0000
NOx	4.0000	4.0000	2.0000	2.0000
SO2	0.3500	0.3500	0.1750	0.1750

* Ozone (O_3) is not a directly emitted substance and the amount of O_3 formed by the fire depends on various external factors such as atmospheric conditions and background levels of NO_x and VOCs.

Plume dispersion and transport models described below need time-resolved emissions inputs. The Fire Emission Production Simulator (FEPS) can be used to generate these inputs (Anderson et al., 2004). The hourly emission profiles depend on the cumulative acreage burned up to that point. In the burns monitored here, typically 80 to 90% of the area is burned by the time ignition is completed and the remainder usually burns over the next couple of hours. FEPS can calculate the amounts of fuels consumed in flaming, short-term smoldering, and long-term smoldering phases. Using this information in conjunction with the emissions factors in Table 1, hour-by-hour emissions of different chemical species can be calculated. Typically, the flaming and short-term smoldering phases are assumed to occur simultaneously involving 90-95% of the fuels. The remaining 5-10% of the fuels is reserved for long-term smoldering. Whenever different emission factors are available for flaming and smoldering phases such as in Table 1, the flaming phase emission factors are applied to the fuels consumed in flaming phase and smoldering phase emission factors are applied to the fuels consumed in short-term and long-term smoldering phases.

3.2 Modeling Methods

The modeling methods will be discussed under four sections: 1) Fire spread model−Rabbit Rules, 2) Dispersion model−Daysmoke, 3) Chemistry-transport model−Adaptive Grid CMAQ, and 4) Coupling of dispersion model with the chemistry-transport model.

3.2.1 Fire Spread Model: Rabbit Rules

The temporal distribution of burn emissions can be better estimated by using a fire spread model. Using cellular automata (CA) models for fire spread by thermal heat transfer to adjacent cells was proposed almost two decades ago (Clarke et al., 1994). Since then, several CA models were developed to model fire spread as a function of fuels, terrain and weather. Rabbit Rules, a recently developed CA model advances the rules for coupled fire-atmosphere circulations so that the complexity of fire induced wind fields approach those found in full-physics models (Achtemeier, 2012). Given a description of the fuel type and distribution over the burn plot, along with an ignition pattern, this model can simulate fire progression over the burn plot. The necessary fuel distribution information can be obtained from satellite imagery. Ignition is performed typically by all-terrain vehicles, or helicopter, starting from the downwind edge of the plot and following lateral stripes towards the upwind edge. Rabbit Rules computes the intensities of fire induced drafts converging towards the flames and the resulting pressure fields. Around low pressure zones, smoke organizes into updraft cores the number of which is important for plume rise calculations in the dispersion model, as fewer cores would result in higher plumes. Rabbit Rules also computes the diameter of the cores, their updraft velocities and temporal profiles for fire emissions.

Rabbit Rules represents “elements” of fire by autonomous agents (Flakes, 2000). The purpose of the autonomous agent is to reduce the complexity of modeling fire while minimizing commensurate loss of explanatory power. Therefore, the agent should not be too much like fire or else modeling complexity will not be reduced nor should the agent be too little like fire or else the result will be too little explanatory power. Furthermore, it is assumed that the primary mechanism for fire spread is spotting. Local spotting advances a fire line as burning fuels (embers) within a bed of finite depth collapse forward to ignite adjacent unburned fuels. Distant spotting establishes patches of independent fire. Therefore, the rabbit (the animal) is a suitable proxy for fire spread by spotting because of a fundamental similarity in behavior. For example, fire consumes fuel; fire “leaps” from fuel element to fuel element; and fire spreads. By comparison, rabbits eat, rabbits jump, and rabbits reproduce.

The fire spread problem is reduced to finding (a) when a rabbit will jump, (b) how far the rabbit will jump and (c) how long a rabbit will live. The physical domain is converted into a fine mesh regular grid with each grid cell given a fuel type number linked to an array of fuel designations. Regarding (a), the rabbit jumps only once at birth. If it lands on an unoccupied food square (green cell in Figure 3), it survives and passes through the remaining life cycle – adolescent/reproductive (shown by the orange squares) and old/dying (red squares). The reproductive period is the time elapsed after initial landing until new rabbits are launched toward nearby food cells. This period is a function of the size of the food square (defined internally in the model) and the fuel designations and must be linked with empirical data on fire spread (Andrews et al., 2005).

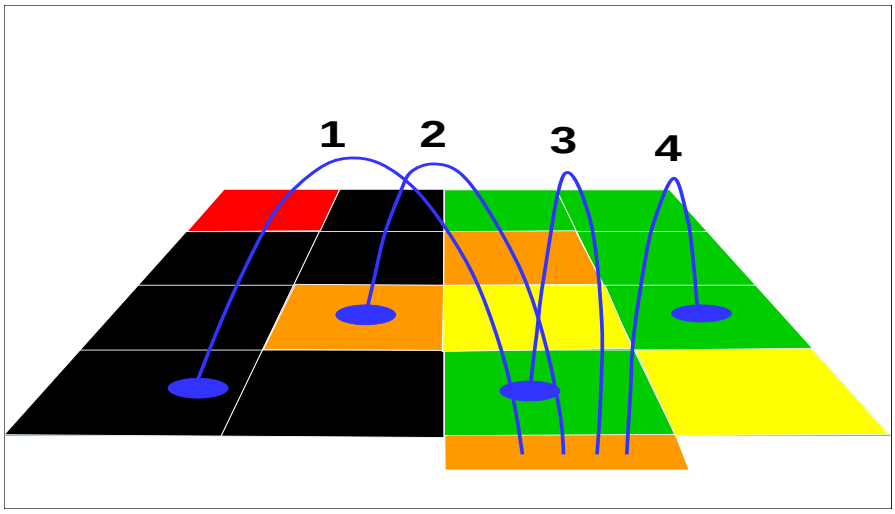

Figure 3. Hopping paths of four rabbits birthed at the lower extension (orange) of the cellular grid. Yellow cells are occupied by baby rabbits, orange cells are occupied by reproductive rabbits, and red cells are occupied by old/declining rabbits. Green cells represent uneaten food and black cells represent eaten food.

Regarding (b), the hopping distance is given by either,

$$
\begin{aligned}
x &= (C_w u|u| + 10 C_f s_x |s_x|)t + C_h z_r (0.5 - ran) \\
y &= (C_w v|v| + 10 C_f s_y |s_y|)t + C_h z_r (0.5 - ran) \\
&or \\
x &= \delta_B C_h z_r (0.5 + ran) \\
y &= \delta_B C_h z_r (0.5 * ran)
\end{aligned}
\qquad (1)
$$

The first and second terms in parenthesis of the first equation set represent the local spread of burning fuel elements by the east-west (x) and north-south (y) components of the wind (u, v) with a correction factor for slope (s_x, s_y). The third term gives background spread in the absence of wind and slope. A random number ($0<ran<1$) adds stochasticity to the hopping distance. If it is determined that the fuel bed is structured so that fire will backspread regardless of wind speed, then $\delta_B = 1$. The total number of rabbits for that fuel type is doubled with the hopping distance for the new rabbits calculated via the second equation set. Each term enters its equation via its respective weight (C_w [$m^{-1}s$], C_f, [$m^{-1}s^{-1}$], C_h [*non-dimensional*]). Thus, in the absence of slope, the hopping distance is proportional to the product of the wind speed with the time the rabbit is airborne. The airborne time t (not the same as the reproductive period) is the time elapsed for the rabbit to complete a hop,

$$
t = 2\sqrt{\frac{2 * z_r}{g}} \qquad (2)
$$

where the acceleration of gravity $g = 9.81$ m s^{-2} and z_r is the rabbit hopping height. The hopping height, analogous to ember (or firebrand) discharge height, is a simple function of a characteristic fuel height f_h that carries information regarding actual fuel height and fuel moisture,

$$z_r = 2(0.1 + ran)\, f_h \tag{3}$$

where *ran* is a random number between zero and one that gives a stochastic component to the hopping height. Should fuel moisture increase, f_h is decreased, hopping height is less, and fire spread rate is reduced.

Regarding (c), the rabbit survives only if it lands on an empty uneaten food cell (Figure 3). Landing on all other cells – cells eaten by other rabbits (black), occupied by other rabbits (orange or red), or non-food cells (other non-green colors) – is fatal. Then its longevity, a function of fuel characteristics which include mass and heterogeneity, is assigned through five time coefficients shown as m_1 - m_5 in Table 2. Specified in units of minutes, for rabbits of a particular fuel type, 100% live through m_1, 50% live through *m2*, 20% live through *m3*, 5% live through *m4*, and 1% live through *m5*. The first cutoff defines the residence time of the fire front as it passes through fuel beds. The remaining cutoffs define the number of old/dying rabbits that represent residual burning. The role of rabbit longevity is described in reference to Rule FA1 below.

Table 2. Fuels data for Rabbit Rules: fn01 – grass/pine needle mixture, fn02 – grass only.

Fn	m_1	m_2	m_3	m_4	m_5	f_h	v_g	C_h	C_w	C_f	δ_B
01	0.5	0.0	0.0	0.0	0.0	0.65	2.00	1.00	0.25	----	1
02	0.1	0.0	0.0	0.0	0.0	1.00	1.00	1.00	0.25	----	1

Equations (1), (2), and (3) describe a simple CA model for “rabbits” hopping over a landscape. The relationship to fire spread rate (ROS) is analogous: fire spreads faster in stronger winds - rabbits hop farther in stronger winds; fire spreads faster uphill than downhill – rabbits prefer to hop uphill rather than downhill; fire spreads faster when embers fall farther from the fire line – rabbits jump higher, hence get carried farther by the wind, subject to food (fuel) characteristics.

The three rules are linked by weights yet to be determined. Once the characteristic fuel height is set, the relationship between fire spread rate, wind and slope is linear. Therefore, Equation (1) cannot represent non-linear dependencies present in a general wildland fire and is thus a departure from simulations based on physics-based models. Nonlinear fire-atmosphere coupling is done through secondary rules, FA1 and FA2.

Rule FA1 posits that each rabbit throughout its lifetime discharges a plume of heated air that drifts downwind from the rabbit location. This plume of warm air creates a hydrostatically-

induced low pressure area at the ground which is too weak to influence the local winds. However, when summed over a large number of rabbits, the low pressure area can be sufficient to impact the local wind field. Thus Rule FA1 defines how temperature anomalies within the plume of ascending hot gases modify surface air pressure to draw the wind field around and through the fire. Each rabbit is assigned a number, n_p, of pressure anomaly "points" which define a plume downwind from the rabbit. The location of the nth point relative to the rabbit is

$$d_n = c_{pn} U (ran)^2 \tag{4}$$

where U is the vector mean wind for the layer containing the heat plume and c_{pn} (c_{pn} = 0.2, 0.5, 1.0; n_p = 3) are distance weights normalized to the grid. Use of the square of the random number forces d_n to concentrate closer to the fire thus making Equation (4) a proxy for heated air within the plume with the hottest air being located just downwind from the fire. The total pressure anomaly at each point of an overlying meteorological grid is the sum of all of the pressure anomalies over all rabbits *nrab* within a specified distance of that grid point,

$$P_{i,j} = P_{0i,j} + 10^{-4} \sum_{k=1}^{nrab} \sum_{n=1}^{np} \delta_{A1} v_{gk} \tag{5}$$

where δ_{A1} = 1 if d_n is located within half a grid space of $P_{i,j}$ else δ_{A1} = 0. $P_{0i,j}$ is a reference pressure here set to 1000 mb. The parameter v_g weights the rabbit "vigor" according to the fuel type consumed. Thus certain cells may hold fuel types and characteristics that produce more/less heat than at other cells. The summation is multiplied by 10^{-4} to render v_g to the order of one.

Rule FA1 defines how temperature-induced pressure anomalies modify surface air pressure to draw the wind field around and through the fire. Air accelerated through the fire line must be replaced by "draw-in" - air drawn in from behind the combustion zone. Rule FA2 posits that a fraction of the air drawn in comes from aloft. The depth of the layer through which a fire draws, and the intensity of the draw-down, is directly proportional to the strength of the fire. Rule FA2 is the mechanism for downward momentum transport in Rabbit Rules. Typically, draw-down would be calculated from the divergence of the winds behind the fire. However, the fire model is to be attached to a simple vertically integrated two-dimensional wind model. Therefore, to avoid vertical momentum transport in divergence not associated with the fire, the draw-down is made a function of the fire-induced pressure anomalies. The quantitative measure for the strength of the draw-down, I, is the Laplacian of the pressure anomaly produced by Rule FA1,

$$I = -\delta_{A2} C_{A2} \nabla^2 P \tag{6}$$

where δ_{A2} = 1 if the Laplacian of pressure is negative else δ_{A2} = 0. C_{A2} scales the draw-down to the order of other rules. Equation (6) is placed in the meteorological model as a forcing term proportional to the vertical wind shear within the surface layer. For this study, the vertical shear is the difference between the vector winds at 100 m and 2 m.

Birth time and number of rabbits birthed are the key links to fire spread rate. Fire spread through a cellular grid must be normalized to the physical size of the cell occupied by the rabbit. In

Rabbit Rules the grid cell is represented by a pixel on the computer monitor screen. The physical area of a pixel is the area of the physical domain imaged on the computer screen divided by the number of pixels contained within that image. The birth time is a constant calculated internally in the model, is proportional only to the physical width of the pixel and therefore can range from seconds to minutes. To the birth time is added a small stochastic component to increase time-variability in hopping.

Tests were conducted and computation time and model behavior were monitored to determine the most suitable number of birthed rabbits. Using four as the number of rabbits birthed keeps the solution from fragmenting, i.e., fire spread becoming too fractal,(Hargrove et al., 2000) while controlling computational overload. When backspread is turned on, the number of rabbits birthed is eight for reasons defined by the discussion leading to Equation (1). However, there exist a finite number of fuel cells to which a rabbit can jump. Birthing many rabbits increases computational load without improving model accuracy because most will perish for lack of empty uneaten fuel cells.

The above rules and associated steps complete the fire model part of Rabbit Rules. Analogous to other cellular automata fire models, a set of parameters must be specified prior to model execution. The values for characteristic food height, wind, isotropic hopping, and vigor (f_h, C_w, C_h, v_g) were assigned by "training" the rabbits through approximately 200 model runs to match the reported rate of spread through tall grass (Andrews, 2008) over the full range of wind speeds ($0.0 – 9.3\ ms^{-1}$).

The above-derived fire model was embedded within a simple high-resolution semi-Lagrangian meteorological "interface" model modified from a shallow-layer wind model (Achtemeier, 2005b). The interface model links the rule-driven fire model with selected output from mesoscale numerical weather prediction models such as the Mesoscale Meteorological Model MM5 (Grell et al., 1994) and the Weather Research and Forecasting Model WRF (Skamarock et al., 2005). However, if there are no terrain-modified circulations and weather patterns are spatially uniform over a relatively small burn area, Rabbit Rules can be initialized with local wind observations at 10-m and at 100-m.

The lower boundary surface for the meteorological interface model is defined by the U.S. Geological Survey 30 m digital elevation data base. Whereas the minimum resolution of the fire model may be less than 1 m, the minimum resolution of winds within the interface model is 30 m. Therefore, the wind model cannot resolve circulations on the scale of the fire but can resolve the bulk circulations initiated by heat flowing through the smoke plume.

3.2.2 Dispersion Model: Daysmoke

The dispersion of the smoke in the near-field is modeled by Daysmoke, an empirical model specifically designed for prescribed burn plumes (Achtemeier et al., 2011). Given the number of updraft cores, core diameters, updraft velocities, plume and ambient temperatures, wind fields, and emission rates, Daysmoke tracks the particles up to a predetermined distance from the burn plot, assuming the smoke is an inert substance.

Daysmoke is an extension of ASHFALL, a plume model developed to simulate deposition of ash from sugar cane fires (Achtemeier, 1998). As adapted for prescribed fire, Daysmoke consists of three models – an entraining turret model that calculates plume pathways, a particle trajectory model that simulates smoke transport through the plume pathways, and a meteorological "interface" model that links these models to weather data from high-resolution numerical weather models such as MM5 and WRF.

The theory for Daysmoke is detailed elsewhere (Achtemeier et al., 2011). Photogrammetric analysis of video footage of smoke plumes from burning sugar cane determined that a rising smoke plume could be described by a train of rising turrets of heated air that sweep out a three-dimensional volume defined by plume boundaries on expanding through entrainment of surrounding air through the sides and bottoms as they ascend (Achtemeier and Adkins, 1997). The plume boundaries of the entraining turret model become an inverted cone centered on the fire and bent over by the ambient wind.

Initial variables needed to calculate plume boundaries are the initial effective plume diameter, D_0, defined as the diameter a plume would have if the fire were placed in a circle, the initial vertical velocity, w_0, and an initial plume temperature anomaly, ΔT_0. These can be derived from an equation for heat release rate (Q) which is simply estimated as 50% of the product of the mass of fuel consumed per hour and the heat of combustion (1.85×10^7 J kg^{-1}) (Byram, 1959). The assumed 50% reduction in the heat release rate is designed to restrict only a portion of the total heat released going into the plume with the other 50% going into the heating of surrounding vegetation and ground surface. The initial values for the plume - D_0, w_0, and ΔT_0 – can be related to the heat of the fire (Mercer and Weber, 2001) by

$$w_0 D_0^2 = \frac{4Q}{\pi C_p \rho \Delta T_0} \tag{7}$$

C_p is the specific heat (J kg^{-1} K^{-1}), w_0 is the vertical velocity entering the plume (m s^{-1}), ρ is the air density (kg m^{-3}) and ΔT_0 is the temperature difference between the plume air and ambient conditions. Representative values for w_0 and ΔT_0 of 25 m s^{-1} and 40 ^{o}C have been assumed based on numerical simulations of coupled fire atmosphere models (Jenkins et al., 2001). Using these assumed values for vertical velocity and temperature difference allows D_0 to be determined.

Equation (7) with the above specified initial conditions is assumed to be valid at some reference height h_0 defined as the base of the plume where flaming gasses and ambient air have been thoroughly mixed and where the incipient plume temperature ΔT_0 of 40 ^{o}C is found. For small prescribed burns, h_0 may be found approximately 10 m above ground and for wildfires, h_0 may be found several 100's of meters above ground. For a typical grassfire (Clements et al., 2007), h_0 can be found near 35 m.

Observations of plumes from large-perimeter prescribed fires revealed the presence of several updraft cores or subplumes. These updraft cores may vary in size depending on the type, loading, and distribution of various fuels. The entraining turret model can be readily adapted for multiple-core updraft plumes by increasing the number of inverted cones to be solved by the model

subject to the condition that the initial volume flux through the ensemble of updraft cores is equal to the volume flux through the single updraft core,

$$f_0 = \frac{\pi}{4} D_0^2 w_0 \tag{8}$$

The volume fluxes of the individual updraft cores may be defined subject to the constraint that

$$f_k = f_0 \frac{(0.01 + ran_k)}{\sum_{k=1}^{n} (0.01 + ran_k)} \tag{9}$$

where ran_k is a random number $0<ran_k<1$. The 0.01 is summed with the random number to render the updraft core diameter unequal to zero. Thus Daysmoke can be set to create simultaneous plume pathways for any number, *n*, of updraft cores. The caveat is that *n* and f_k, k = 1,… *n* are unknown. In the absence of field measurements for each updraft core, the f_k are estimated through the random number *ran*, however, no mechanism to determine *n* exists in Daysmoke. Efforts are under way to determine the appropriate core number from the number of low pressure zones in Rabbit Rules.

3.2.3 Chemistry-Transport Model: Adaptive Grid CMAQ

The base model used for long-range transport and chemistry is the Community Multiscale Air Quality (CMAQ) model (Byun and Schere, 2006). This model is commonly used for regional air quality applications to predict the regional levels of ozone and $PM_{2.5}$. An adaptive grid version of CMAQ (AG-CMAQ) was developed that can dynamically refine the grid around the plume (Garcia-Menendez et al., 2010). An adaptive grid model can better resolve the dynamics and chemistry needed for accurate simulation of a PB plume (Unal and Odman, 2003).

A simulation with AG-CMAQ has two fundamental steps: a grid adaptation step, that is responsible for repositioning of grid nodes according to the grid resolution requirements, and a solution step, that simulates the physical and chemical processes that occur in the atmosphere. The solution (in this case, pollutant concentration fields) remains unchanged during the adaptation step, and the weight function clusters the grid nodes in regions where finer resolution grids are required. In preparation for the solution step, fields of meteorological inputs and emissions must be mapped onto the new grid locations. Efficient search and intersection algorithms are used to perform this task. During the solution step, the grid nodes remain fixed while the solution is advanced in time. Ideally, the adaptation step should be repeated after each solution step owing to the change in resolution requirements. However, since the mapping of meteorological and emissions data is computationally expensive, the adaptation step is applied less frequently. For example, whereas the solution is advanced in time by one hour (or 15 minutes) in multiple time steps, the adaptation step is performed once every hour (or 15 minutes). A description of the operations performed in AG-CMAQ during the adaptation and solution steps follows.

3.2.3.1 Adaptation Step

What drives grid adaptation is a weight function that determines where grid nodes are to be clustered for a more accurate solution. Such a weight function, *w*, can be built from a linear combination of the errors in the concentrations of various chemical species:

$$w \propto \sum_n \alpha_n \nabla^2 c_n \tag{10}$$

∇^2, the Laplacian, approximates the error in c_n, the computed value of the concentration of species *n*. The chemical mechanisms used in AQMs usually have a large number of species. Due to non-homogeneous distribution of emissions and disparate residence times, each species may have very different resolution requirements. Determining α_n such that all pollutant concentrations (e.g., ozone and $PM_{2.5}$) can be estimated most accurately is nontrivial. Here, all α_n are set to zero, except the one for $PM_{2.5}$. Further, the grid adaptation is restricted to the horizontal plane, and the same grid structure, which is determined by the total column $PM_{2.5}$ concentrations, is used for all vertical layers.

The grid nodes are repositioned by using the weight function. The new position of the grid node *i*, $\vec{P}_i^{new}$, is calculated as:

$$\vec{P}_i^{new} = \sum_{k=1}^{4} w_k \vec{P}_k \Big/ \sum_{k=1}^{4} w_k \tag{11}$$

where $\vec{P}_k$, $k = 1,\ldots,4$, are the original positions of the centroids of the four cells that share the grid node *i*, and w_k is the weight function value associated with each centroid.

Once the grid nodes are repositioned, cell-averaged species concentrations must be recomputed for the adapted grid cells. Holding the concentration field fixed and moving the grid is numerically equivalent to simulating the advection process on a fixed grid. Therefore, a high-order accurate and monotonic advection scheme known as the piecewise parabolic method (Collela and Woodward, 1984) is used to interpolate concentrations from the old to the new grid locations.

The calculation of the weight function, the movement of the grid nodes, and the interpolation of species concentration from the old to the new grid locations are three distinct tasks of an iterative process. The process continues until the maximum grid node movement is less than a preset tolerance. A very small tolerance may lead to a large number of iterations. On the other hand, a large tolerance may not ensure adequate resolution of the solution field. Currently, we stop iterating when, for any grid node, the movement is less than 5% of the minimum distance between the node in question and the four nodes to which it is connected.

After the grid nodes are repositioned, emissions and meteorological data must be processed to generate the necessary inputs for the solution step. Note that, unlike the practice with fixed grid AQMs, this processing could not be performed prior to the simulation because there is no *a*

priori knowledge of where the nodes would be located at any given time. In case of meteorological data, an ideal solution would be to run a meteorological model (MM), which can operate on the same adaptive grid, in parallel with the AQM. This would ensure dynamic consistency of meteorological inputs, but such a MM is currently nonexistent. Therefore, hourly meteorological data are obtained from a high-resolution, fixed-grid MM simulation and interpolated onto the adaptive grid.

The processing of emission data is computationally expensive, requiring identification of various emission sources in the adapted grid cells. Here, we treat all emission sources in two categories: point and area sources. For simplicity, the mobile sources have been included in the area-source category, but treating them as line sources would yield better resolution. For the point sources, the grid cell containing the location of each stack must be identified. The search may be quite expensive if there are thousands of stacks in the modeling domain. However, assuming that the cell containing the stack before adaptation would still be in close proximity of the stack after adaptation, the search can be localized. The localization of the search provides significant savings over more general, global searches. As for the area sources, they are first mapped onto a uniform high-resolution *emissions grid* using geographic information systems. This is done in order to avoid higher computational costs associated with processing of emissions from highly irregular geometric shapes presented by highways and counties. Around each adaptive grid cell there is a box of emissions grid cells $E_i, i = 1,\ldots,n$, as illustrated in Figure 4. Once each E_i is identified, then their polygonal intersections with the adaptive grid cell are determined. Finally, the areas of these polygons, S_i, are multiplied by the emission fluxes of E_i and summed over *n* to yield the total mass emitted into the adaptive grid cell. This process is performed for all adaptive grid cells.

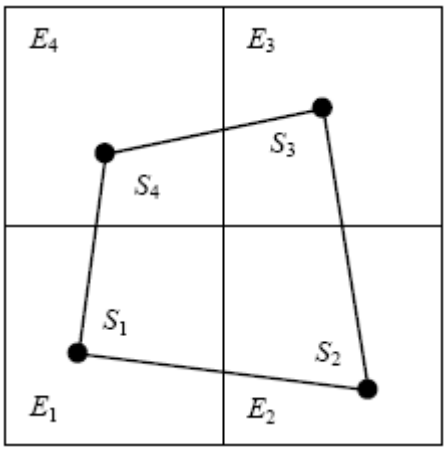

Figure 4. Intersection of an adapting grid cell with the area-source emissions grid.

The final step in preparation for the solution step is reestablishing a uniform grid for easy computation of the solution. This requires computation of a transformation from the (x, y) space where the grid is non-uniform to the (ξ, η) space where the grid would be uniform. The calculation of the Jacobian of the transformation and other necessary metrics (i.e., $\partial\xi/\partial x, \partial\xi/\partial y, \partial\eta/\partial x, \partial\eta/\partial y$) concludes the adaptation step.

3.2.3.2 Solution Step

The atmospheric diffusion equation that CMAQ solves in the (x, y, σ) space is transformed to the (ξ, η, σ) space as

$$\frac{\partial(Jc_n)}{\partial t} + \frac{\partial\left(Jv^{\xi}c_n\right)}{\partial \xi} + \frac{\partial\left(Jv^{\eta}c_n\right)}{\partial \eta} + \frac{\partial\left(Jv^{\sigma}c_n\right)}{\partial \sigma} + \frac{\partial}{\partial \xi}\left(JK^{\xi\xi}\frac{\partial c_n}{\partial \xi}\right) + \frac{\partial}{\partial \eta}\left(JK^{\eta\eta}\frac{\partial c_n}{\partial \eta}\right) + \frac{\partial}{\partial \sigma}\left(JK^{\sigma\sigma}\frac{\partial c_n}{\partial \sigma}\right) = JR_n + JS_n \tag{12}$$

c_n, R_n, and S_n are the concentration, chemical reaction, and emission terms of species *n*, respectively, and σ is a terrain-following vertical coordinate. *J* is the Jacobian of the coordinate transformation:

$$J = \frac{1}{m^2}\frac{\partial z}{\partial \sigma}\left(\frac{\partial x}{\partial \xi}\frac{\partial y}{\partial \eta} - \frac{\partial y}{\partial \xi}\frac{\partial x}{\partial \eta}\right) \tag{13}$$

where *m* is the scale factor of a conformal map projection in the horizontal. The components of the wind vector in ξ and η directions are v^{ξ} and v^{η}:

$$v^{\xi} = m\frac{\partial \xi}{\partial x}U + m\frac{\partial \xi}{\partial y}V$$
$$v^{\eta} = m\frac{\partial \eta}{\partial x}U + m\frac{\partial \eta}{\partial y}V \tag{14}$$

where *U* and *V* are real horizontal wind velocities rotated in the map's coordinate directions. For mass conservation, the vertical wind component v^{σ} is readjusted as described in Odman and Russell (2000).

The turbulent diffusivity tensor is assumed to be diagonal, and its elements, $K^{\xi\xi}$, $K^{\eta\eta}$ and $K^{\sigma\sigma}$, are obtained by tensor transformation. The expressions for $K^{\xi\xi}$ and $K^{\eta\eta}$ involve horizontal diffusivity, $K^{xx} = K^{yy} = K^{hh}$ while $K^{\sigma\sigma}$ is expressed in terms of the vertical diffusivity K^{zz} as:

$$K^{\sigma\sigma} = \left(\frac{\partial \sigma}{\partial z}\right)^2 K^{zz} \tag{15}$$

Since the grid is uniform in the (ξ, η) space, solution algorithms used in CMAQ can be applied directly. However, a computational challenge is encountered due to the numerical stability requirement that the Courant number must be smaller than unity. The presence of very small grid scales (e.g., 100 m) together with high wind speeds in the upper troposphere (e.g., 50 m s^{-1}) necessitates very small solution time steps. This is computationally very demanding and inefficient since using smaller time steps does not necessarily improve the accuracy of the solution. Since the adapted grid contains a large number of coarse cells alongside fine cells, using the time step required by the smallest grid cell everywhere is wasteful. For computational

efficiency, variable grid sizes should be accompanied by variable time steps (Odman and Hu, 2007).

A variable time step algorithm was developed to improve the computational efficiency of AQMs, especially those using adaptive grids (Odman and Hu, 2010). In this algorithm:

- Every cell is assigned its own local time step, Δt_i , which is an integer multiple of the global time step Δt and an integer divisor of the output time step. For example, if the global time step is 5 minutes and the output time step is 60 minutes, local time steps can be 5, 10, 15, 20, 30, or 60 minutes
- The model clock time, t, is advanced by the global time step
- When $t=N\times\Delta t_i$ chemistry, aerosol and cloud processes are applied for the duration of Δt_i
- Transport processes require a reservoir to store the fluxes as shown in Figure 5.

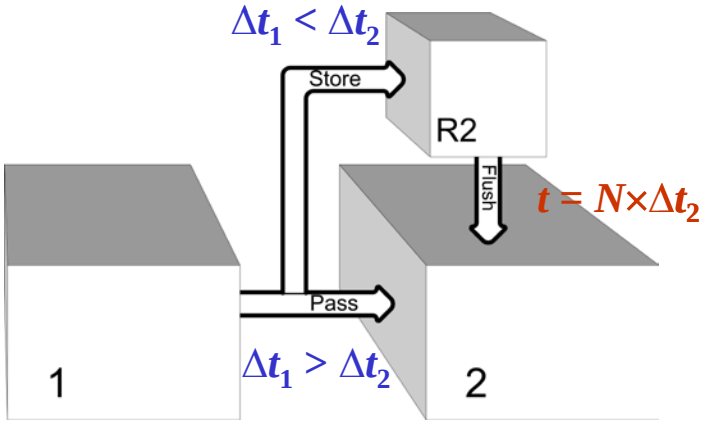

Figure 5. Transport with VARTSTEP algorithm.

All the solution algorithms in CMAQ were revised to operate with local time steps instead of a single global time step. Transport modules were further modified to store the fluxes. A complete description of the VARTSTEP algorithm and its incorporation into CMAQ can be found in Odman and Hu (2010). VARTSTEP and the adaptive grid algorithm described above are the primary additions to CMAQ that form AG-CMAQ. Verification of the AG-CMAQ code and an evaluation of the model can be found in Garcia-Menendez et al. (2010).

3.2.4 Coupling of Dispersion Model with Chemistry Transport Model

This section describes how the dispersion model Daysmoke was coupled with the chemistry transport model CMAQ and its adaptive grid version AG-CMAQ. It includes a Fourier analysis of the accuracy loss during the transfer of PB plume from Daysmoke to CMAQ due to coarse grid resolution. The final coupling methodology was developed based on the results of this analysis.

3.2.4.1 Initial Coupling Methodology

The initial coupling of Daysmoke with CMAQ was accomplished within the framework of the Southern High-Resolution Modeling Consortium Southern Smoke Simulation System (SHRMC-4S) (Liu et al., 2009). Daysmoke was linked to SMOKE, the emission processor for CMAQ, as an addition to Laypoint, the point-source module that is based on Briggs plume-rise algorithm, for distributing PB emissions vertically into CMAQ layers. In this coupling, smoke particles passing an imaginary boundary at a fixed distance downwind from the burn site (3 miles) are extracted from Daysmoke and injected into CMAQ as emissions. Since each smoke particle represents a certain amount of mass of a chemical species (for example, 1 kg of $PM_{2.5}$) the total amount of emissions can be calculated from the particle count. The apportionment of emissions to CMAQ vertical layers is done according to the fraction of such particles in each CMAQ layer (relative to the total number of such particles). The details of the coupling methodology can be found in Liu et al. (2009).

The initial coupling above uses a fixed downwind distance to inject Daysmoke particles into CMAQ grid cells without any consideration of the potential loss of accuracy at the interface. As a drawback of this approach, the detailed plume structure present in Daysmoke particle distribution at the interface may be lost if the CMAQ grid does not have sufficient resolution to support that structure. This drawback can be surmounted by developing a coupling technique that can detect the potential loss of accuracy and set the interface at a distance where this loss is minimal.

3.2.4.2 Fourier analysis

Towards the development of a better coupling approach, a Fourier analysis was performed as follows. First, the smoke particle distributions predicted by Daysmoke were analyzed as spectra of waves with different frequencies. Then, the waves whose frequencies cannot be supported by the CMAQ grid were identified. If the amplitudes of those waves are negligible, then the plume can be handed over to CMAQ without significant loss of accuracy; otherwise it is better to continue to follow the plume with Daysmoke. By conducting this analysis at various downwind distances, the optimal distance for handover can be determined.

To test this new coupling concept, a standalone analysis system was created by borrowing Fast Fourier Transform (FFT) algorithms from MATLAB. Initially, there were some concerns about using MATLAB since some other FFT codes produced numerical noise that dominated the amplitudes of high frequency waves. However, tests showed that the FFT algorithms in MATLAB were able to produce noise-free Fourier transforms for typical Daysmoke particle distributions.

The operation of the Fourier analysis system is illustrated in Figure 6. The smoke plume is modeled by Daysmoke up to a downwind distance of 16 km. The plume span is divided into a "fine grid" of 100×100×100 cells and the Daysmoke particles in each cell are counted. Since each particle represents an assigned mass of smoke in Daysmoke (1 kg of $PM_{2.5}$), the number of particles is converted to smoke concentration by multiplying the number of particles with the assigned mass and dividing the product by the cell volume. At every 160 m downwind from the

fire center, cell concentrations are summed up vertically. The concentration field is now two-dimensional in the physical space, dependent on horizontal location only; this is Step 1 in Figure 6. The next step is to transform this concentration field to a field of frequencies and associated amplitudes in the Fourier space (Step 2). For every cross section 160 m downwind from the fire, the concentration distribution is transformed using forward FFT in MATLAB. The series of frequency-amplitude pairs so obtained can be plotted all together to look like the bottom left panel in Figure 6. Then, the higher frequencies that would not be represented on the "coarser grid" of CMAQ are clipped (Step 3). Inverse FFT transform of the remaining frequencies back to the physical space yields a second concentration field on the "fine grid". This field is an approximation for how the original plume would be represented on CMAQ's "coarser grid" (Step 4). The last step is to assess the differences between the original field and the field that was transformed, clipped and inverse transformed. The downwind distance for handing over the Daysmoke plume to CMAQ can be decided based on this assessment of the differences between the two concentration fields (Step 5).

The metric used for assessing the difference between the original and (forward and backward) Fourier transformed distributions is typically a high moment of the concentration. Here, the square of the concentrations has been used but the third power might be even more discerning. This assessment of the difference between the two concentration fields can help to decide whether to hand over the plume to CMAQ or continue to follow it with Daysmoke. However, there are other considerations in deciding where to set the interface between Daysmoke and CMAQ. For example, a minimum downwind distance is needed to fully benefit from Daysmoke's empirical plume modeling capability. More specifically, the Daysmoke plume does not reach its maximum height or does not show signs of large eddy scale turbulence (LES) up to a certain downwind distance. On the other hand, prolonging the modeling of the plume with Daysmoke, which is an inert model, delays the potential of chemical interactions with the ambient atmosphere. Currently, modeling of chemical reactions does not start until the plume is handed over to CMAQ.

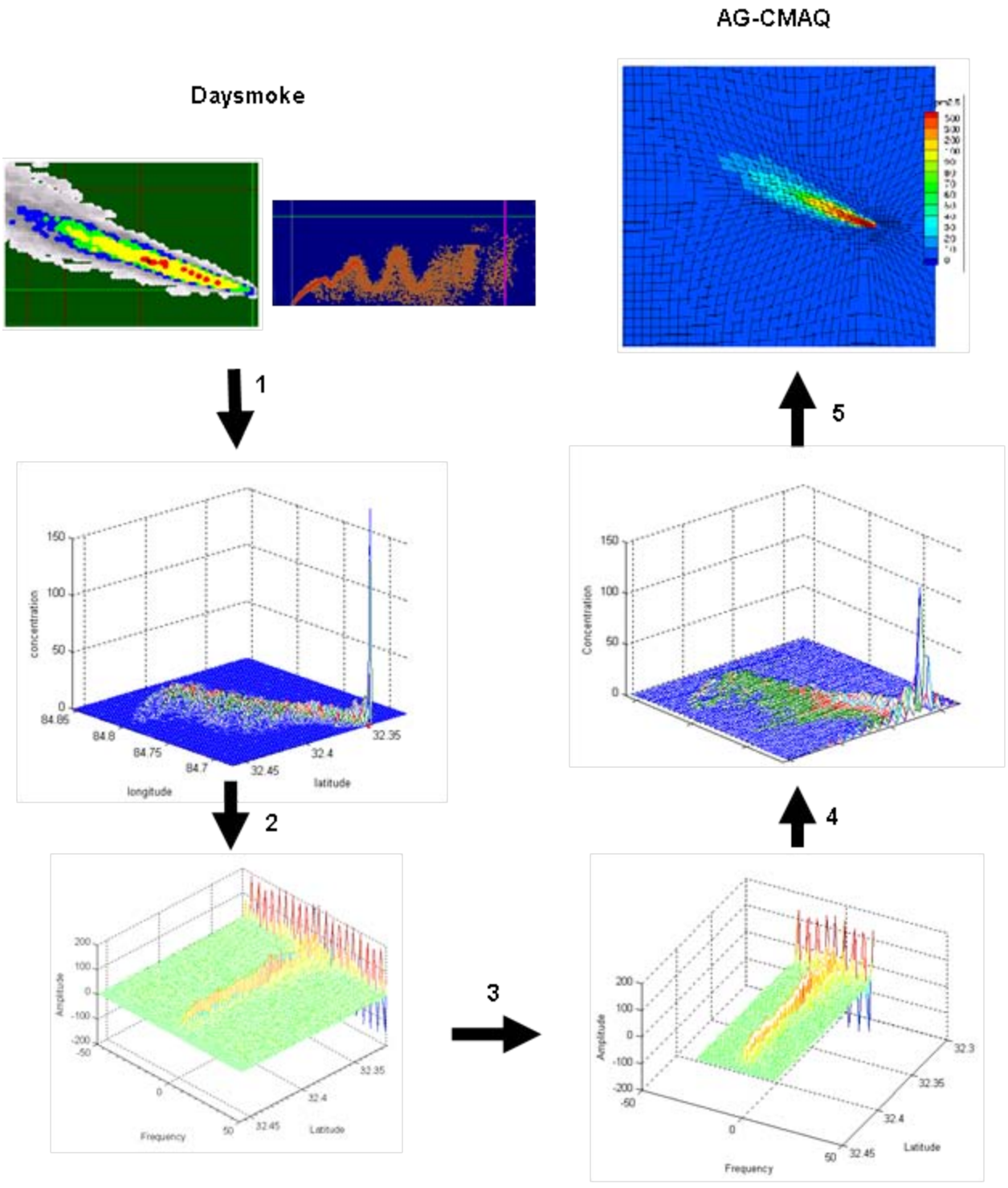

Figure 6. Fourier analysis of the PB plume for coupling Daysmoke with CMAQ.

3.2.4.3 Final coupling methodology

The standalone system developed for the Fourier analysis above has not been used as the final coupling methodology for two reasons. First, the Fourier analysis is time consuming despite the use of FFT. A computationally more efficient method is sought. Second, the coupling will be applied to AG-CMAQ, which does not have a unique grid size. Recall that the adaptive grid is refined gradually around the PB plume, with finer grids where smoke concentrations are large and coarser grids elsewhere, resulting in a spectrum of grid sizes. However, certain elements of the standalone system and the knowledge gained from the Fourier analysis were instrumental in the development of the coupling methodology. The coupled modeling system will be called Adaptive Grid Daysmoke CMAQ (AGD-CMAQ). Daysmoke can be viewed as a sub-grid scale plume model in this system since its primary purpose is to better characterize the smoke plume in AG-CMAQ, which is a grid model.

In the final coupling, instead of using a loose coupling through the emission processor, as was done in the initial coupling, Daysmoke was turned into an AG-CMAQ process module. Daysmoke is called every AG-CMAQ global time step to track the smoke plume for the duration of that time step. Recall that AG-CMAQ uses variable time steps. It was verified that Daysmoke, in this new form, can produce the same results that it did in its original form. Some differences were observed but, given that Daysmoke's internal time step (20 s) did not always evenly divide the AG-CMAQ time step, the differences were deemed to be acceptable. At the end of the CMAQ time step, another process called "handover" was added to determine the interface where Daysmoke will share its information with AG-CMAQ. The conditions sought at the interface will be described below. The information sharing takes place in the form of adding the associated mass of Daysmoke particles into the reservoirs used for the transport processes of AG-CMAQ. In other words, the Daysmoke plume is "handed over" to AG-CMAQ at the interface. Beyond the interface the smoke plume is tracked by AG-CMAQ while the remaining particles continue to be tracked by Daysmoke.

The "handover" process consists of the following major operations. First, Daysmoke particles tracked as mass (1 kg of $PM_{2.5}$ per particle) are converted to concentrations over a 100×100-cell "fine" grid that spans the plume for each vertical layer of the AG-CMAQ model (Figure 7a). The grid columns are perpendicular to the axis of the plume while grid rows are parallel to it. Recall that there is no difference between the vertical layering of AG-CMAQ and that of CMAQ since grid adaptation takes place only in the horizontal. Daysmoke particles are also converted to concentrations over the adaptive grid of AG-CMAQ (Figure 7b). The AG-CMAQ grid is independent from the "handover" process. It has already been adapted by using a fire tracer. The only purpose of this tracer is to adapt the AG-CMAQ grid. The tracer is injected at the center of the burn and it is tracked by AG-CMAQ alone; it has no knowledge of how Daysmoke defines the plume and it has no contribution to the concentrations of $PM_{2.5}$ and other pollutants tracked by the coupled system.

(a)

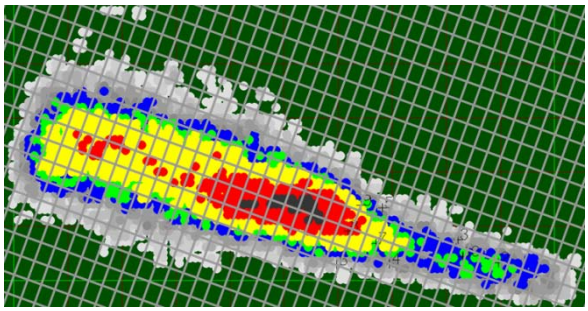

(b)

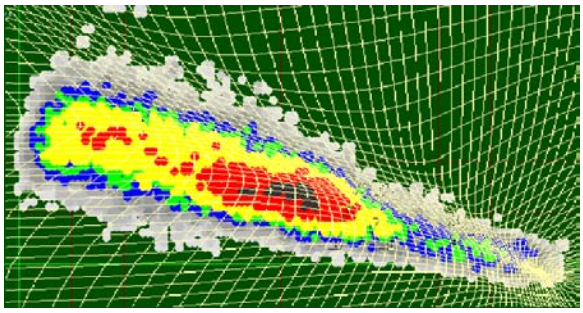

(c)

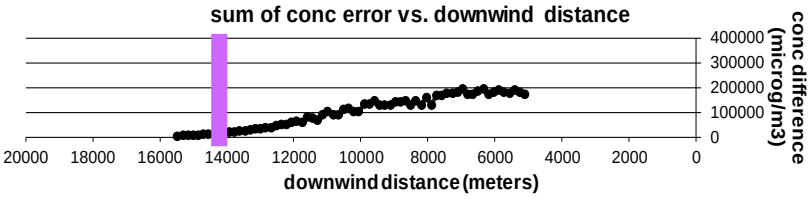

(d)

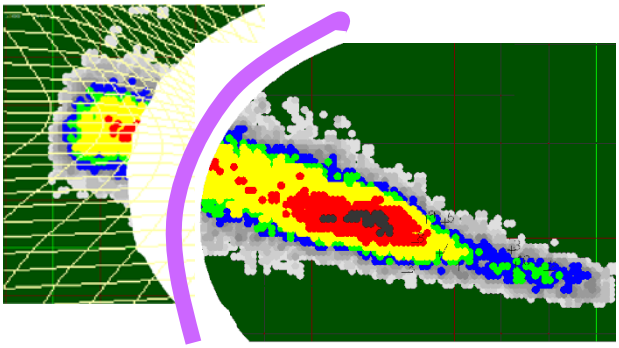

Figure 7. Determination of the interface between Daysmoke and AG-CMAQ: a) Daysmoke plume on the fine grid, b) Daysmoke plume on the adaptive grid, c) determination of the interface from concentration differences, d) separation of the plume into two parts to be tracked by Daysmoke and AG-CMAQ.

Next, the concentration fields calculated on these two different grids are compared to find a suitable downwind distance for the interface. The goal is to set the interface where the difference between the fields is minimal so that the loss of accuracy incurred by "handover" is minimized. The metric used to assess the difference is the cross-sectional sum (sum over lateral grid cells and vertical layers) of normalized differences between concentrations on the two grids, calculated every one hundredth of distance spanned by the plume along the plume axis, as shown in Equation (16).

$$ND_i = \frac{1}{nlays \times 100} \sum_{k=1}^{nlays} \sum_{j=1}^{100} \frac{2 \times \left| c_{i,j,k}^{adp} - c_{i,j,k}^{fin} \right|}{\left(c_{i,j,k}^{adp} + c_{i,j,k}^{fin} \right)} \tag{16}$$

$c_{i,j,k}^{fin}$ is the concentration of the fine grid cell $(i.j.k)$ where $i = 1,\ldots,100$ is the grid column index, j is the row index, k is the layer index and $nlays$ is number of vertical layers in AG-CMAQ. $c_{i,j,k}^{adp}$ is the concentration of the coinciding adaptive grid cell. Note that the actual adaptive grid indices of the adaptive grid cell coinciding with fine grid cell $(i.j.k)$ are different. Also, since the adaptive grid is typically coarser than the fine grid, several $c_{i,j,k}^{adp}$ may have the same value, i.e., the same adaptive grid cell may coincide with several fine grid cells.

Ordinarily, the fine grid column i with the smallest ND_i determines where the interface will be set for transferring the smoke plume from Daysmoke to AG-CMAQ. Small ND_i or difference between the two grids' concentrations will ensure that the error introduced during plume handover will also be small. However, two constraints are placed on this error minimization. First, the interface must be set at a downwind distance which allows for full development of the Daysmoke plume. This condition is checked by the height of the plume in Daysmoke. The plume is assumed to be fully developed when Daysmoke particles reach their potential height. Hence, the constraint becomes that the interface cannot be closer to the burn than the Daysmoke particle with maximum height. The second constraint is that the interface cannot be farther than a predetermined distance, typically 16 km, from the burn. The reason for this constraint is that Daysmoke is an inert model; therefore, chemical interactions of the smoke plume with the ambient atmosphere cannot be modeled until the plume is handed over to AG-CMAQ. The closer the interface, the sooner chemical interactions will be accounted for.

The interface is defined as an arc at the downwind distance (from the burn) of the fine grid column with the smallest ND_i provided the two constraints are satisfied at this distance (Figure 7c). Otherwise another grid column with the smallest ND_i among the columns that satisfy the conditions of the constraints is selected. Note that the fine grid is not radial but the radius, or distance from the burn, of the arc-shaped interface is typically large enough with respect to the width of the plume that the error introduced by using a rectangular grid is small.

Finally, Daysmoke particles beyond the interface are transferred to AG-CMAQ by adding their associated mass to the reservoir of the appropriate AG-CMAQ grid cell. Recall that in AG-CMAQ every adaptive grid cell has a reservoir for proper handling of the transport processes

using the variable time step algorithm. All other particles remain in Daysmoke (Figure 7d), their fate to be determined by Daysmoke in the next AG-CMAQ time step. Next time, the location of the interface would be different since it would be determined by the conditions prevailing at that time. The process continues until all of the particles emitted from the burn and tracked by Daysmoke cross the interface. This completes the description of the "handover" process.

3.3 Data Collection Methods

In 2008 and 2009, eleven prescribed burns were monitored at Fort Benning Army Base (AB) near Columbus, Georgia. The measurements consisted of plume height and smoke ($PM_{2.5}$ and CO) concentrations downwind of the plume. These data were used in evaluating the performance of the smoke dispersion model, Daysmoke. During model evaluation cycles, additional data elements were identified to be necessary for a more rigorous assessment of Daysmoke's performance. These data elements were emissions, wind speed and direction, and more accurate smoke concentrations. A comprehensive second field study was conducted at Eglin Air Force Base (AFB) near Niceville, Florida in 2011 to collect these data.

Here, the methods used for data collection are discussed in two parts. The first part covers the preliminary and initial data collection phases conducted at Fort Benning AB during April 2008, January 2009 and April 2009. The purpose of the Fort Benning study was to collect plume height and downwind smoke concentrations on the ground. The second part covers the more comprehensive final phase of data collection conducted at Eglin AFB with the added objectives of measuring vertical wind profiles and measuring smoke emissions above the canopy. The ground-based smoke measurements methods at Eglin were different than those at Fort Benning; therefore, they will be described under each study. The plume height measurement method was the same at Fort Benning and Eglin; therefore they will be discussed only under the Fort Benning study.

3.3.1 Fort Benning Field Study

The Fort Benning study consisted of eleven burns monitored in three rounds: 1) three burns during April 8-15, 2008, 2) six burns during January 13-23, 2009 and 3) two burns during April 8-9, 2009 periods. Plume height data and ground-level downwind smoke concentrations were collected. These measurements provided ground-truth information for three cycles of Daysmoke evaluation. The procedures used for data collection were slightly modified after each cycle to improve their value for model evaluation.

3.3.1.1 Plume height measurements

Smoke plume rise was measured using a CL31 Ceilometer (Figure 8). This device employs laser LIDAR (Light Detection and Ranging) technology. It emits short, powerful laser pulses in a vertical or slant direction. The directly backscattered light caused by haze is measured as the laser pulses traverse the sky. This is an elastic backscatter system and the return signal is measured at the same wavelength as the transmitted beam. As many as three smoke layers can be detected with the height up to 7.5 km. The detection frequency is 2 second. Figure 9 shows the measured smoke plume structure for a prescribed burn at Ft Benning on April 9, 2009.

Figure 8. CL31 Ceilometer with smoke plume from a prescribed burn.

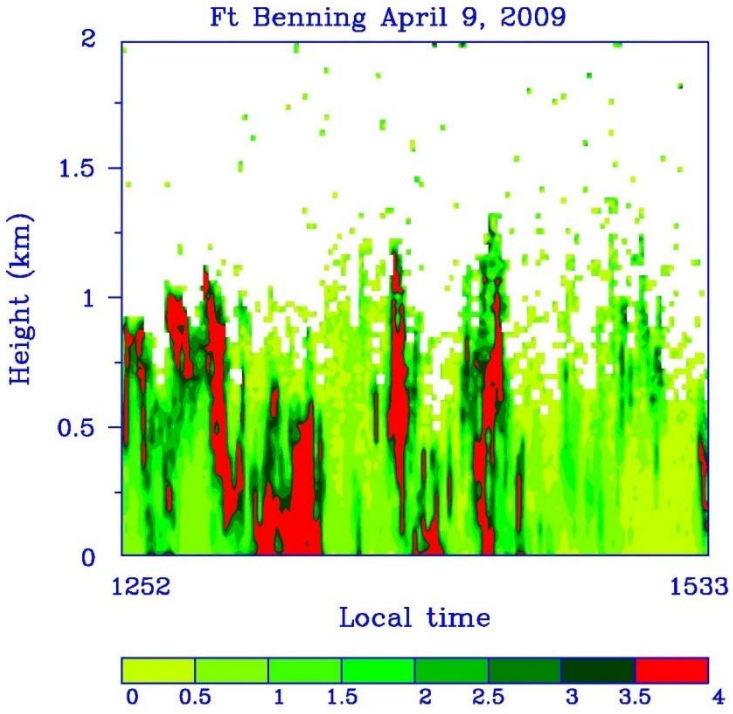

Figure 9. Time-height section of backscattered light of CL31 Ceilometer measurement for the prescribed burn at Ft Benning on April 9, 2009.

During the measurements, the CL31 Ceilometer was mounted in a mobile or on a leveled plate on the ground. The instrument was set up before the start of each burn at a certain distance from a burn in the downwind. The distance ranged between 1 and 5 miles, depending on burn intensity and wind speed. The collected data are vertical distribution and temporal variations of backscatter light intensity. They provide smoke plume properties of plume rise and vertical profile of smoke intensity.

3.3.1.2 Ground-based smoke sampling

Prescribed burns were monitored at Fort Benning using a ground-based real-time measurement technique. Each day, using the burn plan provided by the Fort Benning crew, a grid was laid out on a site map (Figure 10). The grid consisted of a 60 degree arc emanating from the burn compartment and stretching along the predicted wind direction. This arc was divided typically into three sampling zones: Zone 1: 1-3 km; Zone 2: 3-5 km; Zone 3: 5-7 km. A truck was assigned to each zone. Each truck was equipped with two DustTrak $PM_{2.5}$ monitors and two Langan CO monitors at a sampling height of 8 feet. Each truck monitored multiple locations in its zone with a minimum of 30 minutes at each location. Sampling was started at ignition and continued until approximately one hour after completion. Initial sampling locations were on the most direct downwind position from a burn location. Each subsequent position was chosen based on a combination of wind shifts, real-time measurement levels, and road availability. An operator coordinated the movements of the trucks from a fire tower confirming wind shifts and also collected photographical evidence. The truck positions were recorded using Trimble Juno ST GPS units.

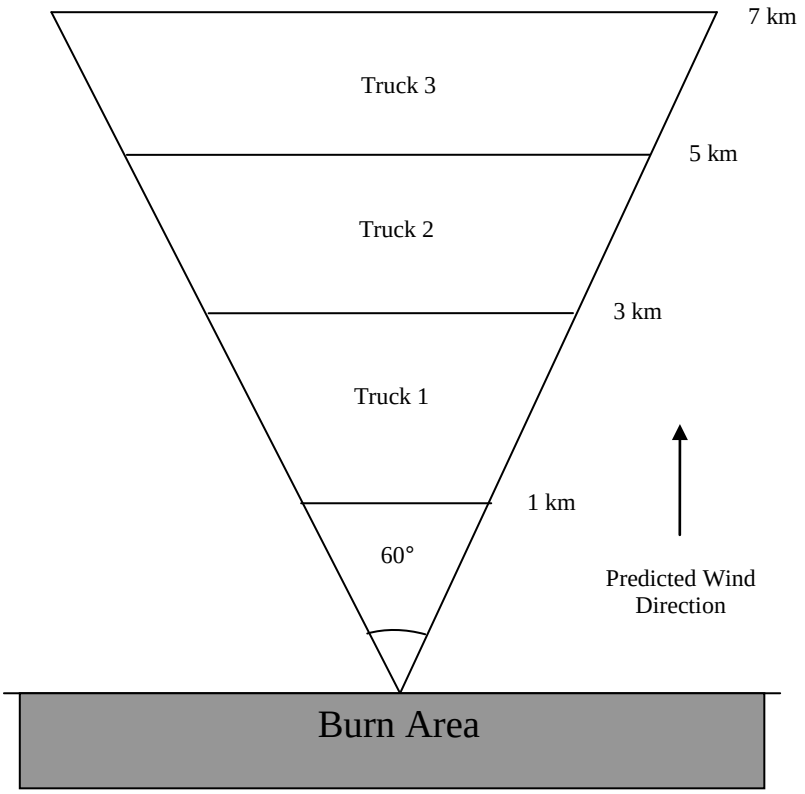

Figure 10. Typical Fort Benning sampling grid.

$PM_{2.5}$ was sampled at 30-second intervals with TSI DustTrak Model 8520 aerosol monitors (DustTrak: range 0.01 mg/m^3 to 100 mg/m^3; resolution 0.01 mg/m^3) with dataloggers (TSI, Minneapolis, MN). CO was sampled at 30-second intervals by two monitors: Langan CO Monitor Model T15v CO monitor (resolution 0.1 ppm) with datalogger (Langan Products, Inc., San Francisco, CA); and PAC III Monitor (resolution 1 ppm) with datalogger (SKC, Inc.). These instruments were calibrated before each round of the study in the Air Quality Lab at the University of Georgia (UGA) and the DustTrak monitors were zero calibrated in the field each day. In addition, all DustTrak monitors were also factory calibrated and serviced annually.

3.3.2 Eglin AFB Field Study

Three burns were monitored at Eglin AFB during the February 5-12, 2011 field study. Previous efforts under this project to evaluate Daysmoke found that emission inputs are critical to Daysmoke performance. While an estimate for the uncertainties in emission factors was established by comparison to laboratory measurements in SERDP project RC-1649 of the fuel collected at Fort Benning, the uncertainties in fuel loads and fuel consumptions remained unknown. As part of Rx-CADRE, the Prescribed Fire Combustion and Atmospheric Research Experiment (Ottmar and Vihnanek, 2009), fuel load and fuel consumption data were collected at Eglin. By conducting the final field study in parallel to Rx-CADRE at Eglin, access was gained to additional data, especially fuel load and fuel consumption measurements. In addition, an

aerostat lofted instrument package was used to collect smoke data above the canopy of the burn plot. These data provided a direct estimate of the actual emissions from the burns. With all these measurements, it was possible to provide more accurate emissions inputs to Daysmoke for a better evaluation of its dispersion modeling performance.

Prior model evaluation cycles also showed that the model predictions were very sensitive to the input wind speeds and directions. The errors in winds predicted by the meteorological models (MM5 and WRF), especially error in wind direction, are believed to significantly affect the plume transport by the Daysmoke model. Therefore, the Eglin field study targeted measurement of the vertical profile of the winds in order to evaluate the impact of the wind direction uncertainties on Daysmoke predictions.

The calibration of real-time instruments used on mobile platforms has been a source of uncertainty in the Fort Benning field study. The calibration factors employed were derived from other studies which may not accurately characterize the smoke conditions of monitored burns. Measurements with stationary but more precise instruments side-by-side with real-time instruments can be useful for deriving burn specific calibration factors. At Eglin, a stationary site was set up to calibrate the instruments used on mobile platforms. This site was set up in the short range (~1 km) and replaced one of the mobile units downwind from the burn unit, which typically required minor movement to capture the smoke plume at Fort Benning.

3.3.2.1 Aerostat based sampling

A 4.3 m diameter tethered aerostat (Kingfisher Model, Aerial Products Inc., USA) was used as an aerial sampling platform. The helium-filled aerostat carried a sampling instrumentation package termed the “Flyer”. The aerostat lofts the Flyer into plumes and is maneuvered by a tether controlled winch attached to an ATV. The aerostat was operated directly at the downwind edge of the burn plots as illustrated in Figure 11.

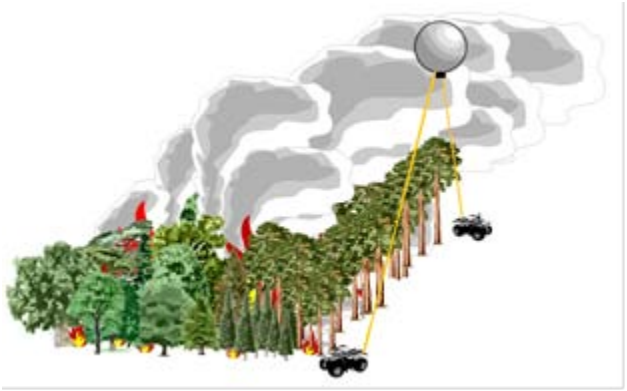

Figure 11. Sampling design to be used by the US EPA aerostat.

The Flyer has an onboard USB based data acquisition (DAQ) card (Measurement Computing USB-2537) controlled by an onboard computer running a LabView generated data acquisition and control program. A ground based computer was used to view data in real time and control the sampling via a wireless remote desktop connection. The computer data was logged at a rate

of 10 Hz. Additionally, in order to avoid dilution of samples the batch samplers are turned on and off by variation of the carbon dioxide (CO_2) concentration in the plume from a set concentration.

The Flyer was equipped for continuous measurement of CO, CO_2, and particle size distribution, and batch sampling of $PM_{2.5}$. The CO_2 is measured with a non-dispersive infrared (NDIR) instrument (LI-820 model, LI-COR Biosciences, USA) at a calibration range set to 0- 4,500 ppm. The LI-820 voltage equivalent CO_2 concentration was recorded on the onboard computer and was three-point calibrated for CO_2 on a daily basis according to U.S. EPA Method 3A (EPA, 2011). Particulate matter was continuously measured and reported in 2-min averages for PM1, PM2.5, PM 7, PM 10 and TSP by use of the MetOne Aerocet Model 531 Laser Particle Counter. The $PM_{2.5}$ was sampled with a constant airflow of 10 L/min (Leland Legacy, SKC Inc., USA) on a 47 mm tared Teflon filter with a pore size of 2.0 µm. The Leland Legacy Sample pump was calibrated with a Gilibrator Air Flow Calibration System (Sensidyne LP, USA).

3.3.2.2 Remotely sensed wind measurements

The plan for Eglin study included remote sensing of the vertical wind profiles. The plan was to use a Doppler sodar to obtain vertical wind profiles in the lowest 500 m of the atmosphere. However, the instrument was damaged during shipment to the site therefore this part of the plan could not be realized. The sodar would have provided wind speed and direction from 100-500 m with 10 m height resolution. The planned method is included here for completeness.

REMTECH Doppler sodar system consists of one sole antenna (phased array type of transducer elements), one computer, one transceiver, one power amplifier, cables and a small mount for the antenna. The system allows for full control of the antenna beams: four of the electronically steered beams are tilted (30° or 15°) from vertical and turned 90° from each other to provide the horizontal component of wind velocity. The last beam is pointed vertically and provides that component of the wind. The system software controls the sequence and rate of operation for each beam.

Linux OS based software provides a signature to the transmitted pulse. The basic coding consists of transmitting 9 (up to 15 optional) frequencies in the pulse. Upon reception, this coded pulse is easily detected from noise and fixed echoes within the backscattered signal. This is particularly useful for turbulence studies since it allows quicker detection for full analysis on the noise spectrum. The frequency transfer function (in phase and amplitude) between the “active antenna” and the “reference antenna” (made of 4 transducers at the 4 antenna corners) allows a very efficient noise subtraction (especially for a fixed noise source such as an air conditioner, an aspirated shield on a meteorological tower close to the sodar). The final acoustic frequency power spectrum can be cleaned by more than 15dB’s decrease of the jamming source in the considered frequency zone.

The Doppler sodar has 52 transducer elements. Its nominal central operating frequency is 3500 Hertz (9 frequencies are emitted on each tilted beam during one “beep”). The size of the antenna is 0.4×0.4 m. Its maximum range is 1,000 m with an average range in typical conditions of 200−600 m.

3.3.2.3 Wind velocity measurements at altitude

The wind velocity aloft was measured by means of a 3D anemometer affixed to the underside of the Flyer (Figure 12).

Figure 12. Aerostat with Flyer and 3D sonic anemometer.

A lofted data acquisition and sampling system (DASS), described previously (Aurell et al., 2011) consists of an onboard PC that controls a Measurement Computing™ USB-2537 data acquisition (DAQ) card via USB using Labview™ generated software. The 16 bit DAQ has 32 differential analog inputs, 24 configurable digital input/output ports, and 4 analog outputs. The sonic anemometer and AHRS were controlled by the onboard computer via RS232 ports. Power is supplied using a 52 V lithium ion polymer rechargeable battery. In addition to wind velocities and motion correction data, the DASS logged CO_2 and PM concentrations in real time and volatile organic compounds and semivolatile organic compound (VOC and SVOC) sampling data. The DASS is lofted by a helium filled 14 ft Kingfisher™ aerostat with a rear sail that keeps the front of the aerostat oriented into the wind. The aerostat remains tethered to an ATV for the duration of the flight. The position of the aerostat sampler is changed by tether length and ATV position. The length of time that the aerostat can remain aloft is primarily determined by battery life which is determined by the number of sampling devices running and their respective power demands. The maximum height of the aerostat is determined by tether length. Currently, it is estimated that a devoted wind sensor could run at an altitude of 500 m for an entire 8 hour day.

An R.M. Young 81000 sonic anemometer measured wind velocity along its 3 internal axes (u, v, and w) with a resolution of 0.01 m/s and an accuracy of ± 1%. These anemometer data were recorded serially using an onboard computer. Wind data presented here were logged serially using the onboard computer. A wireless remote desktop connection to the DASS allowed for real time control and viewing of data. A flexible shaft connected the anemometer to the bottom of the flyer approximately 1.5 m away from bottom of the aerostat. The flexible mount and relatively short distance was chosen to prevent the anemometer from getting tangled in the tether line during turbulent conditions. Visual observation of smoke around the balloon suggests that any boundary layer is much shorter than the distance between the balloon surface and the anemometer. Therefore, the aerostat should not affect the wind measurements by the

anemometer. The orientation of the anemometer was fixed relative to the aerostat and was such that a wind velocity vector with magnitude, *M*, blowing parallel to the aerostat from the front to rear would be recorded as [0,–*M*,0] in the UVW coordinate system (Figure 13). The anemometer zero velocity reading was checked daily by placing a bag over the anemometer for at least 30 seconds.

In order to correct raw wind velocities for aerostat motion, the Xsens MTi-G, a GPS-aided inertial measurement unit with an attitude heading reference system was used. As shown in Figure 13, the MTi-G was mounted directly onto the electronics enclosure of the sonic anemometer. The position, orientation, linear, and angular motion were recorded serially onto the onboard PC using Labview® generated software. MTi-G and anemometer data were logged asynchronously and then aligned in time after acquisition using linear interpolation.

Using the data from the MTi-G, the sonic anemometer data were corrected using the equation

$$\vec{v}_{corr} = \underline{R_{GS}}(\vec{v} - \vec{\Omega} \times \vec{Q}) - \vec{v}_{NWU} \tag{17}$$

Where $\boldsymbol{v_{corr}}$ is the corrected wind velocity data in NWU coordinates, $\boldsymbol{R_{GS}}$ is a unitless rotation matrix such that when multiplied by a vector in the MTi-G's coordinate system, the product is a vector of the same orientation in the global (*i.e.* NWU) coordinate system. The observed 3D wind velocity, $\boldsymbol{v}$, is measured by the sonic anemometer with local coordinates u, v, and w, which are aligned with the local coordinates of the MTi-G. $\boldsymbol{\Omega}$ is the 3D angular velocity measured by the MTi-G in rad/s and **Q** is the vector describing the distance between the MTi-G (XYZ) and the anemometer origin (UVW). The cross product of $\boldsymbol{\Omega}$ and **Q** represents the angular component of the sonic motion. Lastly, $\boldsymbol{v_{NWU}}$ is the linear velocity of the MTi-G and sonic anemometer in NWU coordinates.

Wind velocity data were acquired on 2/08/11 and 2/12/11 at Eglin Air Force Base (Eglin AFB). Wind velocity measurements at Eglin Air Force Base were coincident with a prescribed forest burn and were part of an effort to sample for emissions and predict pollutant dispersion downwind. During this study, a 4.3 m diameter aerostat lofted the sampling array and wind velocity measurements were acquired at 10 Hz.

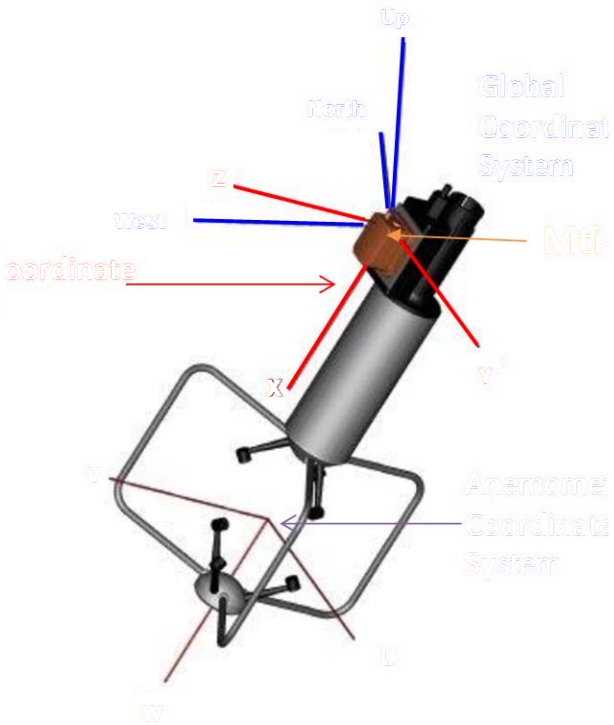

Figure 13. Sonic anemometer/MTi-G schematic.

3.3.2.4 Ground-based smoke sampling

We measured the concentration of several gas- and particle-phase components of the smoke plume downwind of three prescribed burns at Eglin Air Force Base in February 2011. These measurements included both real-time data from continuously-operating devices as well as time-integrated data from particulate filters. For each burn, extensive measurements were made at a stationary site approximately 2 km downwind of the burn sector, while measurements of particle mass were performed at two mobile sites positioned 1-11 km downwind. The stationary site was co-located with US Forest Service Lidar Ceilometer instrument for the measurement of plume heights. The mobile sites consisted of portable, battery-powered devices positioned using 4-wheel drive pickup trucks.

3.3.2.4.1 Stationary site

The stationary sites were established prior to each burn and utilized non-portable instrumentation requiring a source of AC power. This power was supplied by a Honda Model EU3000IS 3000 Watt gasoline generator placed 100' from the instrumentation in the downwind direction. Instruments at the stationary site included a Tapered Element Oscillating Microbalance or TEOM (ThermoScientific) for continuous measurement of the mass concentration of particulate matter smaller than 2.5 µm ($PM_{2.5}$). This device calculates particle mass as a function of the resonant frequency of an oscillating filter element and is a U.S. EPA recognized instrument for measuring $PM_{2.5}$. In addition, the size distribution of particulate matter was measured using a

Scanning Mobility Particle Sizer (SMPS, TSI Inc.). This instrument measures the number concentration and size of particles in the range of 5-600 nm with a time resolution of four minutes.

The concentration of the gas-phase species CO and CO_2 was continuously measured using the ThermoScientific instruments Model 48i and 410i respectively. The 48i measures CO in the range 40 ppb to 10,000 ppm with a resolution of 1 ppb and response time of 60 seconds, while the 410i measures CO_2 in the range 200 ppb to 10,000 ppm with a resolution of 10 ppb and response time of 90 seconds.

In addition to these non-portable instruments, the stationary site also utilized the same portable instrumentation as the mobile sites (described below) and included a meteorology station for continuous measurement of wind speed and direction as well as temperature and relative humidity.

3.3.2.4.2 Mobile sites

Both mobile platforms continuously measured $PM_{2.5}$ mass using an AeroTrak handheld particle counter (TSI Inc., Model 9306) and in addition, collected several particulate filter samples for time-integrated analyses. The AeroTrak measures the light scattered by aerosols as they intercept a laser diode to count the number of particles in six size ranges in real-time. The largest size range was configured to correspond to particles larger than 2.5 µm, and the measured number concentration for each channel was converted to a volume concentration by assuming particles are spherical with diameter equal to the log-midpoint of each channel. The volume concentration of particles smaller than 2.5 µm was converted to a mass concentration using a "synthetic density" factor derived from calibration with the TEOM. This calibration was performed for all three AeroTraks simultaneously by co-locating the instruments with the TEOM at the stationary site. The instruments were operated for 1-2 hours prior to burn ignition, and the mass measurements recorded by the TEOM were compared to the calculated volume values from the AeroTraks to calculate the synthetic density of the particle population. The measurement range of the AeroTrak is 0-70 particles/cm^3 with a resolution of 1 particle/cm3. This measurement range in terms of $PM_{2.5}$ mass is variable depending on particle size and synthetic density, but is generally in the range 0-70 µg/m^3. In addition, the aerosol number concentration was measured using condensation particle counters (CPC), the TSI P-Trak (TSI Inc., Model 8525). This model of CPC is capable of measuring particles in the size range of 20 to 1000 nm in the concentration range of 0-500,000 particles/cm^3 with a resolution of 1 particle/cm^3. Although this instrument does not provide information on particle size, the ambient aerosol number concentration is typically dominated by particles in the ultrafine size mode (< 0.1 µm).

The mass concentration of coarse mode (> 2.5 µm) and fine mode (< 2.5 µm) particles was measured using a 2-stage Harvard Compact Cascade Impactor operated at a flow rate of 30 L/min. The single impaction stage had an aerodynamic cutpoint of 2.5 µm; hence particles collected on the impaction plate were greater than 2.5 µm in aerodynamic diameter while those collected on the after-filter were smaller than 2.5 µm. The impaction filter was a Polyurethane Foam (PUF) substrate while the after filter was a 47 mm Teflon filter. Flow rate spot checks were performed at the beginning and end of each sampling period. Gravimetric measurement of

particle mass were conducted in a controlled-environment clean room facility at Georgia Tech with a temperature of 25°C and relative humidity of 20%. Both Teflon and PUF filters were equilibrated to the clean room environmental conditions for 48 hours prior to weighing, and each filter was weighed three times. The clean room microbalance has a precision of ±5 µg.

Additional time-integrated characterization of $PM_{2.5}$ elemental and organic carbon (EC-OC) content was performed using two parallel filter samples on both mobile platforms. Each sample line was operated at a flow rate of 30 L/min and was equipped with a 2.5 µm cutpoint impactor upstream of the filters to remove coarse-mode particles. One sample line was equipped with a 47 mm Teflon filter followed by a 25 mm quartz fiber filter while the other sample line contained just a quartz fiber filter. Flow rate spot checks were performed at the beginning and end of each sampling period. EC-OC analysis was performed at Georgia Tech using the Thermal-Optical Transmittance (TOT) method. The sampling artifact produced by the adsorption of volatile and semi-volatile organic compounds onto quartz fiber filters was assessed by subtracting the OC content of the quartz filter which follows the Teflon filter from the stand-alone quartz filter. The upstream Teflon filter was used to produce a duplicate gravimetric measurement of $PM_{2.5}$ mass (as described above) as well as an aqueous extract of water-soluble compounds. The extract was produced by immersing the filter in 30 mL of ultrapure water and sonicating in an ultrasonic bath for 20 minutes at a temperature of 30°C. A 20 mL aliquot of this extract was analyzed for water-soluble organic carbon (WSOC) content using a Sievers Model 900 Portable Total Organic Carbon (TOC) analyzer. The ratio of WSOC to EC is useful for parameterizing secondary organic aerosol content. In addition, two separate 200 µL aliquots were analyzed for ion content using a Dionex ICS-2000 ion chromatograph.

3.4 Model Evaluation Methods

The dispersion and chemistry-transport models described in Section 3.2, together with the emissions estimation methods described in Section 3.1 and the weather prediction models MM5 and WRF, constitute a complex modeling system for predicting the downwind air quality impacts of prescribed burns. The system incorporates several new elements into emission, dispersion and transport process components, all with significant potential for improving the accuracy of the predictions. These elements must be verified and evaluated to build confidence in the validity of the modeling system. Determining the uncertainties in emission estimates and meteorological inputs, evaluating the models individually and together using field data from monitored burns and observations from regional networks, and conducting sensitivity analyses have been the three major elements of the model evaluation process. Synthesis of results from uncertainty estimations, model component evaluations, and sensitivity analyses is expected to identify where future research would be most beneficial for increasing the accuracy of the modeling system.

3.4.1 Determining the Uncertainties in Model Inputs

The emission estimates described in Section 3.1 and meteorological parameters from weather prediction models like MM5 and WRF constitute the two major inputs to the dispersion and chemistry transport models described in Section 3.2. Input uncertainties propagate in a model and reflect to the accuracy of its predictions. Therefore, it is important to determine the

uncertainties in the emissions and meteorological inputs and evaluate the predictive skill of a model in view of those uncertainties. Input uncertainties combine with modeling and parametric uncertainties, as well as the uncertainty inherent to atmospheric turbulence, to yield uncertain smoke concentration predictions. Quantifying the range of input uncertainties is a first step towards determining the range of uncertainties in model predictions.

Here, the primary method used for determining the uncertainties in model inputs has been direct comparison of emission estimates and meteorological modeling results to field measurements. As described in Section 3.3.2, data collection at Eglin AFB included measurements of: 1) fuels before and after the burns, 2) emissions with aerostat, and 3) winds with ground-based and airborne instruments. In Section 4.1.4, using the measurements of fuels and emissions, not only the uncertainties in emissions will be determined but they will be linked to major steps involved in emission estimation. Here, the determination of the uncertainties in wind speed and wind direction will be focused.

The meteorology during the week of 6-12 February 2011 was simulated by MM5 and WRF models using nested grid configurations starting with 36-km grid over the contiguous US, followed by 12-km and 4-km grids, and finally a 4/3-km grid over the Eglin AFB. The uncertainties in predicted wind speed and direction were estimated using data available from various sources. Wind data were available from surface weather stations at three airfields in Eglin, a nearby remote automatic weather station (RAWS), a temporary weather station about 3 km downwind from the burn, a pilot balloon launched from a nearby field 3 hours before ignition, UAVs flown at about 100 m altitude over the burn site after the helicopter completed ignition, and a sonic anemometer attached to the aerostat operated at the downwind edge of the burn plot (see Section 0).

Comparisons of wind speed and direction to the balloon soundings on 6 February 2001 will be discussed briefly here; comparisons to data from other sources and for other days can be found in Appendix A. The vertical profiles of model predictions at the location of the launch between 15:00 and 16:00 GMT are compared to temperature, humidity, and wind measurements from the pilot balloon in Figure 14. Note that the sounding balloon may have drifted as much as 400m by the time it reached 1000m altitude.

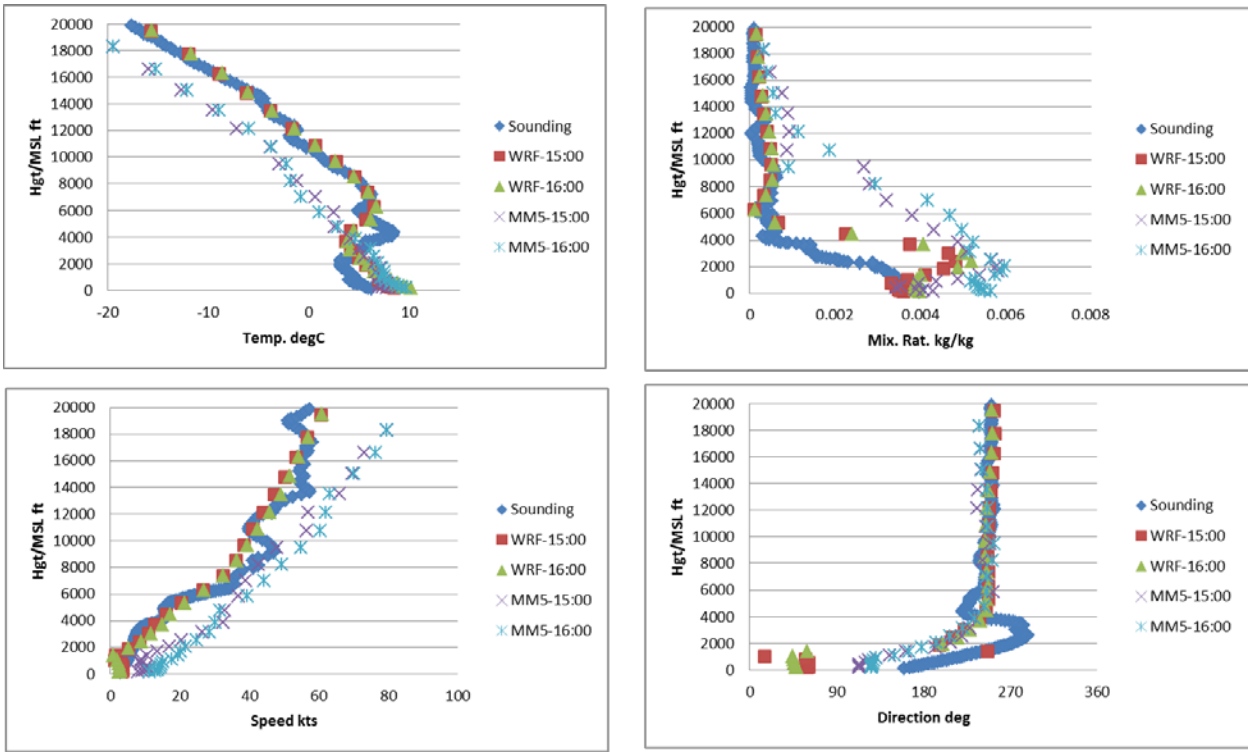

Figure 14. Comparison of MM5 and WRF model predictions with the 6 February 2011 sounding: temperature (top left), humidity (top right), wind speed (bottom left) and wind direction (bottom right).

A large discrepancy in wind direction is evident: while the measured wind direction varies from 140 degrees (southeasterly) at the surface to 270 degrees (westerly) at 2000 ft, predicted wind direction ranges from 60 to 245 degrees (northeasterly to southwesterly) in the WRF model. The reason for this is that WRF still predicts land breeze at 15:00 GMT with return flow at 300 m above ground in layer 7 of the model. In comparison to MM5 predictions, WRF predictions have more vertical structure. WRF-predicted temperature, mixing ratio, and wind speed agree better with observations. Only the surface wind direction predicted by MM5 agrees better with observations.

3.4.2 Evaluating Model Results

Several prescribed burning events have been simulated with the dispersion model, chemistry-transport model, and the coupled modeling system. Components of the system were evaluated individually and together using field data from monitored burns and observations from regional networks. Model predictions were compared to available data as well as to the “base model” predictions in terms of various plume dispersion and air quality parameters. For example, in evaluating the Adaptive Grid CMAQ model, the base model has been the CMAQ model. Improved agreement of predictions with available data indicated success for the newly developed models.

The data used in model evaluations included field measurements described in Section 3.3 and routine observations from regional networks such as the Clean Air Status Trends Network (CASTNet), the Speciated Trends Network (STN), and the Interagency Monitoring of Protected Visual Environments (IMPROVE). These networks are relatively sparse around the study sites and the closest monitors are typically located at 25 km or larger distances. On the other hand, most measurements were within 1-10 km radius of the burn plots.

The two most commonly used metrics in comparisons have been the mean normalized bias (MNB) defined as

$$MNB = \frac{1}{N}\sum_{i}^{N}\left(\frac{C_{obs} - C_{\mathrm{mod}}}{C_{obs}}\right)_i \tag{18}$$

and the mean normalized error (MNE)

$$MNE = \frac{1}{N}\sum_{i}^{N}\left(\frac{\left|C_{obs} - C_{\mathrm{mod}}\right|}{C_{obs}}\right)_i \tag{19}$$

where C_{obs} is a measured or observed value, typically a concentration, and C_{mod} is the corresponding model predicted value, and N is the number of observed-predicted values being paired.

Small values of observed concentrations can lead to a large normalized value that can outweigh the other values in the sum of Equations (18) and (19). To avoid this from occurring, mean fractional bias (MFB)

$$MFB = \frac{1}{N}\sum_{i}^{N}\left(\frac{C_{obs} - C_{\mathrm{mod}}}{\left(C_{obs} + C_{\mathrm{mod}}\right)/2}\right)_i \tag{20}$$

and mean fractional error (MFE) have been used in some instances.

$$MFE = \frac{1}{N}\sum_{i}^{N}\left(\frac{\left|C_{obs} - C_{\mathrm{mod}}\right|}{\left(C_{obs} + C_{\mathrm{mod}}\right)/2}\right)_i \tag{21}$$

Note that the denominator is now the average of the observed and modeled concentrations. Comparisons with other models were typically performed by comparing biases and errors with the biases and errors of those other models.

After initial evaluations, the gaps in data were identified and filled with additional field studies. The models were re-evaluated with the new data. Model evaluations helped to identify weaknesses in the models, which have been revised and/or refined as necessary. These data-collection and model evaluation cycles were iterated two times at Fort Benning and a third time at Eglin AFB.

3.4.3 Analyzing Model Sensitivities

Sensitivity analyses can be used to quantify the responsiveness of modeling results to specific inputs or parameters and provide information about the relative importance of each to select model outputs. Furthermore, sensitivity estimates are essential to enhance model performance and achieve successful simulations. Here, we explore the sensitivities of $PM_{2.5}$ concentrations simulated with CMAQ to the spatial and temporal allocation of fire emissions as well as meteorological inputs.

Sensitivities of CMAQ-modeled concentrations to emission inputs were quantified by calculating the difference between two simulations in which a parameter was perturbed,

$$s_x = \frac{C_{x+\Delta x} - C_{x-\Delta x}}{2\Delta x} \tag{22}$$

where s_x is the first-order sensitivity coefficient of concentration C response to parameter x, and $C_{x+\Delta x}$ and $C_{x-\Delta x}$ are the concentrations resulting from simulations under $+\Delta x$ and $-\Delta x$ perturbations to x. These sensitivity estimates, also known as "brute-force" sensitivities, can be applied to any simulated variable and model parameter or input (Hwang et al., 1997). Note that perturbations that are too small may lead to unreliable sensitivity estimates because of the numerical errors in the simulations leading to $C_{x+\Delta x}$ and $C_{x-\Delta x}$ (Hakami et al., 2004).

Equation (22) provides first-order sensitivity coefficients capable of fully reproducing the exact model response to specific perturbations. The ability of these sensitivity coefficients to replicate response to larger or smaller perturbations is dependent on the response's linearity. Although most atmospheric aerosol-phase processes included in CMAQ are linear, some, such as thermodynamic aerosol interactions, cloud processes, and secondary aerosol formation, are not (Napelenok et al., 2006). For concentrations involving significant nonlinearities, higher-order sensitivity coefficients are required to accurately reproduce model response across a broad range of perturbations. Similar to first-order brute-force sensitivity approximations, higher-order sensitivity coefficients can also be estimated using finite differencing methods. Extending on equation 1, second-order sensitivity coefficients can be approximated from three simulations as

$$s_x^2 = \frac{C_{x+\Delta x} - 2C_x + C_{x-\Delta x}}{\Delta x^2} \tag{23}$$

where s_x^2 is the second-order sensitivity coefficient and base-case concentration C_x is included.

The analyses of $PM_{2.5}$ concentration sensitivity to fire emissions conducted here focus on primary carbonaceous emissions. While secondary formation may contribute to fire-related $PM_{2.5}$ impacts, these impacts can be mostly attributed to primary fine particle emissions. For many primary pollutants, the response of atmospheric concentrations to emissions perturbations can be expected to be mostly linear (Cohan et al., 2005). Previous sensitivity analyses have in fact shown a nearly linear source-receptor relationship for primary emissions (Koo et al., 2009). Furthermore, although fire-related $PM_{2.5}$ impacts may not be entirely linear, treatment of fire emissions in air quality modeling applications typically is. Limited information about fire-

associated emission of secondary aerosol precursors and non-linear atmospheric transformations affecting fire-related particle pollution generally constrains smoke simulations to primary sources and linear response. The adequacy of linear extrapolation for this study will be demonstrated in Section 4.4.3.3.3.1.

4 Results and Discussion

The results will be highlighted and discussed under five sections: 1) Emissions estimation, 2) Model development, 3) Field Measurements, 4) Model evaluation, and 5) Simulations of alternative burning strategies.

4.1 Emissions Estimation

The estimation of emissions will be discussed in four parts: 1) estimation of fuel loads, 2) estimation of emissions, 3) fuel collection for laboratory analysis, and 4) uncertainties in emission estimates.

4.1.1 Fuel Loading Estimation

A subset of the burn plots at Fort Benning was surveyed and the fuel loads were estimated using the photo-series method as described in Section 3.1.1. A model was prepared for estimating the fuel loads on any of Fort Benning's burn units. The fuels at Fort Benning are quite uniform as they are burned so regularly. The main factors determining fuel loading are (1) time since last burn and (2) the underlying soil type (clay versus sand hill). The clay sites are far more productive than the sand sites and therefore have higher fuel loads for a given time since last burn. Figure 15 depicts typical conditions for 1, 2, 3 and 5 year burn intervals on sandy soil sites.

Figure 15. Typical fuel conditions for 1, 2, 3, and 5 year burn intervals (clockwise from upper left) at Fort Benning.

The photo series method produced reasonable fuel loading estimates for the Fort Benning sites. The fuel loading by fuel bed component as a function of time since last burn is shown in Figure 16 for sandy soil sites. The values used in this chart are given in Table 3 for the benefit of future modeling efforts. Fuel loading increases rapidly with each year since last burn as the longer time period allows shrubs to become a significant part of the fuel bed. Fuel loads begin to show asymptotic behavior by five years as the fuel bed begins to reach a balanced state.

Table 3. The fuel loading profiles as a function of age at sandy Fort Benning sites.

Age	Canopy	Shrub	Grass	Woody	Litter	Bdcast	Piles	Duff
1 yr	0	0.90	0.47	0.60	0.71	0	0	0.98
2 yr	0	1.05	0.49	2.93	2.60	0	0	1.06
3 yr	0	2.47	0.20	3.13	3.17	0	0	2.08
5 yr	0	2.75	0.23	4.01	2.66	0	0	2.55

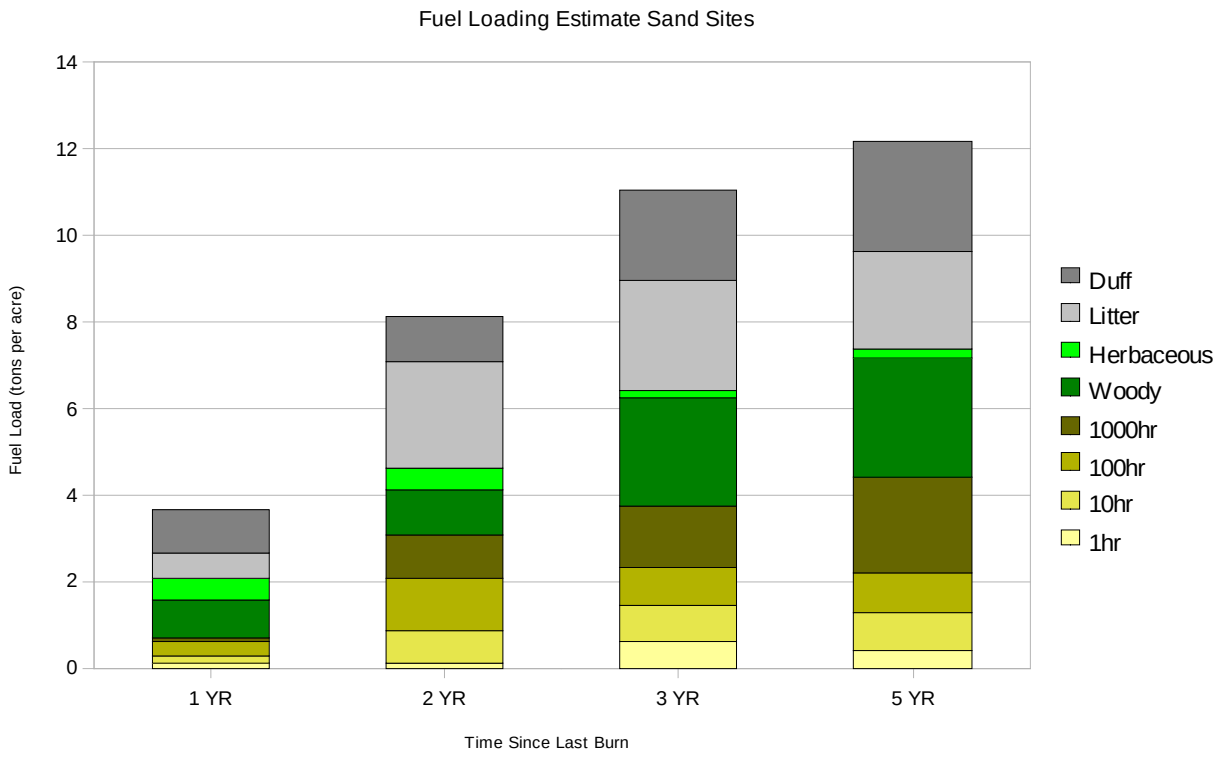

Figure 16. Fuel load by fuel bed component for sandy soil sites at Fort Benning.

Estimating fuel loadings using the digital photo series is the first component of the fuels model being developed. The next component will examine stand data from the sites already analyzed so that a dynamic fuel bed model can be built for Fort Benning that can predict fuel loads based on stand and soil parameters. This component will provide information on the loading of each fuel bed component as well as a crosswalk to FCCS fuel classification system. The development of this dynamic fuel model component was left for future research.

4.1.2 Emissions Estimation

The fuel load estimates reported in Section 4.1.1 were used to estimate the emissions for all the burns at Fort Benning. Digital photographs taken at Eglin AFB right before the burns were used in the method described in Section 3.1.1 to estimate the fuel loads of Eglin sites. The most appropriate fuel loading profile for the time since last burn of each burn unit was input to CONSUME, which yields total emissions based on fuel consumption, and then to FEPS for time varying emissions as described in Section 3.1.2. Both of these models have several parameters that must be set by the user.

A sensitivity analysis was conducted to determine the most important parameters of these models (Figure 17). It was found that the emissions estimates are most sensitive to the selection of fuel moisture, involvement in flaming phase, and duration of ignition were found to be the most sensitive parameters. The likely ranges of these parameters were tested to determine the level of

uncertainty in emission predictions. The uncertainties that were identified in this manner will later be used in estimating the uncertainties in downwind concentration predictions by the dispersion models.

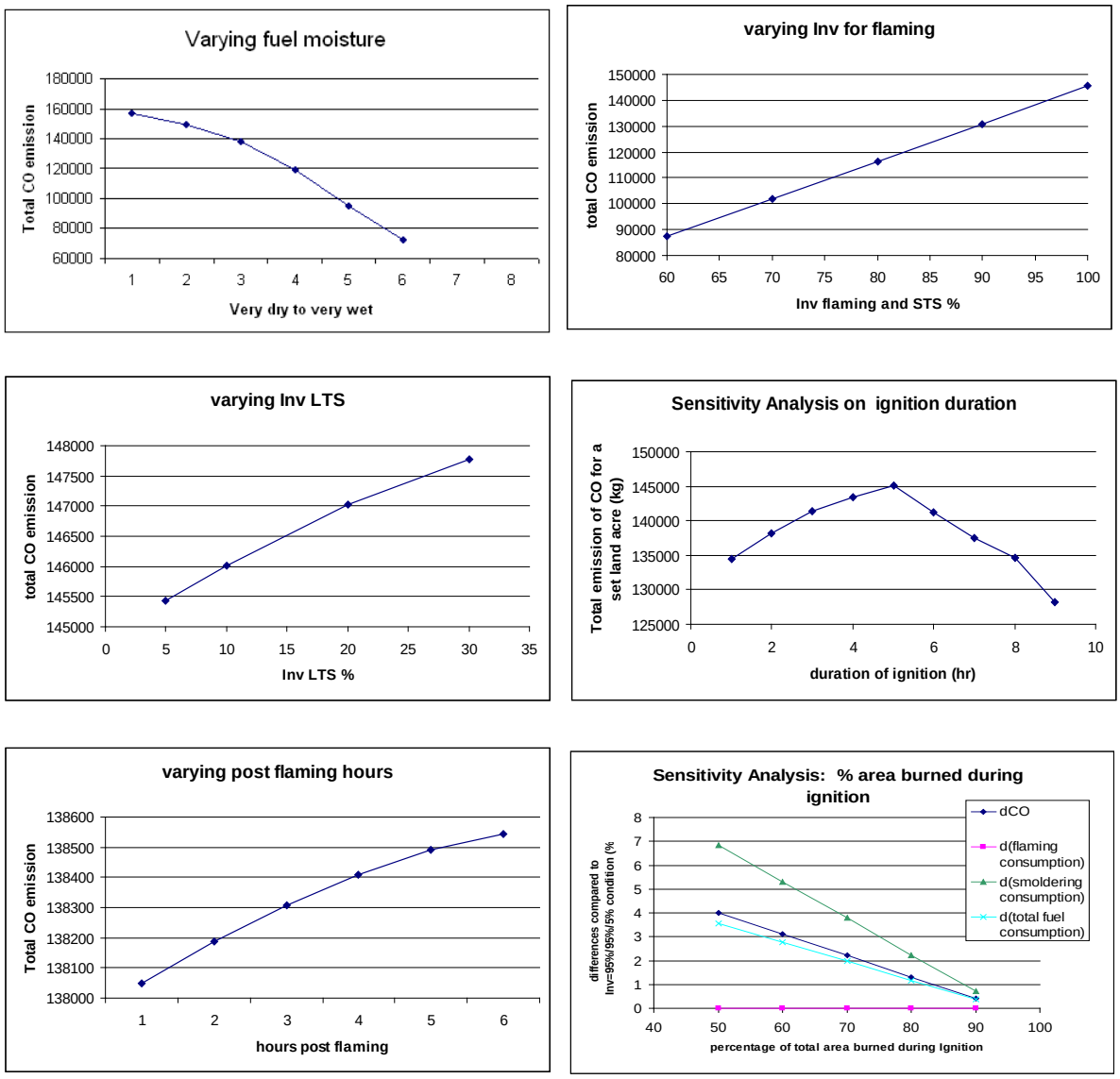

Figure 17. Sensitivity of CO emission estimates by FEPS to various model parameters: a) Fuel moisture, b) Involvement for flaming phase, c) Involvement for long-term smoldering, d) Ignition duration, e) Post flaming duration, and f) Area burned during ignition.

The sensitivity analysis has shown that one of the most important parameters in FEPS is fuel moisture. Most of the burns were conducted under moderate fuel moisture conditions. Another important parameter is involvement in the flaming phase. The long-term smoldering consumptions are generally very low at Fort Benning as most sites have very little of the fuels that would fall into this category. The hourly emission profiles depend on the cumulative acreage burned up to that point. Typically, 80 to 90% of the area is burned by the time ignition is

completed and the remainder usually burns over the next couple of hours. The amounts of fuels consumed in flaming, short-term smoldering, and long-term smoldering phases according to FEPS were used in conjunction with the emissions factors in Table 1 to calculate emissions for different species.

Hourly $PM_{2.5}$ emissions for two of the burns that will be analyzed later in this report are presented here. The first burn was conducted at burn unit F5 on April 9, 2008 (Table 4). The second burn was conducted at burn unit A9 on January 15, 2009 (Table 5). The data in these tables are the emissions inputs to Daysmoke. Emissions for the other burns and chemical species other than $PM_{2.5}$ can be found in Appendix A.

Table 4. Hourly $PM_{2.5}$ emissions estimated for the burn at Unit F5 of Fort Benning on April 9, 2008. This unit, centered at 32.3515° North and 84.6795° West, has an area of 1.2 km^2.

Hour (UTC)	Fire Diameter (m)	Emissions (kg)
1100	0	0
1200	53.2	6128.023
1300	56.6	6626.102
1400	19.4	498.0795
1500	19.4	498.0795
1600	2.6	9.2928
1700	0.4	0.1702
1800	0	0.0031

Table 5. Hourly $PM_{2.5}$ emissions estimated for the burn at Unit A9 of Fort Benning on January 15, 2009. This unit, centered at 32.3230° North and 84.8524° West, has an area of 2.4 km^2.

Hour (UTC)	Fire Diameter (m)	Emissions (kg)
1700	0	0
1800	41.6	10354.58
1900	43.3	10961.08
2000	43.5	11043.16
2100	12.9	688.5792
2200	12.9	688.5792
2300	4.8	94.9277
2400	1.8	12.8471
2500	0.6	1.7386
2600	0.2	0.2353
2700	0.1	0.0318
2800	0	0.0043

4.1.3 Collection of Fort Benning Samples for Laboratory Analysis

Fuel samples were collected using 1-square-meter areas from a Fort Benning plot (Burn Unit I3) that was burned on January 23, 2009. This plot was previously burned on 9 March 2006; therefore, it was assumed to have 3-year old fuels for the purposes of fuel load estimation. The samples were collected at 5 different locations of this 455-acre plot: (1) Planted slash mixed longleaf pine, 44 years old; (2) Shortleaf pine, 70 years old; (3) Planted loblolly pine, 20 years old; (4) Loblolly pine, 68 years old; and (5) Planted longleaf, 4 years old. The samples were shipped to the Fire Science Laboratory in Missoula, MT for measurement and analysis.

The results of the laboratory analysis on Fort Benning fuel samples were published in Burling et al. (2010). The emission factors measured in the Fire Sciences Laboratory (marked SMRFS) were compared to existing sets, namely the US Forest Service southeastern fuels set used here (Urbanski et al., 2009), a set from an earlier Georgia Tech study at Fort Benning (marked Baumann), and the EPA AP-42 set (Figure 18). It should be noted that a logarithmic scale is used in Figure 18 for emission factors. In general, there is good agreement between the flaming phase emissions factors used here (marked Urbanski) and the laboratory measurements (marked SMRFS), for which there is no phase distinction.

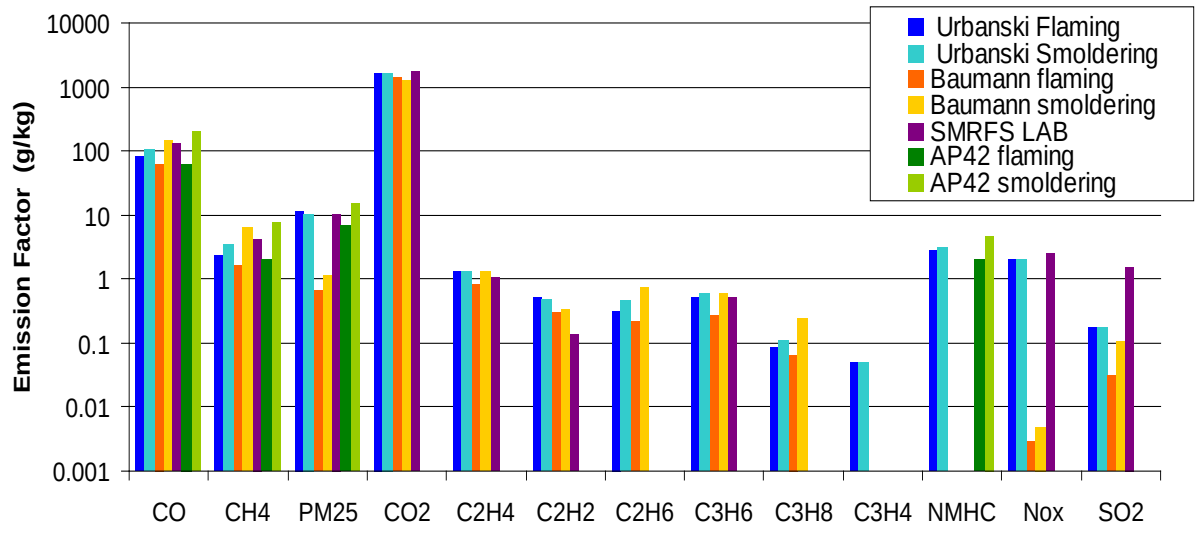

Figure 18. Comparison of emission factors for burn units at Fort Benning.

The values of the emission factors for flaming and smoldering phases are listed in Table 6 and Table 7, respectively. The US Forest Service southeastern emission factors for the flaming phase are generally in closest agreement with the laboratory measurements. This increases confidence in the emission factors used in estimating emissions.

Table 6. Comparison of flaming emissions factors (in g/kg).

	AP42	Baumann	Urbanski	SMRFS
CO	63.0	63.7	82.0	128.6
CH4	2.00	1.63	2.32	4.25
PM25	6.70	0.66	11.50	10.30
CO2		1437	1664	1710
C2H4		0.8400	1.300	1.048
C2H2		0.2986	0.500	0.138
C2H6		0.2179	0.320	
C3H6		0.2664	0.510	0.500
C3H8		0.0635	0.086	
C3H4			0.050	
NMHC	2.00		2.770	
NOx		0.0029	2.000	2.468
SO2		0.0312	0.175	1.547

Table 7. Comparison of smoldering emissions factors (in g/kg).

	AP42	Baumann	Urbanski
CO	205	149.28	106
CH4	7.4	6.49	3.42
PM25	14.7	1.1453	10.5
CO2		1247.68	1649
C2H4		1.357	1.3
C2H2		0.3277	0.48
C2H6		0.7387	0.46
C3H6		0.584	0.59
C3H8		0.2476	0.11
C3H4			0.05
NMHC	4.6		3
NOx		0.005	2
SO2		0.1035	0.175

4.1.4 Uncertainties in Emissions Estimation

Emission inputs are critical to the performance of a smoke dispersion model like Daysmoke; therefore, one of the objectives is to provide accurate emissions inputs to dispersion models. The uncertainty in emission factors has been addressed in Section 4.1.3 by comparing the emission factors used to those measured in a laboratory, but this is not sufficient. The simulated burns in a

laboratory do not exactly reflect the field conditions. Further, the uncertainties in fuel loads and fuel consumptions are still unknown at this point. Recall that the emission estimates here rely on a photo-series based approach for estimating fuel loads and a model (CONSUME) for fuel consumptions. Participation in the Prescribed Fire Combustion and Atmospheric Dynamics Research Experiment (Rx-CADRE) conducted at Eglin Air Force Base near Niceville, Florida between 4-12 February 2011 provided a unique opportunity to evaluate the uncertainties in emissions and their impacts on smoke dispersion predictions.

As part of Rx-CADRE, fuel loading and fuel consumption field data were collected (Ottmar and Vihnanek, 2009). During this study, each fuel bed type in a burn unit was sampled before and after the burn for fuels, which include trees, shrubs, grasses, small woody fuels, and litter. This provided an opportunity to compare the fuel loads estimated by the photo-series method and consumptions estimated by CONSUME to actual field data for an assessment of the uncertainties in those estimates. Further, conducting aerostat-based emissions sampling at Eglin AFB, during Rx-CADRE enabled another evaluation of the uncertainties in emission factors used, this time with field data. Finally, the uncertainties in emissions estimates being input to the dispersion models could be deduced from the uncertainties in fuel loads, fuel consumptions and emission factors. Simultaneous ground-based downwind smoke sampling at Eglin also provided an opportunity to evaluate the impacts of emissions uncertainties on dispersion predictions, as will be discussed later in Section 4.4.3.2.2.2.

Three burns were monitored during Rx-CADRE; here we will focus on the one conducted on February 8, 2011. Burn unit 608A of Eglin AFB, a 2050 acre plot filled with long leaf pines, oaks, and palmettos last burned on February 27, 2009, was ignited by helicopter (i.e., aerial ignition) at 18:00 GMT (12:00 local). A total of 6000 self-igniting balls were dropped from the helicopter, which followed a stripe pattern perpendicular to wind direction starting from the downwind edge of the plot, approximately every second. The helicopter ran out of self-igniting balls and went to reload at 18:50 GMT, returned at 19:20 GMT and completed ignition by 20:00 GMT. The burn continued until 20:20 GMT.

Direct comparison of the measured fuel loads to those estimated by using photo series provided examples of the uncertainty levels introduced by the photo series approach. Similarly, comparison of the consumption estimated by CONSUME to the amount of fuels consumed based on the difference of pre- and post-burn amounts provided examples of the uncertainty in the consumption estimates. Finally, by comparing emissions measured using the tethered aerostat to the emissions per unit mass of fuel consumed from laboratory and other field studies, one can also estimate the uncertainty in emission factors. The uncertainties in fuel load, fuel consumption, and emission factors constitute the major sources of uncertainty in fire emissions. By propagating the emission uncertainties in dispersion models, their impact on dispersion predictions can be assessed. Emission uncertainties combine with modeling and parametric uncertainties, as well as uncertainties in meteorological inputs, to yield the uncertain dispersion predictions.

The emissions calculated using the fuel load and fuel consumption measurements along with the measured emission factors will be used as the nominal value in this study. These emissions will be input to Daysmoke, which is a plume dispersion model that calculates three-dimensional

downwind smoke concentrations as a function of time. Then, the nominal emissions will be perturbed by the amounts of uncertainties attributed to the use of photo series for fuel load, CONSUME 3.0 model for fuel consumption, and emission factors from different sources. Eventually, spatial and temporal smoke distributions obtained by perturbing emission inputs will be compared to the base distributions that the nominal emissions yielded. The differences will be evaluated relative to the measured smoke dispersion parameters such as plume height and downwind smoke concentrations.

Prescribed burning is a necessary activity in the Southeastern U.S. but the resulting emissions can contribute to exceedances of air quality standards. In a dynamic management environment, decisions have to be made to moderate the potential impacts on air quality from PB, and to obviate the air quality constraints that limit PB. Knowing the uncertainties in emissions and how these uncertainties will impact smoke predictions is critical for effective decision making. Presumptively, predictions with known uncertainties should lead to fewer exceedances of air quality standards and subsequent benefits to human health and welfare, and allow more acreage to be treated by fire and more frequently, thereby improving ecosystem health and wildlife habitat, and decrease the risk of wildfires.

4.1.4.1 Uncertainties in estimated fuel loads

Fuel loadings were measured prior to and after the burning of Unit 608A at Eglin for the fuel types shown in Table 8. Fuel moistures were also measured before the burn for different fuel types.

Table 8. Fuel types measured at Eglin AFB during Rx-CADRE in February 2011.

Shrub	live and dead palmetto, woody shrub, yucca, turkey oak
Grass	wiregrass, other grass, live and dead forbs
Woody	1hr, 10 hr, 100 hr, and 1000 hr woody fuels*
Litter	litter

* The moisture in dead fuels tends to equilibrate with the moisture in ambient air. Dead fuels are classified according to the time it takes to reach equilibrium as 1-hour, 10-hour, 100-hour, or 1000-hour fuels. 1-hour fuels reach moisture equilibrium with ambient air in one hour, 10-hour fuels in 10 hours and so on. Typically, 1-hour fuels are less than 1/4 inch in diameter, and 10-hour, 100-hour, and 1000-hour fuels are respectively 1/4 to 1 inch, 1 to 3 inches, and 3-8 inches in diameter.

Figure 19 compares the estimated fuel loads to the measurements. The hardwood litter category consist of live and dead palmetto, woody shrub, yucca, and turkey oak Conifer litter was estimated well probably since it is more uniform throughout the burn site than any other plant species. On the other hand, hardwood litter and duff were overestimated; only 100-hour fuels were underestimated by the photo-series method. Overall fuel total was overestimated by 20% compared to the measured value.

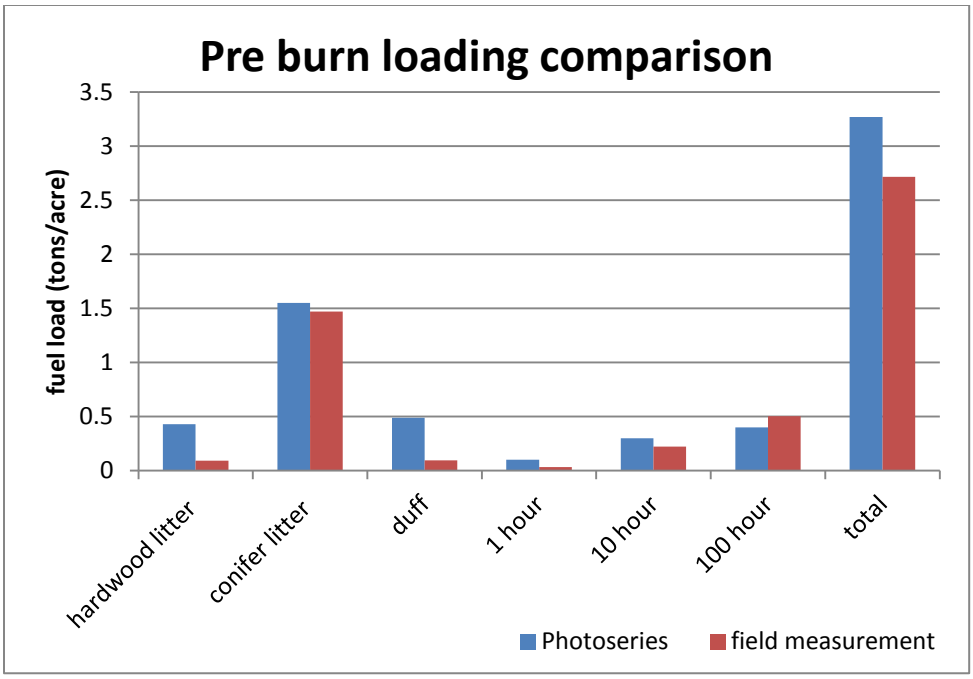

Figure 19. Comparison of photo-series estimated fuel loadings to fuel measurements for Eglin burn unit 608A approximately two years after last burn.

4.1.4.2 Uncertainties in modeled fuel consumptions

Both estimated and measured fuel loads were used to model consumption with CONSUME. Fuelbed 185, long leaf pine-turkey oak with prescribed fire, was taken as the base profile, and then the default fuel loads for each vegetation type were adjusted to match the estimated or measured fuel loads. Since data were not available to set all the parameters of CONSUME it was assumed that: 1) canopy consumption is zero, 2) duff moisture is 70% while 100-hr fuel moisture is 40%, 3) 80% of shrubs are live, and 4) litter is 1 inch deep and covers 70% of the ground.

Figure 20 compares the consumptions for different fuel types obtained from CONSUME, both with measured and estimated fuel load inputs, to “measured consumptions” which are calculated by taking the difference between the the fuel loads measured before and after the burn. The consumption values used in preparing Figure 20 are given in Table 9 for potential use in future modeling efforts. The total consumption is the sum of consumptions for all fuel types except duff.

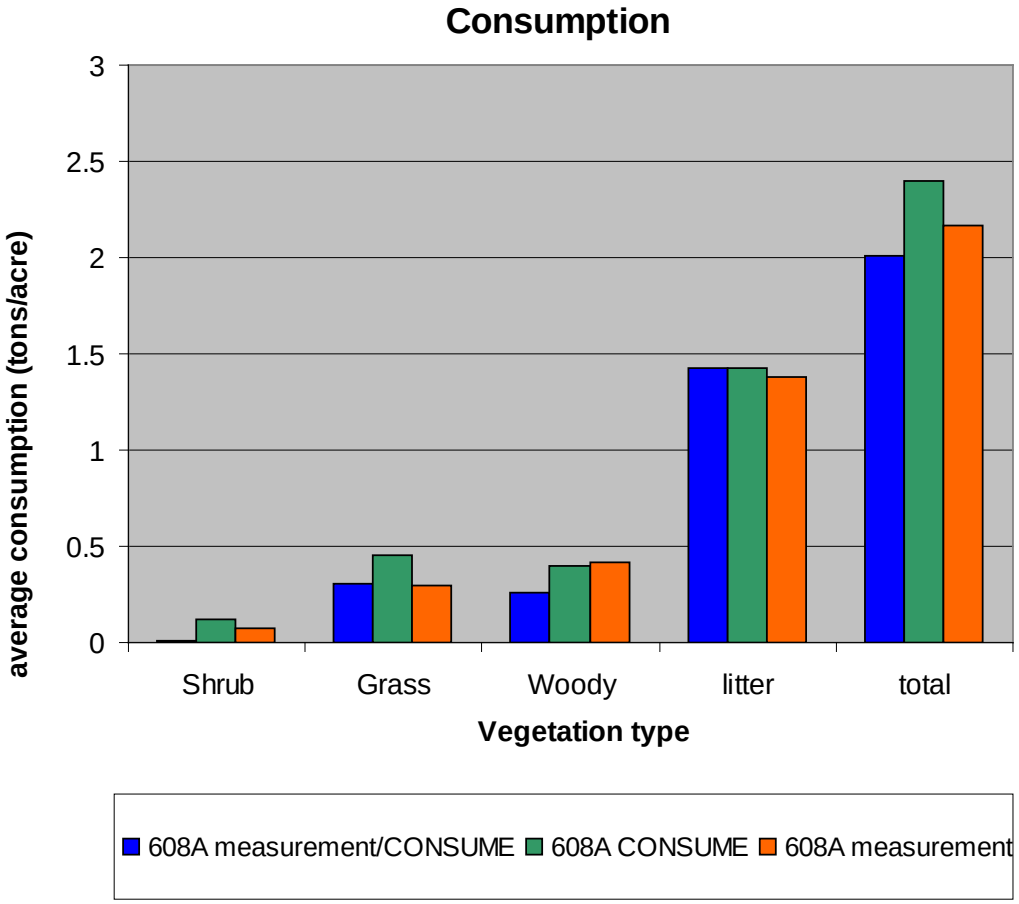

Figure 20. Comparison of CONSUME results with measured and estimated fuel load inputs to the difference in fuels measured at Eglin burn unit 608A before and after the burn on February 8, 2011.

Table 9. Modeled and measured consumptions for Eglin unit 608A burned on February 8, 2011.

Consumption (tons/acre)	Shrub	Grass	Woody	Litter	Duff	Total
Modeled (with measured fuel loads)	0.01	0.31	0.26	1.43	0.44	2.01
Modeled (with estimated fuel loads)	0.12	0.45	0.40	1.43	0.30	2.40
Measured	0.07	0.30	0.42	1.38	0.00	2.16

Total fuel consumption estimated by inputting measured fuel loads to CONSUME resulted in 7% underestimation of consumption (difference between pre- and post-burn fuel load measurements). This is primarily due to underestimation of shrub and woody fuel consumptions. Model predictions of grass and litter consumptions are in good agreement with the measurements. Then fuel loads estimated by the photo-series method were input to CONSUME, total consumption was overestimated by 11%. This is due to overestimating shrub and grass fuel consumptions. Recall that the load for the hardwood litter fuel category, which includes shrubs, was overestimated (Figure 19); this is the main reason for the overestimation of consumption. Also recall that the estimated total fuel load was 20% higher than the measured total fuel load; this resulted in an 18% difference between the consumptions calculated by CONSUME.

4.1.4.3 Emission factors calculated from aerostat based sampling

Emission factors were determined by the ratio of the co-sampled target analytes and the sampled carbon species (Table 10). With knowledge of the fuel carbon content (a carbon fraction of 0.52 was derived from analyses of collected biomass), this allows calculation of the analyte concentration per mass of fuel burned. In this work, the carbon species measurement relied solely on CO_2 measurements. CO was sampled but was always non-detectable as the response time of the chemical cell was too slow to pick up the rapidly fluctuating CO. Other carbon species, such as hydrocarbons, were not measured and were deemed to have little influence on the calculated emission factor.

Table 10. $PM_{2.5}$ Emission Factors derived from Aerostat measurements.

Date	Media Sampled	EF $PM_{2.5}$ by filter g/kg Carbon burned	EF $PM_{2.5}$ by filter g/kg biomass burned
02/06/2011*	Aerostat plume		
02/08/2011	Aerostat plume	28	14
02/12/2011	Aerostat plume	24	13

* No emissions were collected on 02/06/2011.

4.1.4.4 Uncertainties in emission factors used

The emission factors published in the literature (Arakawa, 2004; Burling et al., 2010; EPA, 1996; Urbanski et al., 2009; US-EPA, 1996) are compared to $PM_{2.5}$ emission factor calculated from aerostat measurements during the prescribed burning of Eglin unit 608A on February 8, 2011

(Figure 21). As in Section 4.1.3 the EFs marked SMRFS are those derived from laboratory measurements with fuels collected at Fort Benning.

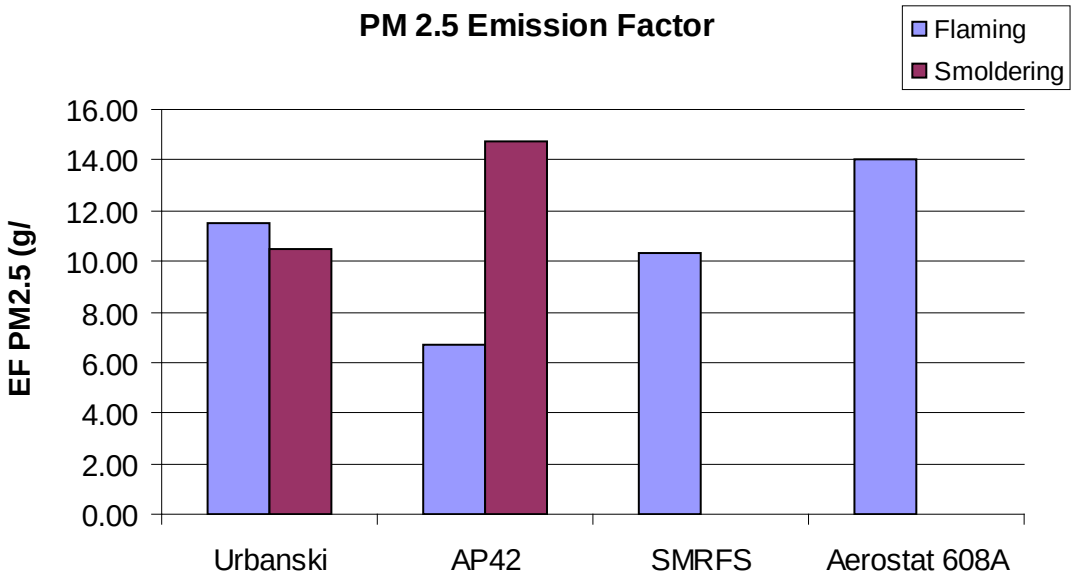

Figure 21. Comparison of various $PM_{2.5}$ emission factors to that derived from Aerostat measurements during the prescribed burning of Unit 608A at Eglin AFB on February 8, 2011.

4.1.4.5 Uncertainties in emissions estimates

A $PM_{2.5}$ emission estimate was obtained by multiplying the total fuel consumption estimate, which resulted from inputting the photo-series based fuel load estimates to CONSUME 3.0 model, by the US Forest Service southeastern fuels emission factor for $PM_{2.5}$ (Urbanski et al., 2009). This emission estimate (marked "Modeled") is compared to the emissions measured by Aerostat at Eglin AFB Unit 608 on February 8, 2011 in Figure 22. In this case, $PM_{2.5}$ emissions are underestimated by 15%. The reasons for this underestimation may be fire induced emissions from the canopy (Alessio et al., 2004) and secondary organic aerosol formation. Both of these factors may have influenced Aerostat-based measurements but they are not considered in traditional emission factors.

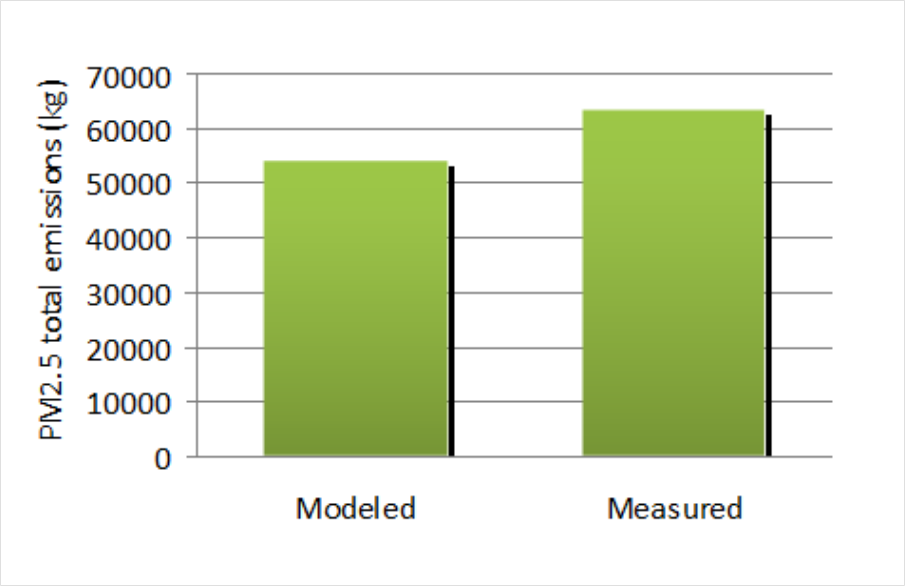

Figure 22. Comparison of total $PM_{2.5}$ emissions estimate (modeled) to the emissions measured by Aerostat at Eglin AFB Unit 608 on February 8, 2011.

4.2 Model Development

This section describes the achievement related to the model development activities. It starts with the incorporation of the adaptive grid technology in the impact prediction system. Not only an adaptive grid algorithm was implemented in the chemistry-transport model, it was also experimented with in the mesoscale meteorological model MM5. The section continues with detailed descriptions of the modifications made to the dispersion model Daysmoke and chemistry-transport models CMAQ and AG-CMAQ. The section ends with a description of the coupling of Daysmoke with the chemistry-transport models.

4.2.1 Incorporation of the Adaptive Grid Method in the Modeling System

One of the objectives was to use the adaptive grid methodology in the smoke impact prediction system. The method was developed for long-range transport and chemistry, and considered for meteorological modeling.

4.2.1.1 Adaptive Grid CMAQ

The incorporation of the Dynamic Solution Adaptive Grid Algorithm (DSAGA) in CMAQ started using not the most current version available at the time (Version 4.6) but Version 4.5 since the direct sensitivity analysis method (Decoupled Direct Method or DDM) that was planned to be employed for determining the air quality impacts of the burns was previously incorporated into this version. The next step was to transfer the variable time step (VARTSTEP) algorithm originally developed in Version 4.3 to Version 4.5. CMAQ advances all the grid cells with the same time step. With a non-uniform grid, this time step would be dictated by the

smallest grid cell. Advancing all the cells with the same short time step is inefficient because scale considerations allow for longer time steps in larger grid cells. Eventually, VARTSTEP has been an important supplement to the adaptive grid CMAQ by significantly increasing its computational efficiency. Later, both algorithms (VARTSTEP and DSAGA) were transferred to CMAQ Version 4.7.1 but the code has not been verified rigorously. In February 2012 CMAQ 5.0 was released but this version is so different in structure from previous versions that a transfer was not attempted as of June 2012.

During the incorporation of VARTSTEP in Version 4.5 of CMAQ, robust verification procedures were employed. For example, the use of the rotating cone test helped improve the accuracy of the algorithm. In this test, a cone-shaped puff is released into a rotational wind field and its evolution is tracked. Ideally the shape of the puff should remain intact but deformations occur due to numerical errors. Figure 23 shows the slightly distorted shape of the puff after one full rotation. VARTSTEP uses larger time steps near the center due to smaller wind speeds there but in the one-time-step-everywhere case, the larger wind speeds near the outer edges determine the time step. Because of the difference in time steps, a different solution is expected from VARTSTEP but this difference is almost invisible to the naked eye (compare left and right panels in Figure 23). The improvement in computational performance due to the use of the VARTSTEP algorithm and the changes in CMAQ's ozone and $PM_{2.5}$ predictions are documented in Odman and Hu (2010).

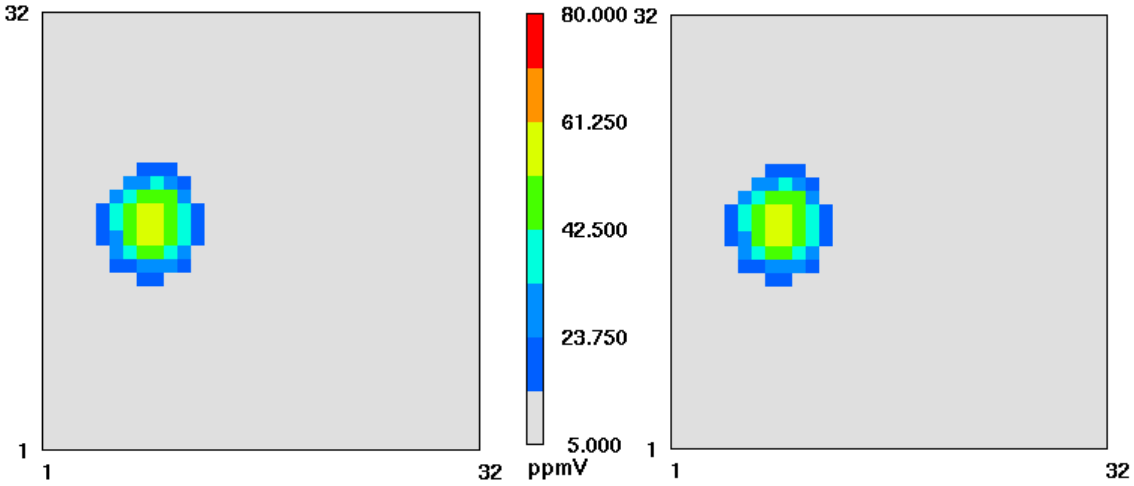

Figure 23. Rotating cone test results with fixed (left) and variable time steps (right).

The incorporation of DSAGA (Srivastava et al., 2000) in CMAQ required substantial modification of the CMAQ code. This included modifications to the main program, the emission/vertical diffusion/dry-deposition module, horizontal advection module, horizontal diffusion module, vertical advection module, gas-phase chemistry module, aerosol module, and cloud dynamics/chemistry module. The resulting code was named Adaptive Grid CMAQ (AG-CMAQ) to emphasize its adaptive grid capability and to distinguish it from CMAQ that employs a static grid. Since the modifications were extensive, rigorous code verification was necessary.

The goal of the first test was to see if the AG-CMAQ code in a "non-adapting" form can match the results of standard CMAQ code. Adaptation of the grid was suppressed by forcing the weight function, which is the driver of grid adaptations, to be and remain uniform, thereby resulting in a fixed, uniform grid. During this test, several mistakes were discovered in the AG- CMAQ code; they were corrected. The differences in the results of the two codes were reconciled with the exception of some small (less than 0.1 μg m^{-3}) differences in the concentrations of aerosol nitrates and secondary organic aerosols of biogenic origin (Figure 24). Those differences were tracked to the aerosol module. Further analysis showed that the differences resulted from lack of stability in CMAQ's treatment of aerosol equilibrium. The problem was reported to the developers of the aerosol module. Since the differences were small and their impact on smoke predictions is expected to be negligible, it was concluded that AG-CMAQ code is able to repeat CMAQ results when its grid is not adapting.

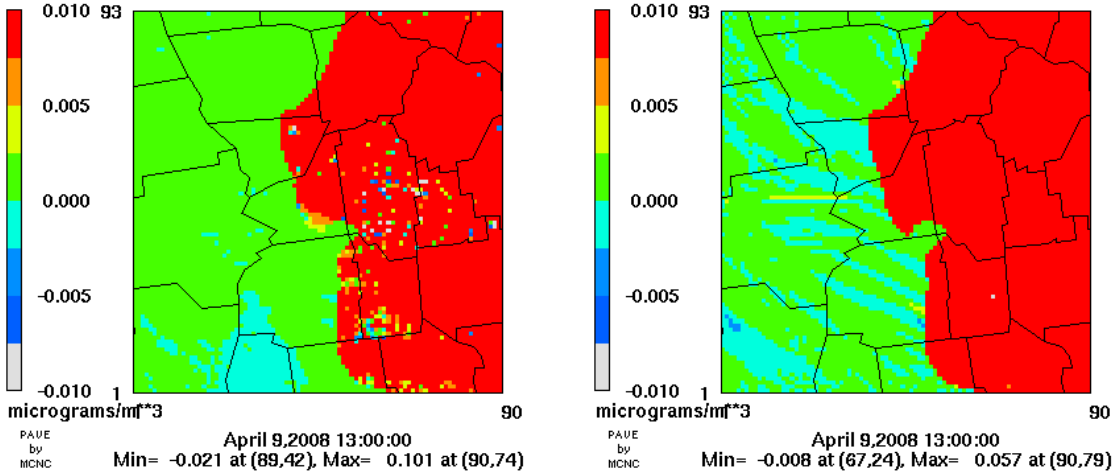

Figure 24. Difference (adaptive minus standard) in nitrate (left) and biogenic organic aerosol (right) when only transport and aerosol modules are turned on (i.e., no gas-phase chemistry or clouds).

The second verification test aimed to show that AG-CMAQ code in adapting mode can refine the grid around smoke plumes and track them more accurately. The April 9, 2008 burn at Fort Benning was simulated with CMAQ and AG-CMAQ codes and the results were compared to each other. In the AG-CMAQ simulation, $PM_{2.5}$ concentrations from the prescribed burn were used as the variable that derives grid adaptations. The static CMAQ grid had a uniform resolution of 1.3 km × 1.3 km; the same grid was used as an initial condition to grid adaptations in AG-CMAQ. As expected, AG-CMAQ increased the grid resolution in the regions of highest $PM_{2.5}$ concentration (Figure 25). In the area of highest resolution, grid cell sizes were reduced to approximately 100 m × 100 m. A reduction in the artificial (numerical) dispersion of plume features, which is typical for long-range transport models like CMAQ, was also evident from the simulation. The smoke plume tracked by AG-CMAQ was narrower and pollutant concentrations remained higher at the core of the plume compared to the plume tracked by CMAQ. Detailed results of this test and highlights of AG-CMAQ development can be found in Garcia-Menendez et al. (2010).

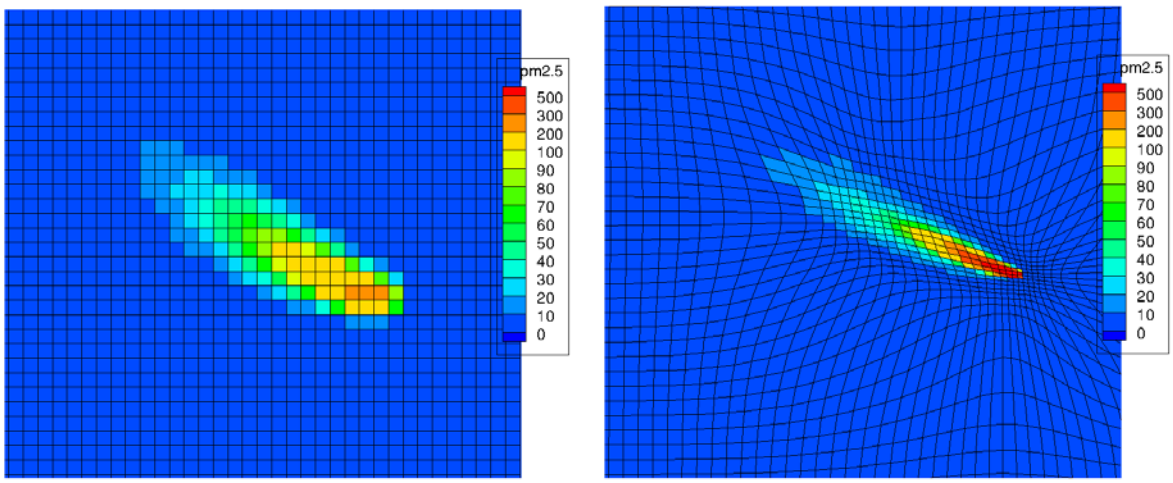

Figure 25. Comparison of $PM_{2.5}$ concentrations ($\mu g\ m^{-3}$) at Fort Benning, GA during a prescribed burn on April 9, 2008: (a) standard CMAQ with 1.33 km grid resolution, (b) adaptive CMAQ with dynamically adapting mesh. Boxes shown are cutouts of the Fort Benning area from the model domain.

The last code verification involved the incorporation of Daysmoke in CMAQ as a process module. The test was designed to assess if Daysmoke-CMAQ can produce the same results that it did in its original standalone form. In Daysmoke-CMAQ, the sub-grid scale plume dispersion module, which has essentially the same function as Daysmoke, is called upon with the same frequency as other transport/chemistry process modules. Hence particle tracking is not continuous in Daysmoke-CMAQ as it was in Daysmoke; there are interruptions by other processes. Figure 26 compares the particle distributions of Daysmoke-CMAQ and standalone Daysmoke in an application to the April 9, 2008 burn at Fort Benning. The distributions from the two models are overlapped on a vertical plane as well as a horizontal plane.

Note that there is no one-to-one match between particle positions of the two models in Figure 26. Also, in the top view, the particle distribution of original Daysmoke is wider than the particle distribution of Daymoke-CMAQ. Some of these differences are due to the necessity of using a different time-step in Daysmoke-CMAQ. Original Daysmoke's time step is 20 s but AG-CMAQ's process synchronization time step was not always divisible to 20 s. Therefore, a different internal time step may be necessary for the plume dispersion process in Daysmoke-CMAQ. Another reason for the differences is the stochastic nature of Daysmoke. As described in Section 3.2.2, Daysmoke makes use of random number generator to simulate atmospheric turbulence. For this reason, Daysmoke is not expected to produce the same result even in two consecutive runs of the original standalone model. Considering these two sources of potential differences, it was concluded that Daysmoke-CMAQ acceptably reproduced the particle distribution of original Daysmoke. Hence the incorporation of Daysmoke in CMAQ was successful.

(a)

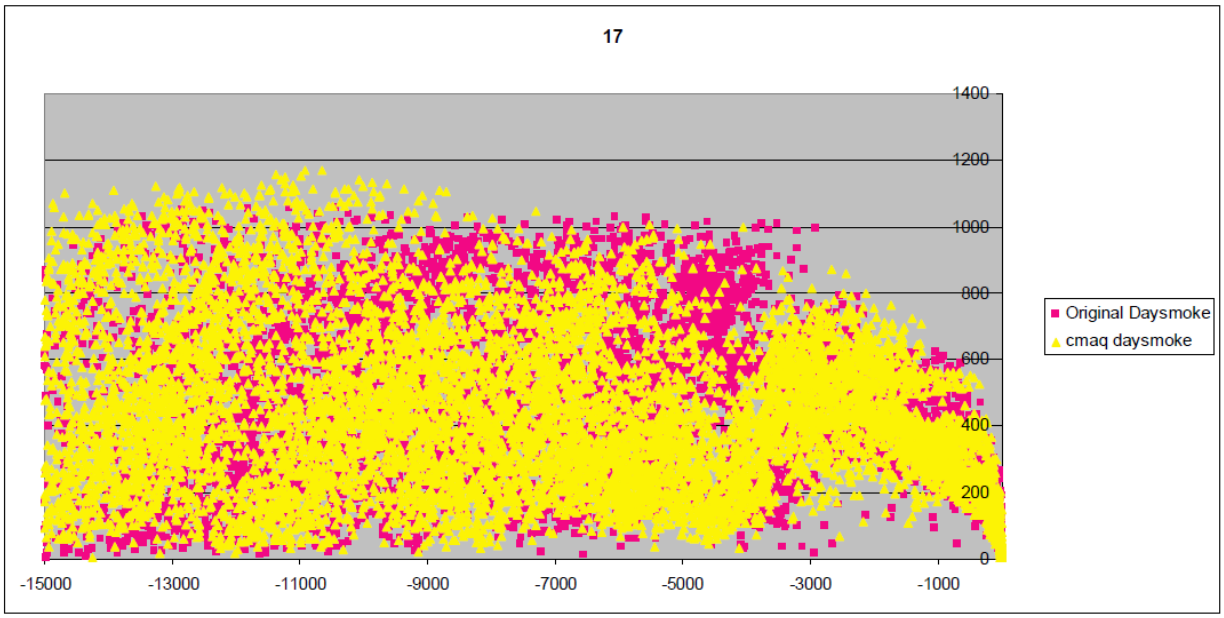

(b)

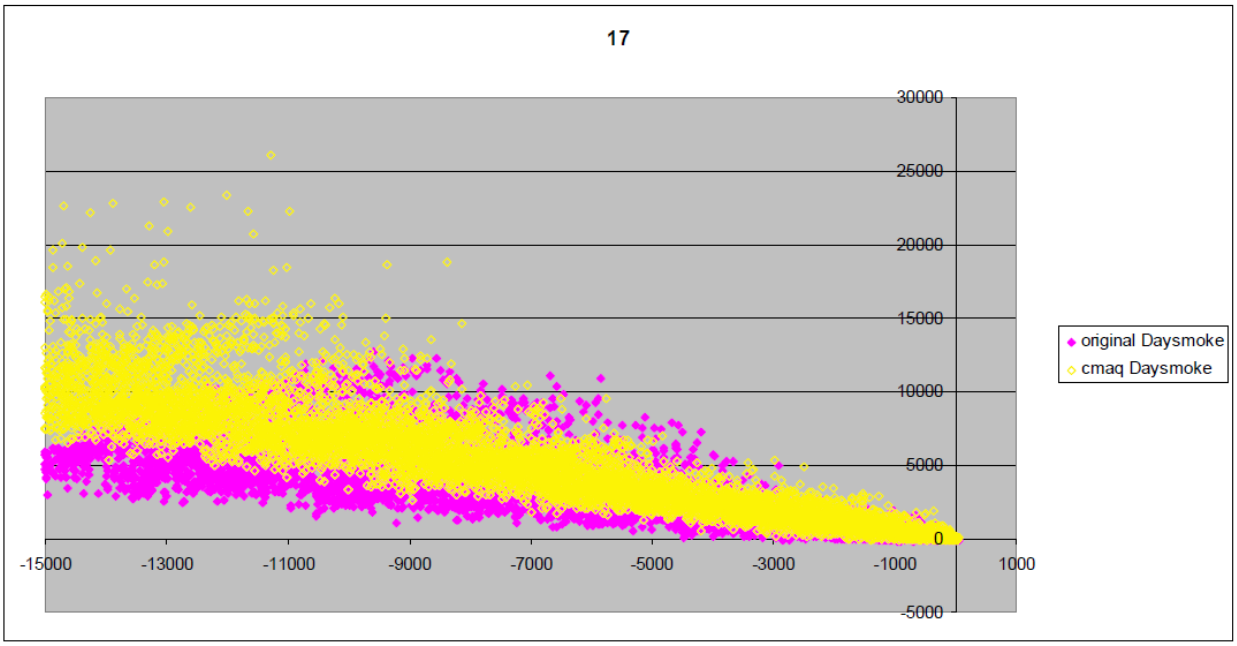

Figure 26. Particle distribution comparison of Daysmoke-CMAQ to original Daysmoke at 17:00 GMT during the April 9, 2008 burn of Fort Benning unit F5: a) side view, b) top view.

4.2.1.2 Exploration of Adaptive Grid MM5

One of the objectives was to explore the possibility of using an adaptive grid weather prediction model as the meteorological modeling component of the smoke impact prediction system. One such model, Adaptive grid MM5 (AG-MM5) was developed at North Carolina State University (NCSU) under the sponsorship of the Air Force Research Laboratory (Xiao et al., 2006). The provided test case, which involves optical turbulence over the Vandenburg AFB in California, was repeated successfully (Figure 27). Typical vertical resolution of MM5 is not adequate to resolve optical turbulence but using adaptive grid technology it is possible to reduce the grid scales to 10-100 m range. AG- MM5 also includes the NCSU k-zeta (enstrophy) hybrid turbulence model, which is based on 4 equations (for variance of velocity, variance of vorticity, variance of potential temperature, and potential temperature dissipation rate) derived from the Navier-Stokes equations. As can be seen in Figure 27, the AG-MM5 solution is in better agreement with observed optical turbulence then the uniform grid solution. Part of the improvement is due to the new turbulence model.

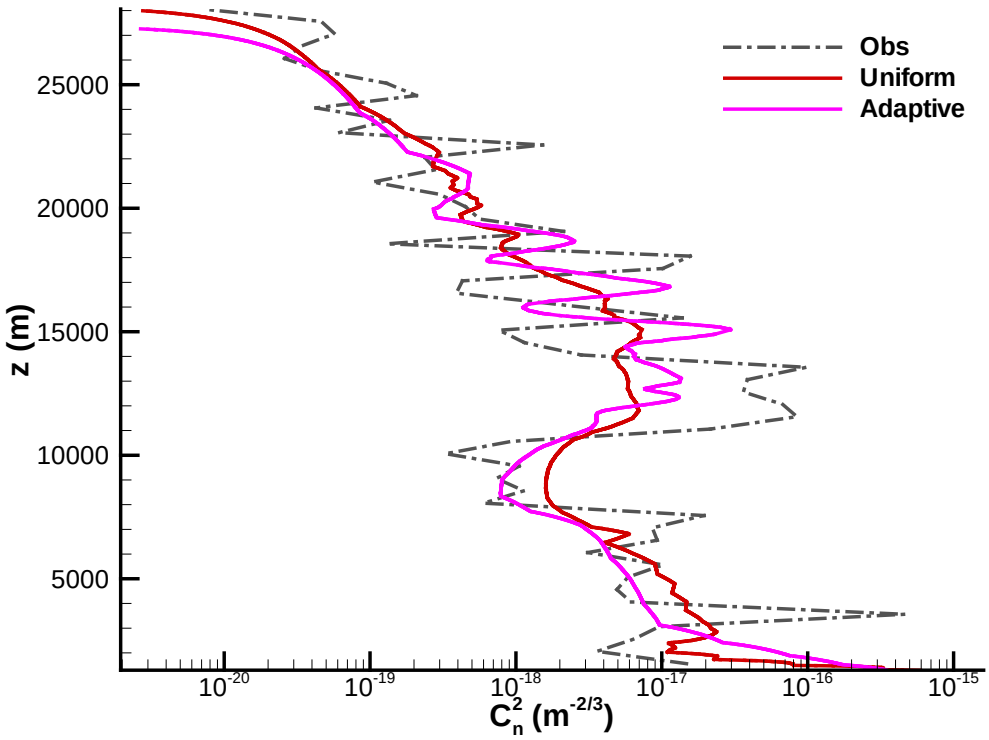

Figure 27. Comparison of C_n^2, a quantitative measure of atmospheric optical turbulence, in uniform and adaptive grid MM5 simulations.

In this optical turbulence application, grid adaptations were performed in the upper troposphere using the vorticity as a measure of the need for fine resolution. However, in prescribed burning

applications the grid must adapt to smoke plumes in the boundary layer. Therefore, AG-MM5 was tested in an application to the 9 April 2008 burn at Fort Benning, first without grid adaptation. The comparison of wind fields to standard MM5 showed that AG-MM5 was promising for wind predictions in the PBL (Figure 28). The wind field obtained by WRF is similar to the standard MM5 wind field shown in Figure 28. Too much synoptic influence, excessive damping, and smoothing of the terrain in MM5 and WRF lead to very little variability in the wind fields. The wind fields by adaptive grid MM5 have much more variability, even without grid adaptation. This is due to less damping in the model. Also, the influence of the terrain on the wind fields is more apparent.

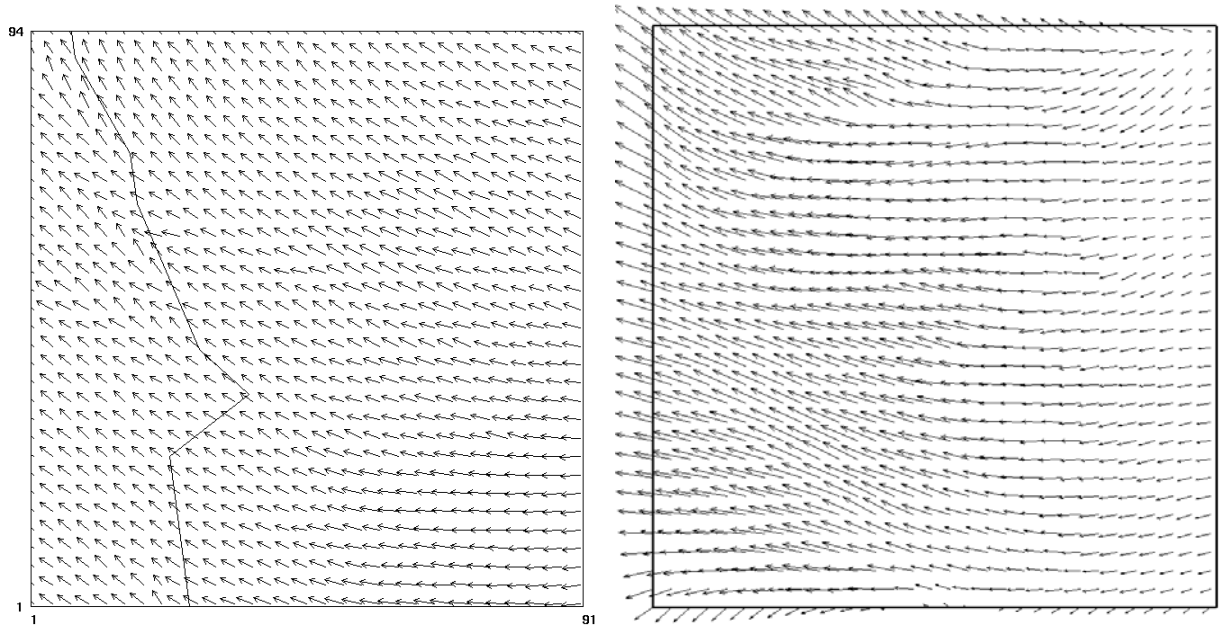

Figure 28. The wind fields obtained by standard MM5 (left) and adaptive MM5 but no grid adaptation (right) in applications to the 9 April 2008 burn at Fort Benning. The domain is 91 x 94 cells of 1.33 km resolution covering Fort Benning and surrounding areas in Georgia and Alabama.

The lack of wind field variation in the Fort Benning application of standard MM5 mirrors the lack of wind variation found in the stratosphere application (Xiao et al., 2006), as compared to detailed ~1.5 m radiosonde observations by AFRL (Figure 29). WRF was also reported to show much reduced variation. AG- MM5 wind field results in the stratosphere showed increased variability as compared with radiosonde observations when no adaptation was used, thereby indicating the benefit of the NCSU LES/RANS turbulence model (Figure 29). When mesh adaptation was used, the wind field variability approached that of the binned radiosonde observations. The improved agreement with observed winds in the PBL (Figure 29 inset) shows the potential of AG-MM5 for benefiting the prescribed burning applications. The dramatic improvements over the standard MM5 results also demonstrate the need for duplicating the adaptive capability in WRF in the future.

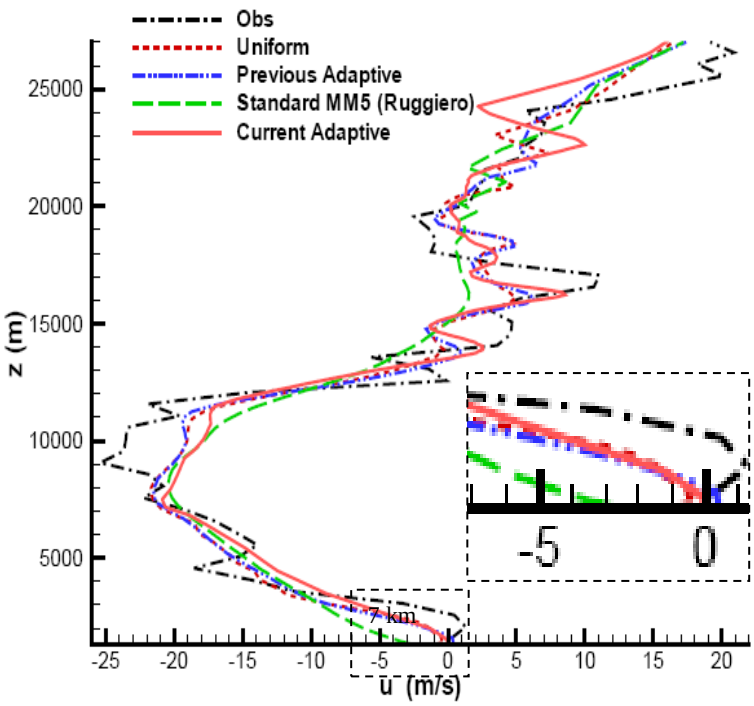

Figure 29. Comparison of zonal wind profiles in applications to the Holloman Air Force Base (Xiao et al., 2006). Adaptive Grid MM5 (both with and without grid adaptation) agreed better with the Radiosonde observations than the standard MM5, even in the PBL although the focus of this application was the stratosphere.

When grid adaptation was tested in the application to the 9 April 2008 burn at Fort Benning, the differences between the non-adapting and adapting AG- MM5 results were significant. While the temperature fields were comparable, the wind speeds were much lower in adapting AG- MM5 and the wind directions differed in several locations. These differences could not be caused by grid adaptation alone; they suggested that there may be a problem with the AG-MM5 code in the PBL, perhaps a problem with the surface boundary conditions. The results were sent to NCSU for review and an explanation for the differences was requested. AG-MM5 developers responded that further investigation, and possibly more development, was needed to calibrate the model in the PBL.

Encouraged by the findings that AG- MM5 could provide significant improvement over uniform grid MM5 if it were allowed more evaluation and development, we submitted a proposal to SERDP to include the developers of AG-CMAQ in our research team. The goal of the proposed work was to continue the development and validation of adaptive MM5 to achieve full meteorology model functionality, thereby resulting in a heretofore unobtainable capability to resolve local detail in wind fields required for accurate smoke plume propagation. The proposal was rejected; therefore, the application of AG- MM5 was not pursued any further. The meteorological inputs for the adaptive grid CMAQ model were derived through interpolation from a uniform but fine resolution grid (e.g., 1.3 km) in WRF.

It should be noted however that WRF wind fields at 1.3 km grid resolution are not problem free. In addition to the lack of variability due to excessive damping and lack of resolution of the terrain, stability issues were discovered. During the simulation of the 15 April 2008 burn, there was a time period with significant disagreement between the predicted wind direction and the direction suggested by the position of the trucks that were chasing the plume to measure its concentration. A closer look at the wind fields revealed a pattern of alternating NNW and NNE winds during the burn (Figure 30). This problem was announced to the community in October 2009. Several suggestions were received thereafter including 1) reducing the time step, and 2) increasing the damping coefficient. Changing the values of these two parameters did not result in significant improvement: the oscillatory wind direction pattern persisted in all cases.

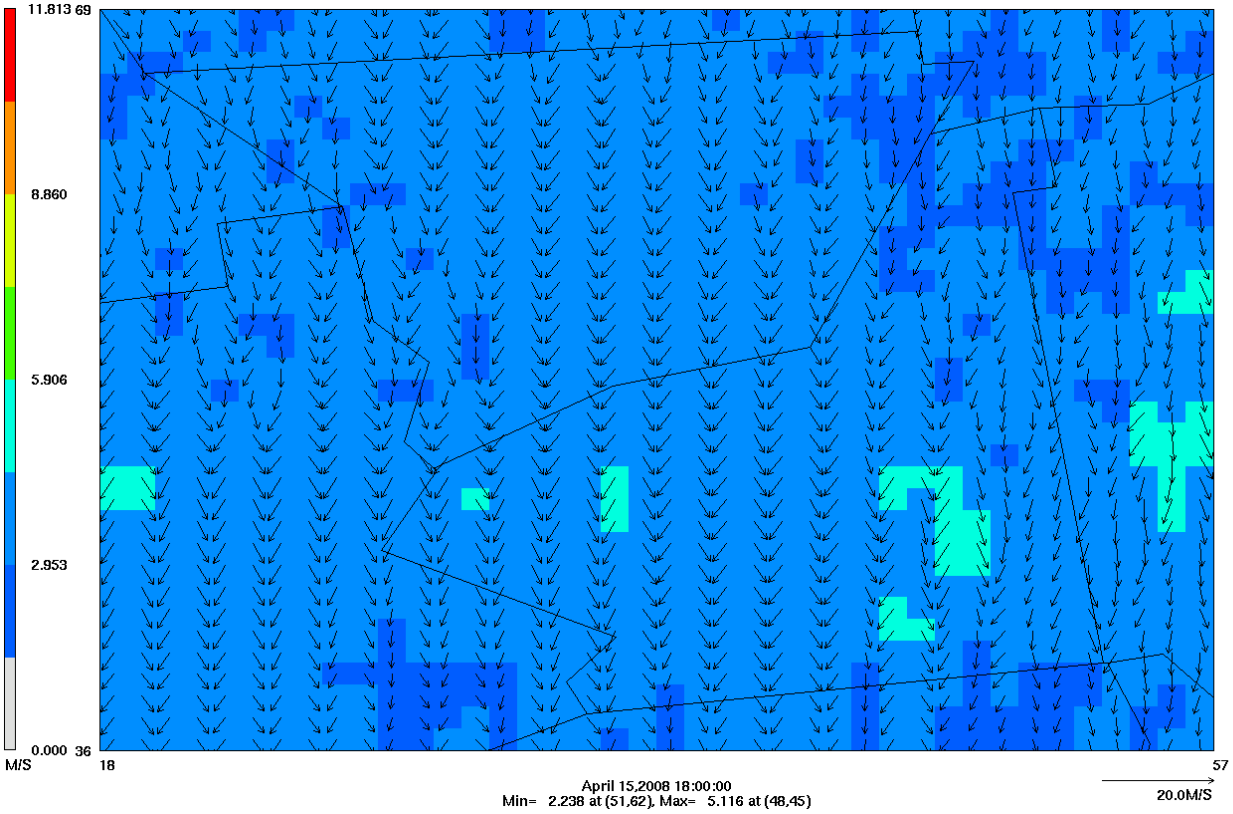

Figure 30. The wind field obtained by WRF in an application to the 15 April 2008 burn at Fort Benning. The grid resolution is 1.33 km.

4.2.2 Modification of Daysmoke and Adaptive Grid CMAQ models

In this section, modifications made to Daysmoke and AG-CMAQ models will be reviewed.

4.2.2.1 Daysmoke Modifications

A thorough review of the Daysmoke model was conducted. All facets of the model theory and computer code were evaluated for accuracy and completeness. The following modifications were completed by the US Forest Service team.

4.2.2.1.1 Adiabatic Expansion:

For adiabatic processes, the first law of thermodynamics relating pressure, volume and temperature reduces to

$$\frac{dp}{p} + \frac{dV}{V} - \frac{dT}{T} = 0 \tag{24}$$

Furthermore, pressure can be related to temperature via

$$\frac{dp}{p} = \frac{c_p}{R}\frac{dT}{T} \tag{25}$$

where R is the gas constant and c_p is the specific heat capacity of dry air at constant pressure. Substitution of (25) into (24) yields a relationship between change of volume and change of temperature

$$\frac{dV}{V} = (1 - \frac{c_p}{R})\frac{dT}{T} = -2.48\frac{dT}{T} \tag{26}$$

Equation (26) relates changes in volume to changes in temperature only for adiabatic processes as a smoke turret rises. The relationship between temperature and height for adiabatic processes is $dT = -9.76\times10^{-3}dz$. Thus the change in volume is related to the ratio of the change in height with the average turret temperature,

$$\frac{dV}{V} = 2.42\times10^{-3}\frac{dz}{\overline{T}} \tag{27}$$

4.2.2.1.2 Data Site Geo-Referencing

Daysmoke outputs PM concentrations above background on a simple graphic plan view surrounding the burn site (Figure 31). Each square represents one square mile. Concentrations are plotted in shades of gray except for greater than 50 μg m^{-3} (dark blue), greater than 75 μg m^{-3} (light green), greater than 100 μg m^{-3} (yellow), and greater than 200 μg m^{-3} (red). The graphic was recoded to allow for geo-referencing the locations of portable PM samplers with reference to the location of the modeled smoke plume. As of this time the exact locations of the sampler trucks have not been reduced from GPS data, however the approximate locations are shown as black crosses near the plume axis.

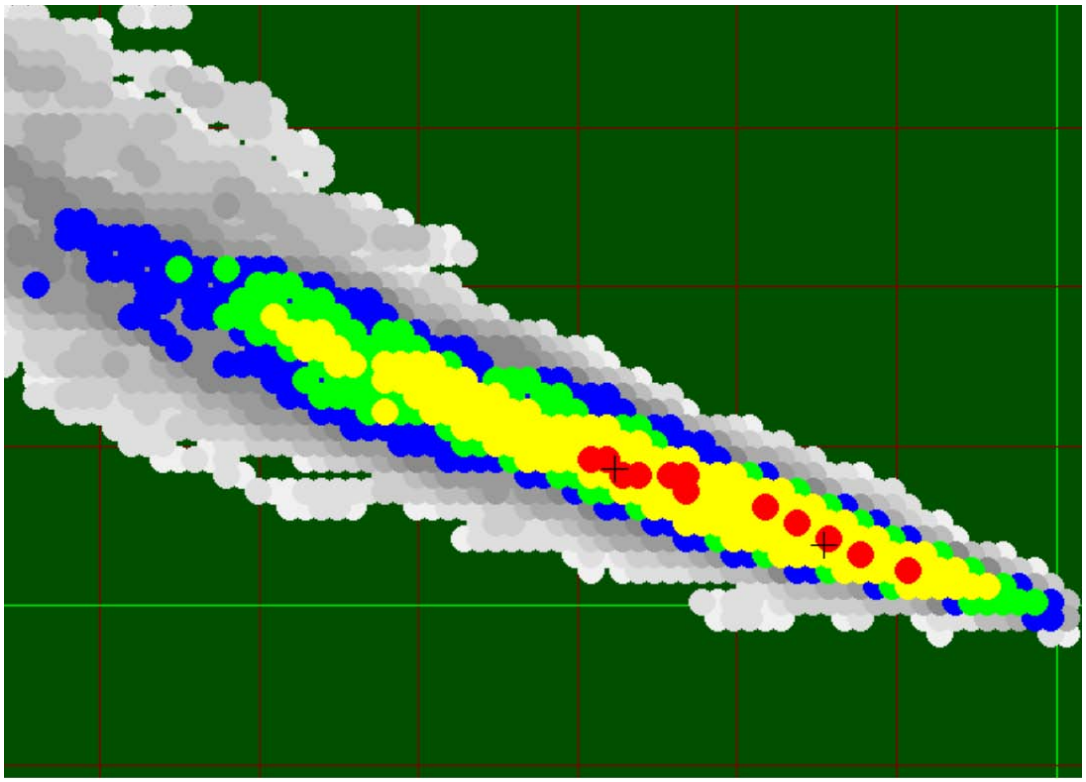

Figure 31. Plane view of Daysmoke $PM_{2.5}$ concentrations for 9 April 2008.

4.2.2.1.3 Multiple-Core Updraft

A feature of Daysmoke different from other empirical plume rise models is that Daysmoke permits multiple plume pathways simultaneously. Plume models that represent multiple-core updraft plumes as a single updraft are likely to overestimate the amount of smoke transported out of the mixing layer and thus underestimate ground-level smoke concentrations. In Daysmoke, the formulas for calculating multiple-core updraft plumes carried the assumption that the cores were all equal in size. This constraint was removed from Daysmoke subject to the new constraint that the sum of the fluxes of smoke through the multiple-core updrafts is equal to the single-core updraft flux given by the emissions production model. Each multiple-core updraft is assigned a stochastic flux component. The resulting spectrum of core fluxes is normalized by the sum of the core fluxes.

Figure 32 shows Daysmoke plume pathways for a 2-core plume. The boundaries of each plume pathway are labeled as “1” or “2”. The horizontal line represents the top of the mixing layer, approximately 550 m.

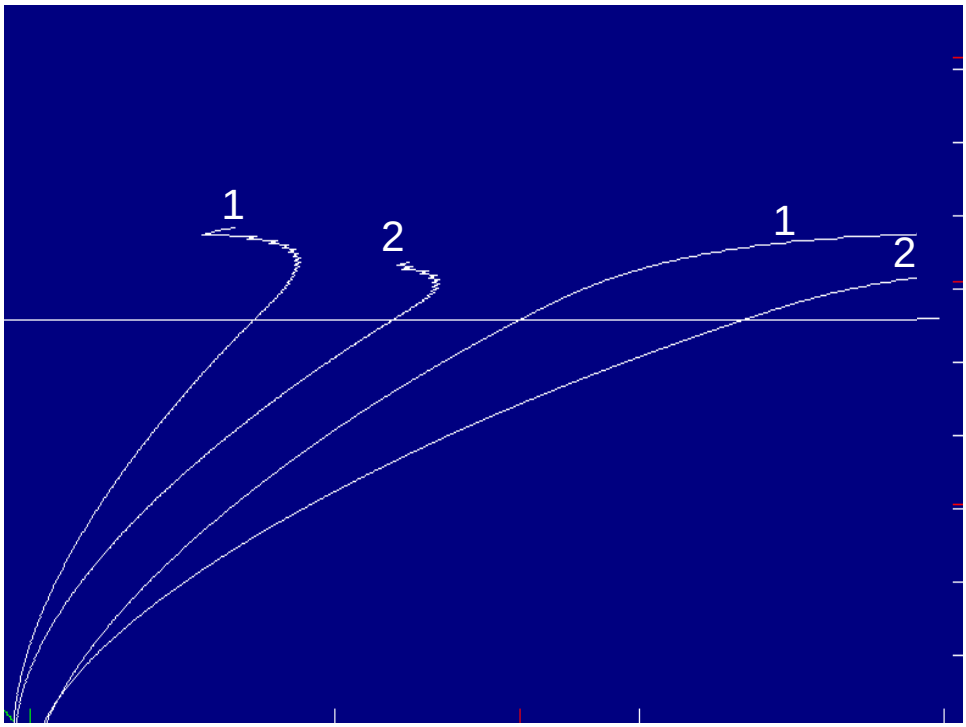

Figure 32. Daysmoke plume pathways for a 2-core updraft smoke plume for 9 April 2008.

4.2.2.1.4 Briggs Constraint

The Briggs Equations for plume rise from industrial and power plant stacks have been extensively validated with stack plume observations. Daysmoke, a plume rise model developed for the simulation of smoke plumes from prescribed burns, was matched with the Briggs Equations for a wide range of plume diameters and for stack-level wind speeds ranging from 2.5 m sec^{-1} to 10 m sec^{-1}. Daysmoke plumes match Briggs plume centerlines almost perfectly when Daysmoke entrainment coefficients are adjusted for the degree of plume "bentoverness" and wind speed. The results show that Daysmoke obeys the so-called 2/3 law for plume rise even though the 2/3 law is not explicitly formulated in Daysmoke.

The Daysmoke re-evaluation removes the Briggs constraint. This step should simplify Daysmoke and increase the range of plume conditions it models. However, if further model validation warrants, the Briggs constraint will be reset.

4.2.2.1.5 Other Daysmoke Modifications

A thorough review of the Daysmoke model computer code revealed a deeply hidden bug in the plume rise code. Testing of Daysmoke with 2008 Fort Benning data sets exposed this bug that could only be found through testing with "weak plume" smoke data. The impact of the bug was to increase plume vertical velocity by 0.5 - 1.0 m/s within the mixing layer. The bug had no impact once the plume entered the free atmosphere above the mixing layer.

The parameterization of the entrainment coefficient was made a function of plume bent-overness. A literature search of the relationship between entrainment and plume structure for single-source plumes found that the entrainment coefficient varies from 0.155 to 0.66 as a function of the bent-overness of the plume. Daysmoke has been modified to calculate entrainment coefficient as a weighted ratio of the transport wind speed and the effective plume diameter. This formulation removes the entrainment coefficient as a degree of freedom.

The detrainment coefficient was removed. The detrainment coefficient has been replaced with the entrainment coefficient thus linking detrainment and entrainment as parts of the same physical process. This step also removes a degree of freedom from Daysmoke.

Upon completion of the review of the Daysmoke model and computer code, a copy of the model code was transferred to GIT along with a draft write-up of the model theory and application to the April 9, 2008 burn. However, due to incompatibility issues, the model could not be immediately compiled at GIT. Daysmoke was developed at USFS using the Compaq Visual FORTRAN compiler, which is no longer available at GIT because it has been superseded by the Intel Visual FORTRAN compiler. When the code was finally compiled after several modifications to the original code, some of the graphical functions that worked under the Compaq compiler could not be reproduced. For this reason, it was decided that the Forest Service would generate a non-graphical version of the code, and deliver it to Georgia Tech to be used in the coupling with CMAQ. An executable version of Daysmoke was also transferred to Georgia Tech to serve as a data generator in the interim. The non-graphical version became available at the end of 2009.

During the analysis of the burns simulated by Daysmoke, it was determined that the 1-hour resolution for fire ignition time was not sufficient for accurate matching with $PM_{2.5}$ observations. Therefore, the Daysmoke code was modified to include the ignition start time. The subroutine that shifts plume data to account for ignitions that are not at the beginning of an hour had to be revised due to a glitch discovered during further evaluation. Also, an equation to add 1° C to the surface temperature was added to ensure there will be no zero-depth mixing layers. These changes improved the comparisons between Daysmoke and observed $PM_{2.5}$.

There were two more places where changes were made. First, just above the fire there exist a steep vertical gradient in vertical velocity in the plume. For bent-over plumes, the 20-second time step cannot resolve plume growth. The current model has code to do local very fine time stepping for the lowest 50 m of the plume. The time steps are calculated internally but can go as small as a few tenths of a second. The outcome is that the code accurately resolves vertical velocity gradients. The code was modified to be able to do the same thing elsewhere. Second, the free atmosphere horizontal velocity turbulence parameter was a constant in the current Daysmoke. The code was modified to make this parameter a function of the depth of the boundary layer as currently is the maximum rotor velocity for convective turbulence. The outcome was that lateral plume spread became a function of the depth of the mixing layer. The deeper the mixing layer, the stronger are the convective turbulence vertical velocities and the stronger are the lateral eddies so the greater the plume spread.

4.2.2.1.6 Highly-Tilted Plume Solution

There were two burns at Fort Benning with plumes characterized by very high concentrations of smoke at the innermost truck (Truck 1) location and very steep gradients of smoke concentration between the trucks. As will be discussed in Section 4.4.3.2.1, Daysmoke greatly underpredicted burn event smoke at Truck 1 locations in these burns; this required further investigation. As can be seen in Figure 33, these two events were extraordinary in terms of peak $PM_{2.5}$ concentrations measured at truck locations when compared to other burns at Fort Benning. Peak $PM_{2.5}$ measurements exceeding 600 μgm^{-3} for 15 January and 23 January 2009 implied that Truck 1 was located within the ascending plume on both days while Truck 2 and Truck 3 were located within particulate matter detrained from the plume as it passed overhead. This implication contrasted with Daysmoke solutions for the other days that placed the trucks either within detrained smoke or within remnants of the smoke plume torn apart and down-mixed by convective circulations.

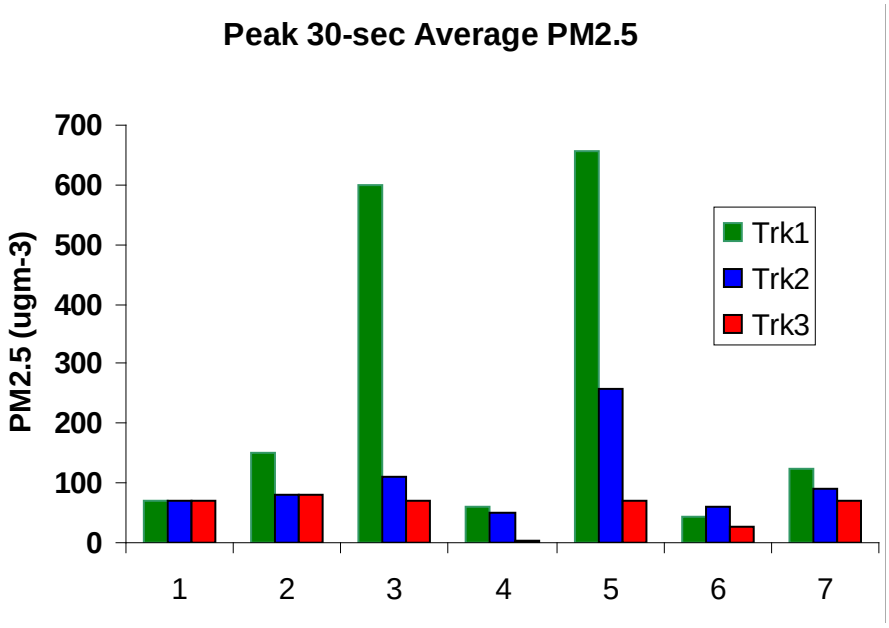

Figure 33. Peak 30-s averaged $PM_{2.5}$ for seven complete data sets from the 2008–2009 burns at Fort Benning. The burn dates are: (1) 9 April 2008; (2) 14 April 2008; (3) 15 January 2009; (4) 21 January 2009; (5) 23 January 2009; (6) 8 April 2009; and (7) 9 April 2009.

Using the initial conditions of $w_0 = 25$ m s^{-1} and $\Delta T_0 = 40$ °C, no choice for updraft core number could produce both the very high smoke concentrations at Truck 1 nor the steep gradients of $PM_{2.5}$ between the other trucks in the events of 15 January and 23 January 2009. Therefore, the initial conditions were varied subject to the constraint that the flux, given by the product of the initial velocity with the square of the initial effective plume diameter, was held constant (Figure 34). The top panel of Figure 34 shows the bent-over solution for a 1-core updraft plume for 23 January 2009. The initial conditions were reduced to $w_0 = 0.5$ ms^{-1} and $\Delta T_0 = 1.0$ °C to obtain the solution for a "highly tilted" plume (middle panel of Figure 34). Conservation of total flux required increasing the initial effective plume diameter from 59 m to 417 m—a requirement that

decreases the impact of entrainment on the plume. Thus the weakly buoyant highly-tilted plume was driven almost entirely by buoyancy and was capable of growth through the depth of the mixing layer.

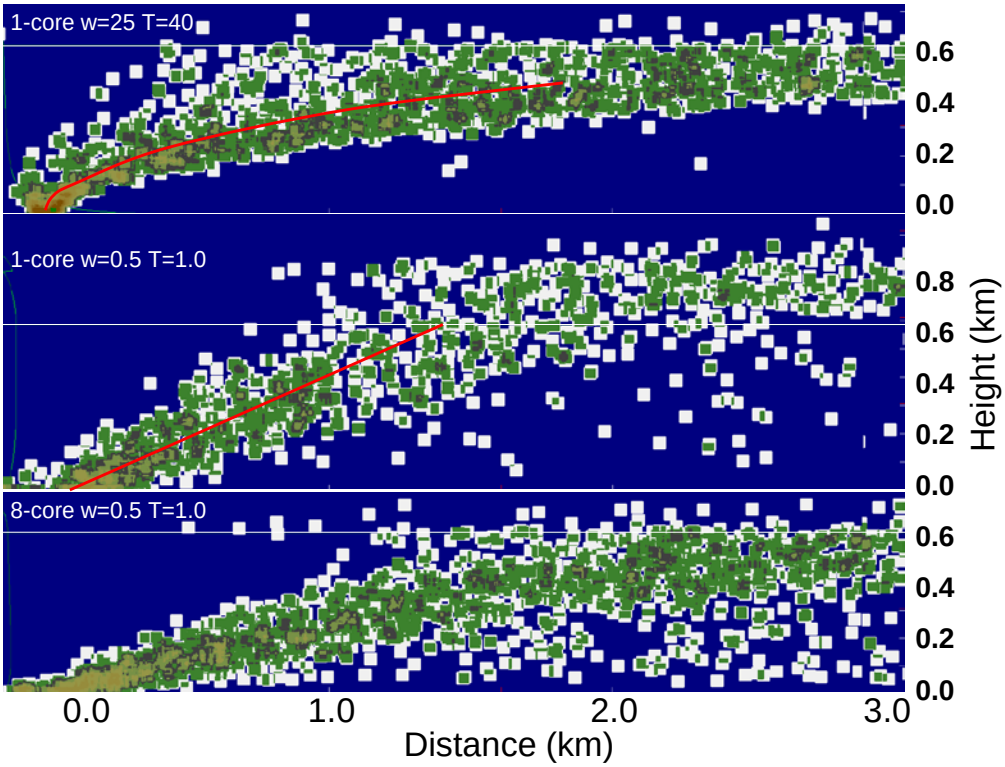

Figure 34. Daysmoke plumes for three selections of initial conditions. The horizontal white line gives the mixing height.

The plume axis is characteristically quasi-linear as compared with the parabolic axis of the bent-over plume (top panel of Figure 34). Running Daysmoke with the updraft core number set to eight (estimated for this burn) yielded the highly tilted plume solution shown in the lower panel of Figure 34. Note how this plume runs along the ground before ascending. The plume tilt of 15 degrees is greater than that for the 1-core plume (middle panel) and the plume is confined to the mixing layer. The $PM_{2.5}$ difference between Daysmoke and observed smoke concentration at Truck 1 location was greatly improved over the bent-over plume solution. Results for Truck 2 and Truck 3 showed minor changes from the original differences for 23 January 2009.

Figure 35 shows plume boundaries (white lines) for the 1-core updraft 23 January 2009 simulation (aspect ratio: $\Delta x/\Delta z = 2$). The plume axis (red line) describes a plume that runs along the ground for approximately 0.6 km then rises at approximate 3.5 ms^{-1} (dark green/light green line) along a quasi-linear axis. The weak buoyancy of the plume, shielded from entrainment by its 417 m diameter, ascended to the mixing height 2 km downwind and rose 100 m above the mixing layer (light blue line). The Briggs solution, shown by the green line, has the plume ascending to 250 m 4 km downwind from the burn. Hence, the highly-tilted plume cannot be represented by Briggs theory.

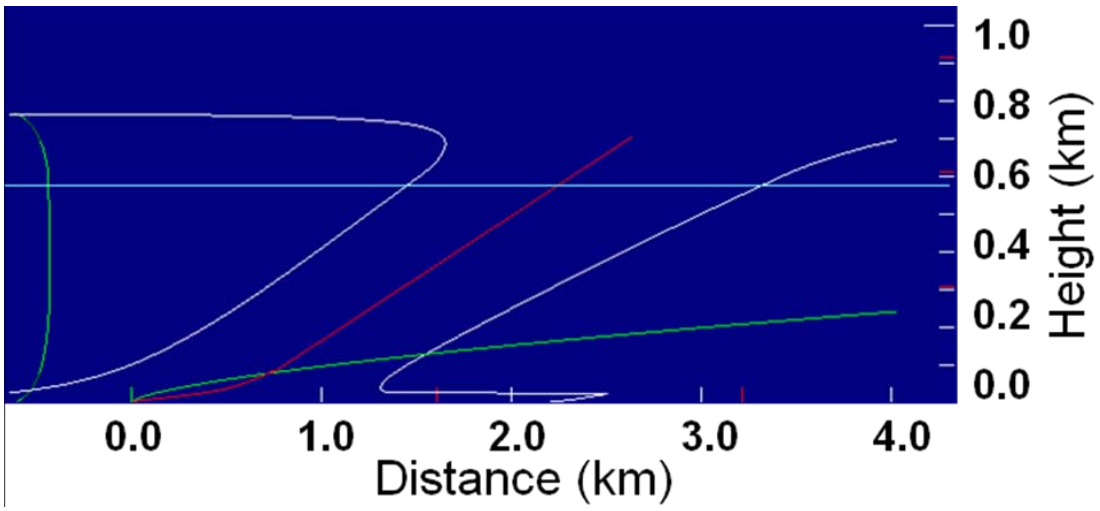

Figure 35. Plume boundaries (white lines) for the highly-tilted plume simulated by Daysmoke for the 23 January 2009 prescribed burn. Other lines are: plume axis (red), the Briggs solution (green), the mixing height (light blue), and the plume vertical velocity (alternating dark green/light green).

Figure 36 shows stack and cooling tower plumes from an electric power generating station. The stack plume shows the strongly bent-over parabolic structure (red line) typical of relative high velocity effluents rapidly slowed by entrainment on ejection through a relatively small plume diameter. The cooling tower plume, tilted along a linear axis (blue line), is characteristic of low velocity effluents ejected within a relative large plume diameter and driven by buoyancy. The plume structures modeled with Daysmoke compare favorably with the plumes shown in Figure 36. This constitutes independent evidence to support the Daysmoke solution for the highly-tilted plume.

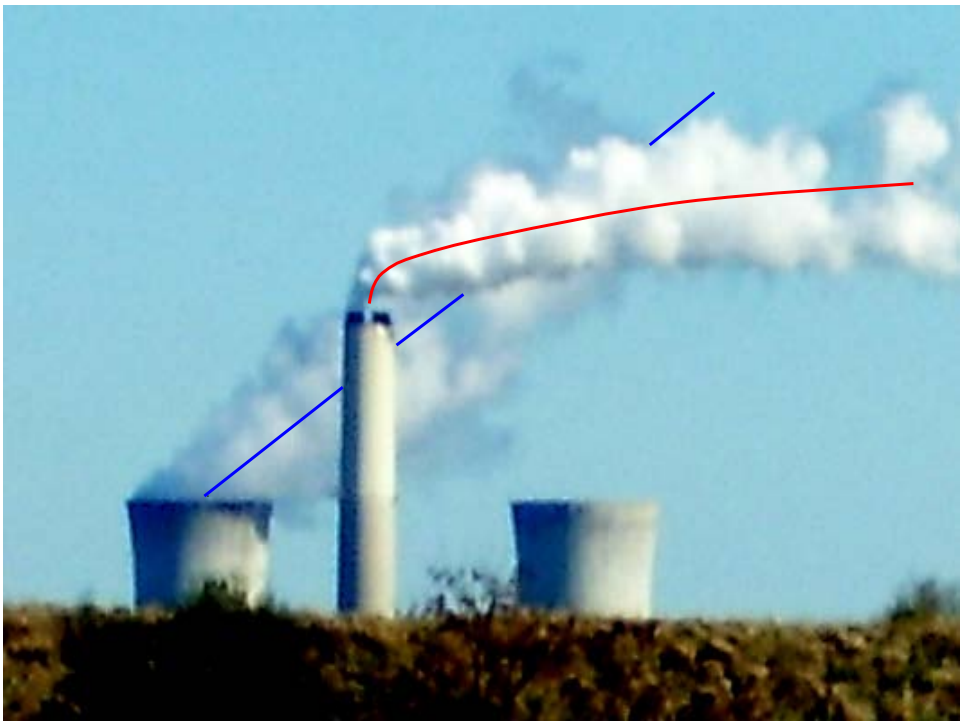

Figure 36. Plumes from an electrical power generating station.

4.2.2.1.7 Determining the number of Updraft Cores

Daysmoke provides no mechanism for determining updraft core number. The user has to set a number for running the model. Two methods are described in this section for determining the number of updraft cores.

4.2.2.1.7.1 Subjective Method for Determining Updraft Core Number

Updraft core number is governed by a complex interaction among a number of factors. Some of these factors are:

- Size of burn area – A small burn area should be expected to produce only one updraft core; large burn areas can support many updraft cores.
- Shape of burn area – A burn area that is highly irregular in shape will require an irregular distribution of fire leading to many updraft cores. This problem can be amplified when wind direction maximizes irregularities.
- Heterogeneity of fuels – Fuels that burn hot relative to surrounding fuels will develop stronger convective currents and will tend to form updraft cores.
- Fuel type, moisture, and loadings – All three factors relate to heat production. High heat production will develop convective columns and lead to fewer updraft cores; low heat production will lead to many updraft cores
- Distribution of fire on landscape − Fire distributed along a long linear line will produce many updraft cores; fire spread evenly over length and depth (mass ignition, stripping) will organize convective columns into fewer updraft cores.

- Amount of fire on landscape – A small amount of fire will reduce emissions per second but decrease heat thus minimizing convective organization. Result: many updraft cores. A large amount of fire will produce the opposite. Result: fewer updraft cores
- Distribution of canopy gaps − Hot air trapped beneath a dense canopy will flow to the gaps thus creating convective columns that produce updraft cores there. Thin (or no) canopies will not be a factor in updraft core development.
- Transport wind speed – Strong winds inhibit convective organization thus leading to many updraft cores. Weak winds allow convective organization resulting in few updraft cores.
- Mixing layer depth – A shallow mixing layer inhibits convective organization thus leading to many updraft cores. A deep mixing layer has less adverse impact on convective organization so fewer updraft cores should be expected.

For all the Fort Benning burns, the updraft core numbers were based on a subjective determination. The thought process will be illustrated for the 09 April 2009 burn. On compartment J6 consisting of 383 acres was burned. Figure 37 shows a Google Earth image of the burn area. Winds at 200 m (approximation to the transport winds) developed by the WRF model were characterized by relatively constant speeds (6.3 m sec^{-1} at 1300 EDT to 7.4 m sec^{-1} at 1500 EDT).

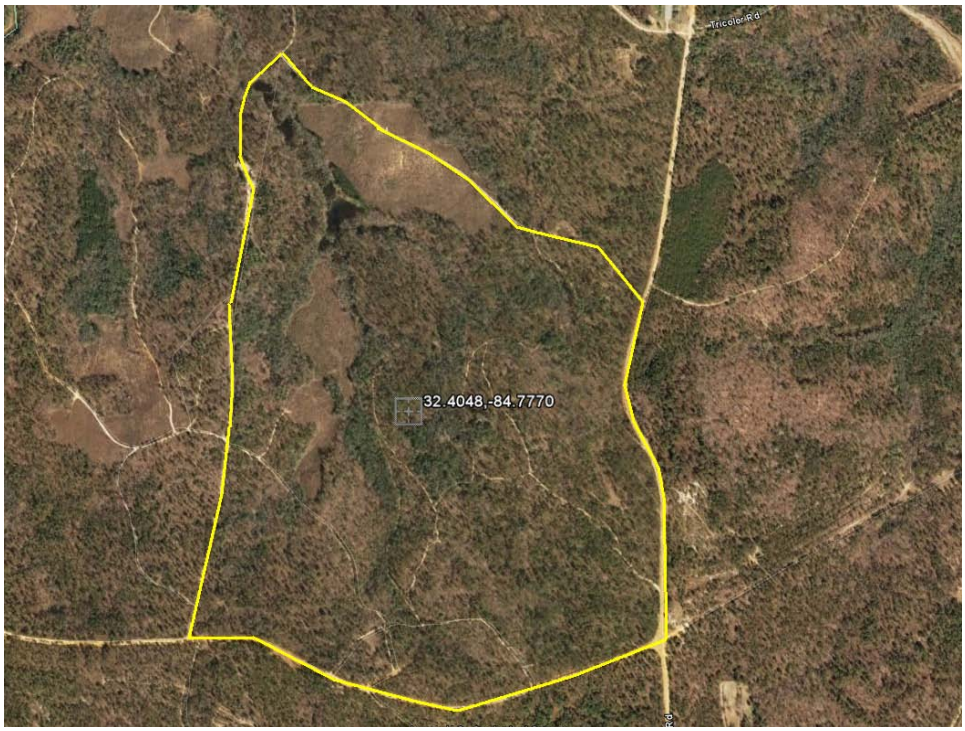

Figure 37. Google Earth image of Fort Benning unit J6 (outlined in yellow) burned on 09 April 2009.

The selection of updraft core number for the 09 April 2009 burn was done as follows.

1) Size of the burn area: A burn area of 383 acres is considered "moderate" in size. Thus the size of the burn area neither adds nor subtracts from the subjective selection of core number.
2) Shape of the burn area: The shape of the block E3 burn was nearly a square. Thus there would be no geometric areas that would set up independent plumes. Thus the shape of the burn area subtracts from the subjective selection of core number.
3) Heterogeneity of fuels: No information was available regarding heterogeneity of fuels.
4) Fuel type, moisture, and loadings: Fuel loadings were considered relatively light. Thus development of hot convective plumes should not be expected. This adds to the subjective selection of core number.
5) Distribution of fire on the landscape: Rapid deployment of fire along many straight strips as was done for this case will favor organization of smoke into convective columns. This subtracts from the subjective selection of core number.
6) Amount of fire on the landscape: The amount of fire under (5) is mitigated by the low fuel loadings under (4) and so neither adds nor subtracts from core number.
7) Distribution of canopy gaps: Areas burned ranged from open to partially closed. Thus canopy gaps do not contribute to the core number selection.
8) Transport wind speed: The relatively strong 200 m transport winds (6.0-7.0 m sec^{-1}) serve to increase updraft core number but not by much.
9) Mixing layer depth: The mixing layer depth of greater than one kilometer should aid (or at least not inhibit) the development of convective plumes. This subtracts from the subjective selection of core number.

Of the nine factors, numbers 2, 5, and 9 subtract from subjective updraft core number. Numbers 1, 3, 6, and 7 are neutral. Numbers 4 and 8 add to the subjective updraft core number. An updraft core number of 4 cores was assigned for this burn.

In retrospect, given results from the Eglin burns, a more appropriate selection may have been 6 updraft cores. The results from this study showed that Daysmoke under-predicted smoke at Truck1 and Truck 3 and matched the observations for Truck 2. Running with 6 updraft cores may have better matched smoke at Truck 1 and Truck 3 although smoke would have been overestimated at Truck 2.

4.2.2.1.7.2 Determining Updraft Core Number by Fire Spread Modeling with Rabbit Rules

A core number identification algorithm has been developed for Rabbit Rules and applied to two burns at Eglin AFB (Blocks 703C and 608A). The analyses of results are shown in the Figure 38.

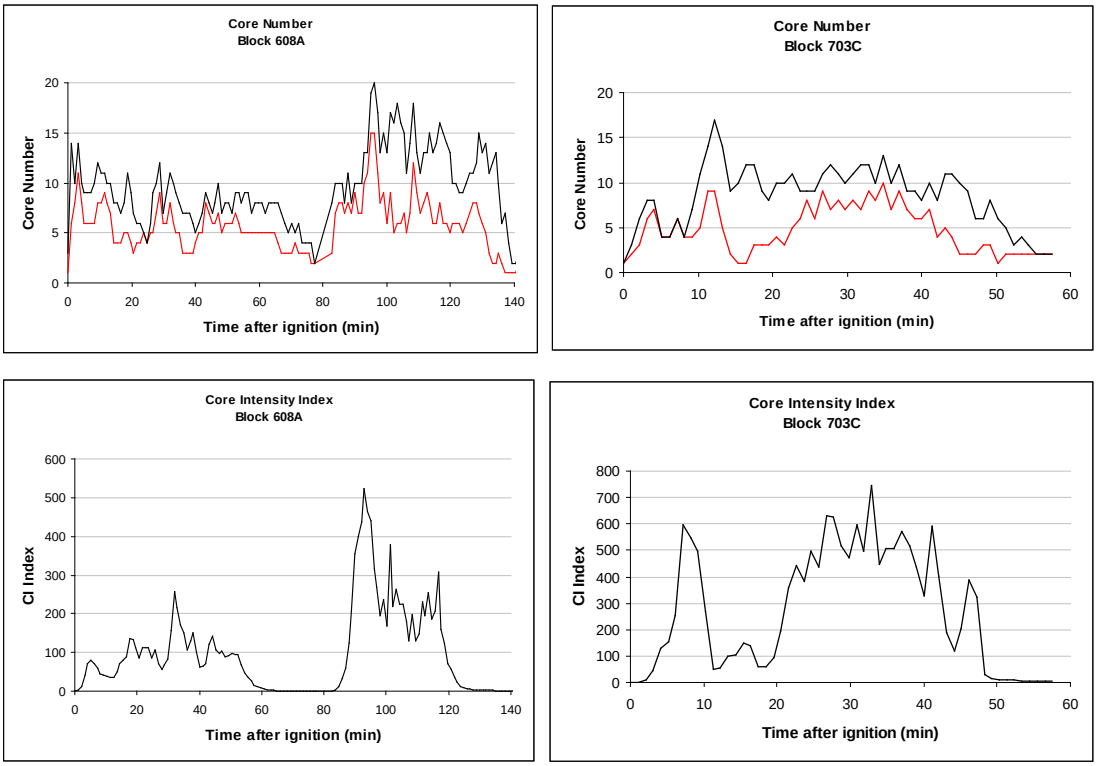

Figure 38. Determination of updraft core number by Rabbit Rules for the 6 February (Block 703C) and 8 February (Block 703) 2011burns at Eglin AFB: Numbers of updraft cores (top) and core intensity indices (bottom).

The left column in Figure 38 is for Block 608A burn on 8 February and the right column is for Block 703C b urn on 6 February 2011. The top row shows the updraft core numbers and the bottom row shows the core intensity (CI) index – defined as the sum of the squares of the core pressure anomalies found each minute during the burns. In the top row, the black line represents total number of cores defined as centers of low pressure in Rabbit Rules regardless of size and the red line represents the number of cores required to account for at least 90% of CI index. Note that there is not much difference in core number between the two burns. Total core numbers for 608A range mostly between 5-10 cores for the first half of the burn and between 10-15 cores for the second half of the burn. 90% CI index core numbers for 608A mostly range between 5 and 8, with several brief periods of lower and higher core numbers. 90% CI index core numbers for 703C mostly range between 6 and 8, with several prolonged periods of lower core numbers.

There is a larger difference in the core intensity (CI) of the two burns as shown in the bottom row of Figure 38. For the 608A burn, CI was around 100 for the first half of the burn and around 200 for the second half with several higher CI events − the highest being about 500. For the 703C burn, there were prolonged periods with CI over 400 with a peak above 700. What this means is that cores during the 703C burn were much stronger and there were more of the stronger cores.

This core number identification algorithm above may be overestimating core number since mergers would occur as the plume rises. However, the merger efficiency is likely a function of ambient wind speed with lower merger efficiency for higher ambient wind speeds. Wind speeds were very low during the 703C burn and moderate during the 608A burn. Therefore, there may have been more cores during the 608A burn and the cores were much weaker than during the 703C burn. A definition of "weaker" based on the heat release rate is under development.

4.2.2.2 CMAQ and AG-CMAQ Modifications

During the verification of AG-CMAQ, four hidden bugs were discovered in the official CMAQ code. These were announced to the CMAQ user community at the CMAS Annual Conference on October 20, 2009 and bug fixes were supplied through a web site[1]. One of these bugs is extremely serious as it leads to instability at fine grid resolution (approximately 1-km), which is damped at the expense of mass conservation errors. Two others bugs were also serious as they lead to incomplete advection and diffusion respectively, also at fine grid resolution. The last one is a potential bug that may affect hemispherical applications of CMAQ.

4.2.2.2.1 Bug fix related to instability

Synopsis: In CMAQ, numerical instabilities may be created during advection calculations. This problem may occur when the maximum wind speed decelerates by more than 1/3 during the course of an output time step.

Description: The advection schemes used in CMAQ are explicit. As such, they are subject to the Courant-Friedrichs-Lewy (CFL) condition for stability. This condition requires that the time step be smaller than the ratio of grid spacing to wind speed. In CMAQ, the CFL condition is applied only in the horizontal plane. Since horizontal grid spacing is uniform, the maximum wind speed in the domain determines the advection time step. In general, the uppermost layers are excluded from the maximum wind speed determination. Advection is sub-cycled in those layers (i.e., applied consecutively several times before other processes are applied) to satisfy the CFL condition.

The wind fields are supplied to CMAQ by a meteorological input file at a certain frequency (usually once every hour, but applications with more frequent inputs are becoming more common). For the time steps between two consecutive CMAQ output records, the wind fields are interpolated from the records in the meteorological input file for that particular time period. As an example, suppose the output time step is 1 hour and the frequency of meteorological inputs is 1/30 minutes. The advection calculations during the first half of the hour involve the winds at the top of the hour and at half past the hour. During the second half of the hour, the winds at half past the hour and at the end of the hour are used for advection. Therefore, all three wind records (i.e., the top, the middle, and the bottom of the hour) must be checked for maximum wind speed in the determination of the appropriate time step. However, only the last record, i.e. the record at

[1] http://people.ce.gatech.edu/~odman/bugs/bugs.htm

the bottom of the hour (or the top of the next hour), is considered in CMAQ. When the maximum wind speeds at the top of the hour and any meteorological input steps in between are larger than the maximum wind speed at the bottom of the hour, there is a chance to violate the CFL condition and introduce numerical instability.

The reason this bug does not lead to problems more often is a factor of safety applied to the time step. In CMAQ, the time step is made smaller than 0.75 times grid spacing over wind speed and even smaller to be an integer number of seconds that divides the output time step evenly. If the maximum wind speed does not decrease by more than 1/3 during the course of an output time step, the factor of safety circumvents any instability.

Remedy: This bug did not exist in MAQSIP, the prototype for CMAQ. Reverting back to how MAQSIP determined the maximum wind speed in subroutine GETSTEP fixed the problem.

4.2.2.2.2 Bug fix related to incomplete advection

Synopsis: In CMAQ, the advection process may be incomplete when it is synchronized with other processes. This problem may occur when advection time step is shorter than the synchronization time step, more likely in upper layers but also in the boundary layer.

Description: The main purpose of SUBROUTINE ADVSTEP is to determine the frequency of calls to process modules, a.k.a. the synchronization time step (SYNC). The characteristic time for advection, which is equal to the grid spacing divided by the maximum wind speed, plays an important role in determining SYNC. The Courant number, an important dimensionless parameter, is equal to the wind speed multiplied by the time step and divided by the grid spacing. In CMAQ, the advection time step (ADV) is selected such that the Courant number is less than 0.75. SYNC is set equal to ADV as long as the following conditions are satisfied.

1) SYNC must divide the output time step, STEP, evenly.
2) SYNC must be smaller than MAXSYNC (default value is 720 s if not user defined)
3) SYNC must be larger than MINSECS (default value is 60 s if MINSYNC is not user defined)

But, if ADV < MINSECS, then SYNC is set equal to MINSECS and advection is sub-cycled, i.e., applied several times before other processes are applied. However, there is a problem when SYNC is forced to equal MINSECS. Suppose MXUOVDX is 0.08. ADV that satisfies the Courant condition is 9 s. Note that 9 divides 3600 evenly (9x400=3600). But, since 9 s is smaller than MINSECS, which is equal to 60 s, SYNC is set to 60 s. The advection process has to be sub-cycled. The code produces the output shown in Figure 39. For layers 1 through 9 the advection time step is 8 s and 7 sub-cycles are performed. Since 7x8=56, the advection process would not be applied for a period of 4 s out of every 60 s.

```
 Top layer thru which sync step determined:  9

     Synchronization step adjusted up to mimimum (SEC):
60
                                                 (HHMMSS):
000100
     Number of Synchronization steps: 60


     Layer   Advection   per Sync
           Step (HHMMSS)  Step
       13      000000      61
       12      000001      31
       11      000002      21
       10      000003      16
        9      000008       7
        8      000008       7
        7      000008       7
        6      000008       7
        5      000008       7
        4      000008       7
        3      000008       7
        2      000008       7
        1      000008       7
```

Figure 39.. Output from CMAQ showing advection time steps per synchronization time step by layers.

There is also a problem in layers above layer 9, where sub-cycling is more common. These layers are in the free troposphere where the wind speeds are much higher than the boundary layer. Here, wind speed over grid spacing increases by 0.08 in every layer above layer 9 (i.e., UOVDX(L) = MXUOVDX + (L-ADVLAYR)*MXUOVDX). Note that every 60 s, advection would be short by 12, 18, and 29 s in layers 10, 11, and 12, respectively. Advection would not be applied to layer 13 at all.

Remedy: The problem in layers where SYNC is determined (layers 1 through 9) has been corrected through the provided new code.

4.2.2.2.3 Bug fix related to incomplete horizontal diffusion

Synopsis: In CMAQ, the horizontal diffusion process is only partially complete when sub-cycling is triggered. This would happen when the characteristic time for diffusion is shorter than the process synchronization time step.

Description: Inside of the DO loop labeled 344, where sub time steps are taken, the CONC array is not updated between the steps. When NSTEPS, the number of sub time steps determined based on the eddy time scale, is larger than 1, CGRID will be updated using the same CONC array loaded from the CGRID before the DO loop labeled 344.

Remedy: The loading of CONC from CGRID should be re-located inside of the DO loop labeled 344 at the very beginning of the loop.

4.2.2.2.4 Bug fix related to hemispherical applications

Synopsis: In CMAQ, the Smagorinsky horizontal diffusion coefficient assumes Cartesian coordinates. This may introduce a directional bias to horizontal diffusion in map projection coordinates, especially when the map scales display a wide range over the modeling domain such as in hemispherical applications with polar stereographic coordinates.

Description: The original horizontal diffusion coefficient of Smagorinsky,

$$K_h \propto \sqrt{\left(\frac{\partial u}{\partial x}-\frac{\partial v}{\partial y}\right)^2+\left(\frac{\partial v}{\partial x}-\frac{\partial u}{\partial y}\right)^2} \tag{28}$$

is valid in Cartesian coordinates. Using this parameterization in other coordinate systems may have undesirable effects.

Remedy: Becker and Burkhardt (2009) revisited Smagorinsky's mixing-length based parameterization of horizontal diffusion and modified it for spherical and terrain following vertical coordinates used in general circulation models. The same thing should be done for the coordinates used in regional-scale atmospheric modeling. Until a more rigorous derivation becomes available, the following form, obtained by intuition from the similarity of the right-hand-side in Equation (28) to divergence, was proposed.

$$K_h \propto \frac{1}{\sqrt{\gamma}}\sqrt{\left(\frac{\partial}{\partial x^1}\left(\sqrt{\gamma}u^1\right)-\frac{\partial}{\partial x^2}\left(\sqrt{\gamma}u^2\right)\right)^2+\left(\frac{\partial}{\partial x^1}\left(\sqrt{\gamma}u^2\right)-\frac{\partial}{\partial x^2}\left(\sqrt{\gamma}u^1\right)\right)^2} \tag{29}$$

In map projection coordinates used in CMAQ, where *m* is the map scale factor,

$$\sqrt{\gamma}=\frac{1}{m^2};\ x^1=x_m;\ x^2=y_m;\ u^1=mU;\ \text{and}\ u^2=mV \tag{30}$$

Therefore,

$$K_h \propto m^2\sqrt{\left(\frac{\partial}{\partial x_m}\left(\frac{U}{m}\right)-\frac{\partial}{\partial y_m}\left(\frac{V}{m}\right)\right)^2+\left(\frac{\partial}{\partial x_m}\left(\frac{V}{m}\right)-\frac{\partial}{\partial y_m}\left(\frac{U}{m}\right)\right)^2} \tag{31}$$

The difference between Equations (28) and (31) may be significant on polar stereographic coordinates.

4.2.2.2.5 Other Modifications

The existing coordinate transformation, which assumed the earth is a sphere, was replaced with a new one assuming, more realistically, the earth is an oblate ellipsoid of revolution. This change

of coordinate transformation leads to differences in calculated distances of the order of 100 m, which is the same order as the resolution targeted in prescribed burning applications.

The modifications made to CMAQ to get to the Adaptive Grid CMAQ model were extensive; they will not all be enumerated here. AG-CMAQ is fully described in Garcia-Menendez et al. (2010). The variable time step algorithm formerly installed in AG CMAQ was revised to allow for outputs more frequently than once per hour (e.g., every 15 minutes).

4.2.3 Coupling of the Models

In this section the results of the model coupling efforts will be discussed. After an ad-hoc coupling of Daysmoke with CMAQ, a detailed Fourier analysis was conducted to study the loss of accuracy incurred during the coupling. Then a coupling method was developed to minimize the loss. Daysmoke was coupled with Adaptive Grid CMAQ (AG-CMAQ) using this methodology. The section ends with ideas for future research towards an ideal smoke prediction system.

4.2.3.1 Initial Coupling of Daysmoke with CMAQ

The 28 February 2007 smoke incident, when plumes from two prescribed burns invaded metropolitan Atlanta, was simulated using the initial coupling of Daysmoke with CMAQ in SHRMC-4S. Satellite imagery and ground-level $PM_{2.5}$ observations were used for evaluating the coupled modeling system. Simulated $PM_{2.5}$ concentrations generally agreed with observed data both in location and timing of the peaks; however, the magnitudes were underestimates (Liu et al., 2009).

4.2.3.2 Fourier Analysis for Coupling Daysmoke with CMAQ

The objective of the Fourier analysis was to understand the relationship between the plume structure and the resolution of the CMAQ grid to find the optimal downwind distance for handing over the Daysmoke plume to CMAQ. Several PB plumes tracked by Daysmoke were analyzed to determine the CMAQ grid resolutions needed to minimize the loss of accuracy during transfer of the plume from Daysmoke to CMAQ. The optimal handover distances (i.e., where the error incurred due to handover is the smallest) were calculates as a function of time as the Daysmoke plumes evolved.

For the case shown in Figure 40, for different grid resolutions there seems to be a different optimal downwind distance at which the transfer results in minimum loss. It should be remembered that the grid resolution required for resolving a wave of wavelength equal to $2\Delta x$ is Δx. When wavelengths shorter than $10\Delta x$ are clipped, which is equivalent to using a grid resolution of $5\Delta x$ (the coarsest grid shown in Figure 40) asymptotic behavior of the C2 error (difference between squared concentrations before the transform and after the inverse transform once short wavelengths that cannot be supported by the grid are clipped) starts at a downwind distance of about $35\Delta x$, if the visible oscillation between $20\Delta x$ and $35\Delta x$ is filtered out. The downwind distance to asymptotic behavior of C2 error gets smaller and smaller as grid sizes are reduced (or grid resolutions are increased) to $2.5\Delta x$, $2\Delta x$ and Δx by clipping waves shorter than

5Δx, 4Δx and 2Δx, respectively. For the finest grid (grid size equal to Δx) this distance is about 25Δx. In other words, for best performance, the interface between CMAQ and Daysmoke should be set at 25 cells away from the fire.

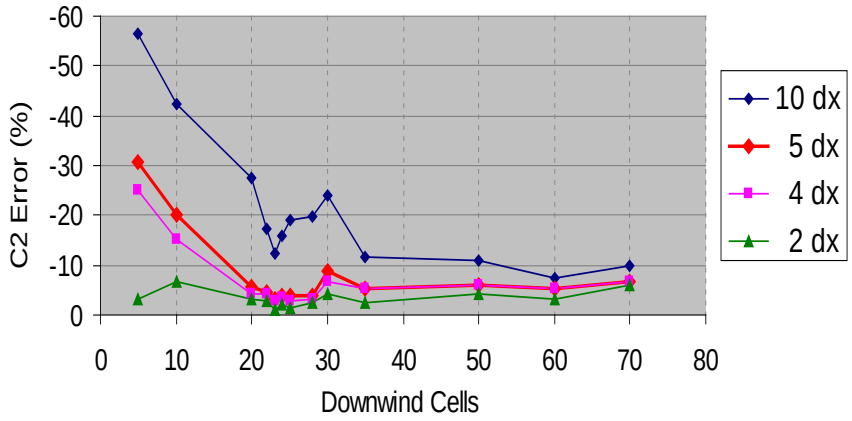

Figure 40. The errors in the sum of squared concentrations obtained by clipping waves shorter than 10Δx (grid resolution of 5Δx) to 2Δx (grid resolution of Δx) as a function of downwind distance measured in Δx.

In the future, the knowledge of what grid resolution would minimize the loss of accuracy can be used as a criterion for grid adaptation in AG-CMAQ.

4.2.3.3 Coupling Daysmoke with AG-CMAQ

Based on the findings of the Fourier analysis, a coupling algorithm was developed that can vary the downwind distance for handover of Daysmoke plume to CMAQ based on the evolving structure of plume as the burn progresses. Two conditions must be satisfied for handover: 1) the Daysmoke plume must reach its potential height and 2) the difference between Daysmoke plume concentrations before handover and CMAQ grid cell concentrations after handover (this difference is the concentration error incurred during handover) must be minimal. Analysis of several burn plumes has shown that the downwind distance where these two conditions are satisfied changes in time. The coupling algorithm was coded in FORTRAN. The review and verification testing of the code have gone through several cycles. At the end, it was concluded that the code performs its intended functions.

Final testing of the handover process was performed by simulating the April 9, 2008 burn at Fort Benning. AGD-CMAQ, the model resulting from the coupling of Daysmoke with Adaptive Grid CMAQ, was used. The results of the handover error analyses are shown in Figure 41. The concentration differences between Daysmoke and AG-CMAQ at different downwind distances from the burn are shown for three different times: 16:30 GMT, 17:00 GMT, and 18:00 GMT. Error analysis does not start until the Daysmoke plume reaches its potential height; this is why the concentration differences are not shown until a certain downwind distance: 2 km at 16:30 GMT, 6.5 km at 17:00 GMT, and 13 km at 18:00 GMT. The concentration difference generally

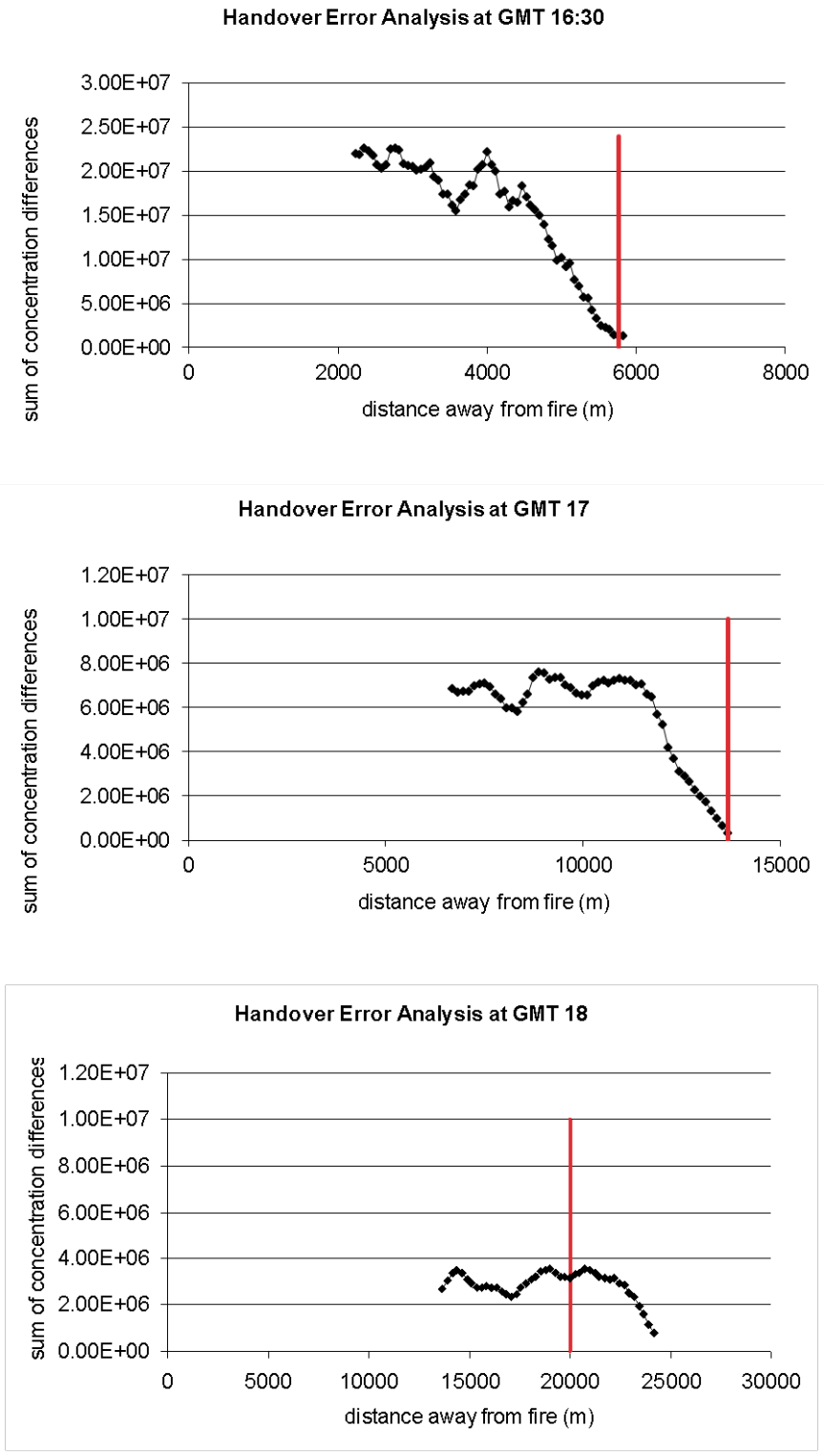

Figure 41. Concentration error versus downwind distance at 16:30 GMT (top), 17:00 GMT (middle) and 18:00 GMT (bottom).

decreases with downwind distance though it can remain flat sometimes and even increase occasionally. In all three cases shown, the difference reaches its minimum at the maximum extent of the plume. The red lines demark the positions of the interface between Daysmoke and AG-CMAQ. The concentration difference at the interface represents the handover error. The interface is drawn at the minimum concentration difference, except at 18:00 GMT. At that time, even though the error would be smaller at 24 km, the interface is drawn at 20km, which was the limit used for avoiding prolonged plume tracking with Daysmoke.

Figure 42 shows how the downwind distance of the interface (measured from the burn plot) varies over time in the application of AG-CMAQ to the 9 April 2008 burn at Fort Benning. The black line displays what happens when the interface is unbounded and is set according to minimum concentration. The green line shows where the interface is set when the distance is limited to 20 km. As the burn progresses, the downwind distance of the interface increases and, if unbounded, reaches its maximum at 40 km around 18:45 GMT. Towards the end of the flaming phase of the burn, the interface recedes. The distance to the interface starts increasing again around 19:00 GMT as it follows the remnant plume from the smoldering phase of the burn.

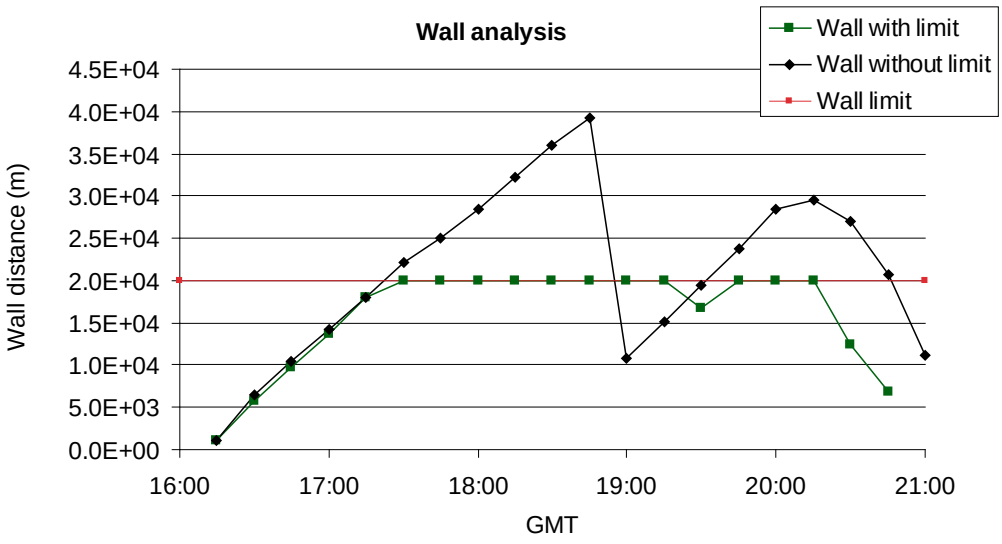

Figure 42. Downwind distance of the interface ("wall") between Daysmoke and AG-CMAQ over time during the application to 9 April 2008 burn at Fort Benning: with no limit (black) and 20-km limit (green).

4.2.3.4 Coupling Ideas for the Future

In our attempts to get the adaptive grid MM5 to provide meteorological data on the same grid as AG-CMAQ, $PM_{2.5}$ concentrations from CMAQ were being passed to MM5, to be used in the weight function which drives grid adaptations. Due to the difficulties involved with this approach, it became evident that, instead of trying to harmonize the adaptor in MM5 with the one in CMAQ, it is easier to make the grid adaptor an entity external to both models. An external grid adaptor can accept information from both models and serve their grid adaptation needs simultaneously and more effectively. We explored the possibility of modifying the adaptive

MM5 code so that it accepts grid coordinates as input, instead of calculating them internally. We found that it is feasible to modify the adaptive MM5 and get it to run with grid coordinates provided externally. Therefore, we changed our concept of an ideal modeling system to accommodate this new idea (Figure 43).

Another important addition to the "ideal modeling system" concept is the chemical feedback coupling of CMAQ with the meteorological model (MM5 or WRF). This is shown with the red arrow in Figure 43. Mathur et al. (2011) suggested that California wildfires of 2008 may have had a significant cooling effect that changed the boundary layer dynamics. Also, photographic and anecdotal evidence of pyrocumulus events suggests that particulate emissions from prescribed burns can act as cloud condensation nuclei. Our ceilometer (lidar) measurements of the burn plume on April 9, 2008 suggested that the plume formed clouds at the top of the boundary layer. This evidence supports the hypothesis that the plume may be creating its own micrometeorology, not just through the interaction of smoke with incoming solar radiation, but also through the interaction of PM with clouds. Therefore, there may be significant benefits in fully coupling the models, i.e., accounting for the feedbacks of aerosol concentrations in CMAQ onto the dynamics in MM5.

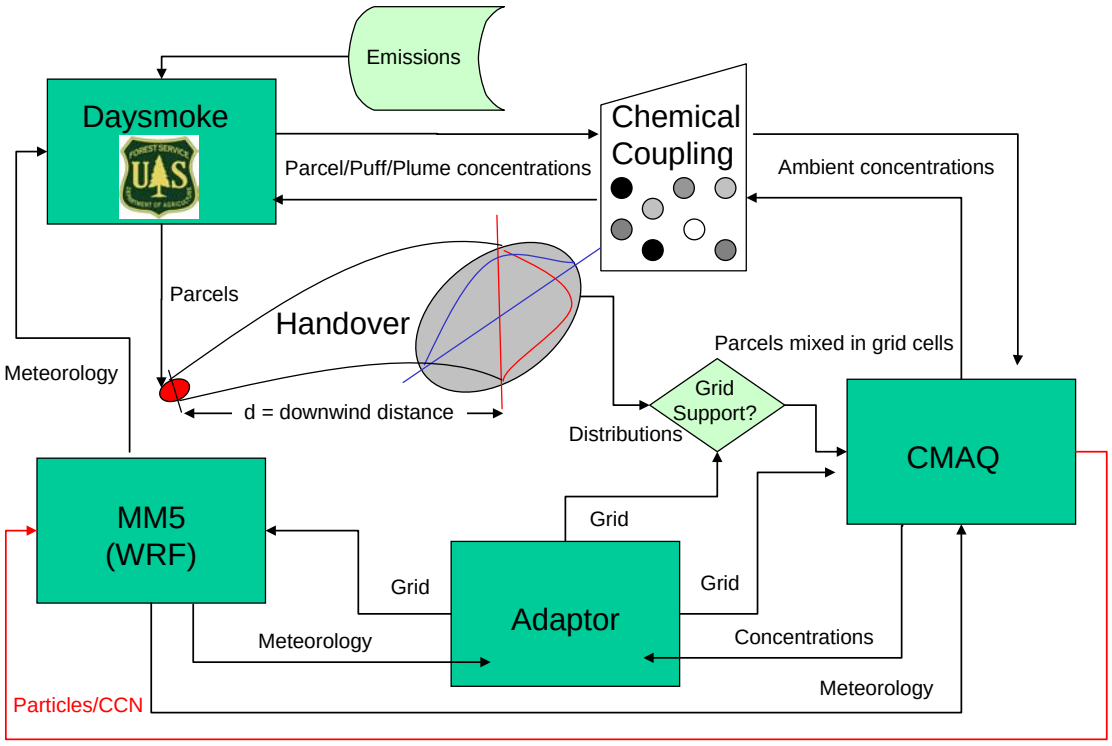

Figure 43. The ideal coupled system of adaptive meteorology and air quality models with embedded sub-grid scale plume model.

Daysmoke is currently an unreactive Lagrangian dispersion model that simulates emissions and transport of $PM_{2.5}$. Given the importance of secondary aerosol formation from gas phase precursors, one objective should be to introduce chemical reactivity in Daysmoke. Emitted gaseous species can be transported by Daysmoke's dispersion mechanism as individual parcels,

each with the same initial pollutant mass and chemical composition upon release. Reactivity can be incorporated into the model by adding a chemistry module that includes a chemical mechanism consistent with the species considered in the background atmosphere photochemical model (CMAQ).

Chemical treatment of a smoke plume requires assumptions to be made about the plume volume, chemistry specificity, and redistribution of reacted mass. A research plan was developed to investigate various assumptions on each of these 3 issues. The first set of assumptions will be about converting pollutant mass at given locations to pollutant concentrations that can be used for reaction kinetics. The second set of assumptions will couple the plume with the background atmosphere through chemical reactions. The last set of assumptions involves redistribution of reacted mass back into the discrete plume volumes and background atmosphere. The coupling should be implemented with the set of assumptions that yield the simplest approach (Figure 44).

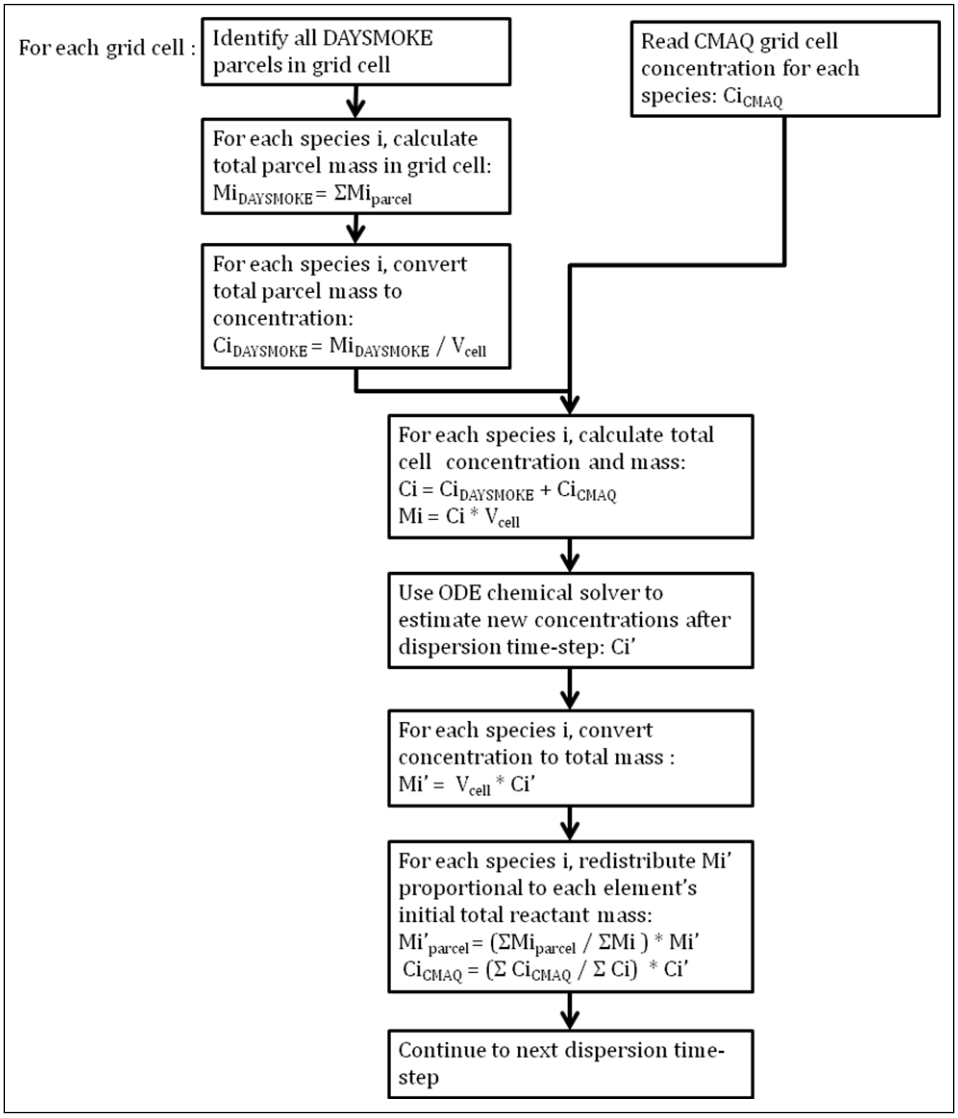

Figure 44. Flowchart for chemical coupling of Daysmoke with CMAQ.

Additional analysis should explore the sensitivity of resultant concentrations to the chemistry time step and determine an optimal call frequency relative to dispersion frequency in Daysmoke.

4.3 Field Measurements

The results of field measurements will be discussed under three sections: 1) Preliminary data collection at Fort Benning, 2) Intensive data collection at Fort Benning, and 3) Data collection at Eglin AFB.

4.3.1 Exploration of Fort Benning Site and Preliminary Data Collection

Three prescribed burns were monitored at Fort Benning as part of the preliminary field program. Each one will be described briefly.

April 9th, 2008: 300 acre burn in compartment F5 with a predicted Easterly wind. Ignition started at 12:30 and completed at 14:45. The protocol for coordination was put to test in this burn.

April 14, 2008: 400 acre burn in compartment N1 with a predicted Northwesterly wind. Ignition started at 12:00 and completed at 15:15. Another 150 acres burned simultaneously in compartment AA but it should not have pushed smoke onto monitored area. Troop exercises were going on in the area of study that did not seem to effect the equipment until the last sampling period of Truck 1. During this final sampling period, Truck 1 was located within 100 yards of simulated battle with smoke grenades at approximately 15:20. Truck 2 was stuck in mud at second sample site but continued to monitor. Truck 1 removed equipment to stationary location in compartment for location 2 to go assist with Truck 2.

April 15, 2008: 200 acre burn in compartment BB3 with a predicted Northerly wind. Ignition started at 12:00 and completed at 14:30. A simultaneous burn was conducted in another small compartment to the southeast. Proximity to a large UXO area allowed sampling only with one mobile unit and one stationary location with Truck 2 equipment. Truck 1 had very limited mobility due to lack of roads, but was able to position directly downwind of the burn.

The air sampling data collected at Fort Benning were quality assured and released for preliminary analysis and access by members of the research team. The $PM_{2.5}$ data from each zone are shown in Figure 45. The *x*-axis is time (not shown) starting approximately at ignition and continuing until approximately one hour after completion. The lidar data collected by the UMASS team were published separately as a technical abstract (Tsai et al., 2009).

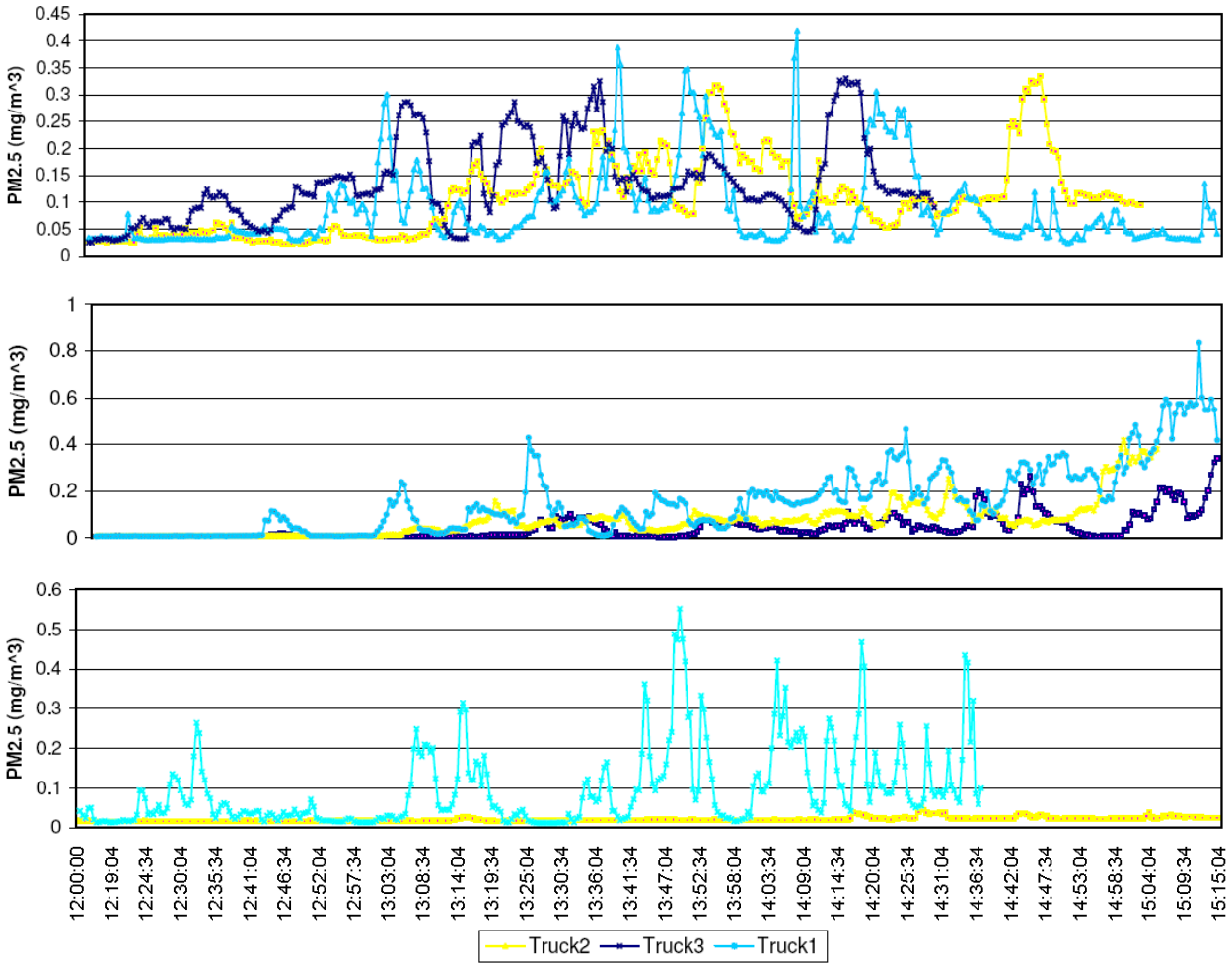

Figure 45. Real-time $PM_{2.5}$ measured by the three trucks downwind from the Fort Benning burns on 9 April (top), 14 April (center), and 15 April 2008 (bottom). Time is EDT.

4.3.2 Intensive Data Collection at Fort Benning and Analysis

In 2009, 8 prescribed burns were monitored at Fort Benning (Table 11). In five of the eight monitored burns ground-based smoke sampling was coordinated with plume height measurements with lidar ceilometer. Attempts to monitor were unsuccessful on 01/16/2009 due to a compartment location which did not allow for any road accessibility and on 01/22/2009 due to cancellation an hour before ignition for aerial photography monitoring being conducted in the area. For the January burns, the sampling pattern used by the trucks was similar to the one in 2008. Increasing the sampling distances of the trucks was attempted for the April 2009 burns.

Table 11. Burns monitored at Fort Benning in 2009.

Date	Burn Unit (s)	Burn Acreage	Ignition Begins	Ignition Ends	Coordinated with USFS	Notes
Jan. 13	O7	276	12:30	14:30	No	All 3 Trucks were able to set-up in the field. The normally sampling grid was not used due to very limited access. Instead all 3 trucks were spaced out in Zone 3.
Jan. 14	S1, S2, S3	309 (76,147, 86)	12:30	14:45	Yes	
Jan. 15	A9	583	12:15	14:00	Yes	
Jan. 20	O11	269	12:20	14:35	No	All 3 trucks were able to successfully monitor a full grid. Truck 1 was stuck in the mud from 14:30 till 15:00, which caused some unusual spikes on the $PM_{2.5}$ data during this time period.
Jan. 21	D15	364	12:30	14:45	Yes	
Jan. 23	I3	455	12:30	14:30	No	Fuel samples were collected before the burn. A second compartment was burned prior to monitored compartment. This earlier burn of 200 acres was conducted in compartment D16 and completed by 12:00.
Apr. 8	E2, E3	112, 127	12:30	13:30 and 15:00	Yes	Two burns were conducted in the same area, but with staggered ignition times.
Apr. 9	J6	383	12: 30	14:20	Yes	Truck #2 was located on a high open ridge during monitoring

Each truck was equipped with real-time $PM_{2.5}$ and CO monitors, as described in Section 3.3.1.2, for all monitored burns. The inlets for all monitors were set at an 8 foot sampling height on the bed of a truck. All monitors collect data in real-time and report samples in 30 second averages. Five of the eight sampling days were coordinated with the US Forest Service team, which operated a real-time weather station and a lidar ceilometer, and conducted photo imaging. After data collection, the recorded GPS locations of the sampling locations were visually analyzed on Google Earth and confirmed by truck drivers. A list of GPS coordinates for all samplers was generated and posted on the project website[2] for access by the members of the research team. Other relevant burn information, such as acreage and time since last burn, was obtained from the Bureau of Land Management at Fort Benning.

All the real-time air samples collected in 2009 were processed and quality assured. The data were first entered into spreadsheets and checked for validity. During this stage of analysis, data with outliers or other problems were removed. In addition, smoke spikes and outliers caused by reasons other than prescribed burning, as noted in data log sheets, were also removed prior to

[2] http://sipc.ce.gatech.edu

data analysis. For example, the data would be removed if the data log sheet indicated that an outside event such as truck movement or any other disturbance (e.g., vehicles passing by, grenade smoke, moving troops). After the analysis was completed, the real-time air sampling data were organized and posted on the project website.

4.3.2.1 Calibration of $PM_{2.5}$ from real-time measurement by EPA standard method

In order to make the recorded $PM_{2.5}$ values comparable to EPA's standard for measuring 24-hour $PM_{2.5}$, a real-time to gravimetric reduction ratio was used to adjust for the bias produced by the real-time monitors. The reduction ratio, 3.64, was generated from a similar study done by the laboratory at UGA during the 2007 wildfires in southeastern Georgia (unpublished). To obtain the real-time to gravimetric reduction ratio, six DustTrak monitors were used to measure concentrations at the same time and location on May 10, 2007, Fargo, GA. An average value was obtained from each of these monitors and a median concentration of 364.9 $\mu g/m^3$ was chosen as the benchmark value based on the six measurements. Second, an average value, 100.3 $\mu g/m^3$, was obtained from two concentrations obtained from the gravimetric method using PQ 200 filter method (EPA's required instrument for measuring $PM_{2.5}$) which was co-located temporally and spatially with the six DustTrak monitors during the same sampling period. The reduction ratio then was obtained by dividing 364.9 $\mu g/m^3$ by 100.3 $\mu g/m^3$.

4.3.3 Data Collection at Eglin AFB

The final field study, originally planned to take place in 2010, was postponed to 2011 in order to give the Technical Advisory Committee (TAC) a chance to review the model evaluation cycles performed thus far. After the In-Progress Review (IPR) meeting on May 7, 2010 the field study plan was revised in accordance with the TAC guidance. An extensive field study was conducted at Eglin AFB in February 2011 with new elements that did not exist in previous studies at Fort Benning. The new elements included a fuels study, more accurate ground-based sampling methods, aerostat-based measurements of emissions and winds, and aerial wind measurements with drones. A total of 3 burns were between February 6 and 12, 2011 using the extended sampling capability.

4.3.3.1 Aerostat based continuous measurements

Continuous results are presented in Figure 46 through Figure 49 as 2-min averages since the continuous PM sampler (Aerocet 531) has a 2 min sample interval. The sampling times and locations are summarized in . Increases in CO_2 track increases in PM, suggesting that concentration of the pollutants are correlated in our measurements. As most of the PM appears to be $PM_{2.5}$ or less in size, these particles tend to follow gaseous CO_2.

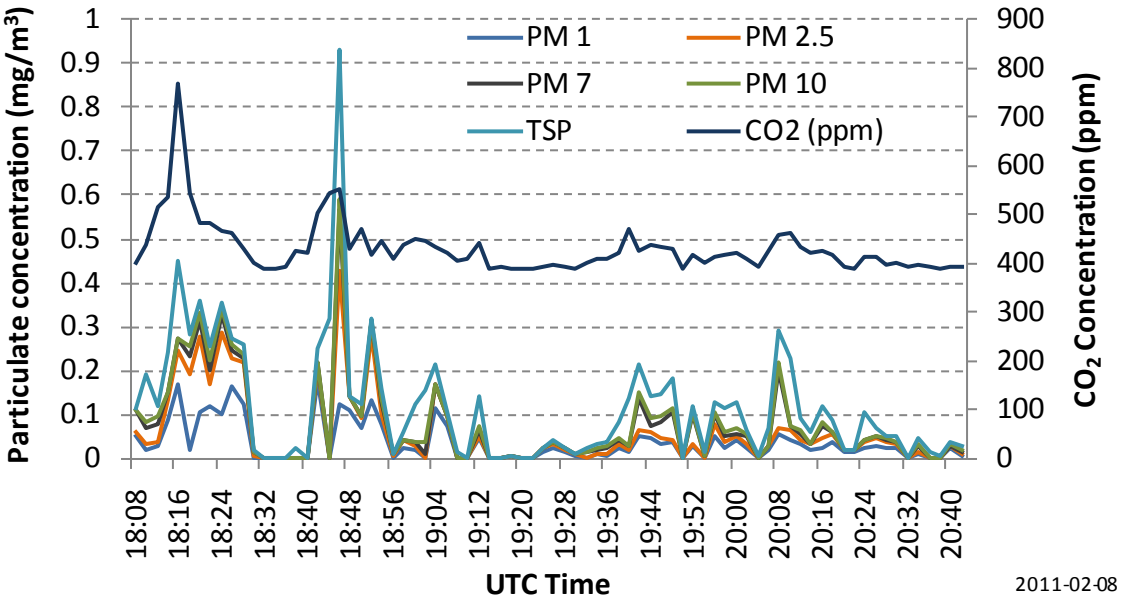

Figure 46. PM by size and CO_2 for 8 February 2011 burn at Eglin AFB.

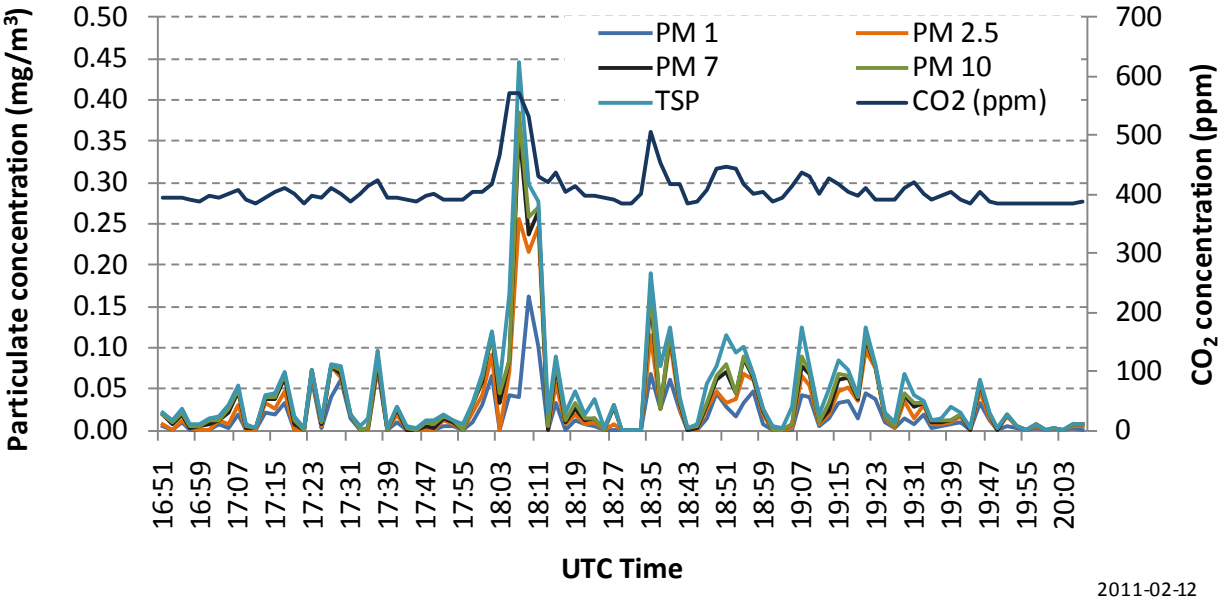

Figure 47. PM by size and CO_2 for 12 February 2011 burn at Eglin AFB.

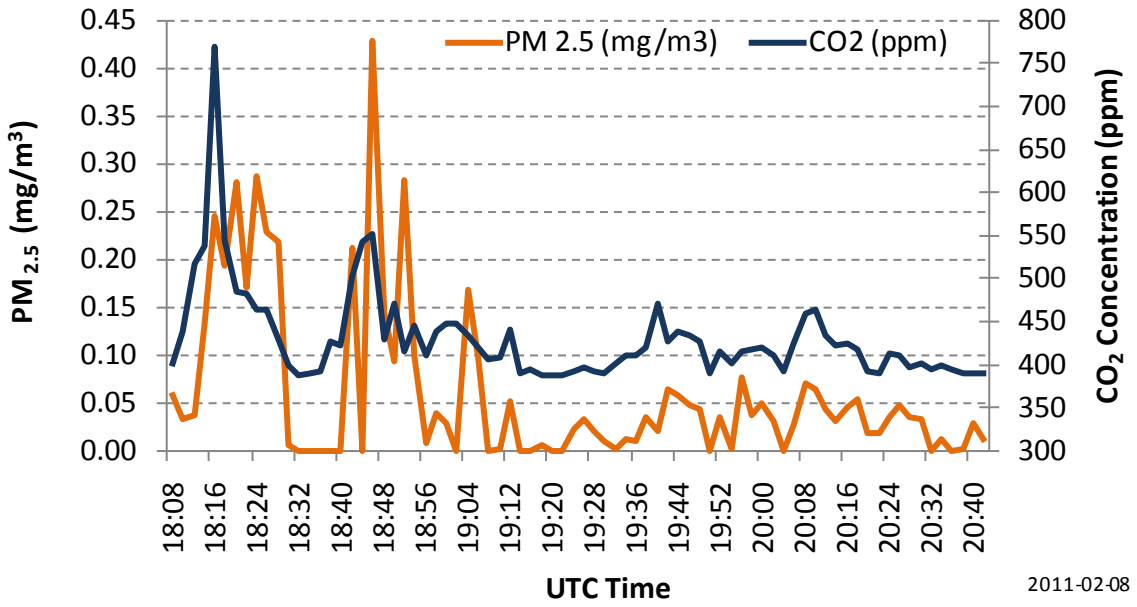

Figure 48. $PM_{2.5}$ and CO_2 for 8 February 2011 burn at Eglin AFB.

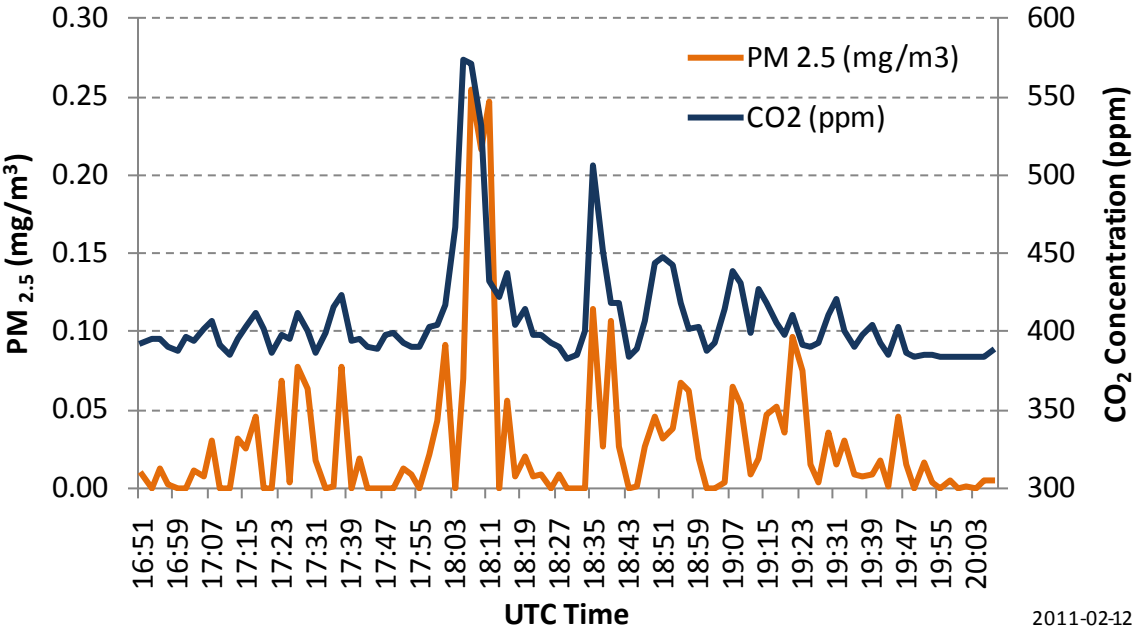

Figure 49. $PM_{2.5}$ and CO_2 for 12 February 2011 burn at Eglin AFB.

Table 12. Aerostat sampling times and initial locations.

Date	Matrix	UTC Time (hh:mm)		Initial	Initial Longitude
		Start	Stop	Latitude	
2/6/2011	Plume	18:09	20:26	30.51511	-86.84875
2/8/2011	Plume	18:11	20:42	30.63155	-86.27769
2/11/2011	Ambient air	14:55	19:11	30.53105	-86.79301
2/12/2011	Plume	16:50	20.07	30.53231	-86.79408

4.3.3.2 Anemometry results

The data presented here were collected during Aerostat flights at Eglin AFB. Wind velocities were measured by sonic anemometer lofted by the Aerostat. Corrections were applied for the motion and orientation of the dangling anemometer. These data were compared with the measurements of another anemometer on the ground and wind data from nearby airfields. The flights lasted between 2 and 4 hours and the aerostat height varied between 10 m and 400 m.

Figure 50 shows wind velocity, anemometer, and altitude data acquired on February 12, 2011 at EAFB. The topmost trace is the aerostat altitude measured by the MTi-G, the middle plot is the vertical velocity component, and the bottom trace is a plot of the magnitude of the horizontal wind $(V_N^2+V_W^2)^{1/2}$. Also plotted on the bottom trace are arrows that indicate the direction from which the wind is blowing. Changes in height are a result of maneuvering of the aerostat to maintain its position in the plume from the prescribed forest burn. The altitude of the aerostat was increased to match the plume height increase during the duration of the burn. The low wind speeds (<5 m/s) and changing wind direction in the Eglin AFB data represent stable to slightly unstable atmospheric conditions.

Figure 50. Wind data from February 12, 2011 burn at Eglin AFB. The blue trace represents the aerostat altitude as measured by the MTi-G. The red trace is the motion corrected and rotated vertical wind velocity component. The green trace is horizontal wind speed. The black arrows indicate the wind direction where up is north and left is west. The data are smoothed using a rolling average with a window of 60s.

Figure 51 demonstrates the ability of the MTi-G to quickly and reliably determine its orientation in the North-West plane despite potential interferences from onboard sampling equipment. The MTi-G uses magnetometers to determine its orientation in the North-West plane which, due to the weakness of the Earth's magnetic field, could give erroneous readings due to nearby magnetic fields from other sampling equipment on the DASS. The most likely source of magnetic interference is a semi volatile organic hydrocarbon (SVOC) sampling pump co-mounted on the aerostat for pollutant sampling. On Figure 51, "SVOC flow rate" indicates the operating status of this pump as well as other sampling equipment. When the flow rate departs from its baseline, the sampling equipment is operating and when it remains at the baseline, this equipment is not running (the sampling equipment is triggered by CO_2 levels).

Figure 51. Anemometer orientation (red), Aerostat tether angle (blue), and compass reference points (•) where zero corresponds to the anemometer facing north. The SVOC sampling flow rate (green) indicates the status of the onboard sampling equipment.

The MTi-G orientation in the North-West plane is directly output from the MTi-G in the form of the r_{31} and r_{32}, terms of the $\mathbf{R_{GS}}$ rotation matrix in Equation (17). These data were compared with handheld compass readings of the anemometer orientation logged manually every 30 s and the azimuth from the balloon to the tether point (*i.e.* the tether angle.) Real time aerostat tether angles were calculated from the GPS positions of the anemometer and the tether point using the Haversine equation (Gellert et al., 1989). The tether angle and anemometer orientation should agree as a result of the sail attached to the rear of the aerostat (see Figure 12.) This relationship is qualitative, however, since the aerostat is capable of rotating about the tether in low stability conditions. These rotations are observed as the spikes in the orientation data shown in Figure 51 at times 17:33, 17:34, and 17:41. Table 13 shows the compass readings and the 10 point (1 second) average of the MTi-G orientation evaluated at the same time. The differences between these values were averaged to determine the reported uncertainty of 5°. The orientation values determined at 17:35 were excluded from this calculation as the twisting of the balloon was noted during the measurement.

Table 13. Anemometer orientation and compass values for direct comparison.

Time (HH:mm:ss)	**Compass** (°CCW from N)	**MTiG Orientation** (°CCW from N)	Δ
17:33:30	100	100	0
17:34:00	35	27	8
17:34:30	10	16	6
17:35:30	10	7	3
17:36:00	5	10	5
17:36:30	10	1	9
17:37:30	15	5	10
17:38:00	10	12	2
17:38:30	20	18	2
17:39:00	23	17	6
17:39:30	25	25	0
17:40:00	32	26	6
17:40:30	15	16	1
17:41:00	10	7	3
17:41:30	8	7	1
17:42:00	2	3	1
17:42:30	8	13	5
17:43:00	8	6	2
17:43:30	2	27	25
		Average Difference:	**5°**

Figure 52 shows a plot of the aerostat wind velocities and altitudes averaged over 15 minutes with ground wind data acquired at a mast height of 10 meters. The green trace represents wind data acquired from a second R.M. Young 81000 3D sonic anemometer positioned on a 10 m mast near the tether point. These provide a direct comparison to the wind data acquired from the aerostat based anemometer. Data are only shown for February 8, 2011 due to the lack of suitable 10 m mast locations near the tether points on the other two days. The black arrows and points indicate wind direction and speed measured from a nearby airfield (ValParaiso/Eglin Airfield) on each sampling day. These data were acquired from the NOAA national climactic data center.[3] There is reasonable agreement between the airfield data and aerostat data. The aerostat measured wind speeds are higher than the 10 m tower data as expected. There is discrepancy between the NOAA wind direction and the aerostat wind direction on 2/06/11 of about 180 degrees. This

[3] www.ncdc.noaa.gov

indicates that, at least under unstable atmospheric conditions, wind data from nearby meteorological stations may not be an acceptable proxy for the plume transport velocities.

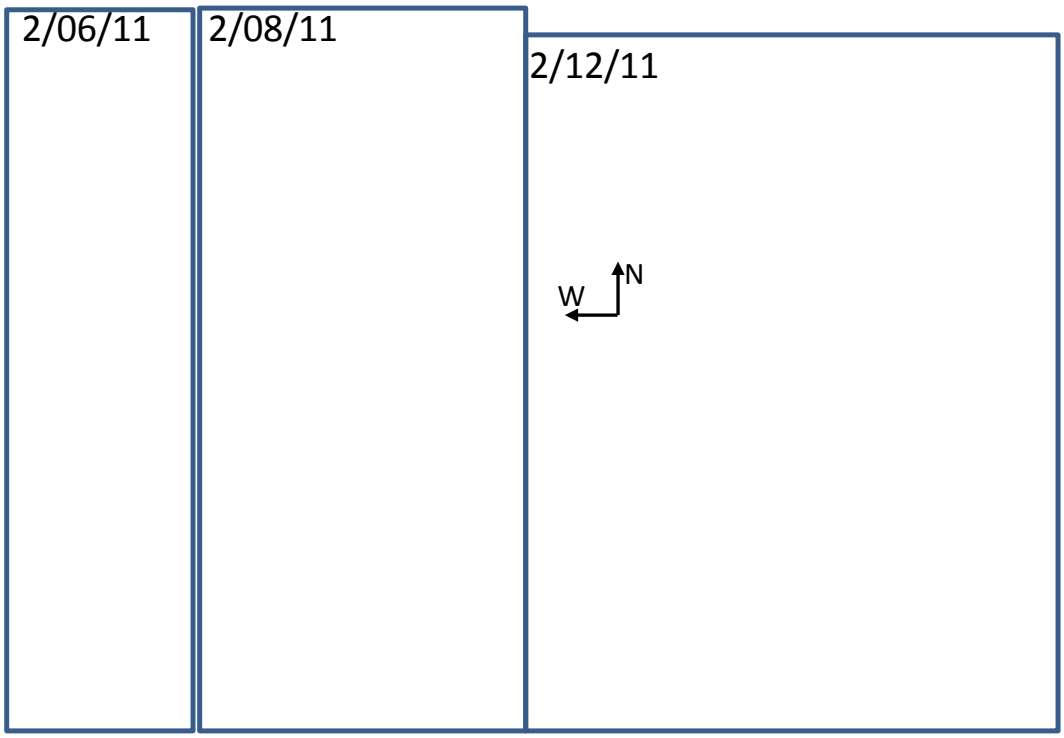

Figure 52. Wind directions plotted at the height and time of day acquired (bottom) and magnitudes (top) observed from the Aerostat based anemometer (blue), ground 3D sonic anemometer mounted to a 10 m tower (green), and 2D anemometer located at a nearby airfield reported to the NOAA weather archive (black). Arrows indicate the direction from which the wind is blowing where north is up and west points to the left.

4.3.3.3 Ground-based sampling results

Burn #1. For the first burn, February 6, 2011, the stationary site was set up approximately 4 km from the centroid of the burn unit in the downwind direction at the time of set up (Figure 53). However, at the time of burn ignition, the wind direction had shifted 12° to the east, and the stationary site was not directly under the plume. In addition, both mobile sites were out of position at their original locations and had to move to find the plume. Mobile site #2 (the furthest downwind) had to drive around a closed sector to find the plume and was eventually located 11 km downwind (much further than planned). For the first burn, both mobile sites were relying on mobile phones for communication, and reception was very poor at both locations. As a consequence, by the time the mobile sites had received updated information about plume

direction and relocated, both had missed the passage of the plume peak concentrations. On the other hand, the stationary site did record the passage of the plume (albeit not the center of the plume) and recorded a maximum black carbon concentration of 9 µg/m^3. The mobile sites did not observe black carbon levels higher than ambient concentrations (Figure 54), and similarly, filter analysis of EC-OC, WSOC, and SVOC were not informative.

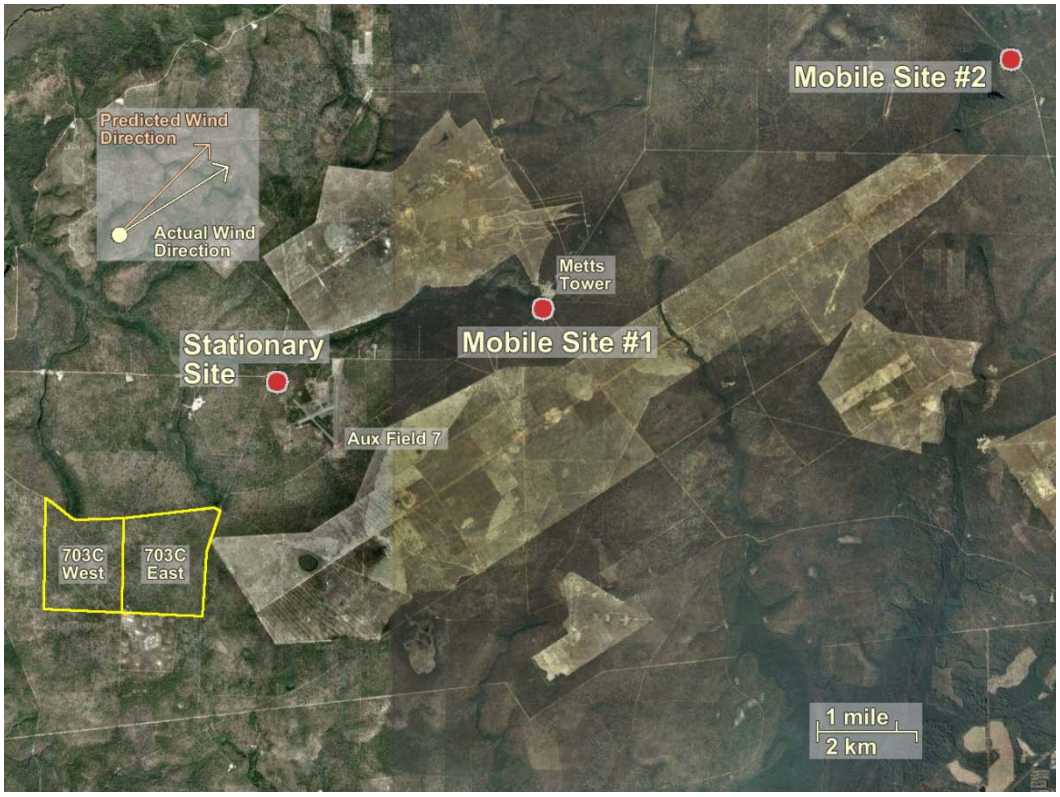

Figure 53. Location of burn area and sampling sites for burn #1 (February 6, 2011).

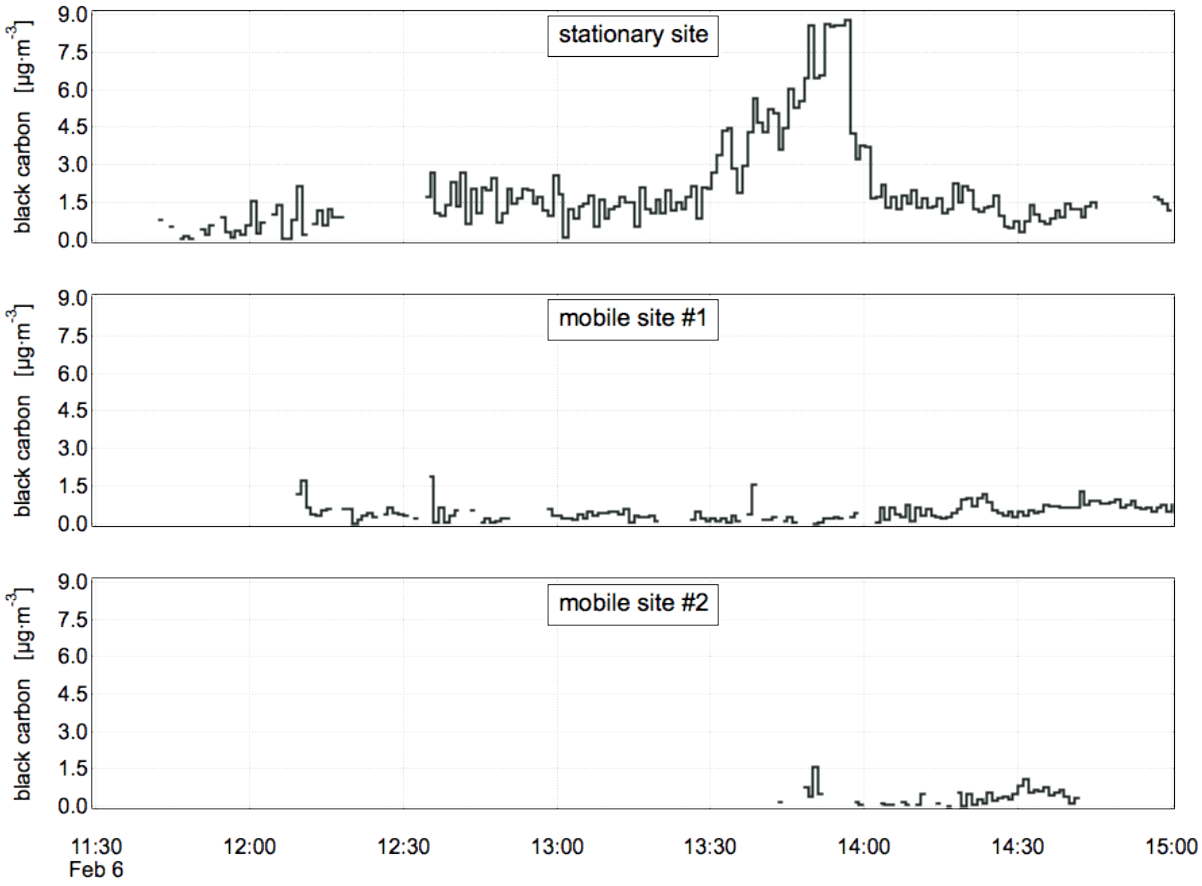

Figure 54. Black carbon concentrations at all three sampling sites for burn #1 at Eglin AFB (February 6, 2011).

Burn #2. For the second burn, February 8, 2011, the wind direction shifted 20° to the west from the predicted direction. The stationary site was set up 4 km south of the burn unit centroid, but once again, this site missed the peak of the plume (Figure 55). In addition, the area to the southwest of the burn was closed for Air Force missions, and the mobile units were unable to follow the plume into these areas. For this reason, both mobile units missed the plume centerline on the second burn as well. However, even at the edge of the plume, black carbon concentrations approaching 20 µg/m^3 were observed at all three sites (Figure 56).

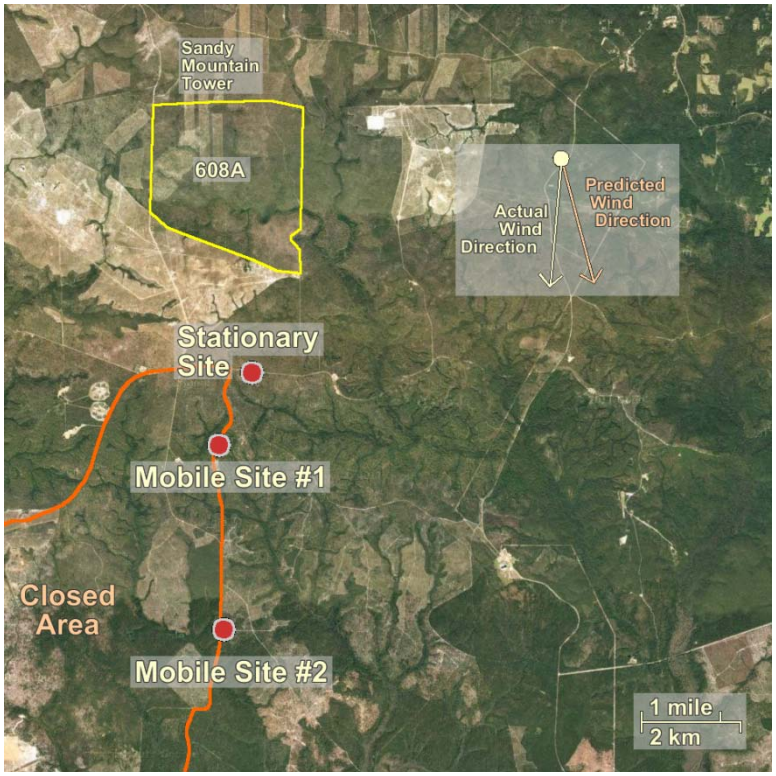

Figure 55. Location of burn area, restricted area, and sampling sites for burn #2 (February 8, 2011).

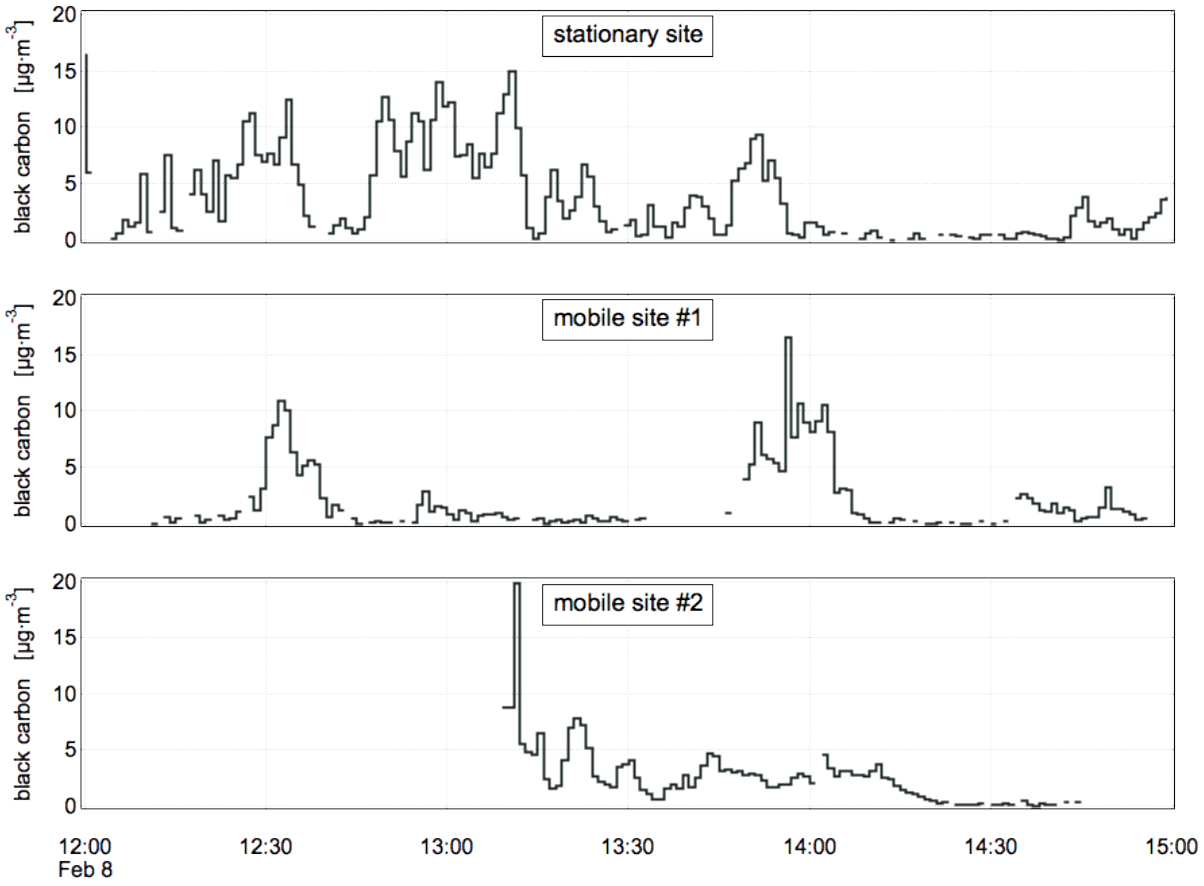

Figure 56. Black carbon concentrations at all three sampling sites for burn #2 (February 8, 2011).

Burn #3. The third burn, February 12, 2011, was the most successful in terms of plume sampling (Figure 57). Wind direction again deviated by 20° from the predicted direction, but travel of the mobile units was not restricted perpendicular to wind direction. On the other hand, they were restricted in the downwind direction and could be no further than 4 km from the burn unit. For this reason, mobile unit #1 was positioned between the stationary site and the burn and was only 1 km downwind of the fire. The stationary site was 2 km downwind, and mobile unit #2 4 km from the fire (Figure 58).

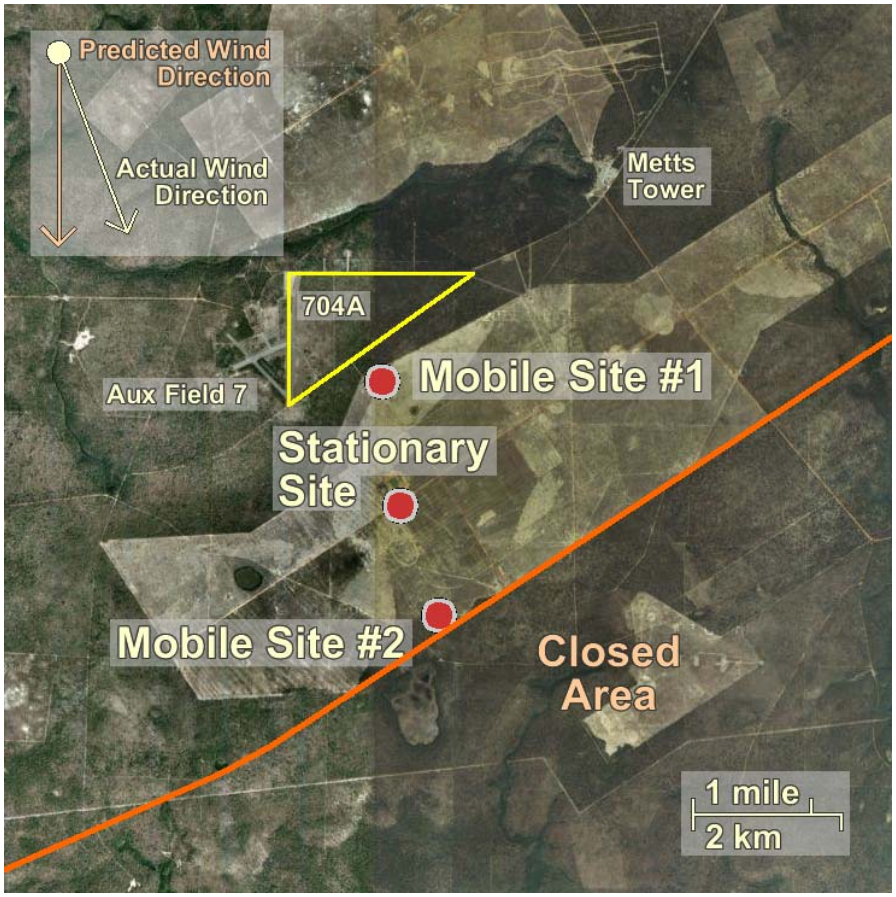

Figure 57. Location of burn area, restricted area, and sampling sites for burn #3 (February 12, 2011).

Figure 58. Photographic image of burn #3 (February 12, 2011) from mobile site #2 (4 km downwind).

Burn #3 was ignited by an ATV traveling across the burn unit perpendicular to wind direction, and repeated passage of the ignition vehicle is clearly observed in continuous measurements, especially those of the closest site, mobile unit #1 (Figure 59). Black carbon levels as high as 100 $\mu g/m^3$ were measured at this proximity to the fire, but values closer to 20 $\mu g/m^3$ were more typical for the sites further downwind. Continuous measurements of $PM_{2.5}$ mass peaked at 250 $\mu g/m^3$ at mobile unit #1, but were still greater than 50 $\mu g/m^3$ at the stationary site and mobile unit #2 (Figure 60).

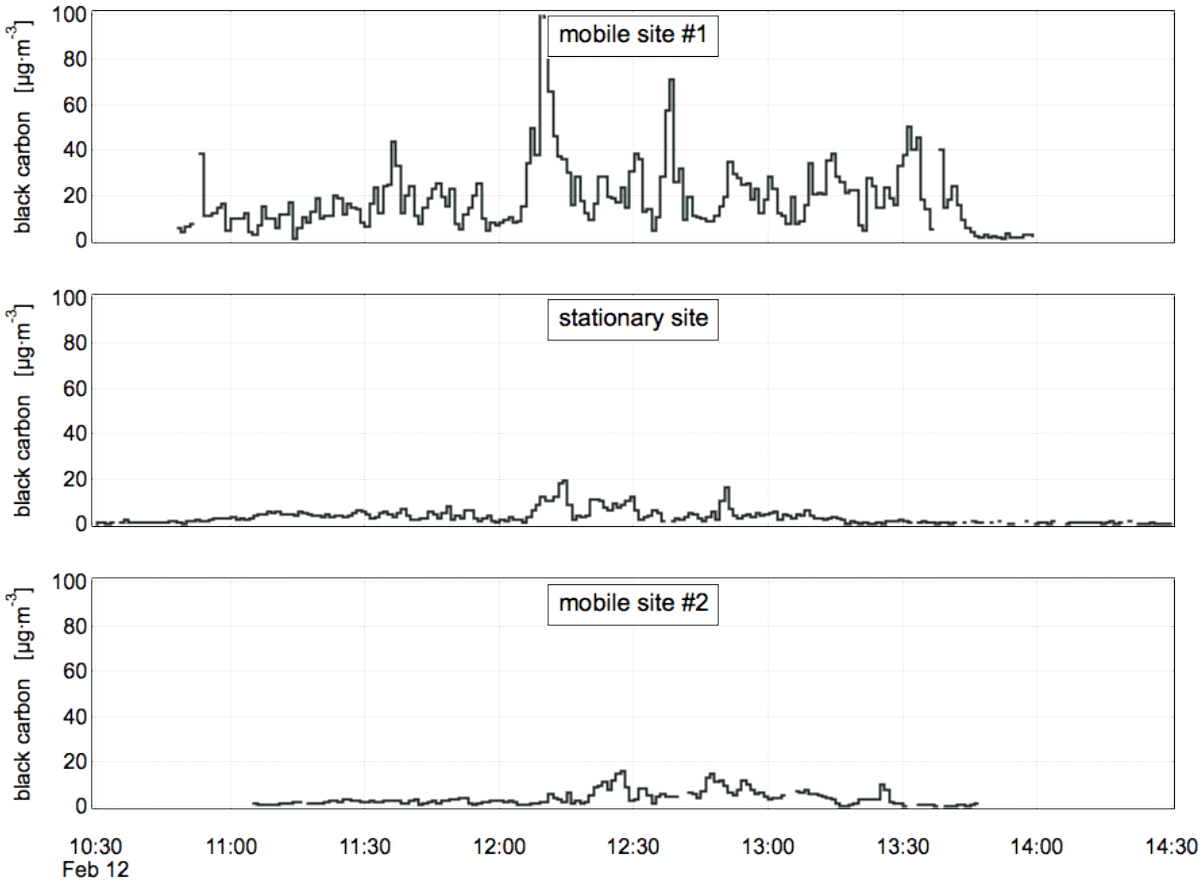

Figure 59. Black carbon concentrations at all three sampling sites for burn #3 (February 12, 2011).

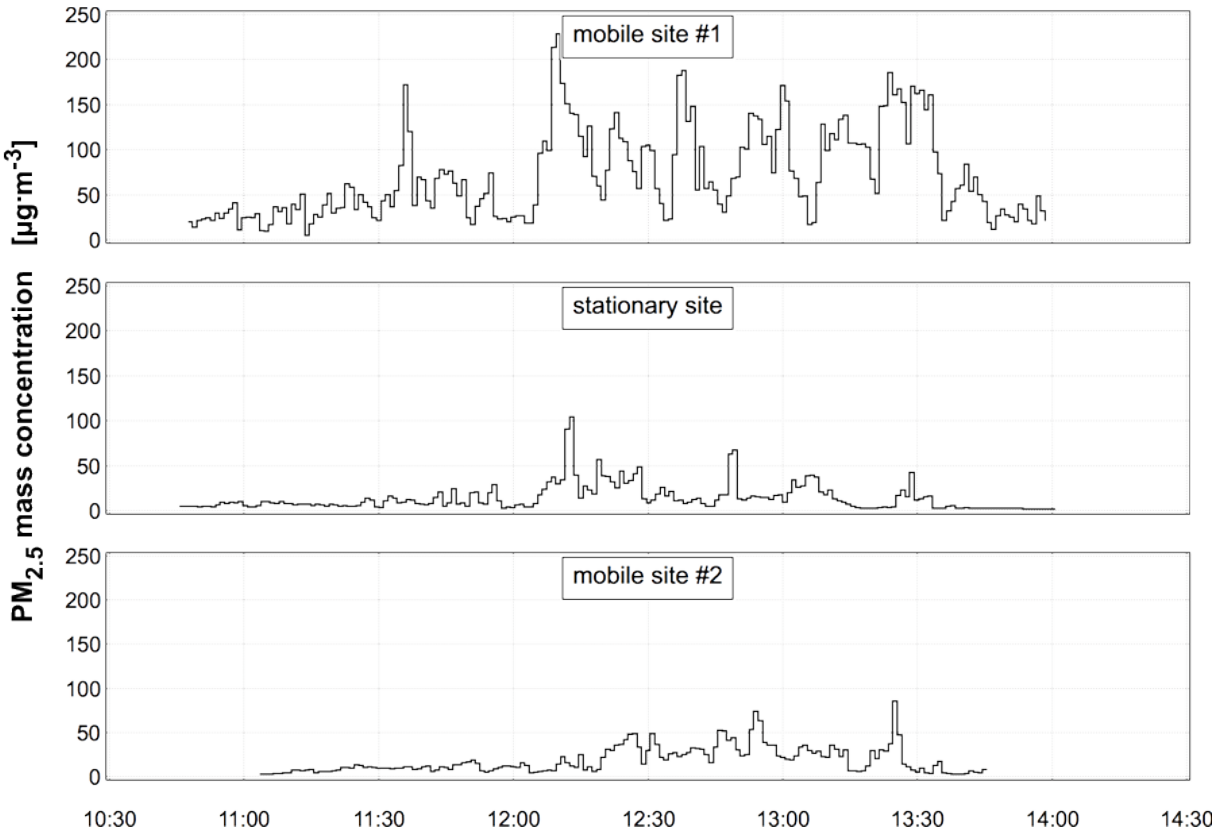

Figure 60. $PM_{2.5}$ mass concentrations at all three sampling sites for burn #3 (February 12, 2011).

SMPS measurements of the particle size distribution at the stationary site displayed simultaneous increases in the number concentration and the geometric mean diameter (Figure 61). As the plume periodically passed directly over the stationary site, the geometric mean diameter was 80-90 nm, but was 20-40 nm (a typical value for ambient PM) at non-burn times.

The concentration of EC and OC was at a maximum at 1 km from the burn, but did not display a significant gradient between 2 and 4 km. The EC concentration was 8.5 µg/m^3 at 1 km and was 1.4 and 1.8 µg/m^3 at 2 and 4 km respectively. The OC concentration was 45 µg/m^3 at 1 km, 5.2 µg/m^3 at 2 km, and 8.7 µg/m^3 at 4 km.

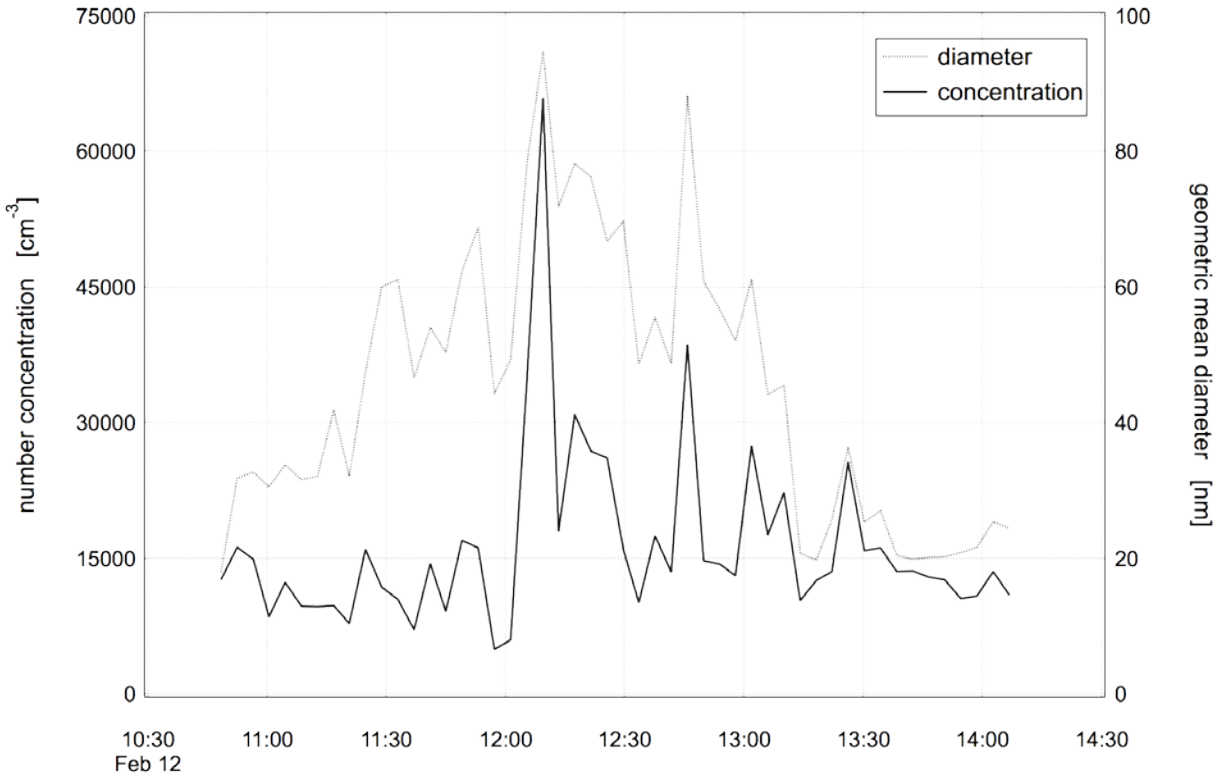

Figure 61. Particle number concentration and geometric mean diameter at the stationary sampling site for burn #3 (February 12, 2011).

4.4 Model Evaluation

Model evaluation was conducted in cycles. In order to capture the progress made in each cycle this section is organized as follows: 1) initial evaluation, 2) re-evaluation with new data, and 3) final evaluation with other data.

4.4.1 Initial Evaluation

Initial evaluation cycle encompassed evaluations of the dispersion model Daysmoke and chemistry-transport model CMAQ. The 9 April 2008 burn monitored at Fort Benning is used as the evaluation case.

4.4.1.1 Initial Evaluation of Dispersion Model

In 2008, smoke data were collected at Fort Benning on April 9, 14, and 15. Initially, Daysmoke was tested with the 9 April data sets only. On this day, winds blew from the southeast taking smoke over Columbus with a possible smoke signal at a PM sampler located at the airport. Some photographical data were obtained and lidar measurements of the smoke plume were taken by a team from the University of Massachusetts Amherst (UMASS).

Daysmoke was evaluated with plume height measurements from the UMASS lidar, and $PM_{2.5}$ concentrations collected by mobile ground-based samplers. Figure 62 shows the UMASS ceilometer (lidar) measurements for 9 April 2008. The ceilometer was located 1-2 km downwind. Dark blue in the plot is background aerosol; lighter blues and green are the smoke. Ignition was at 1200 EDT. The plume height increased from near 700 m initially to about 1200 m by 1500 EDT most likely responding to growth in the height of the mixing layer. Clouds formed once PBL depth reached 1.3 km (red in plot). From the UMASS team's vantage point, it looked like the burn produced these clouds but since there were other clouds around, this cannot be confirmed.

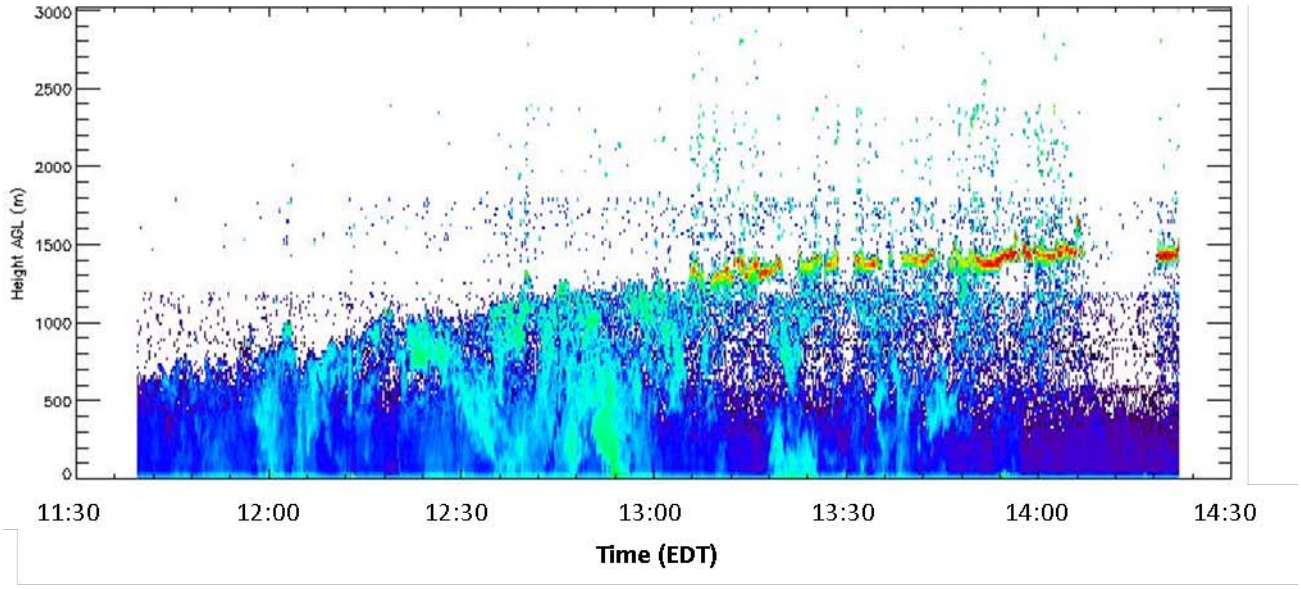

Figure 62. UMASS ceilometer measurements for a Fort Benning burn on 9 April 2008.

Figure 63 (upper panel) shows a vertical view of a 4-core updraft Daysmoke plume (photographs reveal a multiple-core plume) at approximately 1230 EDT. Daysmoke was initialized with WRF weather data. The horizontal line gives the mixing height at 580 m with the Daysmoke plume top at about 700 m. At 1500 EDT (lower panel), the mixing height from WRF is at 1000 m. The Daysmoke plume is confined below this level and subject to intense large eddy mixing. These results compare favorably with the UMASS lidar measurements.

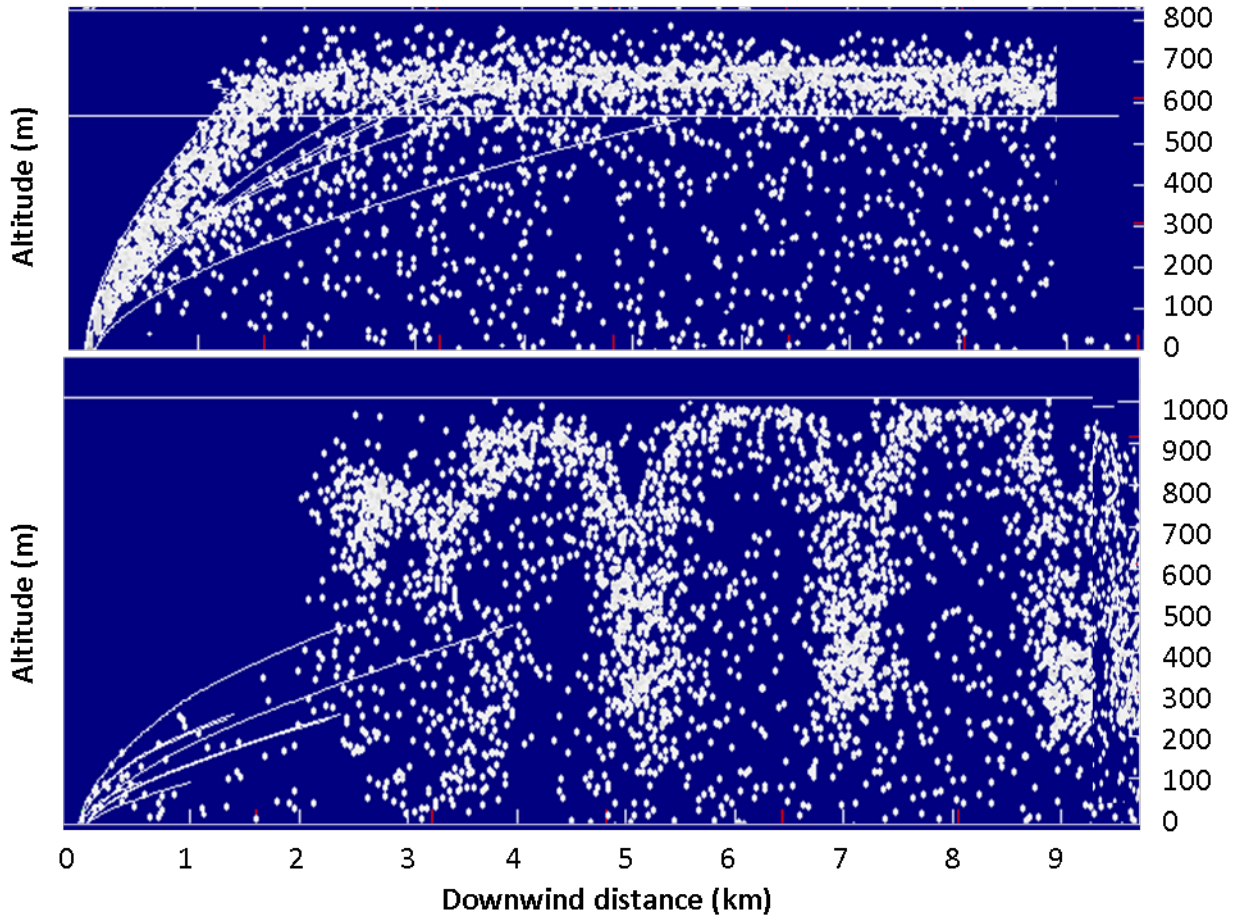

Figure 63. Side views of Daysmoke solution for a 4-core updraft plume. Upper panel – 1230 EDT; lower panel – 1500 EDT.

Figure 64 shows the real-time $PM_{2.5}$ measurements from three mobile trucks located 1-3 km (Truck 1), 3-5 km (Truck 2), and 5-7 km (Truck 3) downwind from the burn. In general, the figure shows $PM_{2.5}$ concentrations exceeding 100 μg m^{-3} for most of the burn with peaks in the range of 250 to 400 μg m^{-3} at all three truck sites. Note that DustTrack $PM_{2.5}$ monitor readings were not calibrated by the reduction ratio of 3.64 described in Section 4.3.2.1 at the time. However, these concentrations can be compared qualitatively with hourly $PM_{2.5}$ concentrations at the Truck 1 and Truck 2 sites as modeled by Daysmoke.

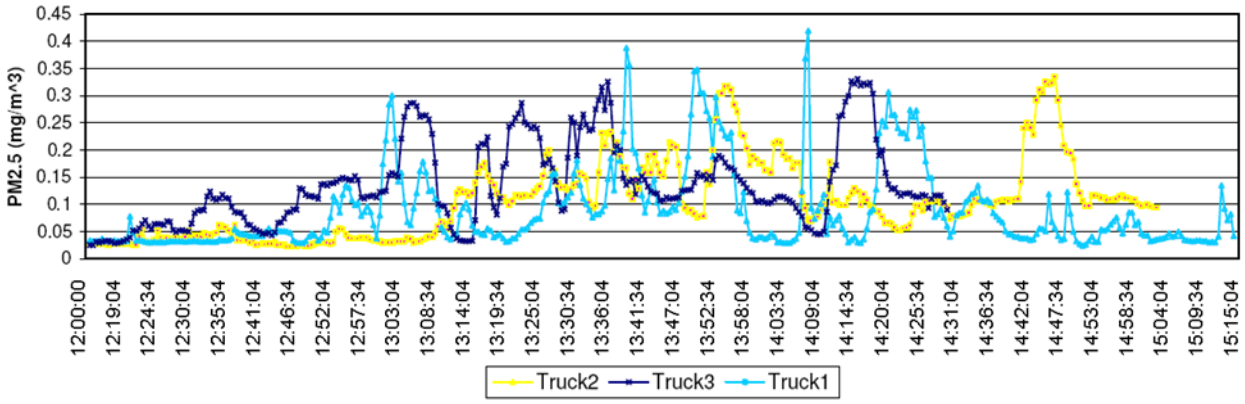

Figure 64. Real-time $PM_{2.5}$ measured by the three trucks downwind from the Fort Benning burn on 9 April 2008. Time is EDT.

Table 14 shows Daysmoke modeled $PM_{2.5}$ concentrations for five locations downwind from the 9 April 2008 burn. Note that the last two columns of each panel carry concentrations for Truck 1 and Truck 2 respectively. The 1-core solution (top left panel) exhausts most smoke from the mixing layer thus producing almost no $PM_{2.5}$ at either truck site. The 3-core and 4-core solutions (see Figure 63 for the 4-core solution) exhaust most smoke above the mixing layer but retain sufficient smoke within the mixing layer to produce $PM_{2.5}$ concentrations in the range estimated from the observations (Figure 64). The 10-core solution (bottom right panel Table 14) confines most smoke to the mixing layer and produces hourly smoke concentrations far in excess of the observed.

Table 14. Daysmoke modeled hourly $PM_{2.5}$ concentrations at five sites downwind from the 9 April 2008 burn. The four panels show results for four different choices of the number of updraft cores.

1 <-- plume core number

	1 <-- burn number				
12:00:00	0	0	0	0	2
13:00:00	0	0	0	0	10
14:00:00	2	0	0	0	0
15:00:00	26	1	0	6	0
16:00:00	7	30	26	0	0
17:00:00	0	0	0	0	0
18:00:00	0	0	0	0	0

3 <-- plume core number

	1 <-- burn number				
12:00:00	0	0	0	45	57
13:00:00	0	0	0	50	126
14:00:00	22	5	0	12	30
15:00:00	26	9	0	6	2
16:00:00	7	29	21	0	0
17:00:00	0	0	0	0	0
18:00:00	0	0	0	0	0

4 <-- plume core number

	1 <-- burn number				
12:00:00	0	0	0	95	140
13:00:00	0	0	0	132	168
14:00:00	49	8	0	19	28
15:00:00	26	15	3	6	2
16:00:00	2	43	23	0	0
17:00:00	0	0	4	0	0
18:00:00	0	0	0	0	0

10 <-- plume core number

	1 <-- burn number				
12:00:00	0	0	0	321	236
13:00:00	0	0	0	561	420
14:00:00	11	19	0	289	221
15:00:00	11	23	11	23	8
16:00:00	0	28	41	0	0
17:00:00	0	0	0	0	0
18:00:00	0	0	0	0	0

4.4.1.2 Initial Evaluation of Chemistry-Transport Model

On 9 April 2008, southeasterly winds carried the PB plume to Columbus, GA presenting an opportunity to compare chemistry-transport model predictions with observations of $PM_{2.5}$ and O_3 at the metropolitan airport. The impact of the plume can be seen in observations with a $PM_{2.5}$ peak of 22 $\mu g\ m^{-3}$ at 18:00 and an O_3 peak of 54 ppb at 17:00 (Figure 65).

The fuel consumption estimate for the plot burned on 9 April 2008 is 4.4 tons per acre. Recall that the area of the burn unit was 300 acres. From these inputs, total emissions were estimated as 100 Mg of CO, 14 Mg of $PM_{2.5}$, 2.4 Mg of NO_x and 3.4 Mg of VOCs. Hourly emissions were also estimated starting with ignition at 12:30 EDT. Emissions peaked during the flaming phase, which ended at 14:45 EDT, and continued during the smoldering phase. A meteorological hindcast was produced using WRF. Air quality simulations were conducted using the CMAQ model (AG-CMAQ without grid adaptation) with and without fire emissions. The difference between the air quality predictions from these two simulations is attributed to the PB. Horizontal grid resolution of 4 km and 1.33 km were tried. The use of finer resolution (1.33 km) resulted in better agreement with the both meteorology and air quality observations.

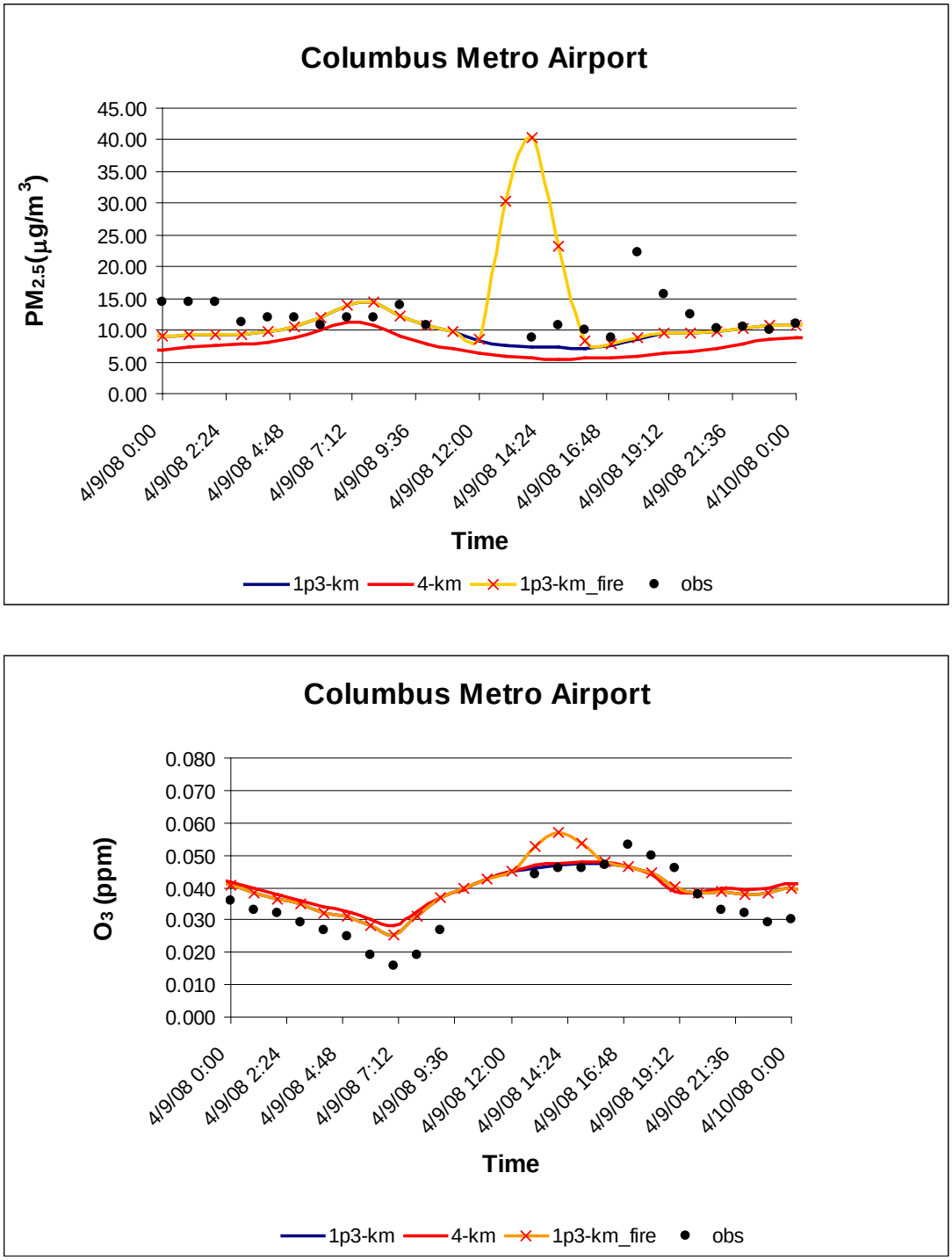

Figure 65. $PM_{2.5}$ (top) and O_3 (bottom) concentrations at Columbus Metro Airport on 9 April 2008. CMAQ model predictions with 1.33-km and 4 km resolutions without fire emissions and 1.33-km resolution with fire emissions are compared to observations.

The model predicts a $PM_{2.5}$ peak of 40 µg m^{-3} and an O_3 peak of 57 ppb both at 14:00 (Figure 65). The predicted $PM_{2.5}$ and O_3 impacts of the PB plume are 33 µg m^{-3} and 10 ppb, respectively.

These impacts are over predicted with an early time of occurrence. One possible reason is over prediction and fast release of estimated PB emissions. The sensitivity of model predictions to various emissions parameters will be evaluated to check this hypothesis.

4.4.2 Re-Evaluation with New Data

Re-evaluation included the evaluation of Daysmoke with data collected at Fort Benning in 2008 and 2009, and the evaluations of AG-CMAQ and the coupled modeling system (AGD-CMAQ) using the Atlanta Smoke Incident of February 28, 2007. Note that Atlanta Smoke Incident is a historic case; "new data" refers to acquired data, previously unavailable to the research team.

4.4.2.1 Re-Evaluation of Dispersion Model

The meteorological simulations of the April 9-15, 2008, January 13-23, 2009 and April 8-9, 2009 periods were performed using the Weather Research and Forecasting (WRF) model. WRF was set up with 1.333-km horizontal resolution and 34 unevenly spaced layers in the vertical, starting with 18-m resolution at the surface, using 10 layers below 1000 m, and extending up to an altitude of 18.2 km. Hourly profiles of the wind speeds and wind directions were extracted at the centroid of the burn unit and input to Daysmoke at WRF's vertical resolution.

The emissions were estimated as described in Section 4.1.2. All the burns were simulated using Daysmoke and the modeling results were compared to the field data collected at the truck locations (Section 4.3.2). The objective of this analysis was to evaluate Daysmoke and confirm the experimental design. The analysis focused on risk of contamination, the positioning of the trucks, accuracy of DustTrak readings, analysis of time averaged data, and discussion of discrepancies between observations and model. Here, highlights from the analysis of the April 9, 2008 and January 15, 2009 burns will be presented. Detailed analyses of all the other burns can be found in Appendix A.

4.4.2.1.1 Re-Evaluation of Daysmoke with April 9, 2008 Burn at Fort Benning

Three trucks were positioned at distances roughly 1.5 mi, 3.0 mi, and 4.0 mi (2.4, 4.8, and 6.4 km) downwind from the 300 acre 9 April 2008 burn. The experiment was designed so that the trucks could be moved if and when wind shifted to blow smoke in different directions. The coordinates of truck locations were recovered from GPS units, plotted on Google Earth, and compared to notes and map markings kept by drivers. When necessary, adjustments were made to better match locations of clearings next to roads where trucks were parked and to reduce the uncertainty in measurement locations.

The positions of the three trucks are numbered and color-coded in Figure 66. Truck 1 (blue), initially 2.2 mi (3.5 km) from the burn centroid and co-located with the UMASS lidar (point 10) from 1112 – 1233 EDT, was stationed closer to the burn (1.4 mi, 2.3 km) from 1240 – 1312 EDT, then moved to point 3 2.5 mi (4.1 km) from the burn from 1325 – 1413 EDT. Truck 2 (yellow), initially at point 4 - (3.9 mi, 6.2 km) from the burn centroid at 1153 EDT, was moved to point 5 (4.2 mi, 6.7 km) at 1245 EDT where it remained until 1424 EDT. Truck 3 (red) was positioned at four locations during the burn: point 6 (5.0 mi, 7.9 km) at the southern edge of the

Daysmoke-simulated plume (white line), point 7 (4.2 mi, 6.7 km), point 8 (4.8 mi, 7.7 km), and point 9 (4.7 mi, 7.6 km). Truck 3 was at the first location from 1200 – 1230 EDT, left the second location at 1315 EDT, and departed the third location at 1405 EDT.

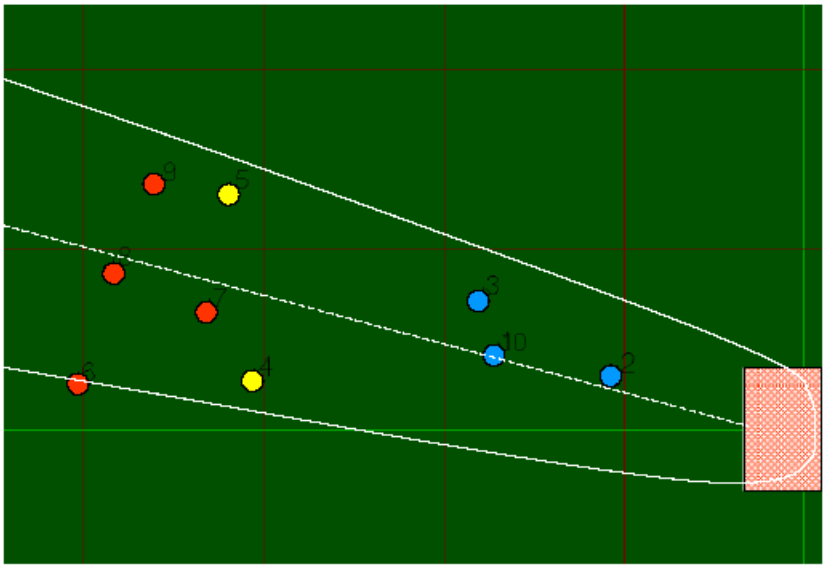

Figure 66. Locations of the three $PM_{2.5}$ collection trucks (blue, yellow, and red circles) and the University of Massachusetts radar/lidar van (point 10) relative to the 9 April 2008 burn site (hatched area) at Fort Benning, GA. The white curve gives the boundaries of the Daysmoke-simulated smoke plume at 1300 EDT. Each square is 1 mi (1.6 km).

4.4.2.1.1.1 Risk of contamination of data

Two DustTrak $PM_{2.5}$ samplers per truck were turned on at approximately the time of ignition and were turned off shortly after ignition was complete. Once the trucks were in position, the engines were turned off. However, there existed risk of contamination by vehicle exhaust and road dust during the period of time when the trucks were moved. The samplers were placed in the trucks so that their inlets would be 8 ft (2.4 m) above ground. This provided an approximate 3 ft (1 m) clearance of the truck cabs thus placing the inlets in the air stream above the trucks during transport. Though there existed risk of contamination during transport, the greatest risk of contamination would have occurred when trucks were moved with the wind and the wind could blow contaminants back over the trucks. Figure 66 shows that movement of Truck 1 from point 2 to point 3 and Truck 3 from point 7 to point 8 would have incurred greatest risk of contamination.

The upper panel of Figure 67 shows the 30-sec $PM_{2.5}$ record for Truck 1. Data were eliminated from the record for the period of transport (lower panel). Comparison between the panels shows a relative minimum in the record during the first transport after 1233 EDT. Transport during the higher risk point 2 to point 3 after 1312 EDT was done beginning at a relative minimum in the record and ended during a maximum which persisted for several minutes after Truck stopped at

point 3. Neither transport produced signals in the $PM_{2.5}$ record that could be judged as out-of-character for smoke.

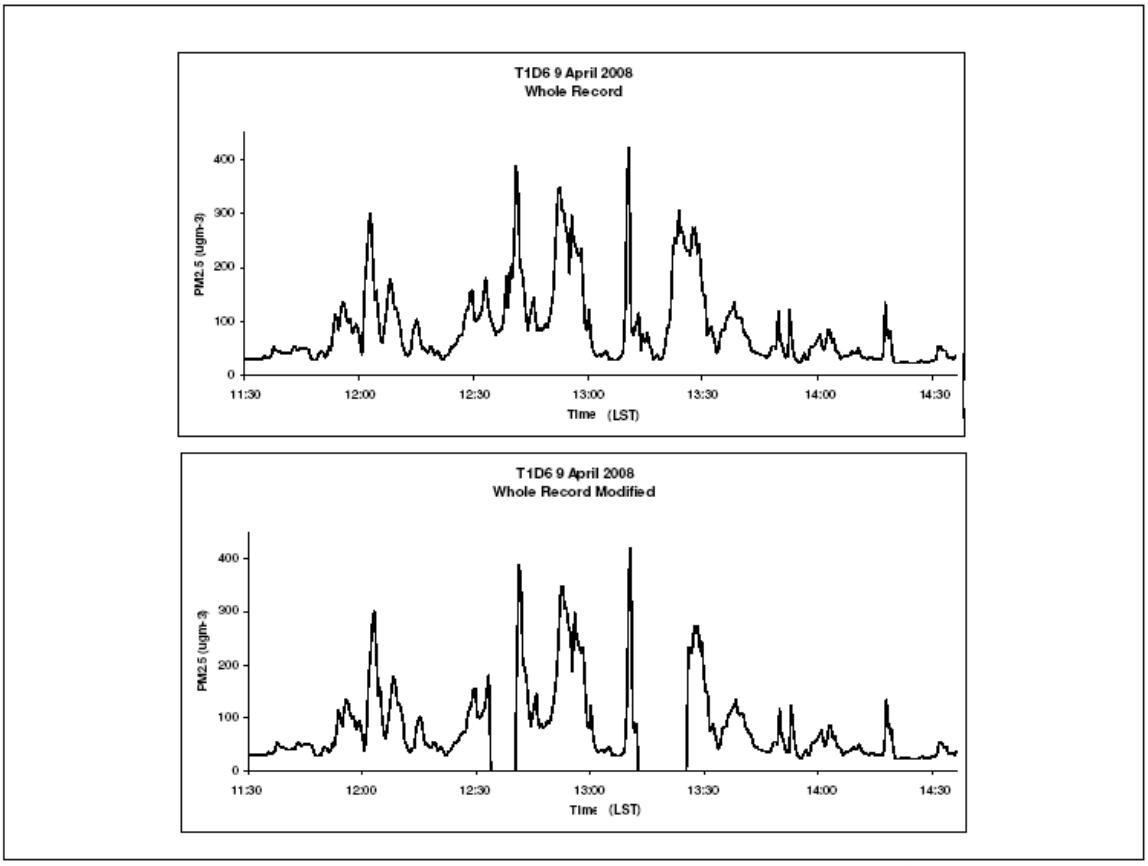

Figure 67. For the 9 April 2008 prescribed burn - Upper panel: The complete Truck 1 DustTrak record (30 sec intervals) for the locations shown in Figure 66 (blue). Lower Panel: Same as the upper panel except data collected during truck transport has been deleted from the record.

Figure 68 shows the $PM_{2.5}$ record for Truck 3 along with gaps during transport. Given the magnitude of variability in the smoke record, it is hard to make a case for contamination for the first transport (gap after 1230 EDT) and the third transport (gap centered at 14:00 EDT as the peak in $PM_{2.5}$ after 14:00 was also observed by Truck 2. The $PM_{2.5}$ peak during the second transport was suspect as it was contained within the gap. Furthermore, the second transport from point 7 to point 8 (Figure 66) was identified as having greatest risk for contamination. Truck 3 traveled against the wind at departing point 6 (red dot at the lower-right of Figure 69) then went cross-wind to the main road. Truck 3 went with the wind along the main road a distance of 0.44 mi (0.70 km) before turning cross-wind to its destination at point 8.

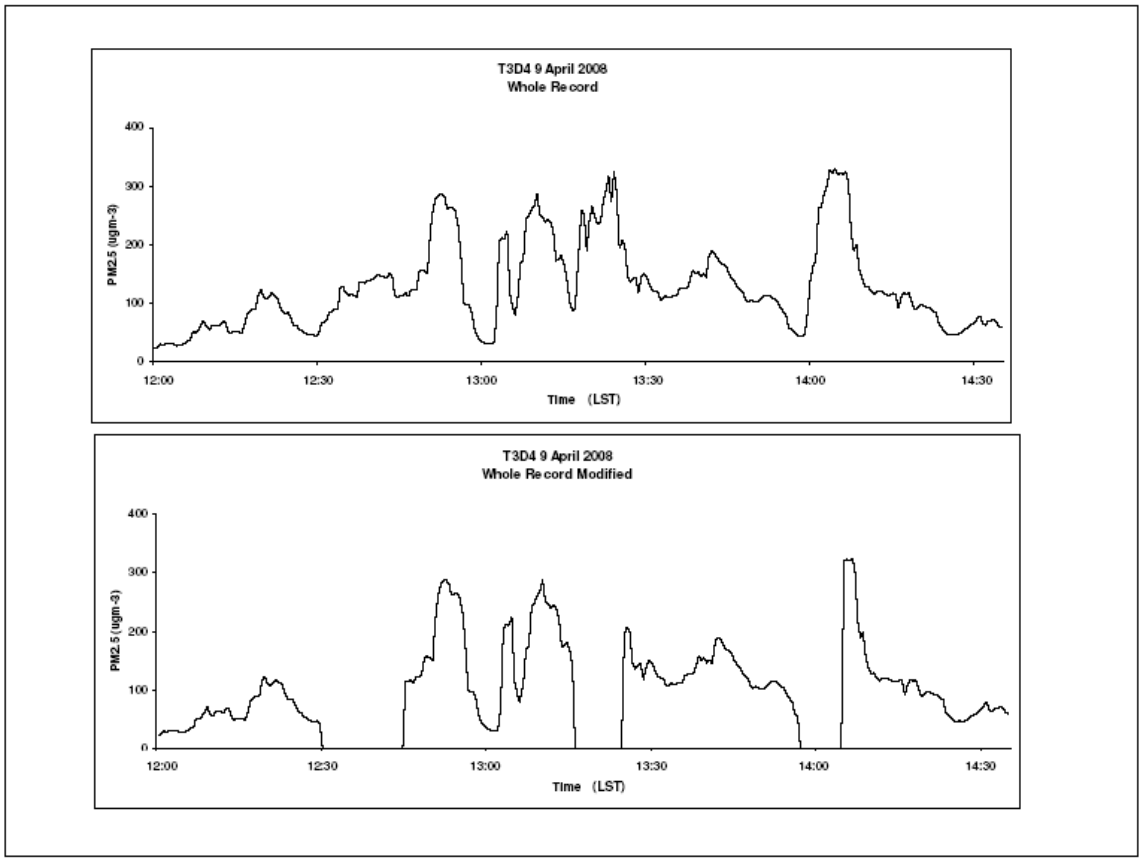

Figure 68. For the 9 April 2008 prescribed burn at Fort Benning- Upper panel: The complete Truck 3 DustTrak record (30 sec intervals) for the locations shown in Figure 66 (red). Lower Panel: Same as the upper panel except data collected during truck transport has been deleted from the record.

Figure 69. Google Earth map showing path of Truck 3 during transport from point 7 (red dot at bottom-right) to point 8 (red dot at top-left) during the 9 April 2008 burn at Fort Benning.

Clearly, the path along the main road placed Truck 3 in high risk of contamination. However, we don't know the magnitude of the contamination and therefore cannot assess its significance to the $PM_{2.5}$ record. Given the magnitudes of the peaks in the smoke record prior to the second transport, there is no reason to assume that the peak in the signal during transport was not the result of Truck 3 passing through dense smoke. Contamination, if any, may be represented by the 20-50 μgm^{-3} spikes superimposed on a smoke signal of amplitude 200 μgm^{-3}.

4.4.2.1.1.2 Creating the Daysmoke $PM_{2.5}$ records

The $PM_{2.5}$ records shown in Figure 67 and Figure 68 were obtained while the trucks were at different locations during the burn. Comparative records were created by Daysmoke in the following way. Continuous records of five-minute averaged $PM_{2.5}$ were obtained from 6-core updraft and 8-core updraft plume Daysmoke simulations at each location shown in Figure 66 during the course of the burn. Then, with the aid of periods of record reported by field crews, segments of the Daysmoke-generated $PM_{2.5}$ records were assembled to give complete model records for each truck. Figure 70 compares the 5-minute averaged observed $PM_{2.5}$ record (upper panel) with two 5-minute averaged 6-core Daysmoke solutions (lower panel). $PM_{2.5}$ mostly ranges between 100- 200 μgm^{-3} with peaks from 200-300 μgm^{-3}. The observed record shows greater variability in amplitudes and frequency than do the Daysmoke records.

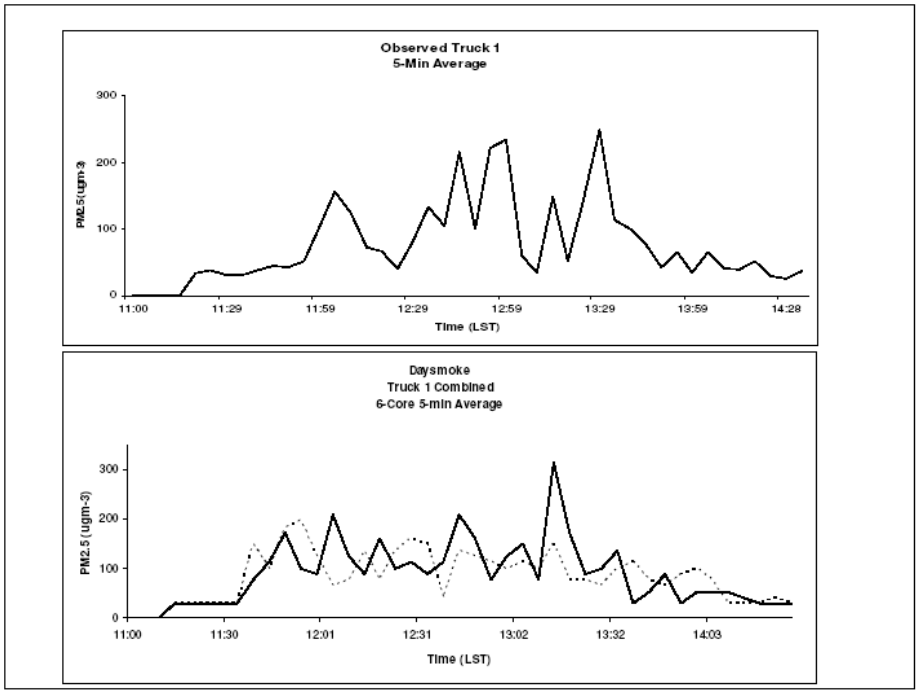

Figure 70. For the 9 April 2008 prescribed burn at Fort Benning- Upper panel: 5-minute averaged $PM_{2.5}$ observed at Truck 1. Lower panel: 5-minute averaged $PM_{2.5}$ for two runs with Daysmoke assembled at Truck 1 locations.

The Truck 2 6-core Daysmoke simulations (Figure 71) underestimate $PM_{2.5}$ concentrations in comparisons with the 5-minute averaged observed record. Furthermore, the Daysmoke simulations do not pick up the concentration maximum occurring after 1400 EDT. Truck 3 6-core Daysmoke simulations (Figure 72) better capture observed smoke concentrations but still fail to pick up the concentration maximum occurring after 1400 EDT.

The small scale peaks in the Daysmoke simulation pairs show little correlation with small scale peaks in the observed record. The timing and magnitudes of these peaks are the outcomes of vertical smoke transport through stochastic mixing in Daysmoke. The stochastic terms are set so that solutions cannot be repeated. Therefore, the timing and magnitudes of the small scale peaks have no physical significance other than that peaks of the magnitudes simulated are possible.

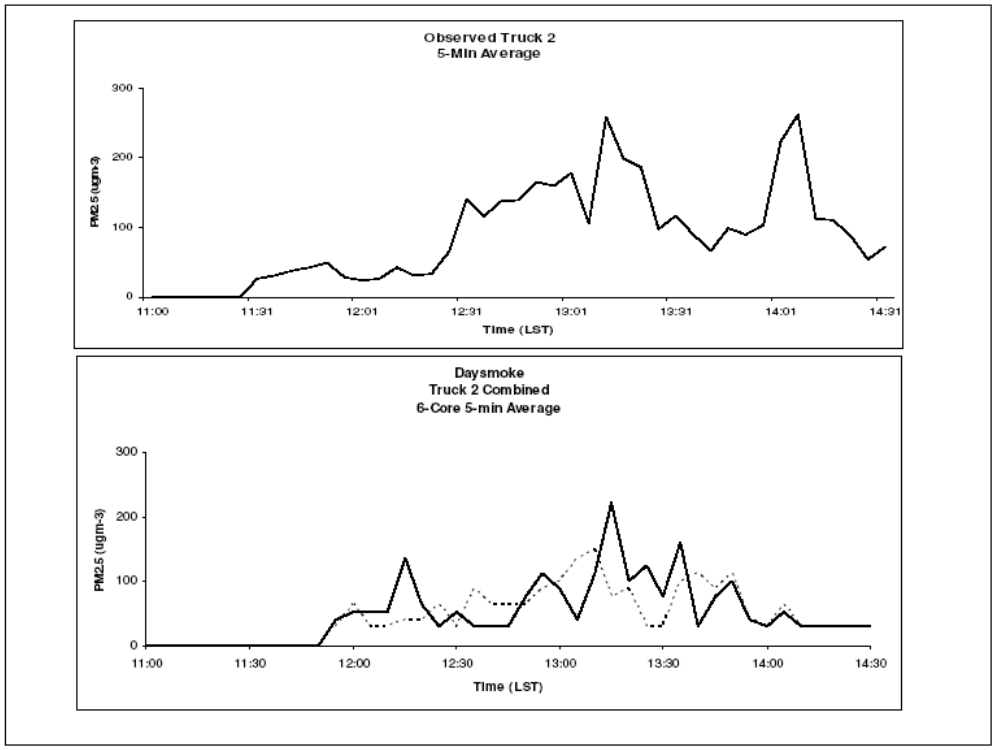

Figure 71. Same as for Figure 70 but for Truck 2.

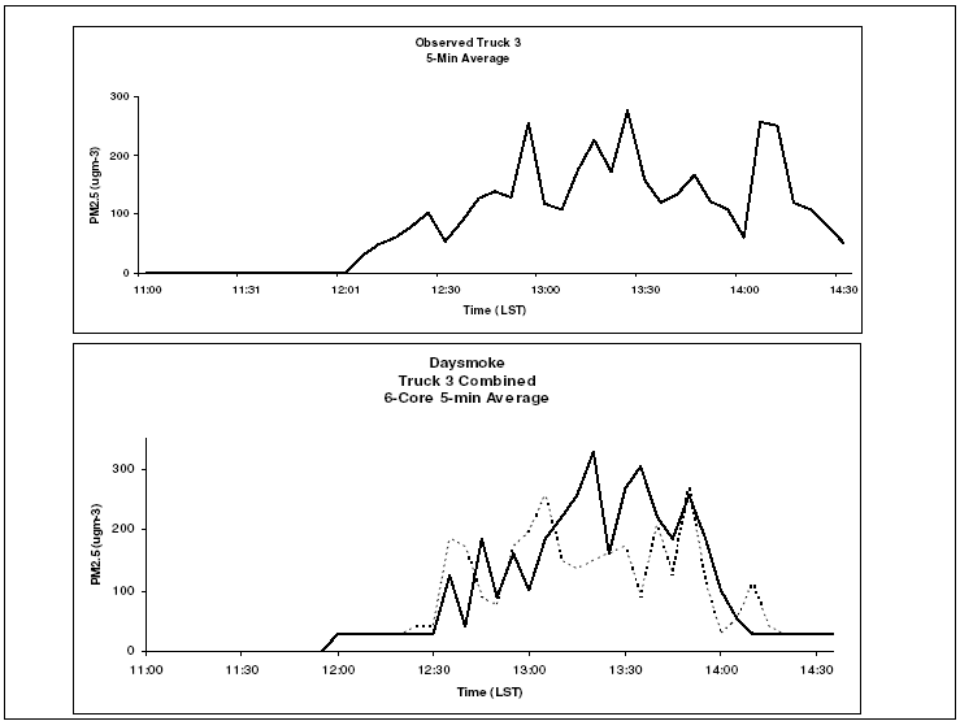

Figure 72. Same as for Figure 70 but for Truck 3.

4.4.2.1.1.3 Analysis of 30-min averaged $PM_{2.5}$ for 9 April 2008

The 5-min averaged $PM_{2.5}$ data described above were averaged into 30-min periods beginning at 1100 EDT. Plots for observed $PM_{2.5}$ for Truck 1 are shown as the solid lines in Figure 73. Ensembles of five Daysmoke runs for 6-core updraft plumes and 8-core updraft plumes were averaged into 30-min periods and shown in Figure 73 as ensemble means (black circles) and high and low ranges of $PM_{2.5}$. The 6-core updraft simulations (left panel) overestimate $PM_{2.5}$ at 1200 and 1230 EDT, underestimate the peak at 1300 EDT and represent the decline in $PM_{2.5}$ after 1300 EDT fairly accurately. The 8-core updraft simulations (right panel) reproduce the $PM_{2.5}$ peak at 1300 EDT but overestimate concentrations at other times. The spreads of $PM_{2.5}$ among the Daysmoke simulations are shown by the vertical lines connecting the horizontal bars. For the 6-core updraft simulations, the spread from 1200 – 1400 EDT ranges from 20-45 μgm^{-3}. The spread for the 8-core updraft simulations for the same period range from 20-120 μgm^{-3} and give a representation of the unpredictability inherent in Daysmoke. For 1330 EDT, the mean is 150 μgm^{-3} with a spread of roughly ± 50 μgm^{-3} or 33%. From another perspective, Daysmoke-simulated $PM_{2.5}$ concentrations at 1330 EDT range from 101 to 209 μgm^{-3} or a factor of two.

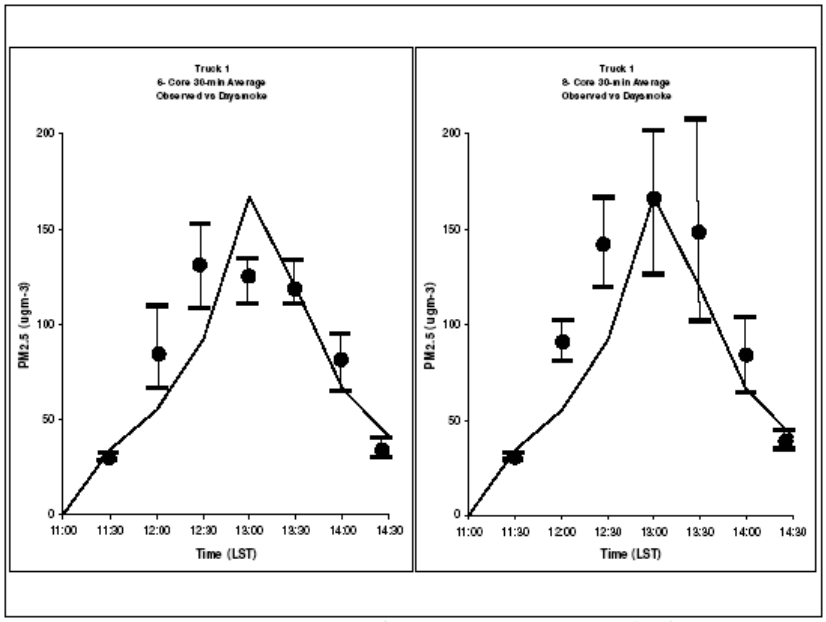

Figure 73. 30-min averaged $PM_{2.5}$ generated by Daysmoke for 6-core updraft plumes (left panel) and 8-core updraft plumes (right panel) compared with 30-min averaged observed $PM_{2.5}$ at the Truck 1 locations during 9 April 2008 burn at Fort Benning.

Figure 74 shows the 30-min averaged $PM_{2.5}$ for Truck 2. The Daysmoke simulations follow the observed trace through 1230 EDT but then fall below the observed $PM_{2.5}$. For Truck 3, both 6-core and 8-core updraft solutions (Figure 75) follow the observed trace from the initiation of smoke to the peak concentration at 1330 EDT. Daysmoke fails to pick up the secondary peak after 1400 EDT (Figure 72).

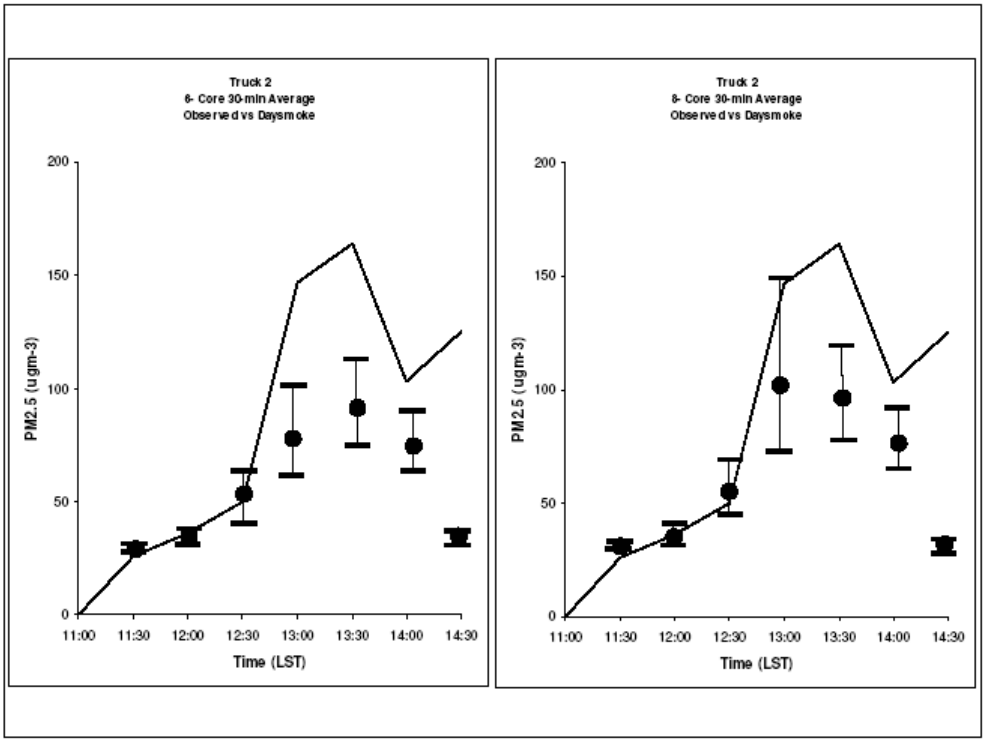

Figure 74. Same as Figure 73 but for Truck 2.

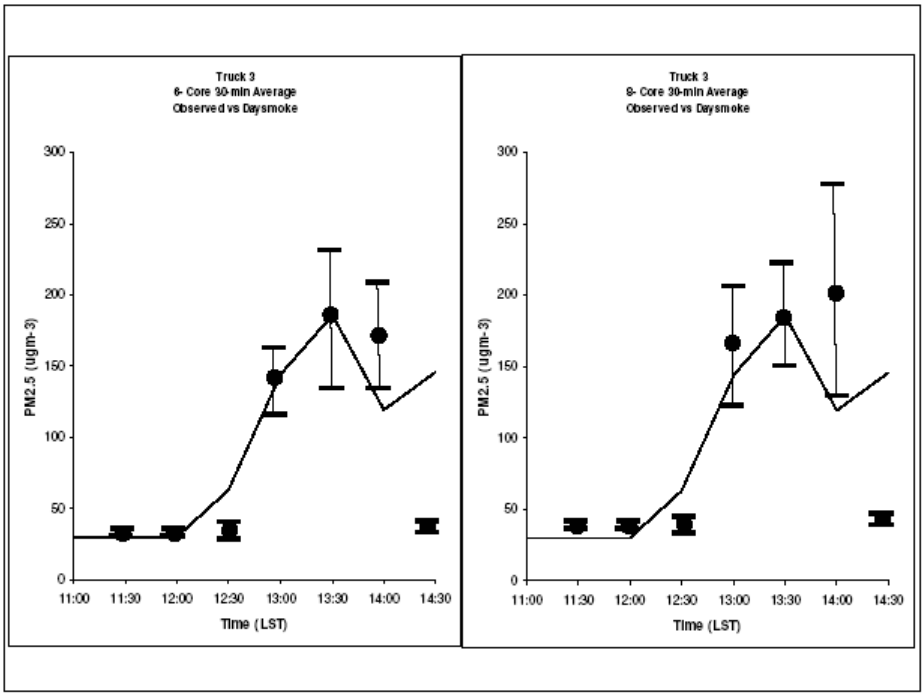

Figure 75. Same as for Figure 73 but for Truck 3.

4.4.2.1.1.4 Discussion of Discrepancies

Two major discrepancies between observed and Daysmoke-simulated $PM_{2.5}$ concentrations – the under-estimation of $PM_{2.5}$ at Truck 2 and the missing of the secondary peaks in $PM_{2.5}$ at Trucks 2 and 3 by Daysmoke need further discussion. Two factors impact the under-estimation of $PM_{2.5}$ at Truck 2.

First, minor shifts in the WRF model wind directions (different from observed wind directions) used to inform Daysmoke could account for the discrepancy. The analysis of truck positions showed a general movement of trucks to the north during the burn as ground crews determined that the winds were shifting to blow more from the south. Because simulated smoke plumes were captured by convective mixing about half-way through the mixing layer, average winds for the lower half of the mixing layer were obtained from the hourly WRF soundings for comparison with truck positions. WRF winds blowing from 103 degrees at 1100 EDT shifted to blow from 108 degrees at 1300 EDT. Truck 2 was initially positioned to intercept a plume carried by winds blowing from 96 degrees (point 4 in Figure 66). Truck 2 successfully captured the plume beginning at 1230 EDT (top panel of Figure 71). Then, at 1245 EDT, Truck 2 was shifted to point 5 (Figure 66) 112 degrees from the burn site and successfully intercepted the plume there. Truck 2 in the WRF/Daysmoke simulations was found at the extreme southern edge of the plume initially then later at the extreme northern edge of the plume. Thus the Daysmoke plume was subject to too strong a wind component from the south early and too weak a wind component from the south late. It should be noted that the discrepancies in wind direction of 7 degrees early and 4 degrees late fall well within the margin of error to be expected with numerical weather models.

Second, it is possible that Truck 2 fell at the edges of the Daysmoke smoke plume because the Daysmoke plume was too narrow. An empirical constant controls the magnitudes of the stochastic terms that govern lateral placement of particles. Increasing the constant would widen the plume albeit at the expense of $PM_{2.5}$ concentrations farther downwind.

There are two explanations for why Daysmoke missed the secondary peaks in $PM_{2.5}$ at Trucks 2 and 3. First, WRF winds shifted from 108 degrees at 1300 EDT to 97 degrees at 1400 EDT. The secondary $PM_{2.5}$ peaks were observed after 1400 EDT. Thus secondary peaks were not observed at Trucks 2 and 3 because WRF/Daysmoke winds shifted to blow the plume elsewhere after 1400 EDT. Second, the $PM_{2.5}$ peaks could have occurred because fire burned into areas with heaver fuel loadings and/or burn crews increased fire on the landscape. However, Daysmoke could not simulate a second peak because the model was initialized with emission rates calculated from a "boxcar-shaped" relative emissions model that held hourly emissions constant for the duration of the period of ignition – 2 hr. In summary, more case studies are necessary to determine the underlying causes for the discrepancies between observed and Daysmoke-simulated $PM_{2.5}$ concentrations.

4.4.2.1.2 Re-Evaluation of Daysmoke with January 15, 2009 burn at Fort Benning

On January 15, 2009, Unit A09 of Fort Benning was treated (Figure 76). Unit A09 is 583 acres and has 2 compartments, which are approximately of equal size (Table 15). This unit was last

burned in 2007 hence the rough is 2 years old. The details of the stand were not used in the emission estimations. Ignition started at 12:15 EST and was completed at 14:30 EST (according to Fort Benning Land Management records; records kept on the field suggest that ignition was completed at 14:00 EST).

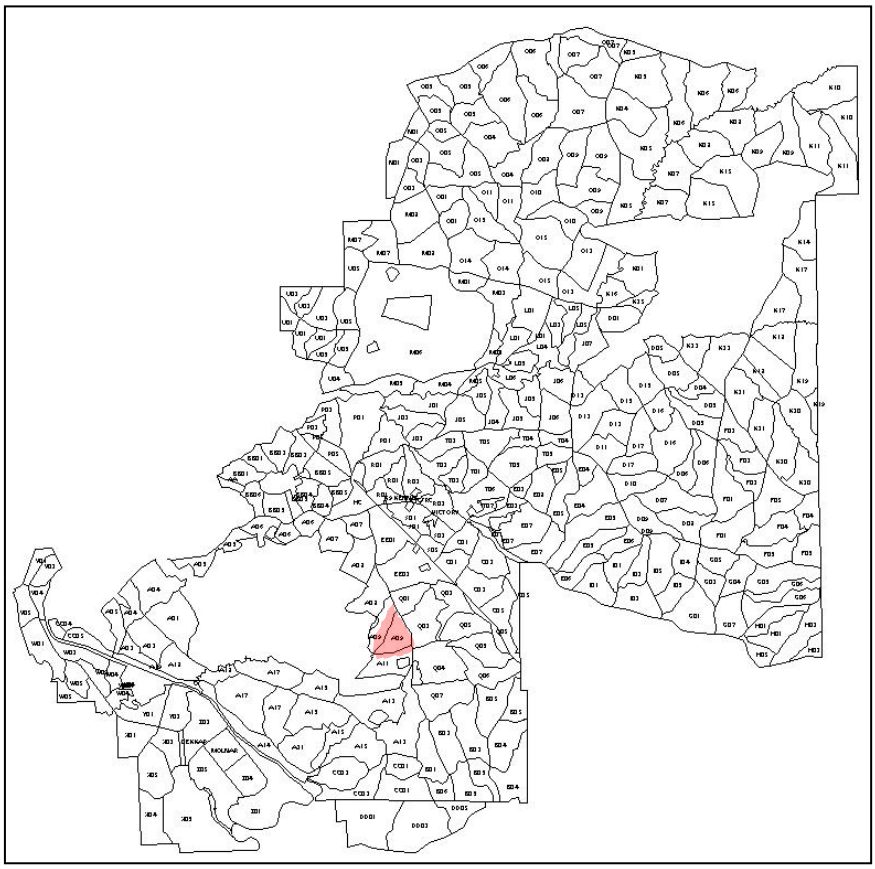

Figure 76. Fort Benning burn units. Unit A09 treated on January 15, 2009 is shaded in pink.

Table 15. Coordinates of burn unit centroids.

Burn Unit	Latitude	Longitude
A09-A (302 acres or 52%)	32.3259° N	84.8552° W
A09-B (281 acres or 48%)	32.3199° N	84.8493° W

The truck locations are shown in Figure 77. Truck 1 sampled at three different locations: from 12:15 to 13:20 EST at location 1 (32.3110° N and 84.8429° W), from 13:23 to 13:53 EST at location 2 (32.3084° N and 84.8411° W) and from 14:07 to 15:30 EST at location 3 (32.3019° N and 84.8433° W). Heavy traffic of trucks, SUVs, and other military vehicles was reported at locations 1 and 3 but no correlation was found in the measurements. It should be noted that

whenever possible the trucks parked on the upwind side of the road. However, location 2 is on a fork downwind from the main road and there is no traffic record for the main road while Truck 1 was at location 2.

Truck 2 tried to sample at 3 different locations also. However, no measurements were made at location 1 (32.2915° N and 84.8295° W) between 12:20 and 13:15 EST. There are measurements at location 2 (32.2951° N and 84.8230° W) from 13:20 to 14:15 EST and at location 3 (32.2925° N and 84.8267° W) from 14:15 to 15:30 EST. There was no traffic reported by Truck 2, except a car driving by at 14:58.

Truck 3 remained at a single location (32.2836° N and 84.8198° W) from 12:28 to 15:30. However, the engine was started twice, at 13:20 and 14:08, and then turned off. No traffic was reported at this location.

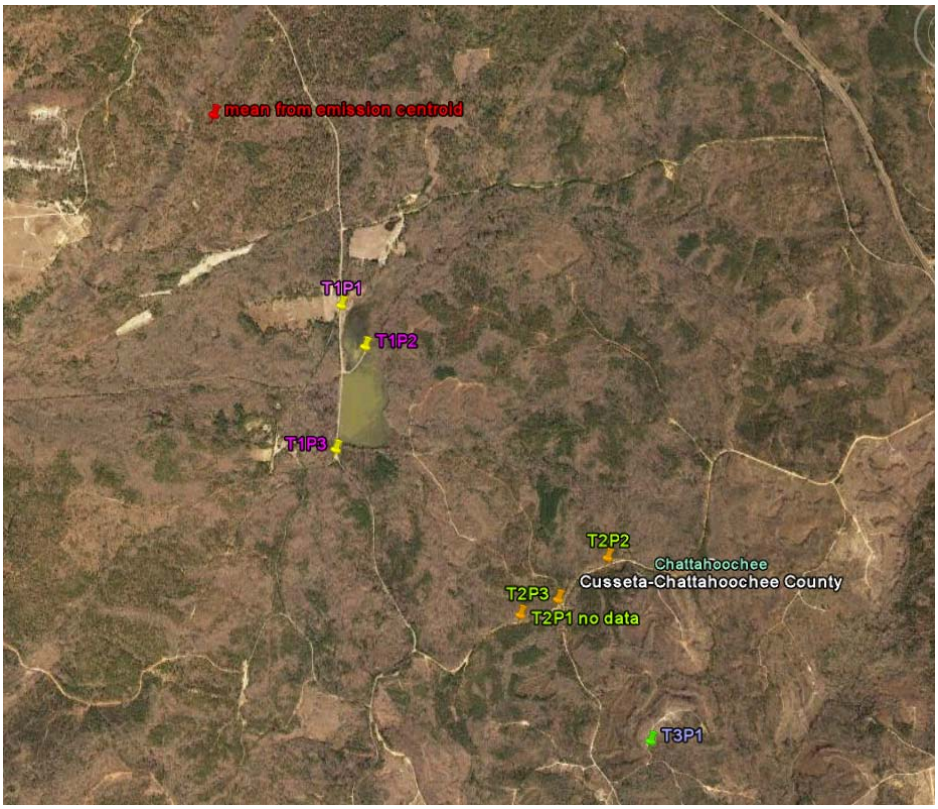

Figure 77. Truck locations on January 15, 2009. Truck 1 (T1) locations marked in yellow, Truck 2 (T2) locations in orange, and Truck 3 (T3) location in green.

The levels of $PM_{2.5}$ measured by DustTrak real-time monitors are shown in Figure 78. Truck 1 recorded high levels of $PM_{2.5}$ both at location 1 and location 2. However, after it has moved to location 3, at 14:07 EST, the levels have dropped significantly. This suggests that location T1P3 in Figure 77 is outside the plume boundary. Truck 2 had a chance to move freely both to the east and to the west on the road it was on, approximately 4 km downwind from the burn. Unfortunately, there is no data at location T2P1. The instrument on Truck 2 recorded higher $PM_{2.5}$ levels at 14:30, shortly after it moved from T2P2 to T2P3 around 14:15 EST. Note that the

log sheet for Truck 2 is not very precise in terms of the time of departure from T2P2 and arrival to T2P3. The southward movement of Truck 1 around 14:00 EST followed by the westward movement of Truck 2 at 14:15 EST suggests that the winds may have shifted to become more northerly. Truck 3 had limited access to the east. The road Truck 3 was on dead ends approximately 400 m to the east.

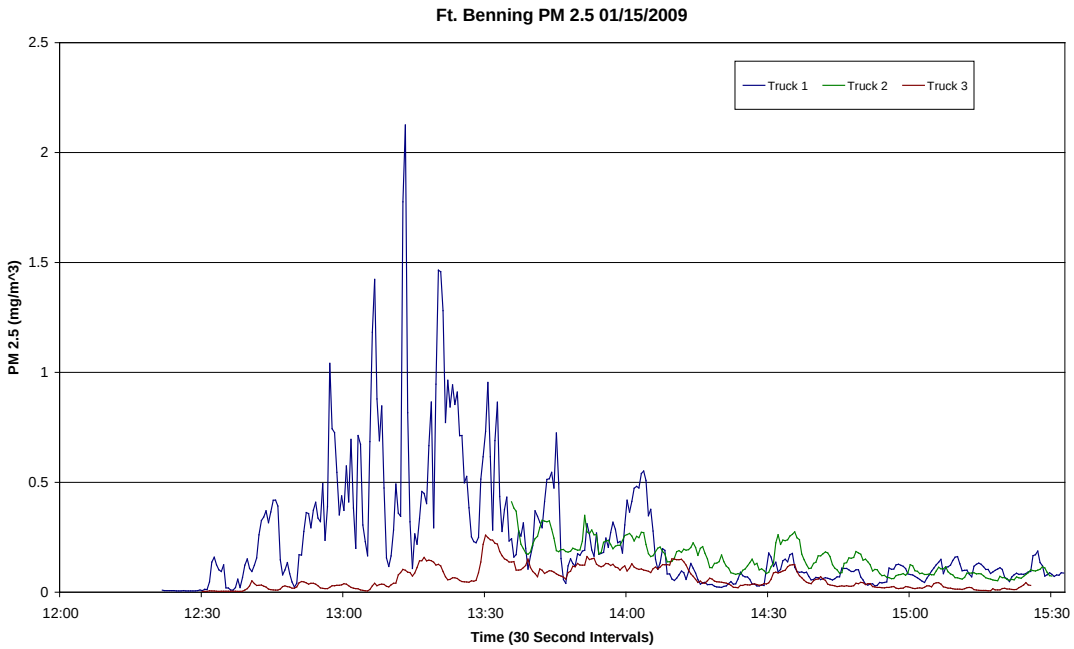

Figure 78. $PM_{2.5}$ levels, in mg m^{-3}, recorded by DustTrak monitors on board of Truck1 (blue), Truck 2 (green), and Truck 3 (red).

Emissions were estimated separately for each compartment (Figure 79). After 3 hours of flaming phase, the fire smolders for two hours according to the emission estimates. The estimated fire diameters for A09-A and A09-B are both 85 m. The emissions from the two compartments were combined and treated as if they were from a single burn, for input to Daysmoke. Note that Daysmoke does not combine the plumes from multiple burns. When the emissions were input separately for the two compartments, the $PM_{2.5}$ levels estimated by Daysmoke were extremely low because Daysmoke treats the fires independently in this case. The centroid of A09 was assumed to be at 32.3229° N and 84.8522° W, which is the average of the centroids of this unit's two compartments (Table 15).

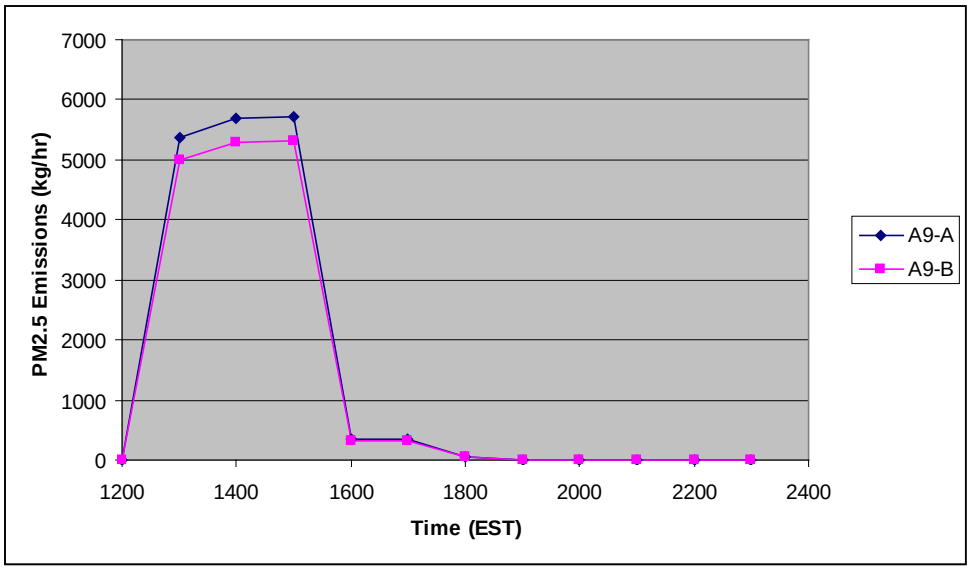

Figure 79. Estimates of $PM_{2.5}$ emissions from burn units A09-A and A09-B.

An important Daysmoke parameter that needs to be input by the user is the number of updraft cores. A picture of the plume provided by the U.S. Forest Service suggests that there are at least 4 distinct cores in the plume (Figure 80). Daysmoke was run with 3, 4, 6, and 8 updraft cores to determine the sensitivity to this important model parameter.

Figure 80. The burn at Unit A09 of Fort Benning on January 15, 2009.

The wind direction suggested by the center of the plume is between 310° and 315° while a line drawn from the centroid of the burn unit through truck locations T1P1, T1P2, T2P3, and T3P1 has a heading of 325° towards NNW (Figure 81). A bias of 10° to 15° in WRF-predicted wind directions is not uncommon. If we assume that the trucks were perfectly aligned with the plume, the true wind direction could have been 325°. To verify this hypothesis, one can refer to the observed wind direction. According to the wind rose located at Fort Benning on the rooftop of the Bureau of Land Management, the winds were from NNW (Figure 82). Note that the wind directions were approximately 330° at 12:00, 300° at 13:00 and 330° at 14:00 EST. Since these are surface winds, and WRF predictions suggest 5° to 10° more northerly winds at 500 m, which is the approximate height of the plume center, it is also possible that the trucks may not have been perfectly aligned with the plume. Recall that Truck 3, whose position was the determinant factor in drawing the line in Figure 81, did not have any room to move further to the east. The wind direction analysis was inconclusive but considering the possibility that the wind direction could have been biased, Daysmoke was also run with winds rotated to align with the trucks.

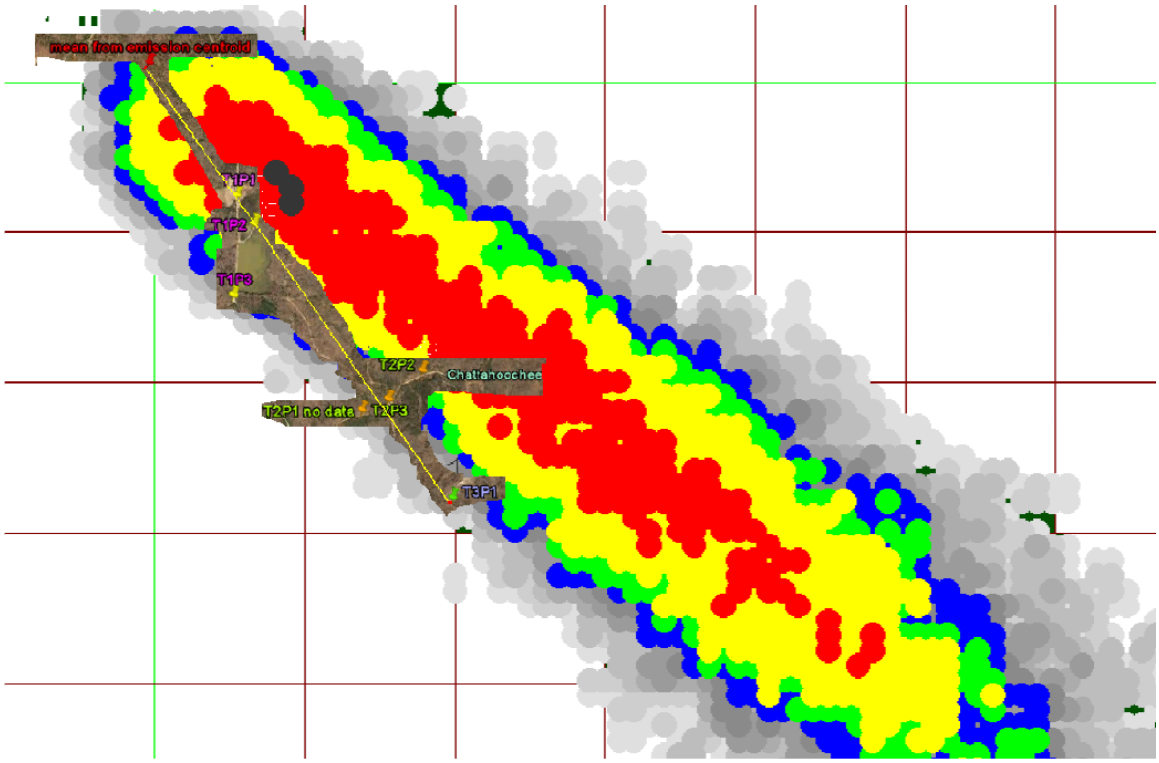

Figure 81. Top view of the Daysmoke plume at 17:45 EST and the truck locations.

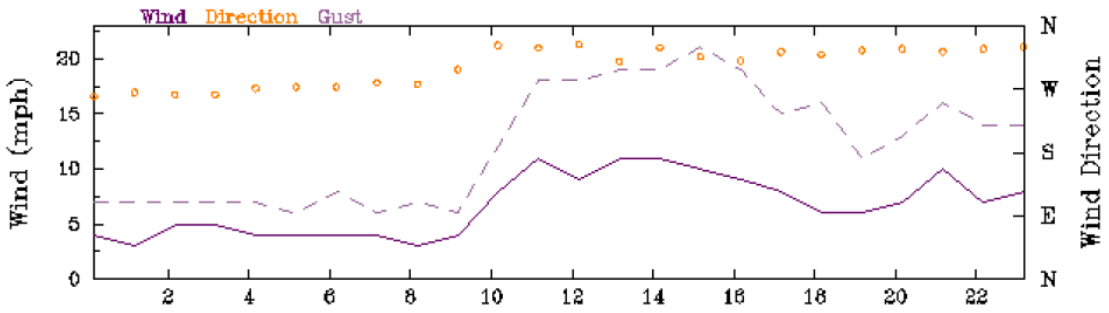

Figure 82. Wind speed and direction at Fort Benning (rooftop of the Bureau of Land Management) on January 15, 2009.

The plume in Figure 81 would also align with the truck locations if the centroid of the burn unit were shifted to the west. The centroid used in Daysmoke runs is the mean of the coordinates for compartments A09-A and A09-B. Another set of coordinates calculated independently suggests that the centroid of Burn Unit A09 is 1.46 km to the NNW of the centroid used. Considering possible uncertainties in burn location, Daysmoke was also run with the centroid shifted to the west by about 1.5 km (32.3230° N, 84.86724° W).

Perhaps the most important factor in this evaluation is the interpretation of the DustTrak readings. While DustTrak is a reliable instrument in relative terms, its absolute readings do not represent the actual $PM_{2.5}$ levels. In the past, collocation of DustTrak monitors with Federal Reference Method (FRM) monitors revealed that DustTrak readings can be higher by a factor of 2 to 5. As described in Section 4.3.2.1, the readings were later divided by 3.64 (or multiplied by 0.275). Since Daysmoke predictions were 15-minute averages, the 30-second DustTrak measurements were also averaged over 15-minute intervals to match the time scales of the measurements and the model.

Among all the Daysmoke runs with different combinations of the number of updraft cores (3, 4, 6, or 8), wind direction (WRF winds or winds rotated to an average of 325°), and burn unit centroid (original and shifted to the west by 1.5 km), the best agreement with the scaled DustTrak readings was obtained for the case of 4 updraft cores, WRF winds, and the original burn unit centroid (mean of compartments A09-A and A09-B) (Figure 83). For Truck-1 locations, after a more rapid increase, Daysmoke predicts a very similar rate of decrease in $PM_{2.5}$ concentrations to the scaled DustTrak measurements. Neither rotated winds nor shifted centroid resulted in similar rates of decrease and both maintained high levels of $PM_{2.5}$ for about 3 hours longer than the measurements (not shown). For Truck-2 locations, the rate of decrease in $PM_{2.5}$ levels is also in agreement with measurements. The rotated wind and shifted centroid cases result in much higher concentrations, and longer smoke duration than observed (not shown). Daysmoke predicted $PM_{2.5}$ levels are 20 to 30 $\mu g\ m^{-3}$ lower than the scaled DustTrak measurements.

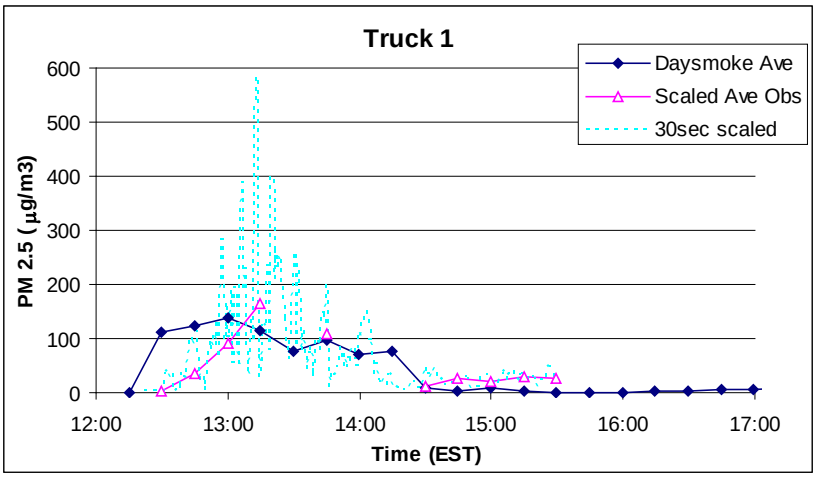

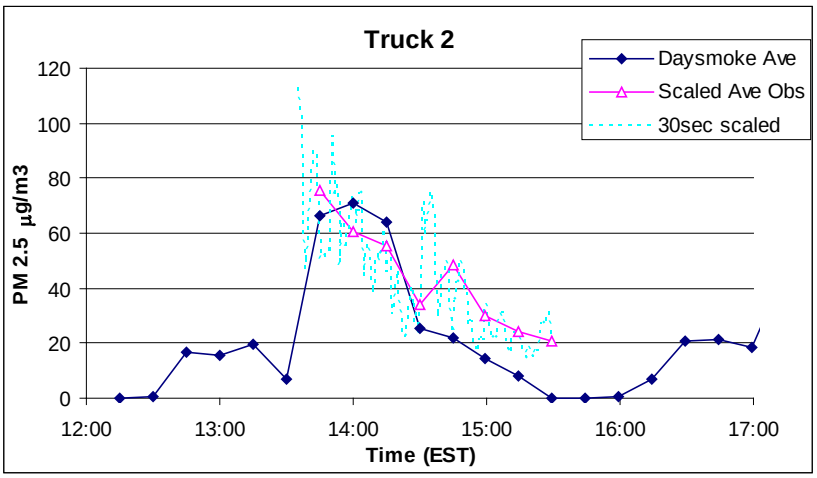

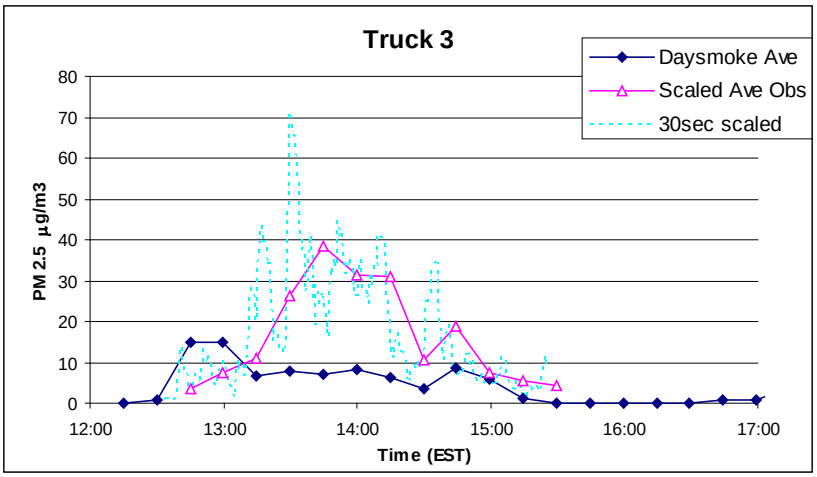

Figure 83. Modeled versus measured $PM_{2.5}$ concentrations at truck locations. Modeled concentrations are the average of 5 Daysmoke runs using 4 updraft cores. Measured concentrations are DustTrak readings scaled by a factor of 27.5%.

While the agreement between the model and the measurements is encouraging, there are several questions that remain to be answered. First, are the WRF winds biased by 10 to 15 degrees to result in less northerly and more westerly flow? Alternatively, is the actual center of the burn more to the west? The misalignment of the truck locations with the Daysmoke plume center may also be due to the inability of the trucks, especially Truck 3, to access the plume centerline. This was assumed to be the case here. Second, is the emissions model assuming too fast an ignition rate, as suggested by the rapid increase in Daysmoke concentrations at Truck 1 and Truck 3 locations? Unfortunately there are no measurements from Truck 2 for this ramp-up period. The uncertainties involved in emissions estimation are likely to cause large differences between the modeled and observed $PM_{2.5}$ levels. The longer smoke durations modeled by Daysmoke when the plume is aligned with the trucks suggests that emissions may be too high. The sensitivity of Daysmoke to fire diameter is another unknown in this analysis. Third, is the large uncertainty of DustTrak readings in determining the absolute $PM_{2.5}$ levels affecting the calibration of the number of updraft cores in Daysmoke? Note that 6 updraft cores proved to be ideal for the April 2008 burns when Daysmoke was being compared to DustTrack readings. After the readings were calibrated with the reduction factor of 3.64 to represent gravimetric $PM_{2.5}$ levels, 4 updraft cores is being used in Daysmoke. Using a smaller number of updraft cores (4 instead of 6) lifts up the plume and results in lower concentrations at the ground. While this approach seems to work for Truck 1 and Truck 2, the concentrations are underestimated for Truck 3, which is 5.5 km away from the burn.

4.4.2.2 Re-Evaluation of Chemistry-Transport Model

In this section, Adaptive Grid CMAQ (AG-CMAQ) and the product of its coupling with Daysmoke (AGD-CMAQ) are evaluated in applications to the Atlanta Smoke Incident of February 28, 2007. For chemistry-transport model evaluation, this incident is preferred over the 9 April 2008 burn at Fort Benning for the following reasons. The burn at Fort Benning was only detected by one regional monitor at Columbus Airport while the smoke incident was captured by several regional monitors around Atlanta. While the signal at Columbus Airport monitor is weak and not associated to the burn for sure, the detected $PM_{2.5}$ levels at metropolitan Atlanta monitors are very high, showing strong connection to two prescribed burns that day. The Atlanta Smoke Incident was studied on several occasions, including independent investigations, while the 9 April 2008 burn is being studied here for the first time. Finally, the Columbus Airport monitor is only 25 km away from the burn, metropolitan Atlanta monitors that detected the smoke incident range from 30-80km distance from the burns, providing data for a better evaluation of the long-range transport. An evaluation of AG-CMAQ with the 9 April 2008 burn at Fort Benning can be found in Achtemeier et al. (2011). A recap of the Atlanta Smoke Incident follows.

On February 28, 2007, air quality in the Atlanta metropolitan area was impacted by heavy smoke caused by prescribed burns. Within hours fine particulate matter levels at monitoring sites throughout the area increased to nearly 150 µg/m3 and ozone levels exhibited increments as large as 30 ppb (Hu et al., 2008b). Not surprisingly, an increase in asthma attacks was also observed. Although several prescribed burns were carried out in the region throughout the day, the dramatic increase in pollution levels is mainly attributed to 2 prescribed fires 80 km southeast of Atlanta in the Oconee National Forrest and Piedmont National Wildlife Refuge. In these two prescribed burns about 12 km^2 of land were subjected to treatment over a period of about 5

hours. The smoke from the burns was completely gone when it started raining at noon the next day. Simulation of air quality resultant from the February 28 Atlanta smoke episode with the CMAQ model has been previously carried out as discussed in Hu et al. (2008b).

4.4.2.2.1 Evaluation of Adaptive Grid CMAQ

Here the incident was re-simulated with the adapting and non-adapting (fixed grid) versions of the Adaptive Grid CMAQ model (AG-CMAQ) using previously unavailable information about the 2 major prescribed burns blamed for the incident. Recall that the non-adapting version of AG-CMAQ was evaluated previously and found to produce essentially the same results as CMAQ (Section 4.2.1.1). Therefore, any reference to non-adapting (or fixed grid) AG-CMAQ in this section can be viewed as a reference to the standard CMAQ model and vice versa. Also, whenever no specification is made in reference to AG-CMAQ as to whether the grid is adapting or not, it should be assumed that the grid is adapting.

Model inputs (emissions, meteorology, initial and boundary conditions), configuration and setup for AG-CMAQ were the same as those used for the fixed-grid simulation at 4-km horizontal grid resolution over a domain covering Northeastern Georgia. The vertical distributions of the PB plumes were input from Daysmoke using the initial coupling methodology described in Section 4.2.3.1. AG-CMAQ was initialized with the same 4-km resolution uniform grid used in fixed-grid simulation. Note that meteorological inputs as well as emissions from all sources other than the two prescribed burns mentioned above are also available on the same 4-km grid. Grid refinement in AG-CMAQ was driven by $PM_{2.5}$ concentrations. The simulation started from 21:00 UTC (16:00 EST) on February 27 and continued until 05:00 UTC (00:00 EST)on March 1. Grid adaptation commenced at 15:00 UTC (10:00 EST) on February 28 consistent with the initial emissions release from the Oconee National Forrest and Piedmont National Wildlife Refuge fires.

The results of the AG-CMAQ simulation were compared to the results obtained from the fixed-grid simulation. Figure 84 shows $PM_{2.5}$ concentrations on the modeling domain at 04:45UTC on March 1 after full plume development from both the AG-CMAQ and standard CMAQ simulations.

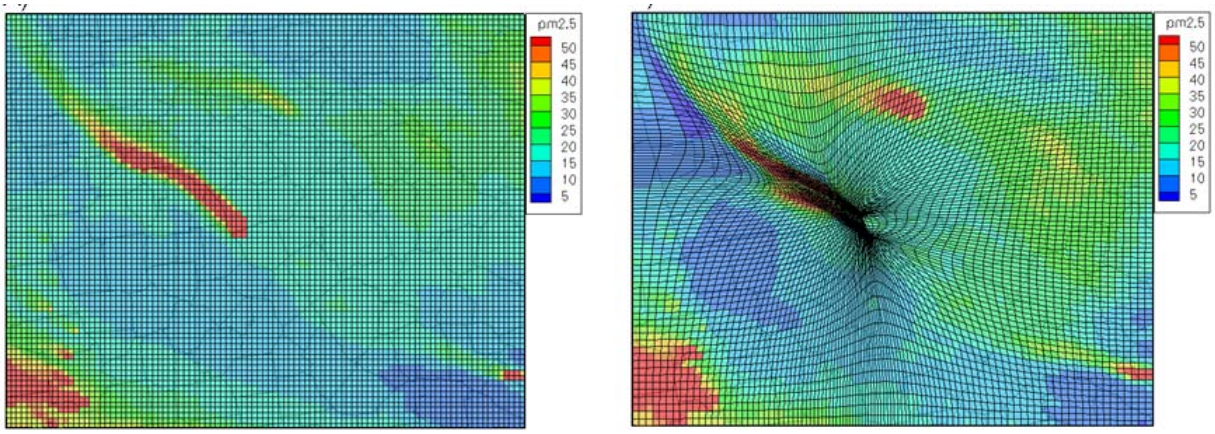

Figure 84. Simulated $PM_{2.5}$ concentrations (µg/m3) in modeling domain at 04:45 UTC on March 1, 2007 using fixed grid CMAQ (left) and AG-CMAQ (right).

Visual inspection of the modeled $PM_{2.5}$ concentration fields provides evidence of significant differences between the adaptive grid and fixed grid simulations. The artificial dilution effect generally present in gridded photochemical models appears to decrease when applying an adaptive grid. The smoke plumes drawn with AG-CMAQ appear better defined and pollutant concentrations remain higher near plume cores. Most significantly perhaps, plumes from both ongoing prescribed burns can be distinctly observed when applying an adaptive grid. When using a static grid, the plumes cannot be distinguished from each other and appear as a single thicker plume. We believe results from AG-CMAQ better describe local air quality and pollutant dispersion.

Modeled concentrations from both adaptive grid and fixed grid simulations were compared to concentration measurements at several air quality monitoring sites in the Atlanta metropolitan area that experienced a significant increase in $PM_{2.5}$ concentration during the incident. Results for both simulations are plotted along with hourly measurements at four monitoring sites in Figure 85. Concentrations resultant from a fixed grid simulation of the smoke incident consistently under-predict peak $PM_{2.5}$ concentrations at the locations of monitoring sites that recorded a significant increase in measured concentrations. Additionally, in some instances modeled concentrations from the fixed grid simulation appear higher than measurements outside the pollution spike and exhibit two distinct concentration peaks.

The simulation with AG-CMAQ results in higher concentration peaks compared to the fixed grid simulation and reduces the initial over-prediction of $PM_{2.5}$ concentrations and significance of the double peak behavior observed with a fixed grid. We believe the differences in simulated concentrations between the fixed grid and adaptive grid simulations reflect the improved replication of plume dynamics and decrease in artificial dilution that can be achieved through grid refinement. However, we believe that underestimation of secondary organic aerosol formation and volatile organic compound emissions are still largely responsible for the differences between modeled results and measurements and that other model characteristics unrelated to grid resolution contribute significantly to the error.

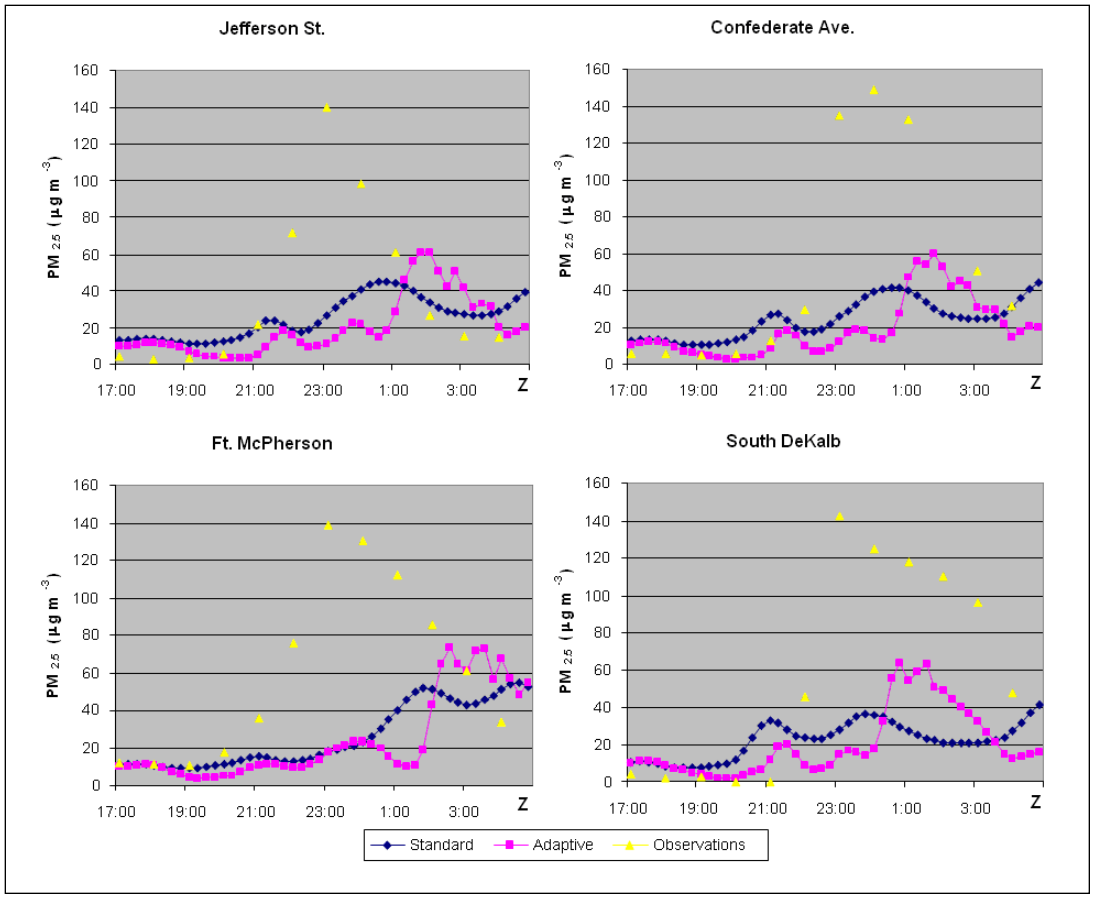

Figure 85. Modeled $PM_{2.5}$ concentrations using standard CMAQ and AG-CMAQ and concentration measurements at the Jefferson Street, Confederate Avenue, Fort McPherson, and South DeKalb air quality monitoring sites in the Atlanta metropolitan area.

Vertical resolution of the model and the plume height with respect to the boundary layer may be important factors leading to the underestimations in Figure 85. A three-dimensional visualization of the results revealed important clues. Figure 86 is a 3-D version of Figure 84-A after rotation; X and Y are the easting and northing (y) axes, respectively. The elevated plume coming out of the paper bifurcated from the leading part of the plume heading northwest to Atlanta (to the right of the figure) due to wind shear. The trailing part of the plume heading to Atlanta formed after the bifurcation, when the plume height dropped with respect to the boundary layer height. There is no data to verify if the bifurcation really occurred. If it did not, then it is partially responsible for the underestimations in Figure 85. The underestimations may also be due to the overestimation of the plume height which, together with the coarse model resolution above the boundary layer, may be artificially lofting the plume above the boundary layer and leading to the bifurcation due to wind shear.

Considering these possibilities a new simulation was performed using a different plume height and 34 vertical layers, instead of 13 used in the previous simulation. One of the parameters that plume height in Daysmoke is most sensitive to is the initial plume diameter, which depends on the fuel type. The diameter used in earlier simulations was 200m; this time the diameter was

reduced to 70m. As a result, the mean plume height reduced from 1200 m to 500m. No bifurcation was observed in the standard CMAQ simulation, and the $PM_{2.5}$ concentrations in Atlanta increased by more than 50 $\mu g/m^3$ (Figure 87).

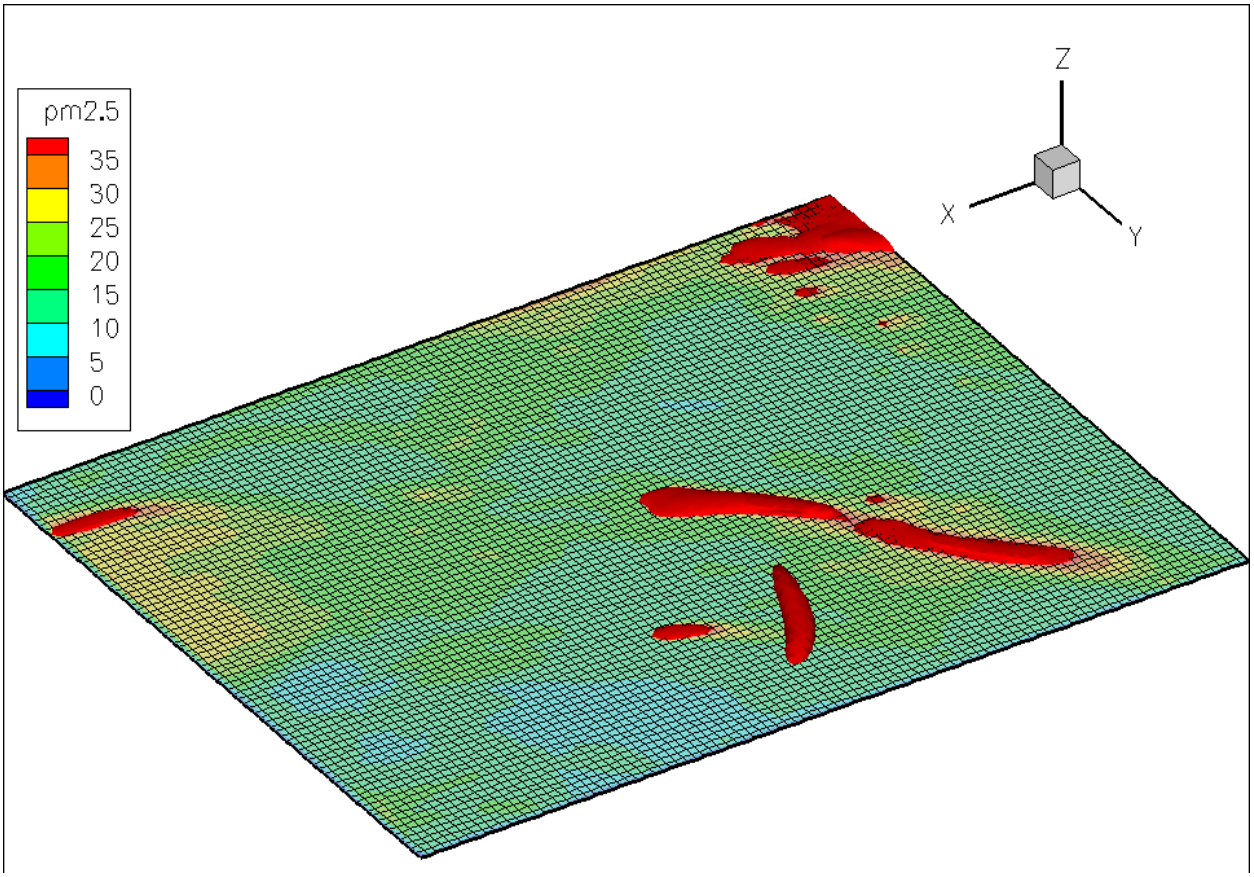

Figure 86. Three-dimensional view of the plumes in Figure 84. Note the different orientation of the easting (X) and northing (Y) axes after rotation. The elevated plume coming out of the paper bifurcated from the leading part of the plume heading northwest to Atlanta (to the right) due to wind shear.

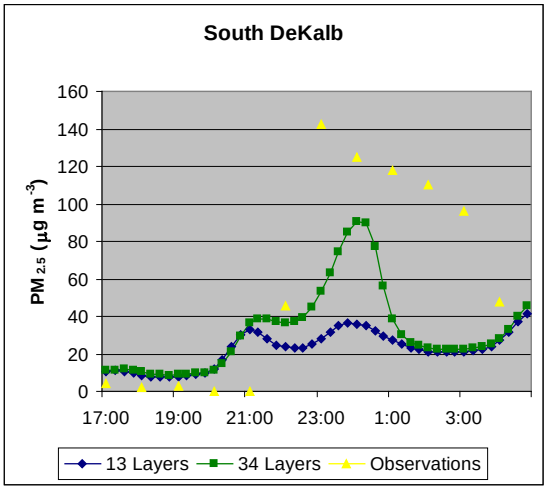

Figure 87. Modeled $PM_{2.5}$ concentrations using standard CMAQ with 13 and 34 layers respectively and observations at the South DeKalb air quality monitoring site in Atlanta. Time is UTC.

4.4.2.2.2 Evaluation of Adaptive Grid CMAQ coupled with Daysmoke

The February 28, 2007 Atlanta Smoke Incident was used for the evaluation of the coupled Daysmoke and Adaptive Grid CMAQ (AGD-CMAQ) modeling system as well. The methodology used in coupling Daysmoke with AG-CMAQ was already described in Section 3.2.4.3 so it will not be repeated here. However any deviation from the described methodology will be noted.

4.4.2.2.2.1 Analysis of Handover Error

During the simulation of the Atlanta Smoke Incident the handover process for the two fires was kept track. The plots of the normalized concentration error analysis are shown in Figure 88. In these plots, the blue line represents the normalized error at a certain downwind distance for the Oconee burn, and the pink line represents the same error for the Piedmont burn. As a deviation from the described methodology, instead of using the sum of the concentration difference to represent the handover error, the differences were normalized by the average of Daysmoke and AG-CMAQ concentrations and then summed. The objective for this was to give the differences in low concentrations as much weight as the differences in high concentrations. Later it was decided to revert back to absolute differences since normalization led to some difficulties in determining the location of minimum error. Here, the interfaces between Daysmoke and AG-CMAQ were drawn at the minimum normalized error location closest to the fire. As described in Section 3.2.4.3, at the interface, the plume tracked as an ensemble of particles by Daysmoke is handed over to AG-CMAQ, which continues to track the plume as grid-cell concentrations.

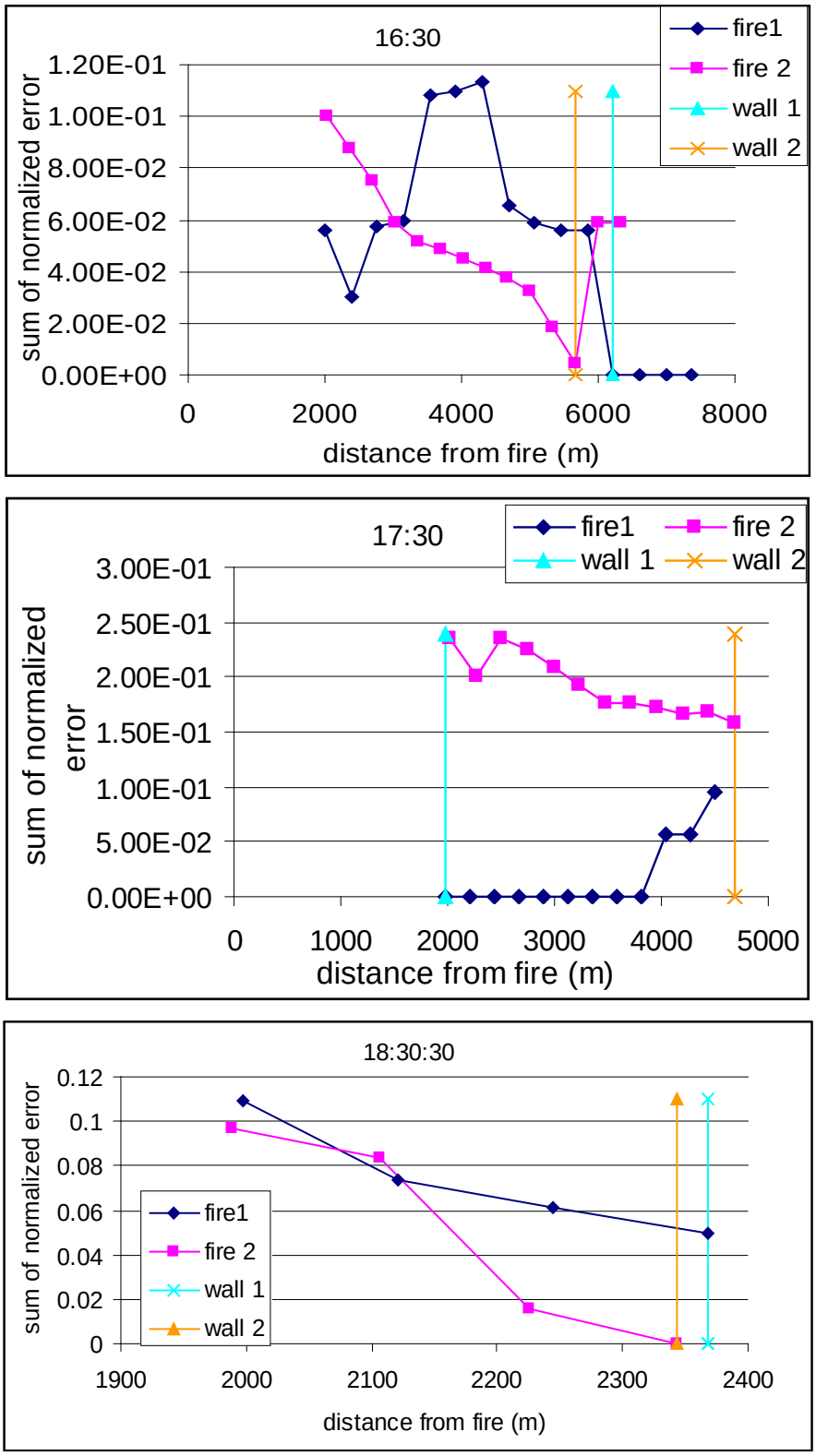

Figure 88. Plots of normalized concentration errors versus downwind distance at 16:30 UTC (top), 17:30 UTC (middle) and 18:30 UTC (bottom) on February 28, 2007.

The vertical light blue line in Figure 88 represents the interface between Daysmoke and AG-CMAQ for the Oconee burn and the orange line is where the interface was set for the Piedmont burn. The plots for 16:30 UTC and 18:30 UTC show cases where the normalized error tends to minimize as distance from the fire increases. Note that the interface is much closer to the fire at 18:30 UTC since it is towards the end of the fire, when both burns are in the smoldering phase. At 17:30 UTC, the Piedmont burn shows a pattern where the normalized error decreases farther away from the fire. On the other hand, the Oconee burn displays a minimum error closer to the fire, which is why a constraint was added that the interface be drawn at least 2 km away from the fire once the Daysmoke plume is fully developed.

Figure 89 shows another result from handover where the dots represent the location of where the wall was set for Oconee and Piedmont burns. Only the period when both burns were active is shown. One can see that as the plume starts to develop, the downwind distance of the wall increases and reaches its maximum around 16:24 UTC. As both fires start to calm down, the distance of the wall tends to stay steady between 2 and 3 km. Towards 19:00 UTC the Piedmont fire has stopped flaming and went into the smoldering phase, which explains the sudden decrease in the distance of the wall.

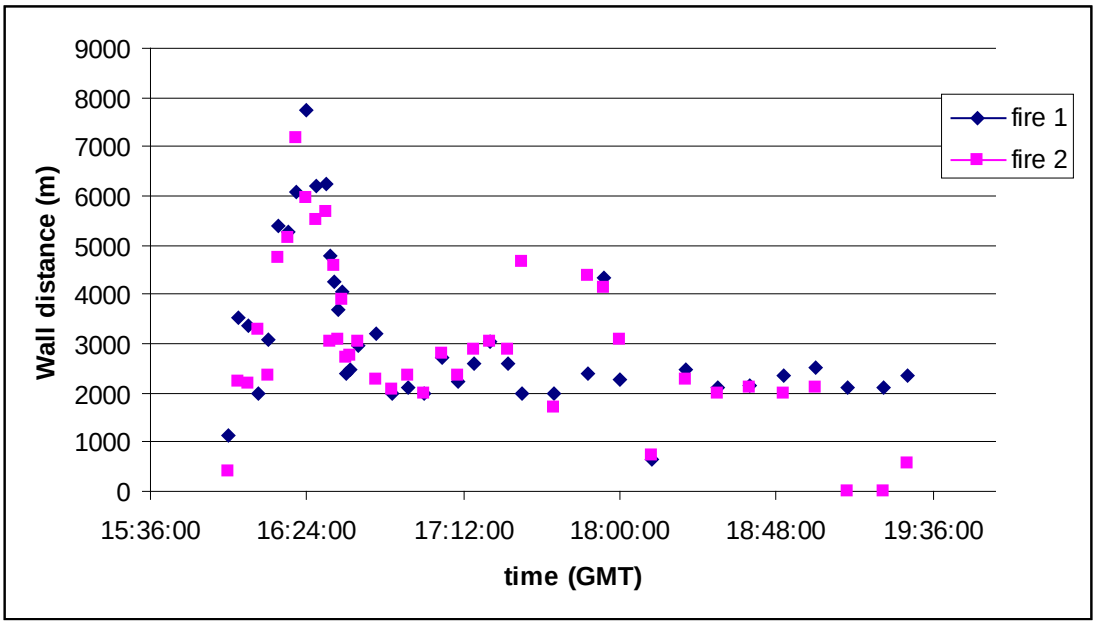

Figure 89. Downwind distance of the Daysmoke─AG-CMAQ interface (wall) over time during the Feb. 28, 2007 Atlanta Smoke Incident: blue for the Oconee burn and pink for the Piedmont burn. Time is UTC.

4.4.2.2.2.2 Evaluation of the Coupled Model

Simulation results from three different CMAQ versions are compared here: CMAQ, AG-CMAQ and AGD-CMAQ. Model inputs, configurations and setups were the same in all cases. Grid refinement in AG-CMAQ and AGD-CMAQ was driven by fire related $PM_{2.5}$ concentrations. The simulations started at 21:00 UTC on Feb. 27 and finished at 05:00 UTC on Mar. 1. The results

(modeled pollutant concentrations) were output with a time step of 30 minutes. The first burn started at 15:00 UTC on Feb. 28, which is also when grids start to adapt, consistent with the initial emissions release from the fires. The concentration peaks from the fires were observed at 6 monitoring sites in/around Atlanta and the sites are numbered from the station closest to the fire in Figure 90.

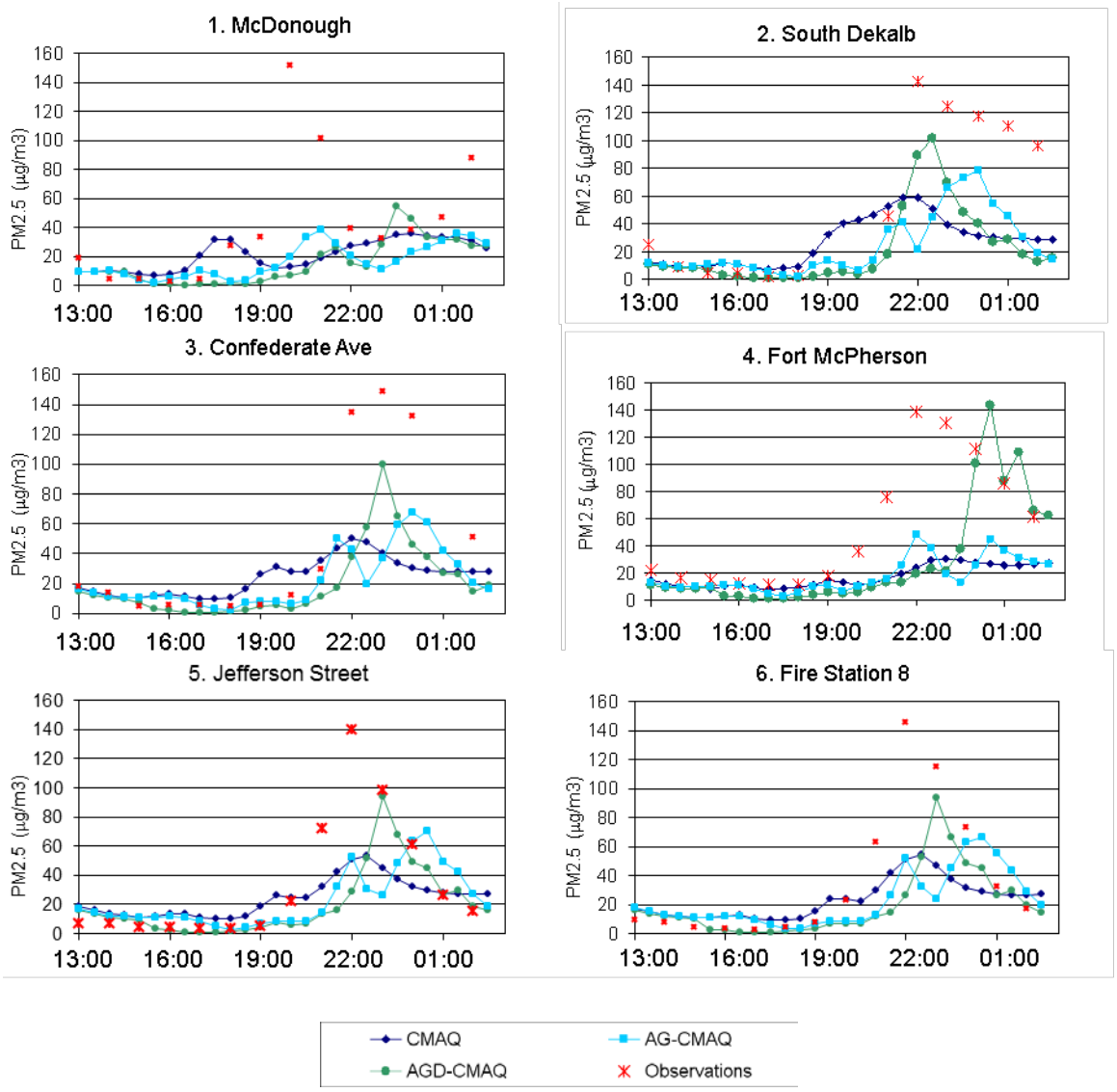

Figure 90. Measured (red) and modeled $PM_{2.5}$ concentrations using standard CMAQ (dark blue), AG-CMAQ (light blue), and AGD-CMAQ (green) at the Mc Donough, South DeKalb, Confederate Avenue, Fort McPherson, Jefferson Street and Fire Station 8 air quality monitoring sites in the Atlanta metropolitan area. All times are UTC.

Figure 90 compares the performances of standard CMAQ, AG-CMAQ and AGD-CMAQ to the hourly measured concentrations at sites near Atlanta that experienced a significant increase in $PM_{2.5}$ concentration from 9am to 10:30pm EST. Significant differences can be observed in all three simulations. The artificial dilution effect in uniform grid is thought to be the reason why

the standard CMAQ concentrations consistently under-predict peak $PM_{2.5}$ concentrations and concentrations generally start to increase sooner than the other two models with adaptive grids. AG-CMAQ reduces the initial over prediction of $PM_{2.5}$ concentrations and predicts higher concentration peaks compared to standard CMAQ results. The double concentration peak behavior is observed with a fixed grid as well but more significantly in AG-CMAQ. The two peaks appear in AG-CMAQ because the two smoke plumes from the two burn sites remain separated and reach out to Atlanta consecutively. On the other hand, the double concentration peaks are no longer apparent in AGD-CMAQ. AGD-CMAQ tends to predict higher concentration peaks, and seems to predict the closest to the observations for most of the monitoring sites. To compare the performances quantitatively, the mean normalized errors were calculated and they are shown in Figure 91.

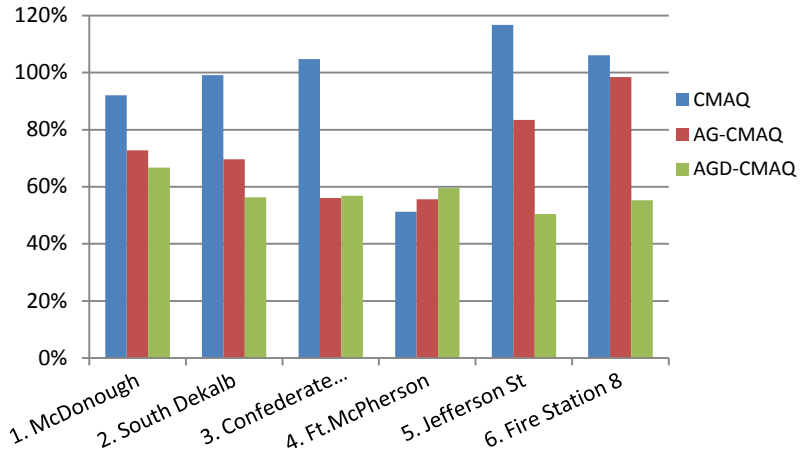

Figure 91. Mean normalized error for modeled $PM_{2.5}$ concentrations using standard CMAQ (blue), AG-CMAQ (red), AGD-CMAQ (green) at the Mc Donough, South DeKalb, Confederate Avenue, Fort McPherson, Jefferson Street and Fire Station 8 sites in Atlanta metropolitan area.

The mean normalized error (MNE) is calculated for the duration of the fires using the following equation, where for every hour i up to N, C_{obs} is the measured $PM_{2.5}$ concentration and C_{mod} is the predicted $PM_{2.5}$ concentration.

$$MNE = \frac{1}{N}\sum_{i}^{N}\left(\frac{|C_{obs} - C_{\mathrm{mod}}|}{C_{obs}}\right)_i \qquad (32)$$

On average, AGD-CMAQ performs the best followed by AG-CMAQ then standard CMAQ. 5 out of 6 times AGD-CMAQ has much lower error than standard CMAQ has, except for Fort McPherson. Going back to the concentration plot for Fort McPherson in Figure 90, AGD-CMAQ was the only model that captured the $PM_{2.5}$ concentration peak well, but it over predicted the concentrations at times. AG-CMAQ performs better than AGD-CMAQ does for Confederate Ave. site as well but only by 0.83%. Decrease in artificial dilution is achieved through adaptive grid refinement. On top of that, deciding when and where to carry the information from the sub

grid model to the air quality model improves the plume impact predictions. The simulation with AGD-CMAQ is believed to better describe local dispersion of fire emissions and their regional air quality impacts.

4.4.3 Final Evaluation with Other Data

In the last evaluation cycle, after re-evaluation with Fort Benning Burns, Daysmoke was evaluated with data collected at Eglin AFB in 2011. The fire spread model Rabbit Rules was used to generate some of Daysmoke's inputs therefore the section starts with the application of Rabbit Rules. The chemistry transport model evaluations focused on the methods used for adaptive grid modeling and coupling with Daysmoke. The sensitivities of model predictions to various parameters related to emissions and meteorological inputs were investigated.

4.4.3.1 Evaluation of Fire Spread Model

This research did not target the evaluation of the fire spread model Rabbit Rules described in Section 3.2.1. Rabbit Rules was evaluated independently by Achtemeier (2012). Here, the model was applied to the 6 February 2011 Burn at Eglin AFB. Different from burns at Fort Benning, this burn involved aerial ignition. However, as long as the ignition pattern is available, Rabbit Rules could also be applied to hand-lit fires.

The purpose of the application of Rabbit Rules to 6 February 2011 burn of Eglin Block 703C is to generate the updraft core number and other input parameters used in Daysmoke. Given the short period of ignition (approximately 1 hr), Rabbit Rules was run with the hourly average wind (1200-1300 CST; Eglin AFB is in the Central Time zone) for 10 m (210 degrees at 1.3 ms^{-1}) and for 100 m (210 degrees at 1.5 ms^{-1}) obtained from MM5 meteorological model, which was used in addition to WRF to predict the weather.

Rabbit Rules was set up to reproduce the helicopter pathway and the time rate of deposition of ignition balls beginning at 1206 CST. Figure 92 shows the distribution of fire over the 660 ha tract at 12:41:57 CST. Fire expanded about the ignition points and merged with adjacent ignitions to form lines spaced at approximately 100 m. Average fire spread rate was 0.20 ms^{-1}.

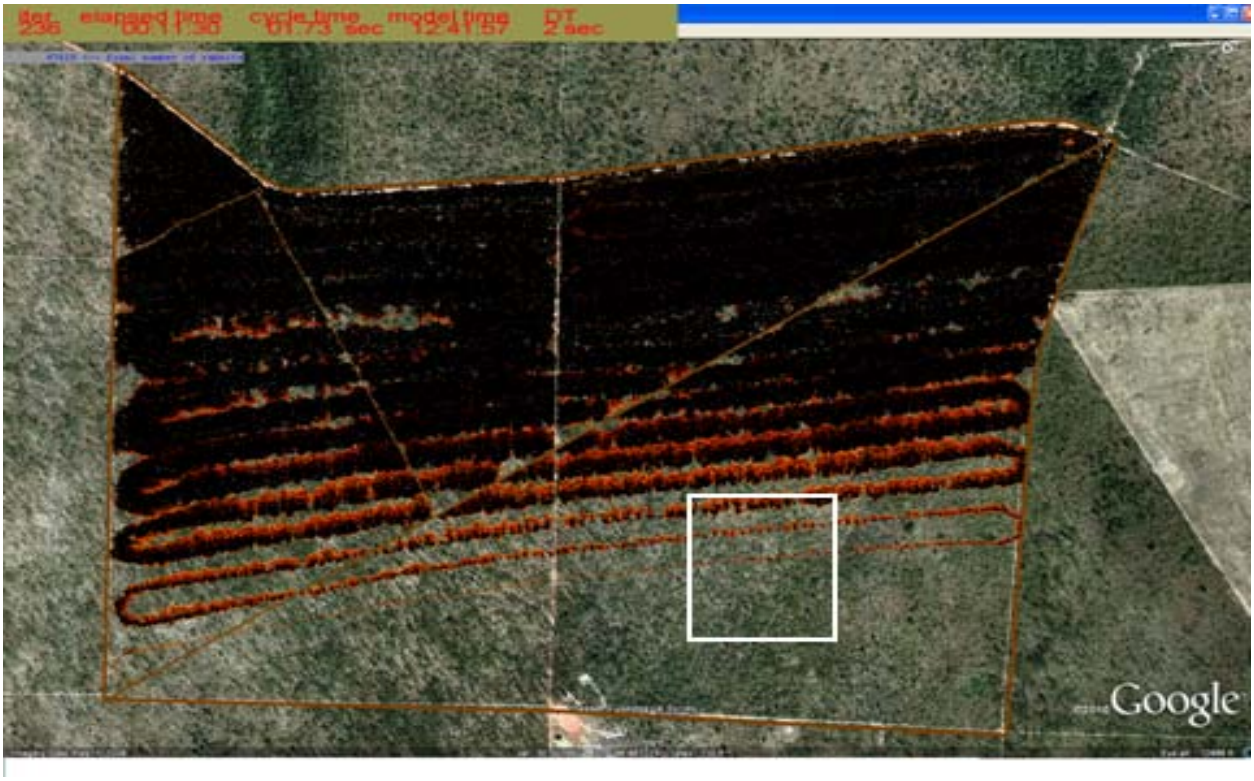

Figure 92. Progress of helicopter ignition and burn-out over Eglin Block 703C for 12:41:57 06 Feb 2011. The sub-area detailed in Figure 93 is denoted by the white square.

The fire behavior in the presence of light ambient winds needs further explanation. Figure 93 shows an example of fire-atmosphere coupling within a sub-area of Block 703C (white square in Figure 92). The meteorological grid spacing in Rabbit Rules is 60 m. Explanations of wind and fire behavior are given in reference to the center point (white dot). The first panel (12:32:43) shows the undisturbed prevailing 1.3 ms^{-1} winds blowing from 210 degrees. By 12:40:02 (second panel) three lines of fire laid down by the helicopter are visible in the upper half of the figure. "Draw-in" of air toward the combustion zone accelerated the winds to 2.5 ms^{-1} at the white dot. These winds increased to 4.0 ms^{-1} at 12:44:55 toward a convergence axis (white dotted line) that locates the center-line of the smoke plume and beyond which winds were blowing from the north. The feed-back was a relatively intense faster-spreading head fire (12:46:58) which increased heat production and maintained the strong "draw-in".

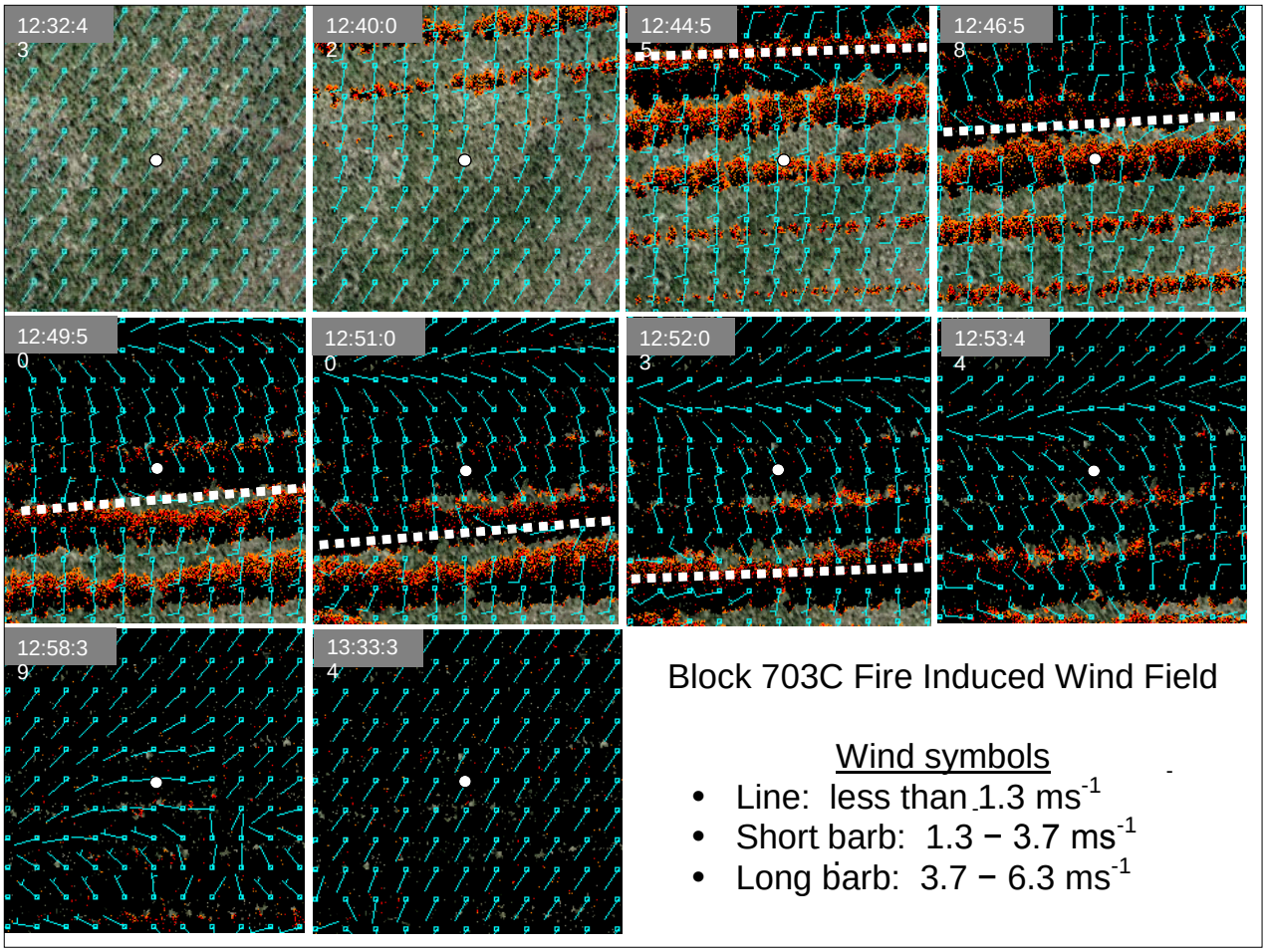

Figure 93. Fire-atmosphere coupling between winds and fire on the landscape within a sub-area of Figure 92.

As the helicopter laid down new fire to the south and areas north of the center point burned out, the plume axis shifted south of the center point (12:49:50), in phase with the zone of maximum heat accumulation. Where the head fire had not burned to the adjacent fire line, the wind shifted to blow from the northwest at 5.0 ms^{-1} and converted the head fire to a slow-moving backfire (12:51:00) creating islands of unburned fuel (12:52:03). As the plume axis moved farther away, the "draw-in" died down (12:53:44) allowing the backfire to consume the remaining fuel (12:58:39). Finally, winds returned to pre-burn ambient conditions (13:33:34). This sequence of helicopter lay-down of fire, followed by draw-in establishing a head fire, passage of the plume axis, local burn-out or conversion to backfire, to final burn-out was repeated over most of Block 703C.

The time-series of the north-south wind (v-component) at the center point in Figure 93 is shown in Figure 94. Draw-in ahead of the plume axis from 12:32 – 12:47 and draw-in behind the plume axis from 12:50 – 12:58 must be compensated by sinking of air from aloft. Slow-down and reversal of winds during the period from 12:47 – 12:50 must be compensated by updraft into the base of the plume. From the spatial distribution of the winds in Figure 93, it can be inferred that

the maximum width for the plume base is not larger than twice the spacing of the meteorological grid or 120 m for this case.

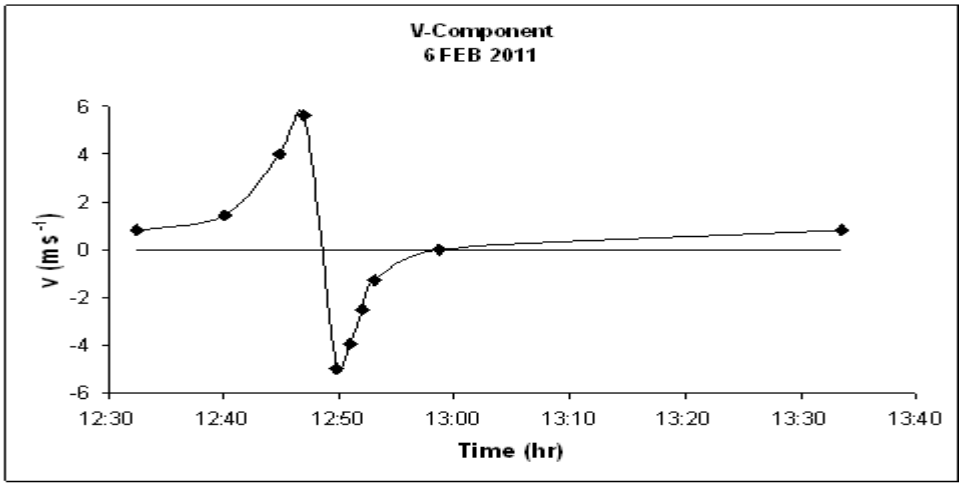

Figure 94. Time series of the north-south wind at the center point shown in Figure 93.

Initial plume rise w_0 for conservation of flux into opposite sides of a box of height, h, and length, x, and up into a linear updraft of width y requires the vertical velocity within the plume above the convergence line in Figure 93 to obey

$$w_0 = \frac{hx}{xy}(U_1 - U_2) \tag{33}$$

However, farther above ground, the updraft organizes into a string of n updraft cores of effective diameter, d. Thus,

$$w_0 = \frac{4hx}{n\pi d^2}(U_1 - U_2) \tag{34}$$

where U_1 and U_2 represent flow through the opposite sides of the box.

For radial draw-in to a single updraft core (Figure 95), the flux of air through the sides of a cylinder of radius, r, and height, h, and draw-in speed, U_0, must equal the flux of air into the updraft core of effective diameter, d, and vertical velocity w_0. The equation for w_0 is,

$$w_0 = \frac{8rhU_0}{d^2} \tag{35}$$

For the convergence line, substitution of the pertinent quantities (U_1 = 5.0 ms^{-1} and U_2 = -5.0 ms^{-1}) in Equation (34) yields $w_0 = 2.12h/n$ if $x = 40\Delta x$ across the length of a fire line in Figure 93 and $d = 2\Delta x$ (120 m). Thus w_0 depends on the choice for h and the number of updraft cores distributed along the length of the fire line. If h = 10 m, $w_0 = 21.2/n$. As regards radial draw-in,

draw-in speed, U_0, and the radius, r, can be obtained from Figure 95, for example, U_0 = 6.3 ms^{-1} on average at $r = 3\Delta x$. Furthermore, an estimate for the effective core diameter is d = 120m. Substitution of these quantities in Equation (35) yields $w_0 = 0.63h$. If h = 10 m for the radial draw-in, w_0 = 6.3 ms^{-1} – about 25 percent of the estimate from the literature for effective plume diameter for a bent-over plume used by Achtemeier et al. (2011) and for the line convergence case, w_0 = 5.3 ms^{-1} if n = 4. Deepening the draw-in depth to canopy height (if at 30 m) triples w_0. Reducing the effective core diameter also increases w_0. Therefore, reasonable estimates for initial updraft core vertical velocities range from 5.0 – 25.0 ms^{-1}.

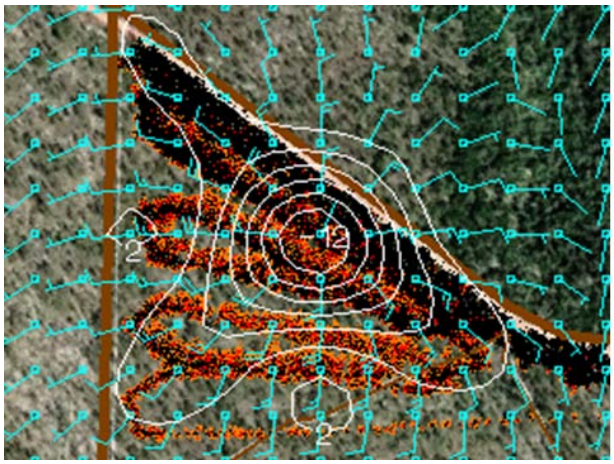

Figure 95. Winds and divergence (1 unit = 0.012 s^{-1}) simulated by Rabbit Rules for a radial-inflow isolated updraft core at 12:22:52. Wind speed convention is the same as that for Figure 93.

Needed to complete calculations for initial plume dynamics is a mechanism for estimating updraft core number. From Equation (5), areas of heat accumulation into an incipient plume are represented in Rabbit Rules by low pressure anomalies. During the simulation of fire spread, pressure anomalies ranged as low as -1.4 mb and the number ranged from one to six but typically was four. At 12:40:41 (Figure 96), largest pressure anomalies of -1.0 mb are located along the zone of maximum fire near the boundaries of Block 703C. A minor center of -0.4 mb is located behind. The yellow ellipses highlight locations of pressure anomaly centers that could direct the winds into updraft cores. The large ellipse encloses three centers joined by an axis of low pressure. It is inferred that these could merge into a single updraft core a short distance above the ground.

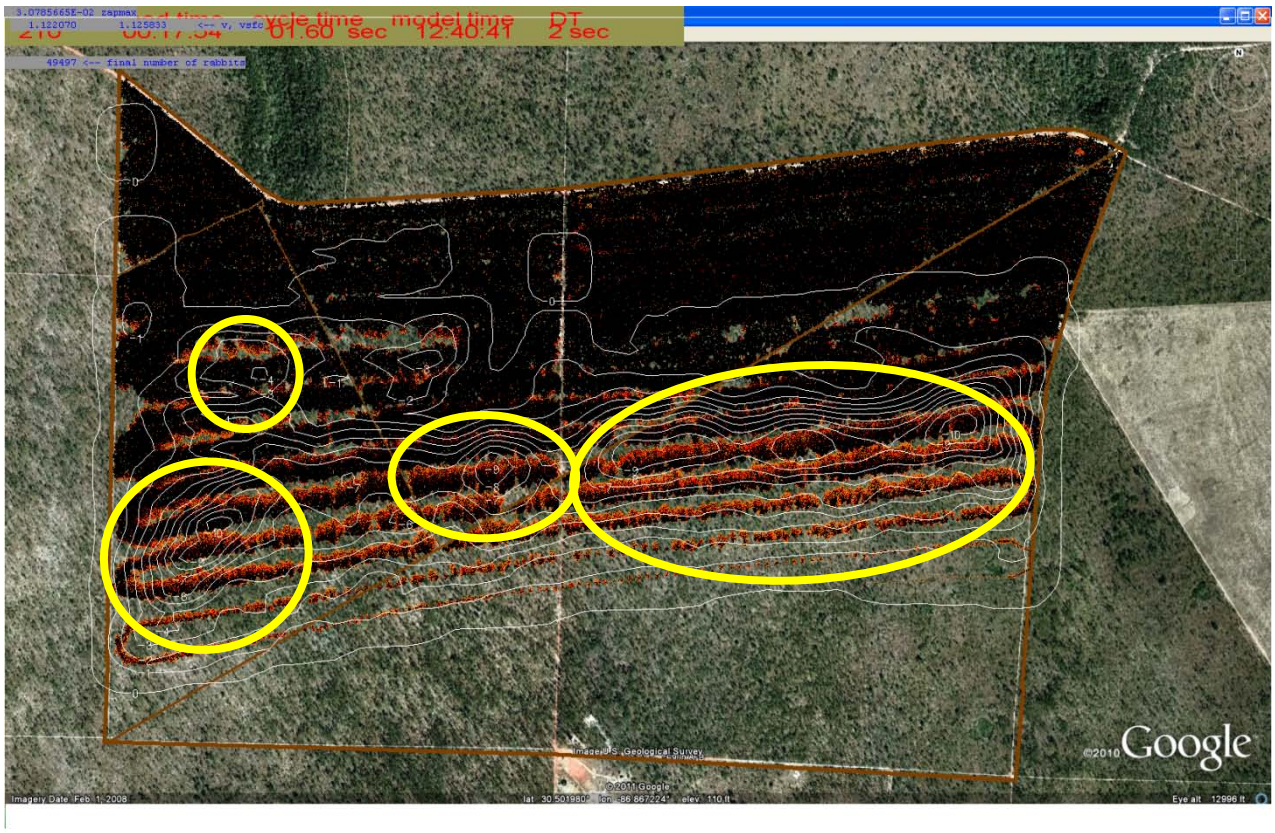

Figure 96. Pressure anomalies (white lines) generated by Rabbit Rules at 12:40:41. The yellow ellipses highlight centers that might correspond to updraft cores.

The multiple-core updraft structure of the Block 703C burn is shown by a photo-image taken from a location 42 km east-southeast from the burn (Figure 97). There were two prominent updraft cores on the far left and far right of the burn (long arrows). In the center, there appear either two closely spaced updraft cores or two updraft cores that merge into one updraft core partway in ascent (two small arrows). The time of the photo-image was not taken. However, the extent of spread of the plume top would infer that the image was taken midway or later during the burn.

Figure 97. Photo-image of the Block 703C plume taken from a bridge 42 km east-southeast from the burn.

Finally, Rabbit Rules provides time-series of relative emissions expressed as a percentage of total emissions per minute. Figure 98 shows that relative emissions peaked twice, first at 1218 CST (12 minutes after beginning of ignition) to 2.73 percent of total emissions, then to 4.26 percent at 1240 CST (34 minutes after beginning of ignition).

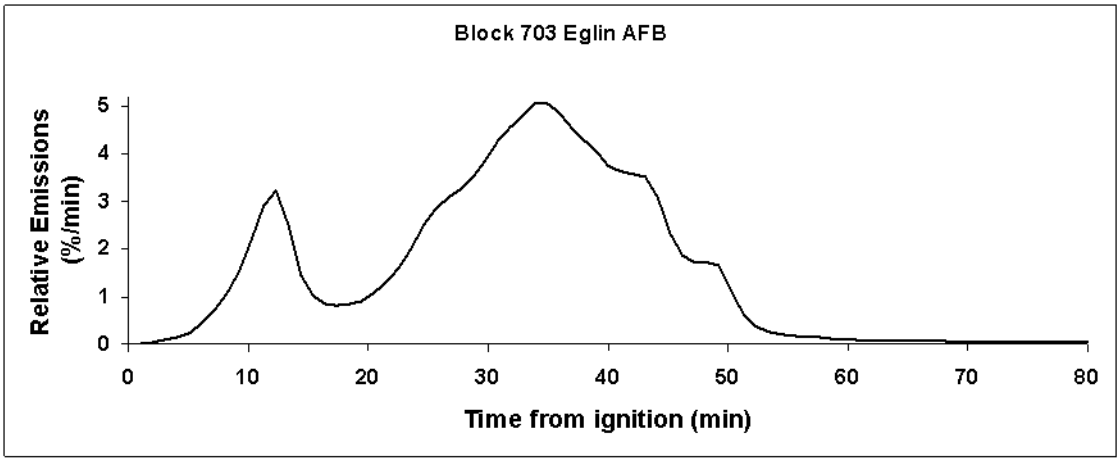

Figure 98. Relative emissions as a function of total emissions for the Block 703C burn as simulated by Rabbit Rules. Ignition started at 1206 CST.

4.4.3.2 Final Evaluation of Dispersion Model

In this section Daysmoke will be evaluated using all of the data collected at Fort Benning and Eglin AFB. The newly developed highly-tilted plume solution and new initial conditions derived from Rabbit Rules are the foci of the evaluation.

4.4.3.2.1 Evaluation of Daysmoke with Burns Monitored at Fort Benning

In 2008 and 2009, a total of eleven burns were monitored at Ft. Benning and plume height and ground-level smoke data were collected for the evaluation of Daysmoke. These burns were analyzed and placed into five categories according to the trend of measured $PM_{2.5}$ concentration with downwind distance (Table 16). The number in parenthesis in front of each burn date is to keep track of the order in which the burns were monitored: the first burn was on 8 April 2008, the second burn on 14 April 2008, and so on. Detailed reports of the burn analyses are included in Appendix A. Note that the updraft core numbers for all Fort Benning burns were set by using the Subjective Method described in Section 4.2.2.1.7.1.

Table 16. Fort Benning burns listed by plume characteristics.

Increase	Decrease	Extreme Decrease	Out of Plume	Misc
(1) 9 Apr. 08	(2) 14 Apr. 08	(6) 15 Jan. 09	(4) 13 Jan. 09	(5) 14 Jan. 09
(8) 21 Jan. 09	(3) 15 Apr. 08	(9) 23 Jan. 09	(7) 20 Jan. 09	
(10) 8 Apr. 09	(11) 9 Apr. 09			

In the middle panel of Figure 99, where Daysmoke performance is illustrated, the burn days are color coded by category and marked by their corresponding number in Table 16. On days coded by orange, measured $PM_{2.5}$ concentrations increased with distance downwind from the burn, Truck 1 measuring the highest concentrations and Truck 3 measuring the lowest. On days coded by magenta, $PM_{2.5}$ concentrations decreased with distance. There were three days in each of these categories. On two days coded by brown, extremely high $PM_{2.5}$ concentrations at Truck 1 rapidly decreased to almost no $PM_{2.5}$ at Truck 3. On two days coded by light blue, analysis has shown that the Trucks were outside of the smoke plume due to access issues (either no roads or movement restricted by military activities). Data did not allow categorization on 14 January 2009 (no color). Discarding the out of plume and miscellaneous categories, eight burns remained for Daysmoke performance evaluation.

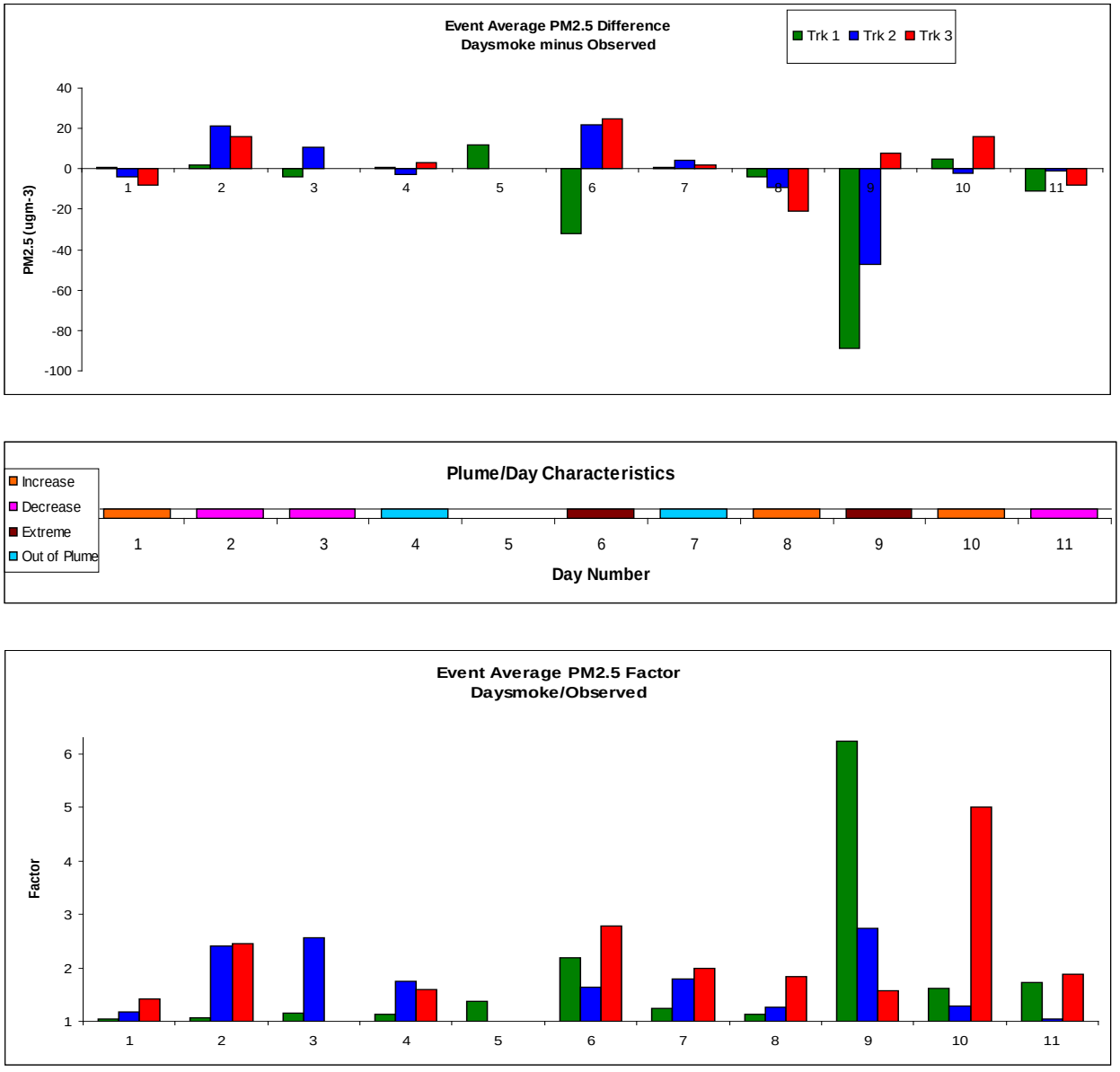

Figure 99. Daysmoke performance for each burn event and at each monitor: difference of modeled $PM_{2.5}$ from observed (top), classification of the burn event by the trend of concentration with distance downwind (middle), and ratio of modeled to observed or vice versa $PM_{2.5}$ (bottom).

Recall that Daysmoke contains stochastic terms for convective circulations that involve random numbers which cannot be repeated. Thus successive Daysmoke runs will give slightly different answers. To smooth out the effects of the stochastic terms, each burn was simulated with Daysmoke five times and an ensemble average was calculated. The top panel of Figure 99 shows the event average departure from observations – the difference between $PM_{2.5}$ concentrations calculated by Daysmoke and $PM_{2.5}$ concentrations observed at each truck for the whole period of observations – generally beginning one half hour before ignition and ending at the completion of ignition. The trucks are color-coded with Truck 1 (green), Truck 2 (blue), and Truck 3 (red).

Note that Truck 3 average departure is missing on 15 April 2008 (Day 3) since the truck was stuck in mud and could not perform any smoke measurements. With data from the other two trucks this day could still be categorized as decreasing $PM_{2.5}$ with distance. However, on 14 January 2009 (Day 5), since both Truck 2 and Truck 3 data were missing (corrupted or lost) this burn could not be categorized; therefore it was thrown into the miscellaneous bin and excluded from model evaluation. The lower panel of Figure 99 shows the event average factor of departure calculated as the larger $PM_{2.5}$, measured or modeled (ensemble average) divided by the smaller of the two $PM_{2.5}$ values.

Most of the departures in the top panel of Figure 99 are less than 20 μgm^{-3}. These results could be excellent or poor depending on the relative magnitudes for both modeled and observed $PM_{2.5}$. Therefore, both departures (top panel) and departure factors (bottom panel) should be considered to correctly interpret Daysmoke's performance. For example, for 14 April 2008 (Day 2), the departures for both Truck 2 and Truck 3 are around 20 μgm^{-3}. This could be interpreted as good performance if $PM_{2.5}$ magnitudes were high (e.g., for a $PM_{2.5}$ magnitude of 100 μgm^{-3} a departure of 20 μgm^{-3} would correspond to 20% modeling error). However, both Truck 2 and Truck 3 Daysmoke $PM_{2.5}$ are off by greater than a factor of 2.

When $PM_{2.5}$ concentrations increased with distance, Daysmoke performed well except for Truck 3 on Day 10: observed $PM_{2.5}$ was small therefore resulting in a large departure ratio. Daysmoke performance deteriorated for the decreasing $PM_{2.5}$ category of burns. On two days (6, 9) in the extreme decrease category, Daysmoke performed poorly as shown by the large event average $PM_{2.5}$ differences plus large departure ratios. The bottom panel shows that, on five of the eleven days, Daysmoke was off by a factor greater than 2 for at least one truck. On a per truck basis, there were 30 events of which seven exceeded a factor of 2.

The analysis in Figure 99 has shown a relationship between the performance of the model and the gradient of the observed $PM_{2.5}$ by downwind distance. A more detailed quantitative analysis including the spreads of the departures can be found in Achtemeier et al. (2011). Daysmoke performance was the best on days when smoke concentration increased with distance downwind from the burn. Given the uncertainty in defining Daysmoke's updraft core number and uncertainties in wind speed and direction, the results for this category are as good as can be expected from an empirical-statistical model. On days when smoke concentrations decreased with distance, Daysmoke performance was not as good but still acceptable. Daysmoke slightly underpredicted $PM_{2.5}$ at Truck 1 and overpredicted $PM_{2.5}$ at Truck 2 and Truck 3. On days characterized by extremely high smoke gradients, from very high smoke concentrations at Truck 1 (1-3 km downwind from the burn) to almost no smoke at Truck 3 (5-7 km downwind), Daysmoke performance in predicting $PM_{2.5}$ concentrations was poor.

Figure 100 shows the ensemble average departures (squares) as well as the spreads (demarcated by horizontal bars) for the three truck locations during the 23 January, 2009 burn at Fort Benning. Daysmoke greatly underpredicted burn event average $PM_{2.5}$ at Truck 1— minus 60 μgm^{-3} with a spread ranging from −32 to −89 μgm^{-3}. The average residual was improved for Truck 2 (−12 μgm^{-3}) but the spread remained high (−47 to 22 $\mu\mu gm^{-3}$). The better results at Truck 3 could be explained by the truck being located near the edges of the plumes.

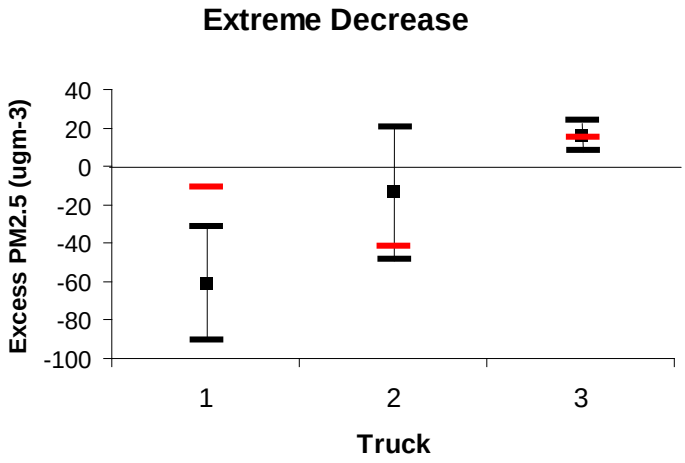

Figure 100. Ensemble average Daysmoke minus observed $PM_{2.5}$ (black squares) at the three trucks for the two days of high smoke concentrations at Truck 1 and steep gradients of smoke between the trucks. The spreads of the departures are shown by the horizontal bars. Red bars: Daysmoke minus observed $PM_{2.5}$ for a highly tilted plume for 23 January 2009.

The poor Daysmoke performance for the burns categorized as "extreme decrease" due to very high $PM_{2.5}$concentrations at Truck 1 locations and steep gradients of $PM_{2.5}$ between the trucks (third column of Table 16) was addressed by the highly tilted plume solution described in Section 4.2.2.1.6. When the initial conditions of w_0 = 25 m s^{-1} and ΔT_0 = 40 °C were modified to w_0 = 0.5 ms^{-1} and ΔT_0 = 1.0 °C and the updraft core number was increased to 8, Daysmoke predicted a plume that first rolls along the ground and then lifts along quasi-linear axis with a slope of about 15°. The red bars in Figure 100 show that the 30-min averaged $PM_{2.5}$ difference between Daysmoke and observed smoke concentration at Truck 1 of $-8 \mu gm^{-3}$ was greatly improved over the $-89 \mu gm^{-3}$ calculated for the bent-over plume. Results for Truck 2 and Truck 3 showed minor changes from the original differences for 23 January 2009.

Figure 101 compares the Daysmoke-predicted plume heights to the heights observed by the ceilometer for six burns monitored at Fort Benning. Plume top heights (squares) and height ranges (connecting lines) for plumes simulated by Daysmoke (red squares) compare favorably with plume top heights measured by ceilometer (black squares). Relative to the observed lower range, Daysmoke plume tops were on the average 8 m high. However, relative to the observed higher range, Daysmoke tops were on the average −200 m low. Thus Daysmoke plume tops were, overall, slightly low.

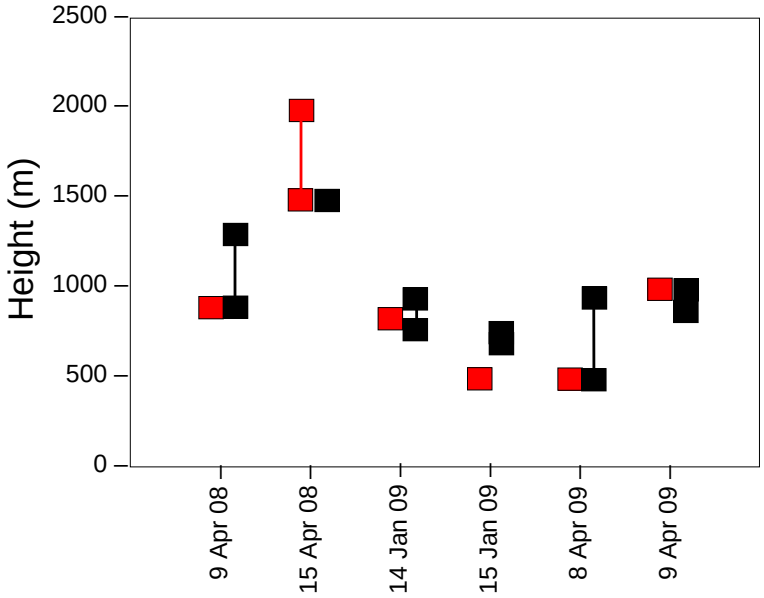

Figure 101. Plume heights for Daysmoke-simulated plumes (red squares) compared with plume heights observed by ceilometer (black squares) for six prescribed burns at Fort Benning. Plume height ranges less than 100 m during the course of the burn are represented by single squares.

4.4.3.2.2 Evaluation of Daysmoke with Eglin Burns

Two burns at Eglin AFB, 6 February 2011 burn of Block 703C and 8 February 2011 burn of Block 608A, were simulated by Daysmoke. What makes these burns different than Fort Benning burns is the ignition method used (aerial ignition). Ignition was performed by a helicopter dropping hundreds of self-igniting balls to the ground.

4.4.3.2.2.1 Daysmoke Evaluation in 6 February 2011 Burn at Eglin AFB

Updraft core number and other Daysmoke plume initial conditions were generated by using the fire spread model Rabbit Rules as described in Section **Error! Reference source not found.**. In applications to Fort Benning burns (except for re-evaluation of Daysmoke in 23 January 2009 burn; see Figure 100) , w_0 and ΔT_0 were set to, respectively, 25 ms^{-1} and 40 ^oC as suggested by Jenkins et al. (2001). However, these values derived from grass fires may not be valid for fires in southern United States pine forests. Depending on assumptions, the initial vertical velocities calculated from Rabbit Rules ranged from 5-25 ms^{-1}. Further reductions on transfer of momentum from the plume to the trees through canopy drag should be expected. Furthermore, transfer of heat from the plume passing through the canopy would be expected to reduce the initial temperature anomaly. Thus the initial vertical velocities for the four updraft cores were set to range from 8-12 ms^{-1} stochastically (shaded area in Figure 102a) and the initial temperature anomaly was set to 30 ^oC. These numbers are approximate and more accurate estimates await future research.

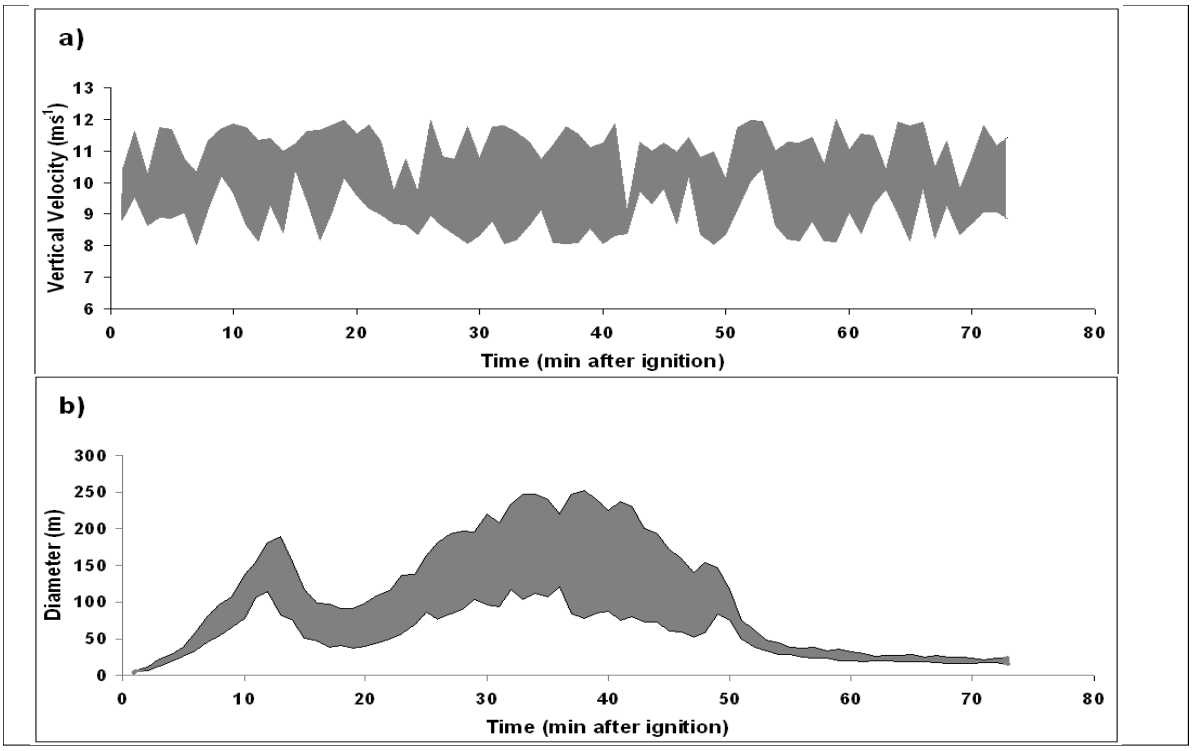

Figure 102. 1-min time-series from Rabbit Rules for a) initial vertical velocity and b) initial effective plume diameter for the range of updraft cores calculated for the 06 Feb 2011 burn. Ignition started at 1206 CST.

Total mass flux (in units of mass flux per minute) and total $PM_{2.5}$ (49,280 kg) was partitioned into 80 minutes, from 1206 CST to 1326 CST, according to the relative emissions production simulated in Rabbit Rules (Figure 98). Thus updraft cores were recalculated for every minute. The volume fluxes of the individual updraft cores were defined subject to the constraints put forth in the derivation of Equation (9). The range of initial plume diameters D_{0k} (shaded area in Figure 102b) were calculated by replacing f_0 with f_k in Equation (8).

Figure 103 shows 5-min time-series of MM5 and WRF-simulated maximum plume top height and plume depth calculated at a reference distance of 12.5 km (7.8 mi) along the plume axis (red asterisk for MM5 in Figure 106) equal to the distance of the ceilometer (yellow square) from the burn. Note that Daysmoke plume heights were obtained from a "projected cross section" – all smoke points were projected onto a vertical plane (arrow) extending from the burn site along the plume axis. Therefore the maximum heights and the minimum heights contained in the cross-sections do not exactly represent plume structures observed at the ceilometer located approximately 3.7 km from the plume centerline.

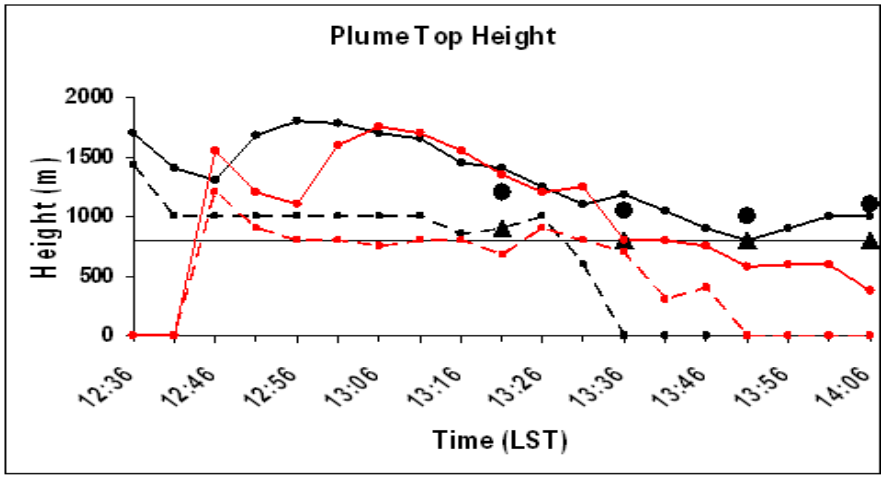

Figure 103. Plume top heights and bases of Daysmoke simulations based on WRF (black lines – solid and dashed) and MM5 (red lines – solid and dashed) for the 6 February 2011 burn of Block 703C at Eglin AFB. The mixing height simulated by MM5 is shown by the horizontal line at 800 m. The plume data were calculated from Daysmoke at 12.5 km (7.8 mi) downwind from the burn. Plume tops and bases observed by ceilometer are given, respectively, by the large circles and triangles.

After ascent into the free atmosphere above the mixed layer, the plume was subject to stronger transport winds in the WRF sounding than in the MM5 sounding (Figure 104). Regarding the WRF-based simulation, the maximum plume top of 1800 m traveled at 6.9 ms^{-1} to arrive at the reference distance at 12:56 (solid black line in Figure 103). That was approximately 10-min before the arrival of the 1750 m plume top in the simulation using the MM5 sounding (solid red line in Figure 103) which was traveling at 5.2 ms^{-1}. The plume top height minimum at 16:46 (WRF) and 16:56 (MM5) corresponds to the minimum in relative emissions at 18 minutes after ignition in Figure 98 and the minimum in updraft core diameter at 18 minutes after ignition in Figure 102b.

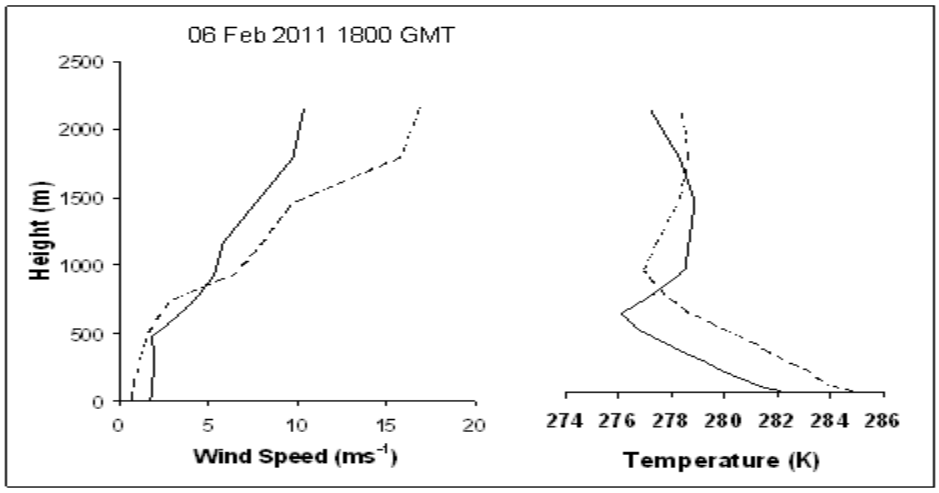

Figure 104. Vertical profiles of wind speed and temperature for the first 2.2 km above Block 703C on 1200 CST 06 February 2011. Solid lines are simulations by MM5 and dashed lines are simulations by WRF.

Ceilometer observations of plume top height (large circles in Figure 103) began at 13:21 and declined slowly from 1200 m to 1000 m at 13:51 then rose again to 1100 m at 13:56. Both Daysmoke simulations came into agreement after 13:06 having declined from the maxima to 1400 m (1350 m) by 13:21 after which the time-series for the WRF-based simulation (black line) continued in relatively good agreement with the observed plume top heights through 14:06. After 13:36, the time-series for the MM5-based simulated plume tops (red line) fell below the observed plume base (solid triangles).

The ceilometer also observed a well-defined plume thickness of approximately 300 m thus giving plume base as shown by the solid triangles. Both MM5 and WRF-based simulations gave plume bases (dashed lines) defined by the mixing height. Thus the WRF-based plume thickness was 800 m at maximum plume height and declined to 400 m by 13:21. However a projected vertical cross-section of the simulation at 12:56 (Figure 105) showed most “smoke” concentrated within an approximate 300 m layer below the plume top.

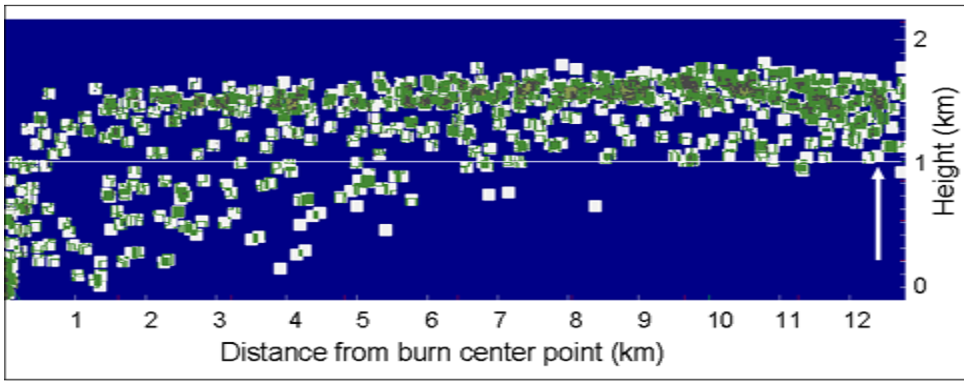

Figure 105. A projected vertical cross-section showing the Daysmoke simulation of the Block 703C burn (WRF sounding) at 12:56 CST. As smoke parcels overlap, their colors go from white to green to brown to indicate increasing particle density. The mixing height is given by the horizontal white line. The "reference distance" is shown by the white arrow.

Average above background ground-level concentrations of $PM_{2.5}$ for the Daysmoke simulation with the MM5 sounding for the period 1200 – 1400 CST are shown in Figure 106. The scattering of white circles along the general plume axis represents above-background concentrations due to smoke of 1-2 μgm^{-3}. Note that simulations were for flaming stage only. Measurements of $PM_{2.5}$ taken at the three sites identified by the red triangles are shown in Figure 107. No smoke was observed at Site 3 (green line) and the absence of smoke at Site 2 (blue line) confirms ceilometer observations of the plume base remaining above 800 m. Smoke was observed at Site 1 after 13:36 at the same time as smoke arrived at the reference distance (red asterisk). Daysmoke did not simulate smoke at Site 1. Therefore the near-simultaneous arrival of smoke at two disparate locations can be explained if smoke was from different sources. Projected vertical cross-sections of the Daysmoke simulations are suggestive that smoke arriving at the reference distance was transported down by convective circulations from the overhead plume passing at higher wind speeds near the top of the mixing layer. Smoke arriving at Site 1 within surface winds blowing at 1.5 ms^{-1} would have departed the closest perimeter of Block 703C 28 min earlier or at approximately 13:08. Aerial ignition had ceased by 12:52. Thus, allowing time for burnout, the source of smoke at Site 1 was likely from smoldering combustion. Figure 107 shows that concentrations increased reaching a maximum at 13:55 CST and remaining at elevated levels thereafter.

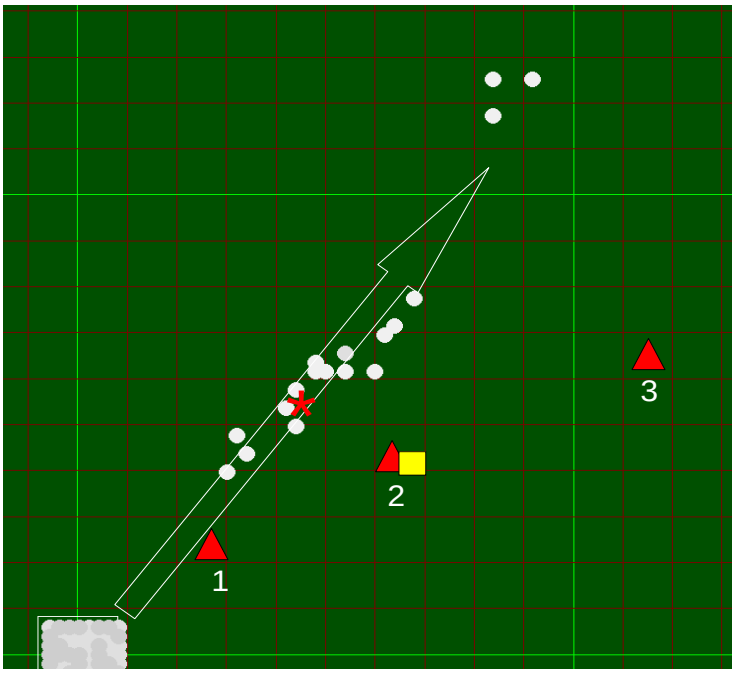

Figure 106. Ground-level $PM_{2.5}$ average concentrations simulated by Daysmoke for a 2-hr period beginning at ignition of the 6 February 2011 burn in Block 703C at Eglin AFB, using the MM5 meteorological sounding. The white dots indicate above-background concentrations due to smoke of 1-2 μgm^{-3}. The small squares represent 1 mi (1.6 km) and the light green square represents 10 mi (16 km). The axis of the plume is given by the white arrow. Also shown are locations of the ceilometer (yellow square) and three $PM_{2.5}$ sampling units (red triangles).

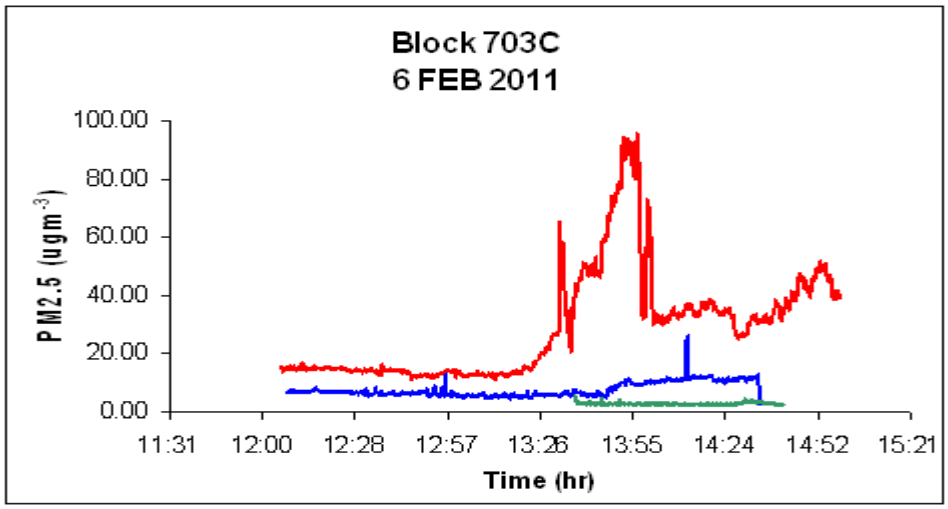

Figure 107. Measurements of $PM_{2.5}$ taken at the three sites in Figure 106: Site 1 (red), Site 2 (blue) and Site 3 (green).

If little flaming phase smoke was recorded and simulated at the ground, where did the smoke go? Recall that Daysmoke also functions as a smoke injector for CMAQ (see Section 3.2.4.1). The amount of smoke injected into a model layer per hour is the smoke passing through a cylinder of radius 11 km (7 mi) at height equal to the layer of interest – the cylinder radius chosen to allow Daysmoke to fully develop the plume. The vertical distribution of smoke shown in Figure 108a (based on the MM5 sounding) has been normalized by layer thickness and is expressed as a percentage of the total smoke passing through the walls of the cylinder for that hour. The mixing height is given by the thin black line at 650 m. For the period 1200-1300 CST (black line) 100 percent of the smoke passing through the wall was above the mixing height where ambient winds were strong enough to carry smoke to the wall. Roughly 84 percent of the smoke passing through the cylinder during the hour ending at 1400 CST was found above the mixing layer (blue line). At 1500 CST (red line) most of the smoke was confined to the mixing layer but this accounted for only 3.5 percent of the total for the burn. Overall, 93 percent of the smoke was confined above the mixing layer. Note that these calculations were done only for particulate matter released during the flaming phase.

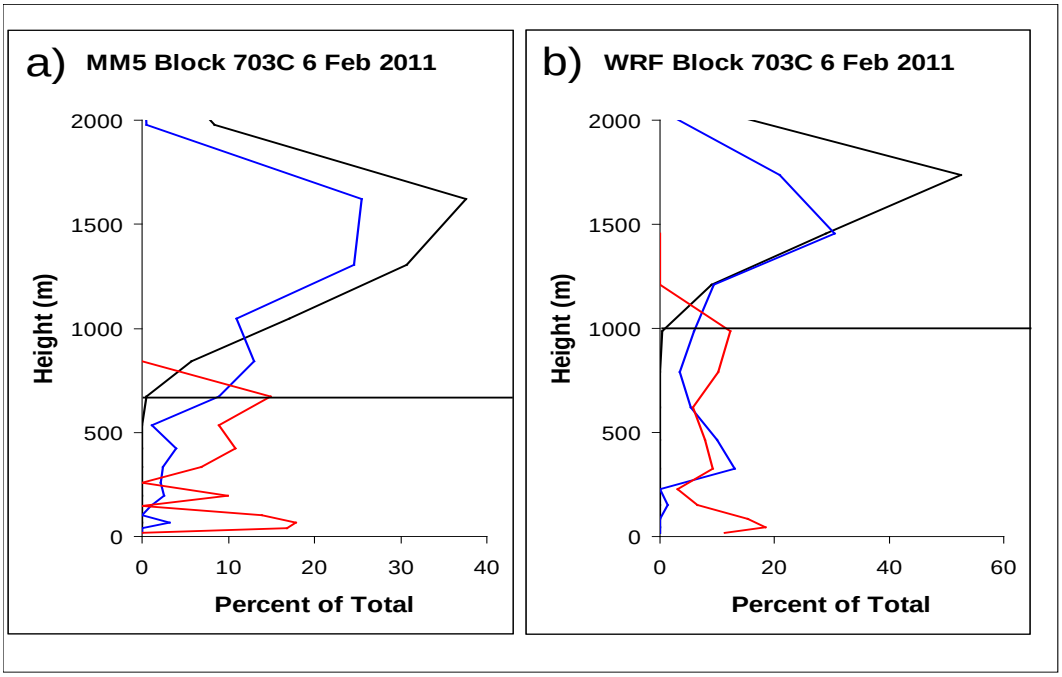

Figure 108. For the Daysmoke simulation done with the a) MM5 and b) WRF soundings: Vertical distribution of smoke within normalized by layer thicknesses and expressed as a percentage of the total smoke passing through a wall of an 11 km radius cylinder for 1300 CST (black line), 1400 CST (blue line) and 1500 CST (red line).

Similar results were found for the simulation done with the WRF sounding (Figure 108b). Note the mixing height at 1000 m. As could be expected from the time-series of plume top heights (Figure 103), particulate concentrations were found higher at 1300 CST than those for the MM5 sounding. By 1500 CST (red line), all smoke was confined below the mixing height. For the total active burn phase, 89 percent of the smoke was confined below the mixing height.

4.4.3.2.2.2 Daysmoke Evaluation in 8 February 2011 Burn at Eglin AFB

One of the objectives in simulating this burn was to determine the uncertainty in smoke estimates of the dispersion model created by the uncertainty in emissions estimates. To generate a range of smoke estimates, four different emissions input sets were generated to be input to Daysmoke. The first set was obtained by multiplying measured fuel consumptions by the $PM_{2.5}$ emission factor measured by the EPA Aerostat at the site (Block 608A). This is considered to be the most accurate $PM_{2.5}$ emissions input set. The second set was generated by multiplying measured consumptions by the emission factors derived from burns simulated in the laboratory using Fort Benning fuels. The difference between Eglin fuels and those from Fort Benning and the difference between actual field conditions and laboratory conditions should create a reasonable approximation to the typical uncertainty found in emissions estimates. The third and fourth sets were obtained by multiplying the consumption estimates of CONSUME by the emissions factors from AP42 tables and US Forest Service southeastern fuels set (Urbanski et al., 2009), respectively. Both of these emission factor sets provide flaming and soldering emission factors for $PM_{2.5}$, Flaming consumption was multiplied by flaming phase emission factors and smoldering consumption was multiplied with smoldering phase emission factors.

Figure 109 shows the hourly $PM_{2.5}$ emissions calculated by the four different methods described above. As mentioned previously in Section 4.1.4.2, measured consumptions were smaller than modeled consumption (see Figure 20 and Table 9). A comparison of the emission factors used can be found in Figure 21. The largest amount of emissions is obtained by using the measured consumption with the EPA Aerostat factor. The two emissions calculated from modeled consumption are very similar and is within 4% of each other but emissions from measured consumption differ by 31.5%.

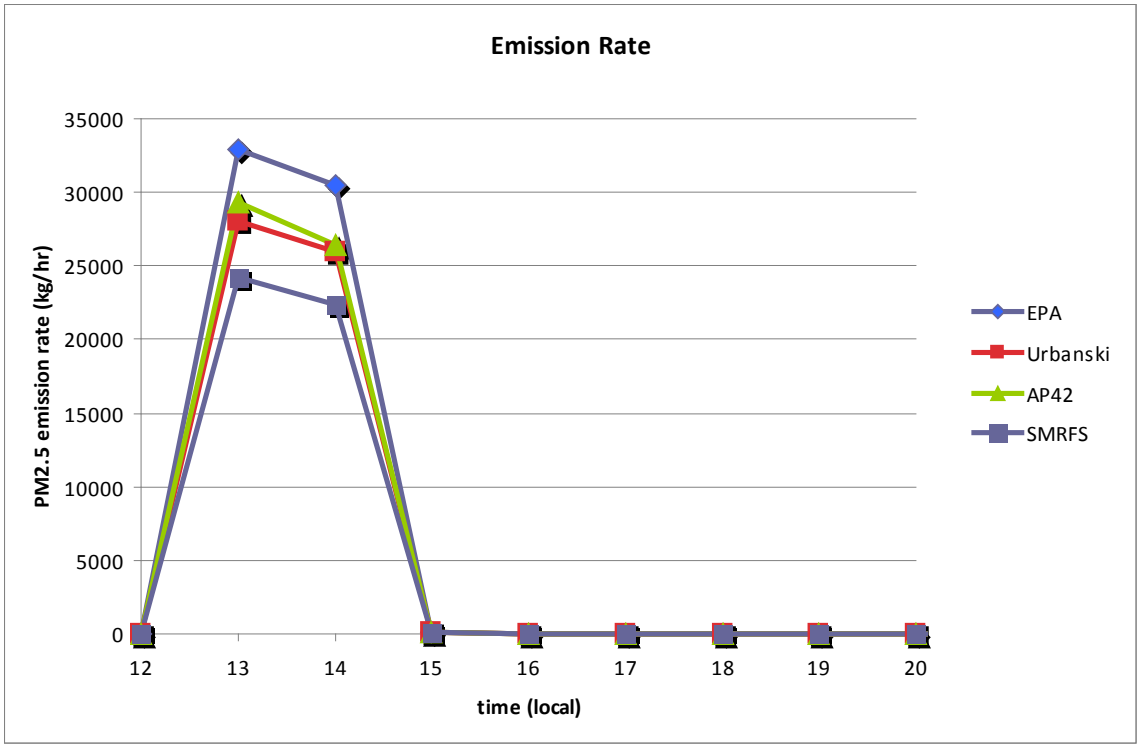

Figure 109. Hourly emission rates calculated by FEPS for the 8 February 2011 burn of Eglin Block 608A using different sets of emission factors.

Figure 110 shows a close-up of the burn area already shown in Figure 55. In this Google Earth picture, the blue balloon marks the approximate operation location of the EPA aerostat, which carried instruments both for emissions and wind measurements. Ground level smoke and plume height were measured at the stationary site, and ground level smoke was measured by the mobile sites.

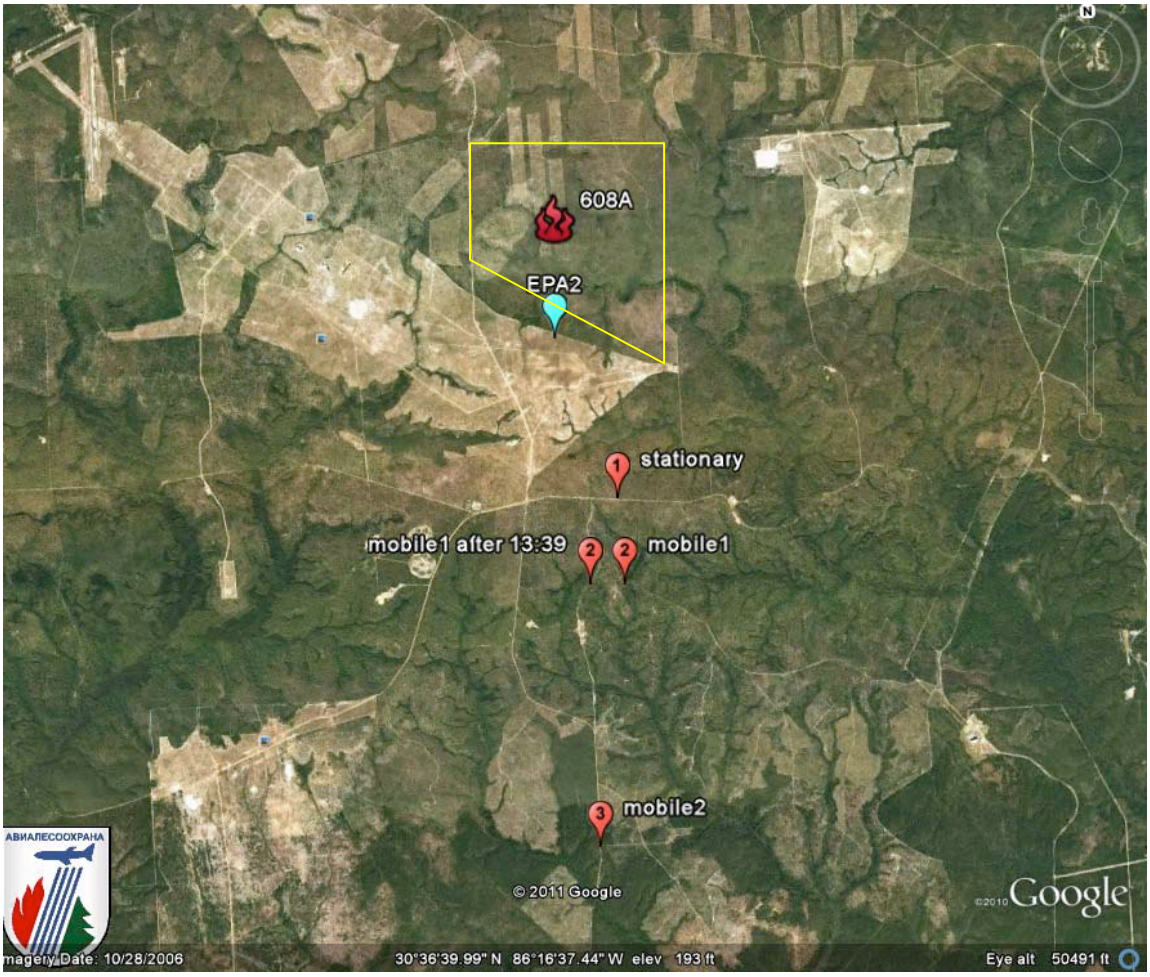

Figure 110. Monitoring locations at Eglin AFB on 8 February 2011: Block 608A is demarcated by yellow line and EPA Aerostat location is marked in blue. Stationary and mobile site locations are marked in red.

The dispersion of smoke was simulated with all four emission inputs shown in Figure 109, first without any adjustments to WRF-predicted winds. The results are compared to smoke measurements in Figure 111. Recall that the stationary site measured $PM_{2.5}$ with a TEOM and AeroTrak particle counter but the mobile units were equipped only with particle counters. Daysmoke was run 11 times with each emission set and the runs with the highest and lowest two $PM_{2.5}$ predictions were discarded. The horizontal bars denote the range of $PM_{2.5}$ predictions from the remaining 7 runs and a line is fitted through the means. Both measurements and Daysmoke results shown are 10-minute averages.

Among the AP42, Urbanski and SMRFS emission sets, the mean of one usually falls within the 63% prediction range of the others. This can be interpreted as the variability due to using a different emission input set being smaller than the Daysmoke predicted variability due to turbulence in the atmosphere. Because of the comparable variabilities, it is difficult to make a judgment about the effects of using these emission input sets. However, the EPA emission set based on consumption and EF measurements results in clearly higher $PM_{2.5}$ predictions both at

the stationary site and at Truck 2 location. Since this set of emissions is nominal (best approximation of actual emissions), it can be concluded that using laboratory derived EFs or estimated consumption with AP42 or Urbanski EFs may lead to significantly lower downwind $PM_{2.5}$ predictions.

The other result that can be deduced from Figure 111 is that, with WRF-predicted winds, Daysmoke overestimated downwind $PM_{2.5}$ levels at the stationary site and more so at Truck 2 location. At the stationary site, there seems to be good agreement between $PM_{2.5}$ measurements and Daysmoke predictions using AP42, Urbanski and SMRFS emission inputs. However, recall that these input sets led to lower Daysmoke predictions than the EPA emission set, which shows a clear overprediction at the stationary site. This overprediction may be due to an error in wind directions predicted by WRF. Recall that the surface wind direction (WD) measured at the stationary site shifted from the forecasted WD by about 20° to the west (Section 4.3.3.3). The truck drivers were able to see the shift and they tried to move to the west (see Truck 1 movement in Figure 110) but ran into a restricted area therefore they could not align themselves with the axis of the actual plume. On the other hand, the predicted plume axis aligned perfectly with the truck locations. This led to the extreme overprediction at the Truck 2 location (bottom panel in Figure 111).

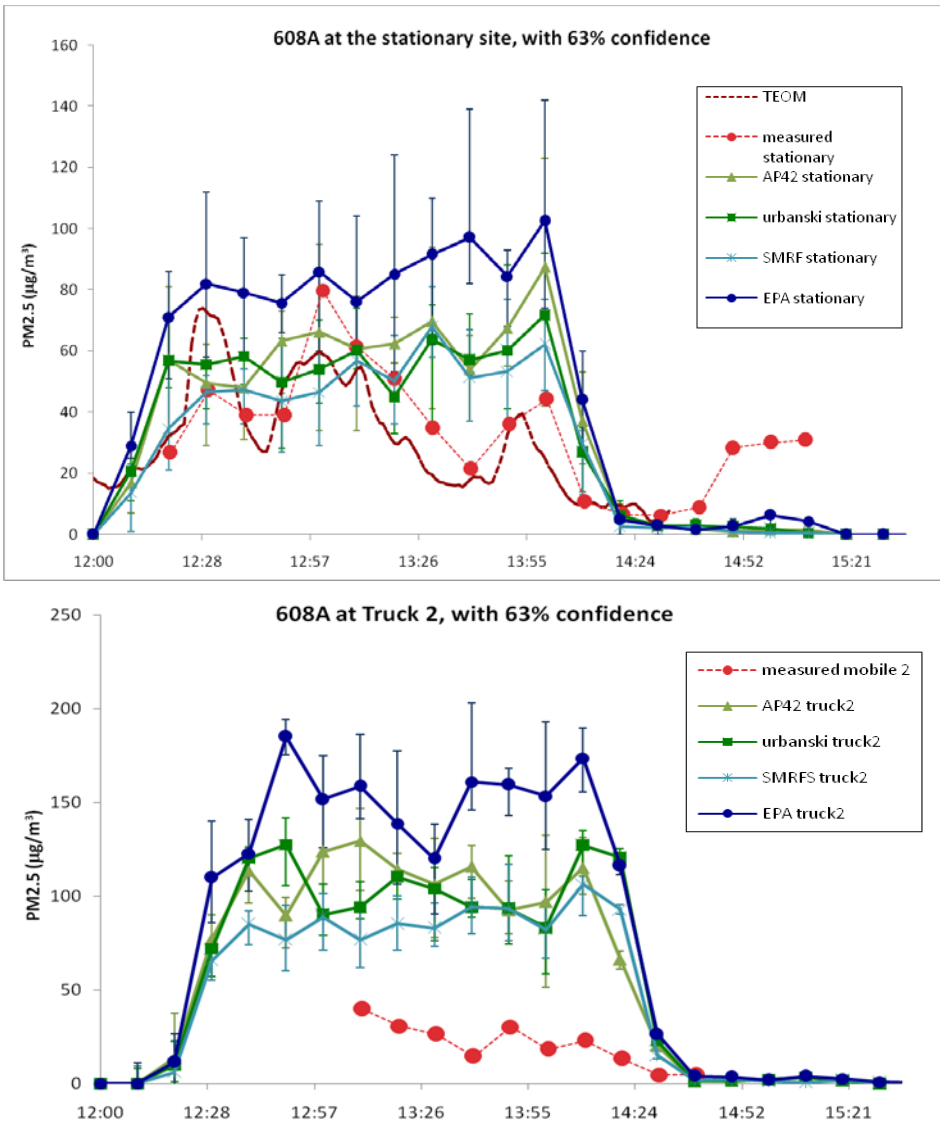

Figure 111. Comparison of $PM_{2.5}$ predictions with observations at stationary site and mobile site #2 whose locations are shown in Figure 110. Daysmoke predictions are shown for four different sets of emission inputs. Both TEOM and AeroTrack observations are shown at the stationary site.

Wind fields are another important input to Daysmoke that can affect model performance. The details of the wind analyses performed for this and other burns monitored at Eglin AFB in February 2011 can be found in Appendix A. Here the part of the analysis focusing on the wind measurements by aerostat-based anemometry will be presented. WRF wind directions will be adjusted to match measured wind directions at aerostat altitudes. Figure 112 shows the wind components at different times of the burn. WRF predicted the winds to be north-northwesterly; however, the measured winds were north-northeasterly. On average, WRF wind directions were underestimated by 26° at aerostat altitudes: therefore, WRF wind vectors used in running Daysmoke were rotated by 26° clockwise.

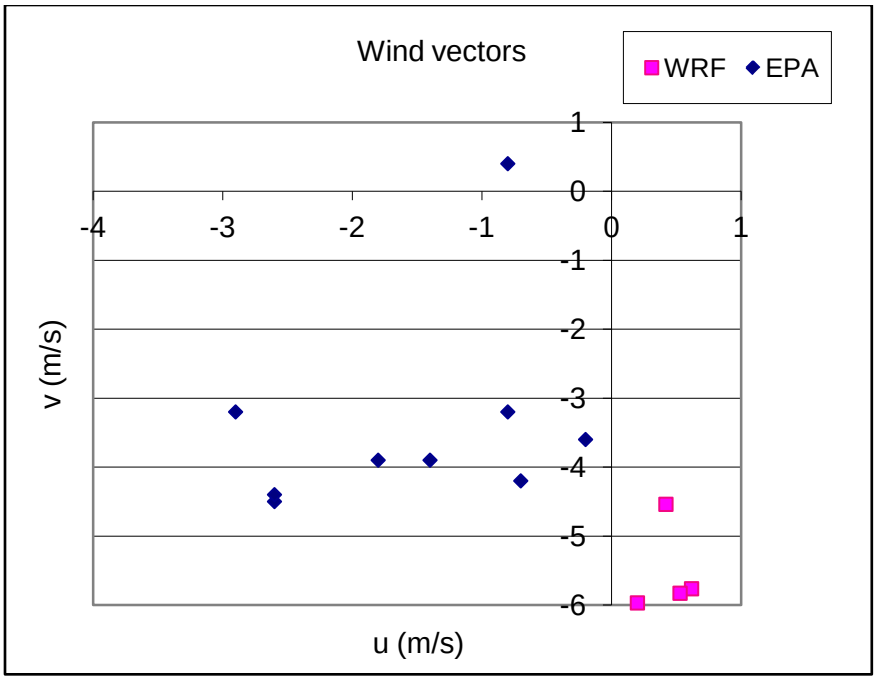

Figure 112. Comparison of WRF-predicted winds to the aerostat-based anemometer measurements during the 8 February 2011 burn of Block 608A at Eglin AFB.

Figure 113 shows the $PM_{2.5}$ concentrations obtained after a 26° clockwise rotation of the vertical wind profiles input to Daysmoke. For each set of emission inputs Daysmoke was ran 40 times. Different from Figure 111, the horizontal bars denote one standard deviation around the mean at a particular time. With all four emission inputs, Daysmoke underpredicts $PM_{2.5}$ both at the stationary site and the second mobile site (Truck 2).

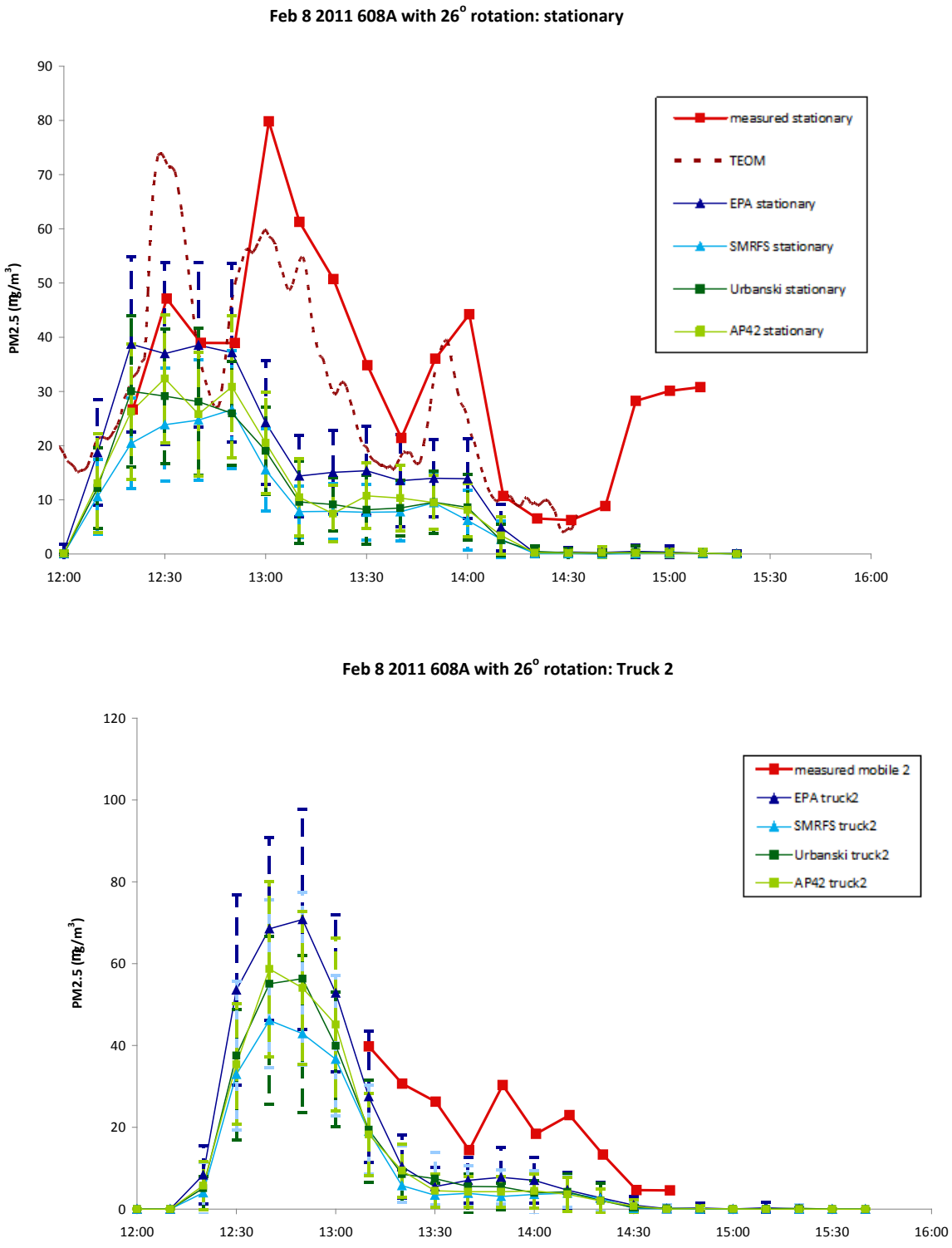

Figure 113. Comparison of $PM_{2.5}$ predictions with observations at stationary site and mobile site #2 after 26° rotation of input winds to Daysmoke.

The 26° rotation of the winds seemed to be excessive since predicted $PM_{2.5}$ concentrations are now lower than the measured concentrations. Therefore this time, the winds were rotated only by 23° clockwise. The three-degree difference from the last time was generated by slightly changing the procedure for averaging of the Aerostat wind measurements. Results of Daysmoke simulations with 23° rotated winds are shown in Figure 114. The model was run three times with each input emission set and the average of those runs was calculated at the stationary site and the location of Truck 2.

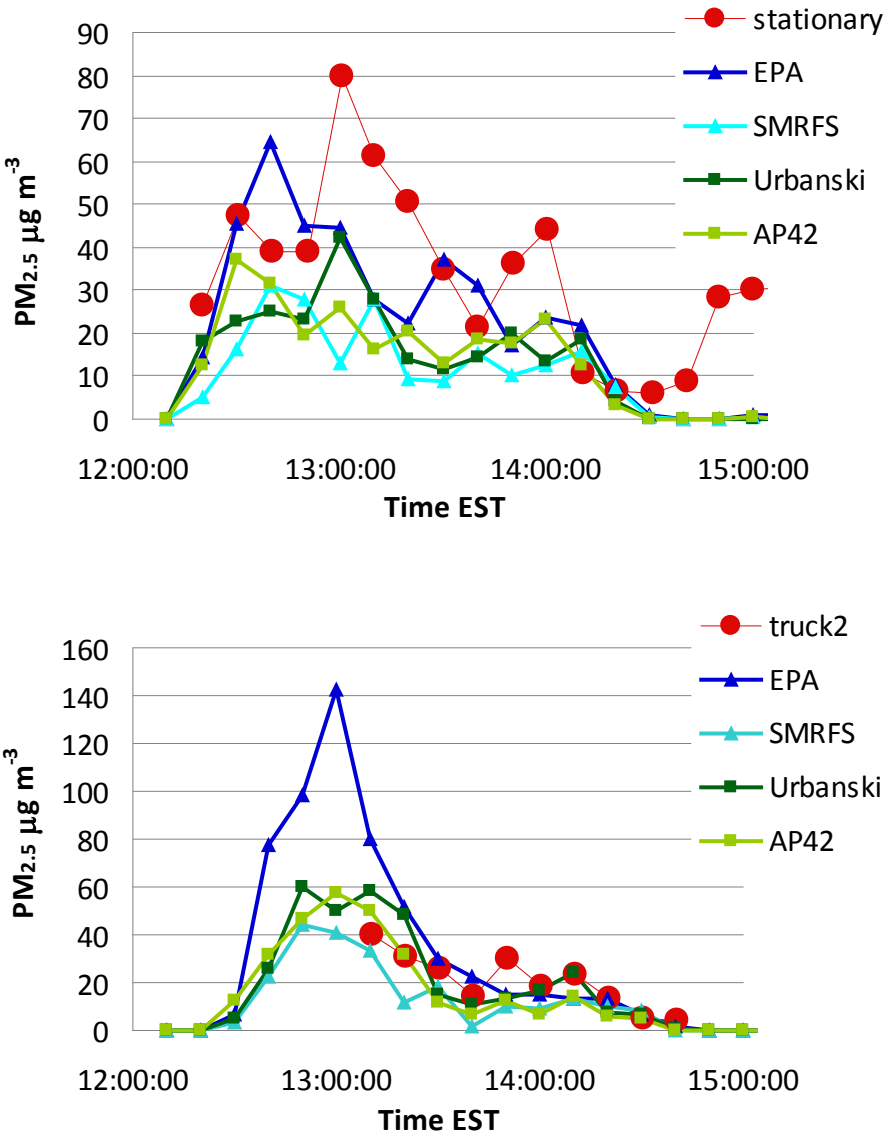

Figure 114. Same as Figure 113, except for a 23° rotation of the WRF winds.

Note that the agreement between Daysmoke predictions and observations of $PM_{2.5}$ improved significantly when the adjustment to the WRF wind directions was reduced from 26° to 23°. Mean normalized biases and errors for the Daysmoke predictions using the nominal emission

inputs (EPA) are listed in Table 17. Though the wind direction is changed by only three degrees, the impact to the $PM_{2.5}$ concentrations downwind is large. Compared to 26° wind rotation case, the mean normalized bias (MNB) improved by 29% and the mean normalized error (MNE) improved by 6% at the stationary site. At the location of Truck 2, MNE improved by 58% when 23° clockwise rotation was used instead of 26°, and the MNE improved by 25%. The 3-degree difference in wind directions made a big improvement especially at Truck 2 location.

Table 17. Daysmoke performance in accurately predicting downwind $PM_{2.5}$ concentrations for the 8 February 2011 burn of Block 608A at Eglin AFB after input winds were rotated by 23^0 and 26^0.

Wind rotation clockwise	Site	MNB	MNE
23°	Stationary	-29.2%	57.6%
26°	Stationary	-58.8%	63.9%
23°	Truck 2	11.7%	44.7%
26°	Truck 2	-69.8%	69.8%

4.4.3.3 Final Evaluation of Chemistry-Transport Model

Recall that the primary evaluation case for the chemistry-transport model has been the Atlanta Smoke Incident of 28 February 2007. During this incident the impacts of two prescribed burns were detected at several regional monitors around Atlanta. The other evaluation case is the 9 April 2008 burn monitored at Fort Benning. AG-CMAQ and AGD-CMAQ were evaluated with these cases.

4.4.3.3.1 Final Evaluation of Adaptive Grid CMAQ

The results from prior evaluation of the Adaptive Grid CMAQ (AG-CMAQ) with the Atlanta Smoke Incident were highlighted in Garcia-Menendez et al. (2010). Based on criteria listed in Section 4.2.2.1.7.1, the numbers of cores used in Daysmoke were revised (reduced) for the burns at Oconee National Forest and the Piedmont Wildlife Refuge that led to the Atlanta Smoke Incident. Also, the fuel type used in FEPS was revised upon further review of the burn information obtained from the Georgia Forestry Commission. These modifications reduced the amount of $PM_{2.5}$ emissions but the rise of the smoke plume in the atmosphere was enhanced. As a result, not only the predicted $PM_{2.5}$ concentrations were in better agreement with observations at downwind regional monitors, some long-range transport characteristics of the plumes were better simulated as well (Figure 115).

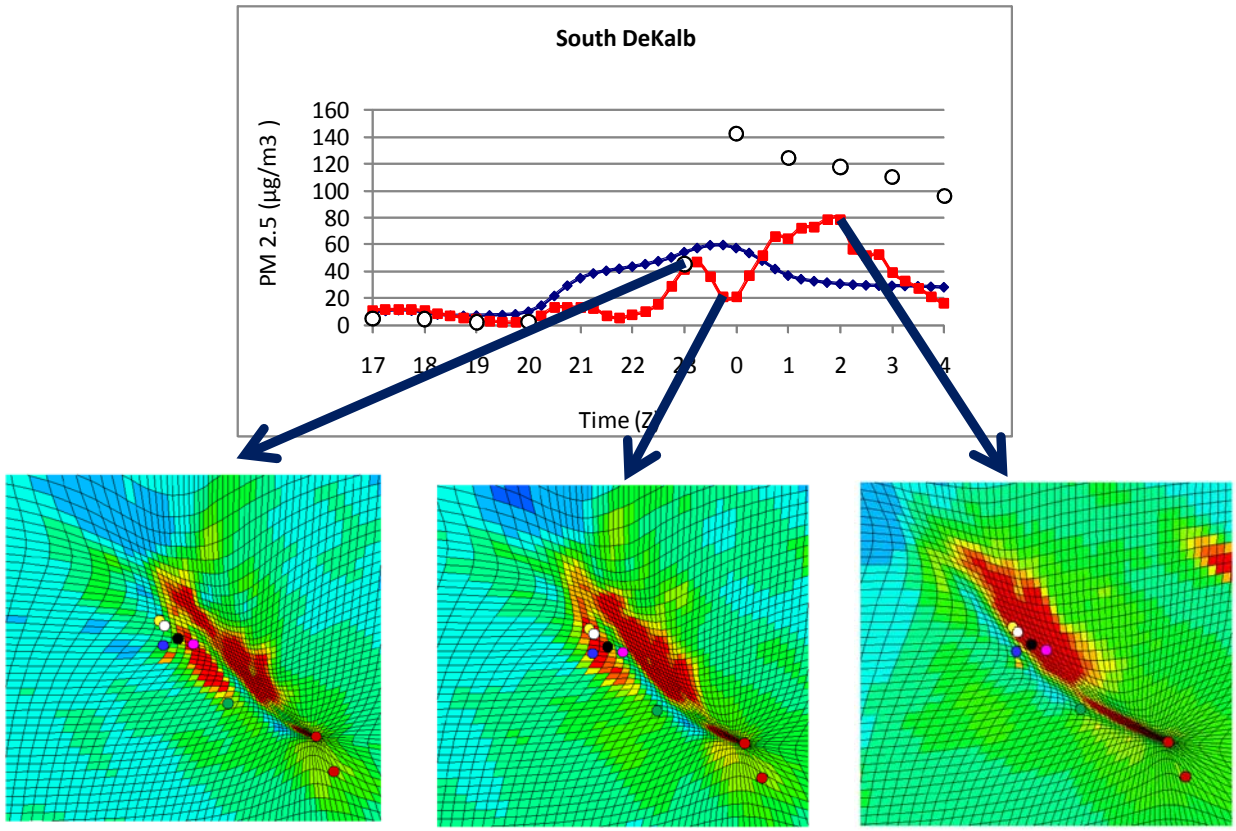

Figure 115. $PM_{2.5}$ concentrations predicted by CMAQ and AG–CMAQ along with measurements at South DeKalb on 28 February 2007 (top). The bottom panels, where the location of the South DeKalb site is marked by the pink dot, show simulated $PM_{2.5}$ at three different instances indicated by the arrow tails. Time is UTC.

Figure 115 shows modeled $PM_{2.5}$ concentrations using static grid CMAQ (blue) and adaptive grid CMAQ (red), along with site measurements at the South DeKalb station during Feb. 28/Mar. 1, 2007. Gridded concentration maps explain the peaks and trough in the AG-CMAQ modeled concentration, where the South Dekalb site is the pink circle. The initial peak corresponds to a plume from the smaller westernmost fire. The second peak corresponds to the larger Oconee fire plume. The transition between plumes leads to a trough in the station's pollutant levels.

4.4.3.3.2 Final Evaluation of Daysmoke coupled with Adaptive Grid CMAQ

The 9 April 2008 burn at Fort Benning was simulated using the coupled modeling system consisting of the dispersion model coupled with the chemistry-transport model. Both the initial coupling methodology (Daysmoke with CMAQ) and the final methodology (AGD-CMAQ) were used and the results were compared. Model inputs and setup are kept the same as those used for the previous April 9 2008 burn case. Grid refinement in AGD-CMAQ is driven by fire related $PM_{2.5}$ concentrations. The simulations start at 16:30 UTC or 12:30 EDT on 9 April 2008 and finish at 00:30 UTC (20:30 EDT) using an output time step of 15min. $PM_{2.5}$ concentrations from the models are compared to the observations at Columbus Airport monitor in Figure 116.

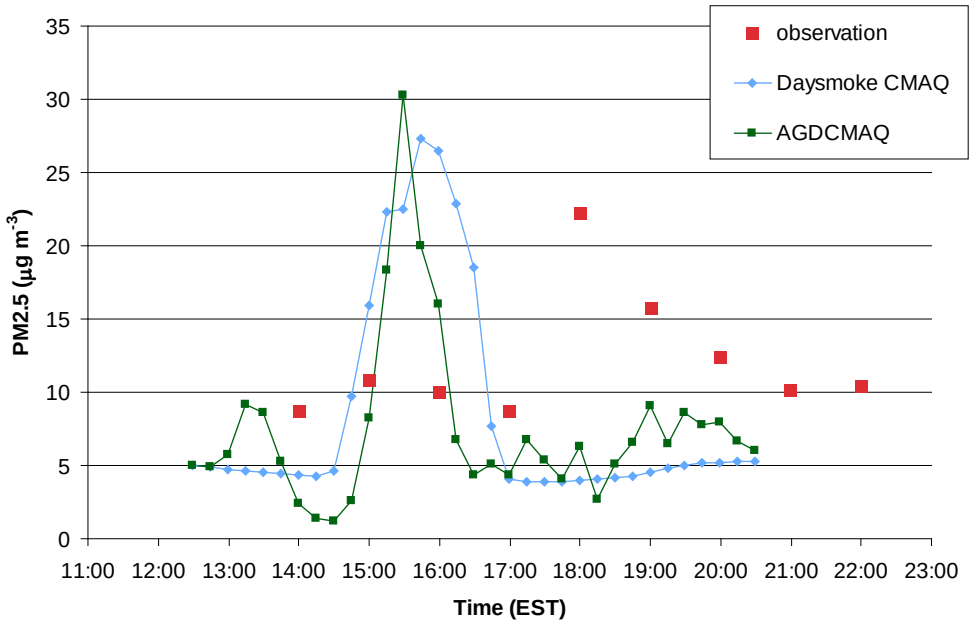

Figure 116. Observed (red) and modeled $PM_{2.5}$ concentrations using CMAQ with Daysmoke as a smoke injector (blue) and AGD-CMAQ (green) at the Columbus Airport site.

$PM_{2.5}$ from CMAQ with Daysmoke run is shown by the blue line in Figure 116; the green line shows $PM_{2.5}$ from AGD-CMAQ. In the CMAQ run $PM_{2.5}$ from Daysmoke plume at 10 miles is injected into CMAQ layers. In AGD-CMAQ the downwind distance of the interface where Daysmoke plume is "handed over" to the adaptive grid varies in time but cannot be larger than 20km. In AGD-CMAQ simulation, although the grid was refined around the burn unit, its resolution near the interface was comparable to the resolution of the uniform grid in CMAQ, which was 1.3 km ×1.3 km.

Both Daysmoke-CMAQ and AGD-CMAQ predicted similar $PM_{2.5}$ peaks of about 30 µg m^{-3} arriving at Columbus Airport between 15:00 and 16:00 EST. AGD-CMAQ peak was slightly higher, about 2µg m^{-3}, and arrived sooner. 1-hr average $PM_{2.5}$ concentration observed at the airport peaked between 17:00 and 18:00. If the observed peak is caused by the burn at Fort Benning and not by any other impact from local sources, then the models are predicting the fire plume reach the airport monitor earlier by more than an hour. This may be due to overprediction of wind speeds by WRF and/or overestimating the fire spread over the burn plot.

4.4.3.3.3 Analysis of Sensitivities to Emissions and Meteorology

Sensitivity analyses were conducted to investigate the reasons for the underestimation of PB impacts in the simulations of the Atlanta Smoke Incident. First, the sensitivity to the magnitude of emissions was analyzed, followed by an analysis of the significance of plume rise by changing the vertical distribution of fire emissions. Then, the sensitivity of simulated pollutant

concentrations to the temporal partitioning of fire emissions into hourly model inputs was analyzed. These emissions sensitivities were followed by analyses of the sensitivities to meteorological parameters such as wind speed, wind direction and boundary layer height. Numerical simulations were performed through the CMAQ model and a "brute-force" method described in Section 3.4.3 was applied to complete the necessary sensitivity analyses. CMAQ was the preferred model in this analysis because AG-CMAQ would produce a different grid every time the inputs were changed and there would be grid related effects in each simulation in addition to the effects of changing the targeted parameter.

4.4.3.3.3.1 Sensitivity to Fire Emissions Strength

As previously discussed, linearity is an important assumption if brute-force sensitivity approximations are used to estimate model response across a range of perturbations. Linear response enables accurate approximations of impacts and source contributions using first-order sensitivity coefficients. For the air quality simulations included in this study, the response of $PM_{2.5}$ concentrations to fire emissions can be expected to be predominantly linear. Fire-related particle emissions are determined from $PM_{2.5}$ emission factors and speciated mostly into primary organic aerosol (90%) and primary elemental carbon (6%). For these species, no significant indirect effects are anticipated. To test the validity of the linear response a series of simulations were performed varying fire emissions magnitude by ±10%, ±30%, and ±50%. **Error! Reference source not found.**Figure 117 shows peak simulated $PM_{2.5}$ concentrations at South DeKalb as a function of these variations. Linear response is evident and was observed at all downwind receptors throughout the simulation.

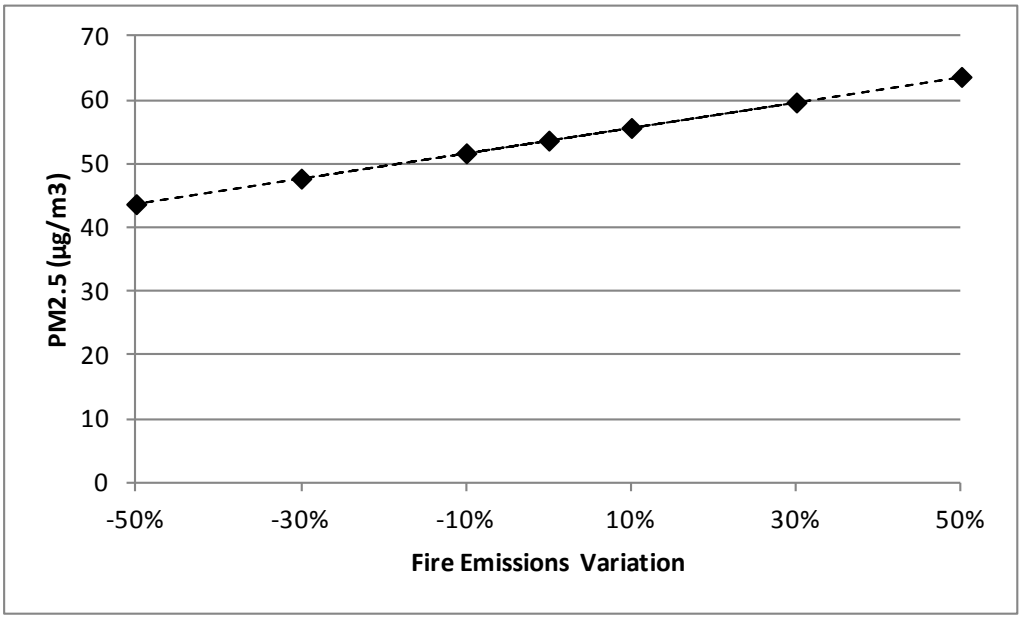

Figure 117. Simulated $PM_{2.5}$ concentrations as function of fire emissions perturbation (% change with respect to baseline) at the South DeKalb monitoring site on Feb. 28, 2007 at 23:45.

Brute-force first-order sensitivity coefficients were estimated at each downwind site using Equation (22) and ±30% perturbations to fire emissions. Sensitivity coefficients for $PM_{2.5}$ concentration response to fire emissions at South DeKalb during the smoke episode are shown in Figure 118. The sensitivity coefficients quantify change in modeled concentration per ton of fire-emitted $PM_{2.5}$ as a function of time. It is important to note that estimates at each instant represent sensitivity to all prior $PM_{2.5}$ emissions (i.e. total fire-emitted $PM_{2.5}$). Sensitivity coefficients were also calculated using ±10% and ±50% perturbations and proved to be nearly equal to those estimated with ±30% perturbations, further confirming linearity.

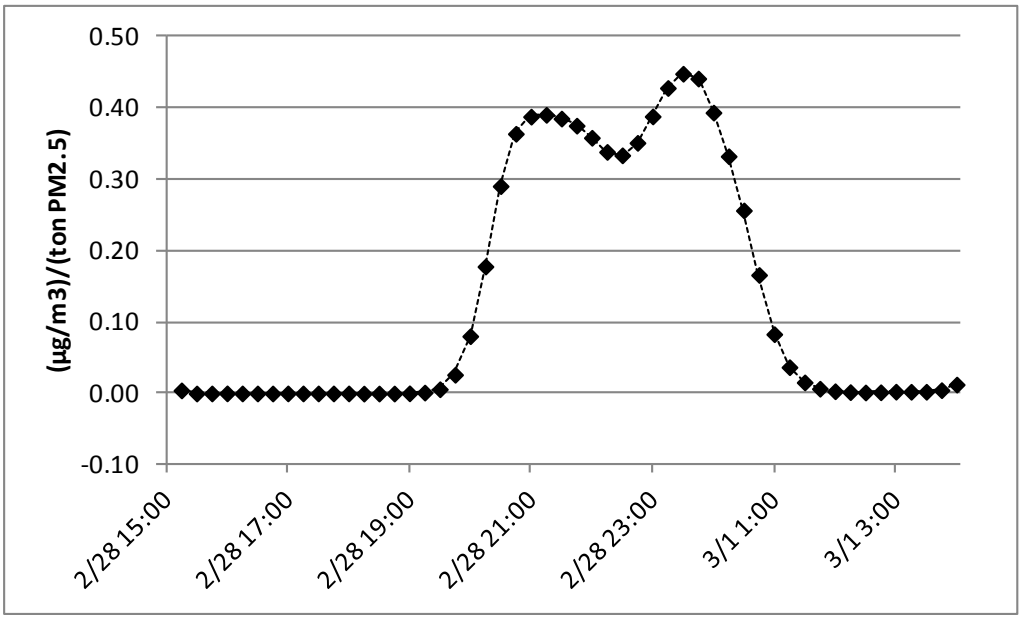

Figure 118. Brute-force sensitivity coefficients for $PM_{2.5}$ response to fire emissions strength at South DeKalb. Time is UTC.

The importance of higher-order sensitivity coefficients to replicate the response of pollutants affected by nonlinearities was discussed in Section 3.4.3. Using Equation (23), second-order coefficients and response were calculated for the simulated episode and second-order response terms proved to be minor compared to first-order ones. Inclusion of second-order coefficients into response calculations only changed total estimated $PM_{2.5}$ impacts by less than 2%. The results demonstrate that for analyses included in this study, modeled $PM_{2.5}$ concentration response to fire emissions can be effectively captured by first-order sensitivity coefficients.

Fire contributions to modeled $PM_{2.5}$ levels at each downwind site were quantified using brute-force sensitivity coefficients. Figure 119 shows fire and background contributions to simulated $PM_{2.5}$ concentrations at South DeKalb. Background contribution was estimated from a CMAQ simulation without fire emissions, while fire contribution was calculated using brute-force sensitivity coefficients. Figure 119 also includes results from a simulation including all emission sources and shows these concentrations closely match the sum of estimated fire and background contributions. A significant fraction of the CMAQ-predicted $PM_{2.5}$ pollution is attributable to fire emissions. For sites near downtown Atlanta, fire-attributable $PM_{2.5}$ impact increases to 20-31

µg/m^3 and can contribute up to 56-67% of total modeled $PM_{2.5}$. At McDonough, the closest site to the burns, the maximum fire contribution to modeled $PM_{2.5}$ concentration is 78% and the largest impact from fires is 70 µg/m^3. However, $PM_{2.5}$ contributions from non-fire sources are also significant throughout the simulation.

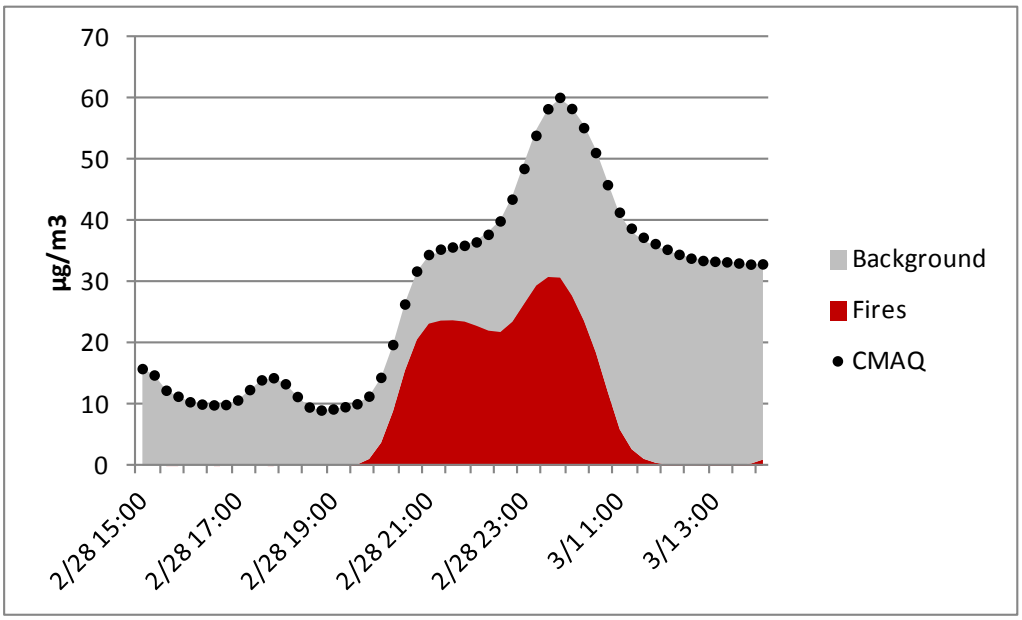

Figure 119. Fire and background contributions to modeled $PM_{2.5}$ concentration and base-case CMAQ results at South DeKalb. Time is UTC.

Brute-force sensitivity coefficients were also used to determine the increase to fire emissions that would match maximum simulated $PM_{2.5}$ concentrations and peak observations. Figure 120 shows the effect of intensifying base-line fire emissions by a factor of 5.1 at Jefferson St. and 3.7 at South DeKalb. Overall, base-line fire emissions would have to be increased by a factor of 4-6 for CMAQ-predictions to reach the highest observed concentrations. The modified simulations also indicate that while modeled maxima are generally well-timed relative to peak observations, important differences exist between the complete evolution of predicted fire impacts and observed $PM_{2.5}$ increments throughout the episode.

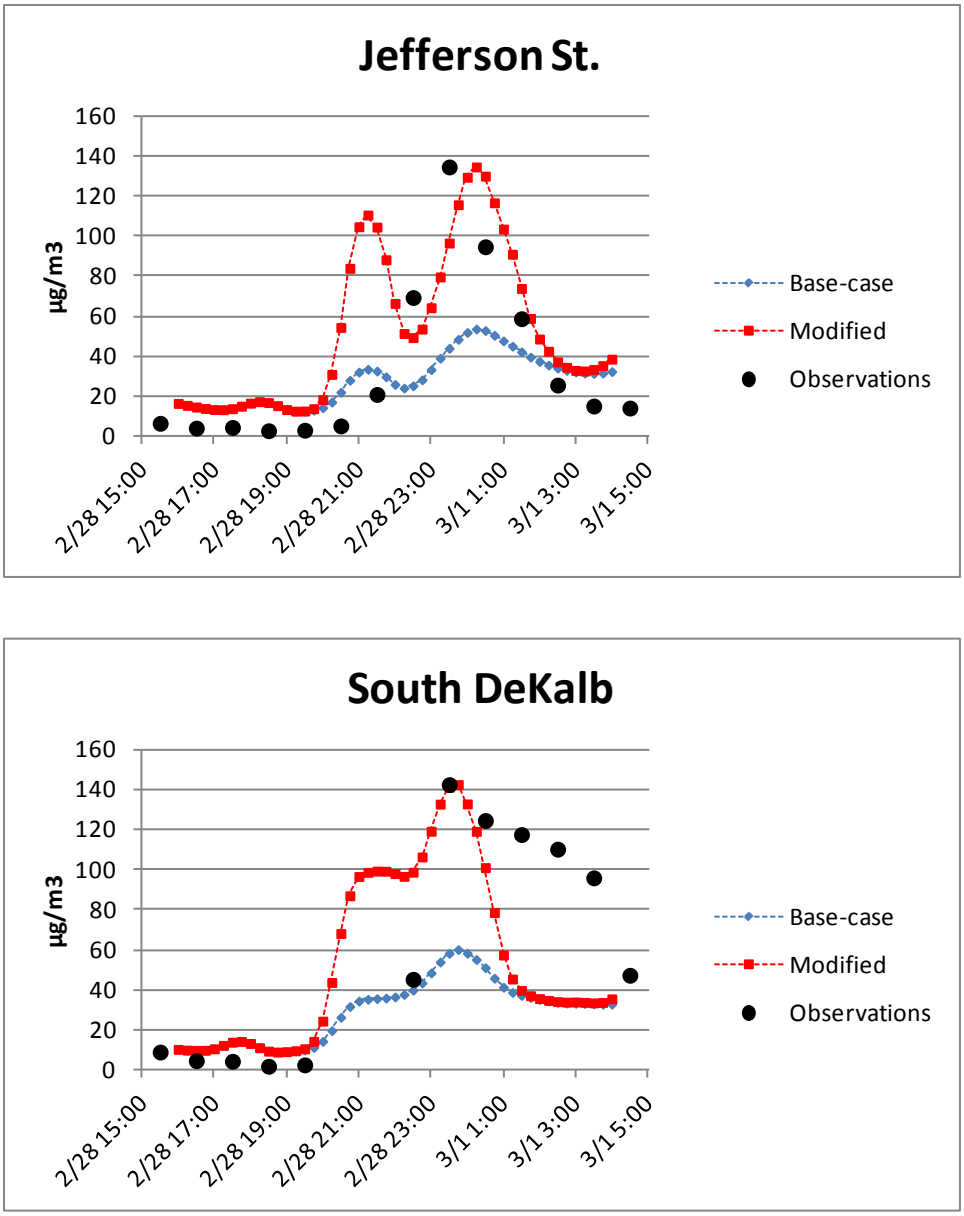

Figure 120. Base-case and modified CMAQ-predicted $PM_{2.5}$ concentrations along with monitoring site observations. Fire emissions for modified simulations were increased by factors of 5.1 (Jefferson St.) and 3.7 (South DeKalb). Time is UTC.

Sensitivity coefficients were calculated for each individual prescribed burn and used to quantify and compare $PM_{2.5}$ concentration contributions specific to the Oconee and Piedmont fires. $PM_{2.5}$ impacts broken down by fire at South DeKalb are included in Figure 121. Although contributions from both fires are significant, about 75% of the total fire-related $PM_{2.5}$ impact is attributable to the Oconee burn at all sites considered. The disparity in contributions is brought about by unequal emissions and differences in concentration sensitivity to each fire. Figure 122 shows hourly $PM_{2.5}$ emissions and brute-force sensitivity coefficients for each burn. It is clear that stronger emissions from the Oconee burn largely drive pollution impacts. However, it is

interesting to note that sensitivity coefficients can be significantly higher for Piedmont burn emissions. While the added impact of Oconee emissions is larger, on average each ton of $PM_{2.5}$ emitted by the Piedmont burn leads to a greater increase in concentrations at downwind locations. Moreover, the timing of peak sensitivity coefficients for the Piedmont fire better agrees with maximum simulated and observed concentrations. Sensitivity coefficients for individual fires are different because of dissimilar spatial and temporal emissions distribution for each. The difference corroborates that allocation of fire emissions into hourly rates and gridded three-dimensional domains may significantly influence predicted pollutant concentrations. Sensitivities related to emissions allocation are further explored in section 3.3.

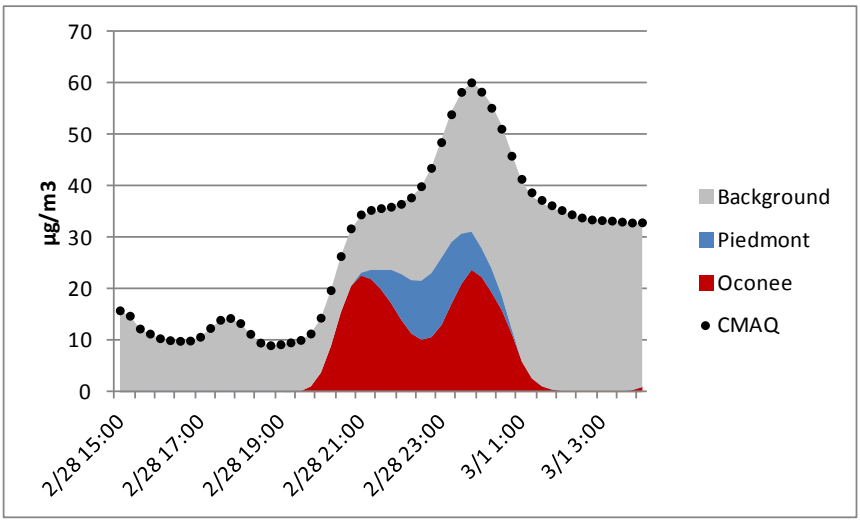

Figure 121. Fire contributions to modeled $PM_{2.5}$ concentration at South DeKalb for the Oconee National Forrest and Piedmont National Wildlife Refuge prescribed burns. Background contribution and base-case CMAQ results are also included. Time is UTC.

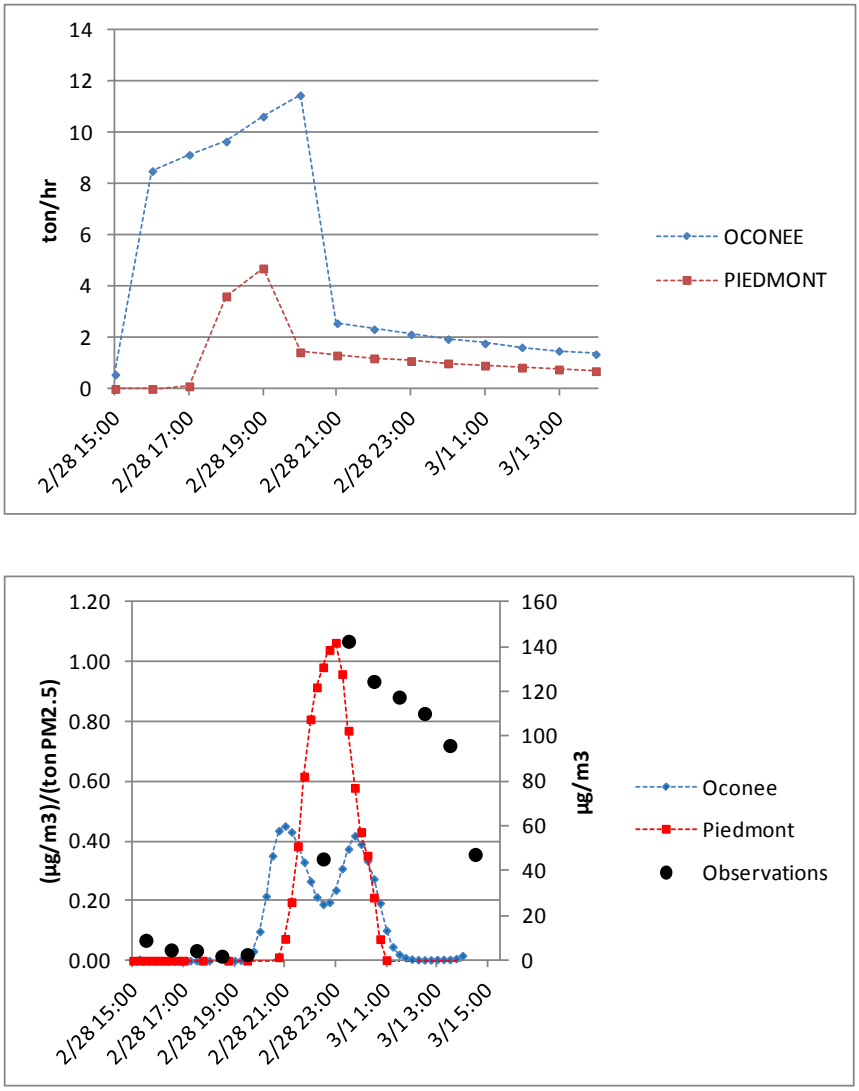

Figure 122. Hourly $PM_{2.5}$ emissions for the Oconee National Forrest and Piedmont National Wildlife Refuge prescribed burns (top panel). Bottom panel shows brute-force sensitivity coefficients for $PM_{2.5}$ concentration response to fire emissions from each fire at South DeKalb (left axis) and site observations (right axis). Time is UTC.

4.4.3.3.3.2 Sensitivity to Vertical Allocation of Fire Emissions

Plume rise approximations are an important component of air quality simulations involving buoyant emissions. As previously discussed, when fires are included as point or area sources on gridded domains, their emissions must be distributed among the domain's vertical layers. Here, hourly vertical distributions of fire emissions were determined using Daysmoke. Figure 123 shows $PM_{2.5}$ injected into each vertical layer from the Oconee and Piedmont fires for the entire simulation. Generally, upper layer injection corresponds to flaming combustion while emissions distributed closer to the surface correspond to the fire's smoldering phase.

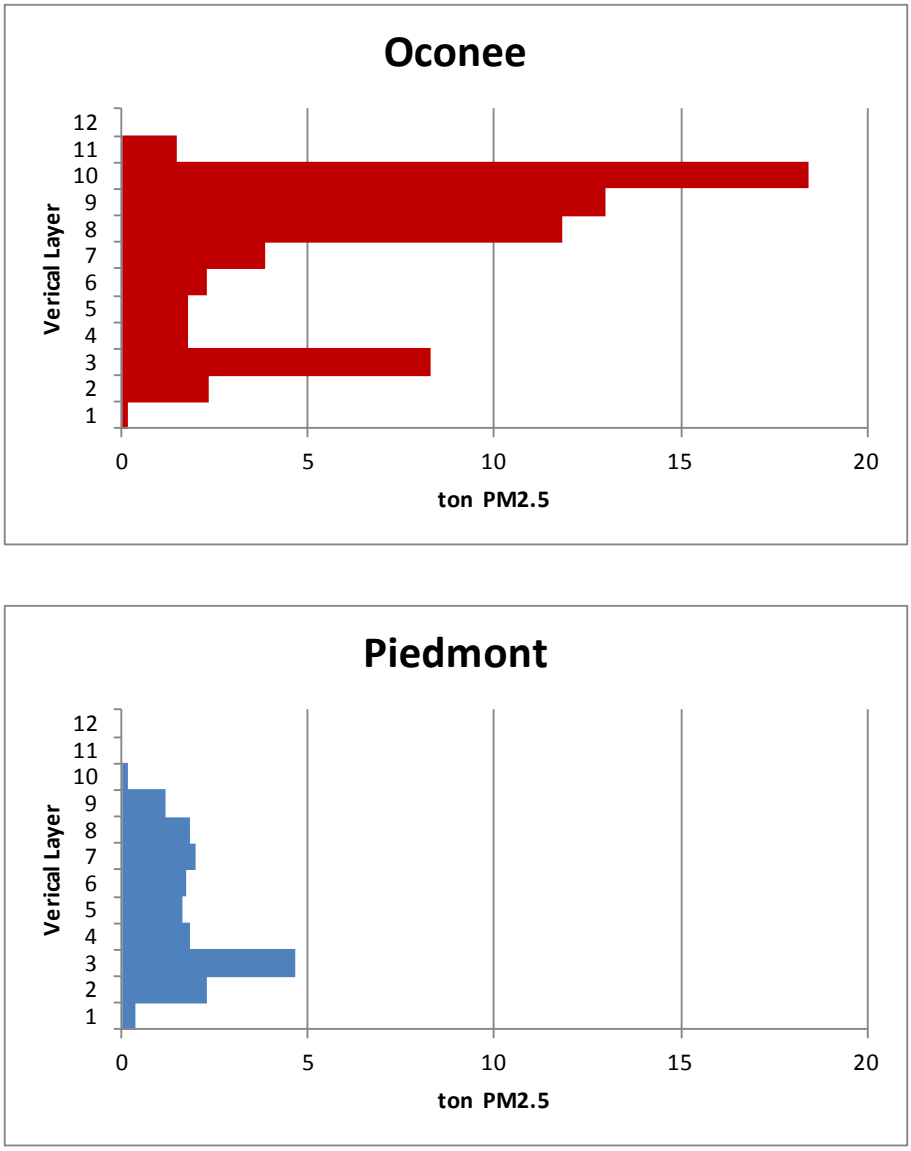

Figure 123. Total fire-related $PM_{2.5}$ emissions by vertical layer for Oconee (top) and Piedmont (bottom) burns.

To assess the significance of vertical emissions allocation in successfully modeling the air quality impacts of PB burns, brute-force sensitivities of CMAQ-predicted $PM_{2.5}$ concentrations to fire emissions were compared for each vertical layer included in our base-case simulation. Sensitivity approximations were then used to quantify the $PM_{2.5}$ impacts attributable to each layer. Figure 124 shows estimated fire contributions to $PM_{2.5}$ concentration at South DeKalb by vertical layer. In the base-case simulation emissions were injected into the lowest eleven layers. The contribution from non-fire (background) sources, determined from a simulation without fire emissions, and base-case CMAQ concentrations are also included. Additionally, Figure 124 shows that the sum of background and individual contributions to $PM_{2.5}$ closely matches base-case predicted concentrations. This agreement, observed at all downwind sites, further confirms

a linear response to fire emissions and validates the adequacy of brute force sensitivities in this analysis.

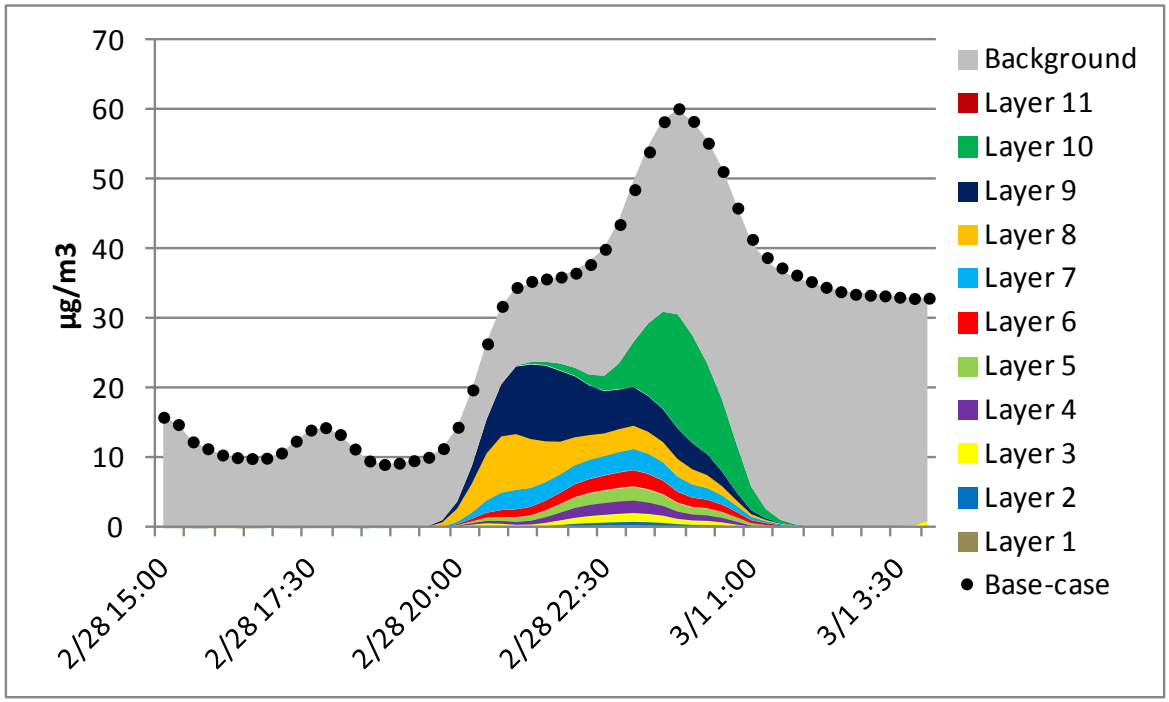

Figure 124. Fire contributions to modeled $PM_{2.5}$ concentration at South DeKalb by vertical CMAQ layer. Background contribution and base-case CMAQ results are also included. Time is UTC.

Figure 125 compares $PM_{2.5}$ concentration sensitivities to fire emissions from each vertical layer at South Dekalb and includes hourly-averaged monitoring station observations. Sensitivities vary significantly between different vertical layers at all the sites considered. As observed concentrations peak at South DeKalb, the sensitivity to fire emissions is clearly largest for layer 10. These results might seem to indicate that CMAQ-predicted $PM_{2.5}$ concentrations are significantly sensitive to the vertical allocation of fire emissions. However, it is important to note that two distinct components of individual vertical layer emissions make sensitivities to them differ: injection altitude and emissions timing. If time-varying vertical profiles are applied, simulated concentrations may be more responsive to emissions from a specific vertical layer due to the timing of injection rather that layer altitude. To isolate the influence of spatial or temporal allocation in brute-force sensitivity calculations, only a single component of fire emissions should be perturbed. Sensitivity to temporal allocation of emissions will be discussed in Section 4.4.3.3.3.3.

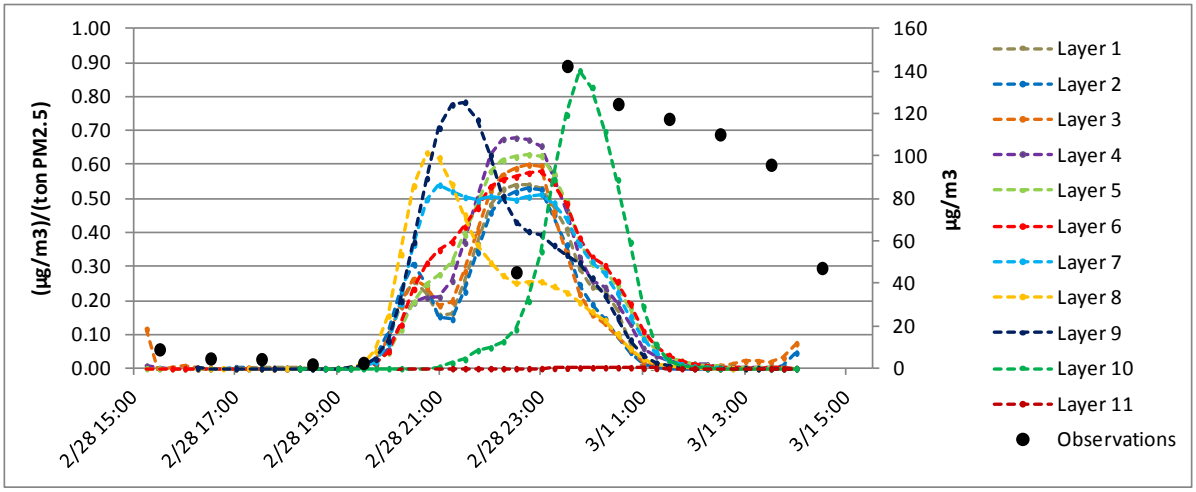

Figure 125. Brute-force sensitivity coefficients for $PM_{2.5}$ concentration response to fire emissions by vertical CMAQ layer at South DeKalb (left axis) and site observations (right axis). Time is UTC.

To remove the temporal variability between different layers, brute force sensitivities were quantified using a constant vertical emissions profile. An accurate assessment of the sensitivity of modeled $PM_{2.5}$ concentrations to injection height was achieved by equally dividing fire emissions into all layers considered throughout the full episode. Further, allocating the same amount of hourly fire emissions to each layer allows for a fair comparison of their respective impacts. Figure 126 shows $PM_{2.5}$ concentration sensitivities to fire emissions by vertical layer at South DeKalb after applying a constant and uniform vertical emissions distribution covering the lowest 16 layers. Contrary to the comparison previously presented in Figure 125, these results indicate that after eliminating the temporal variation in layer emissions, sensitivities are very similar for all vertical layers below layer 10. Sensitivity to layer 10 emissions is markedly lower and modeled $PM_{2.5}$ concentrations are not responsive at all to emissions injected above layer 10 or approximately 1000m. The same conclusions can be drawn from sensitivity estimates at other downwind sites.

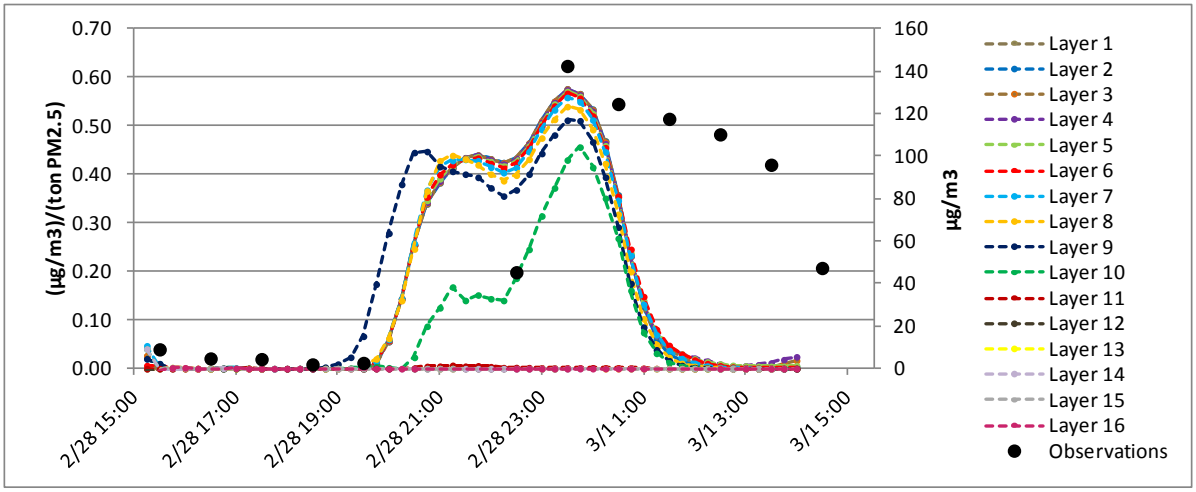

Figure 126. Brute-force sensitivity coefficients for $PM_{2.5}$ concentration response to fire emissions by vertical CMAQ layer at South DeKalb for uniform distribution into 16 lowest layers (left axis), and site observations (right axis). Time is UTC.

The analysis reveals that CMAQ-predicted $PM_{2.5}$ concentrations are not overly sensitive to the vertical distribution of fire emissions other than injection above or below a specific altitude. These results can be explained by analyzing the evolution of PBL height in meteorological input data. Figure 127 shows WRF-predicted PBL height during the episode at the Oconee fire location along with full-layer heights for the lower 11 vertical layers. In Section 4.4.3.3.3.3below, we demonstrate that simulated $PM_{2.5}$ concentrations at South DeKalb are mostly sensitive to fire emissions released between 17:00 and 21:00 UTC. During this lapse the PBL partially extends into layer 10 for only a fraction of the time and does not reach layers above. The analysis indicates that modeled $PM_{2.5}$ concentrations respond similarly to all fire emissions injected within the PBL and are not affected by emissions released into the free atmosphere. Previous studies have reported similar findings. (Yang et al., 2011) conclude that modifying the vertical distribution of fire emissions injection did not significantly affect performance for their CMAQ simulations. Sensitivity analyses performed on the National Oceanic and Atmospheric Administration's (NOAA) Smoke Forecasting System (SFS) determined that model effectiveness is greatly dependent on accurately determining whether smoke injection height occurred within or above the PBL (Stein et al., 2009). Although Liu et al. (2010; 2008) assert that CMAQ $PM_{2.5}$ predictions are highly sensitive to plume rise approximations, concentration differences are most evident between their simulations with emissions distributed within the PBL and that with injection at much higher altitudes.

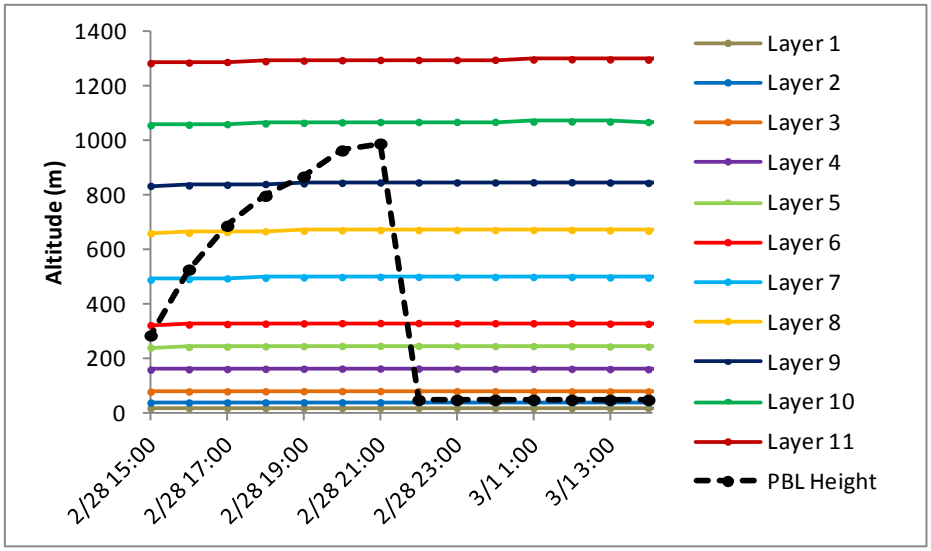

Figure 127. PBL height and full-layer altitudes for lower 11 vertical layers at Oconee fire site. Time is UTC.

4.4.3.3.3.3 Sensitivity to Temporal Allocation of Fire Emissions

While important uncertainties related to the spatial allocation of fire emissions on gridded domains may exist, additional uncertainty associated with the temporal allocation of emissions may affect an air quality model's ability to simulate the impacts of wildland fires. Emissions are generally inputted into comprehensive air quality models as hourly emission rates. Similarly, fire emissions processors typically provide hourly estimates. Partitioning of fire emissions into hourly rates may be complicated by limited information about ignition time, duration, and evolution.

In this study, hourly rates for all fire emissions were prepared through FEPS. Hourly $PM_{2.5}$ emissions were previously shown in Figure 122. To compare the responsiveness of CMAQ-predicted $PM_{2.5}$ concentrations at Atlanta sites to hour-by-hour fire emissions, brute-force sensitivities were estimated for each hour. Perturbations were applied to single hour emissions in order to quantify sensitivities and individual contributions to $PM_{2.5}$ levels at downwind receptors. Figure 128 shows estimated fire contributions to $PM_{2.5}$ concentration at South DeKalb for each hour of emissions. At this site, it is clear that most of the fire-related $PM_{2.5}$ pollution is attributable to fire emissions released during a four hour span. Emissions released from 17:00 to 21:00 UTC are accountable for over 85% of the simulated fire contribution to $PM_{2.5}$ concentration.

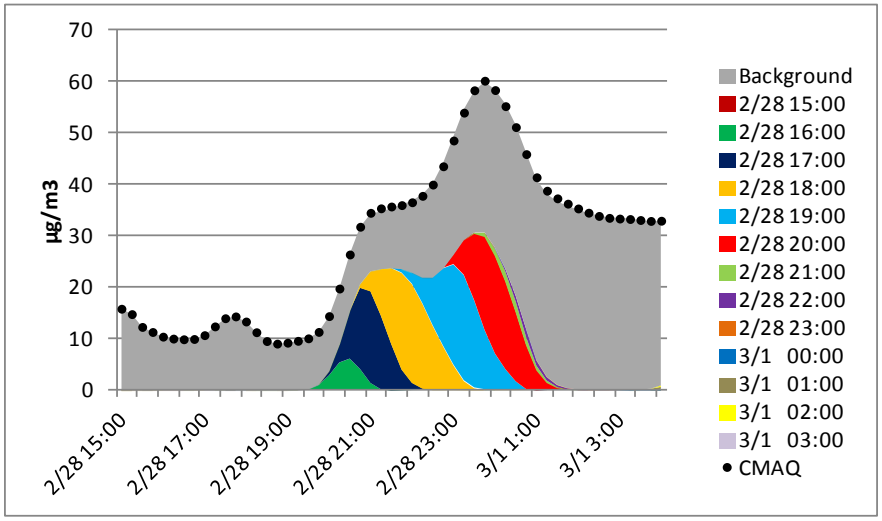

Figure 128. Fire contributions to modeled $PM_{2.5}$ concentration at South DeKalb by hour of emissions. Emissions are labeled at the start of the hour. Background contribution and base-case CMAQ results are also included. Time is UTC.

Differences between fire-related impacts for each hour of emissions are driven by both emissions timing and mass. Sensitivity estimates reflecting concentration responsiveness to fire emissions are more informative. However, an objective comparison between sensitivities to hour-by-hour emission rates must account for the temporal variation in vertical distribution of emissions as described in section 3.4.2. Here again, a constant vertical emissions distribution was applied to remove the influence of time-varying plume rise profiles and allow sensitivity calculations to solely focus on the temporal allocation of fire emissions. Figure 129 shows $PM_{2.5}$ concentration sensitivities to hour-by-hour fire emissions at South DeKalb after equally distributing fire emissions into the lower 10 vertical layers during the entire simulation. Results at all sites considered demonstrate that sensitivities of modeled $PM_{2.5}$ concentrations to hour-specific can be substantially different. In Atlanta, $PM_{2.5}$ concentrations are influenced to varying degrees by emissions released between 15:00 and 23:00 with specific locations responding more intensely to emissions from distinct hours. The analysis also shows that each hour's fire-related emissions only influence concentrations at downwind receptors during a 2-3 hour lapse starting approximately 3 hours after release. Overall, sensitivity estimates illustrate that altering the temporal allocation of fire emissions can significantly change the timing of fire-related impacts and peak simulated concentrations. (Hu et al., 2008a) conclude from their "hindcast" simulations of this same episode that enhanced CMAQ performance is more readily achieved by improving hourly emissions profiles rather than refining fire location or emitted mass. The sensitivity analysis of modeling results to diurnal variability in wildfire emissions reported by (Hodzic et al., 2007) finds that hourly resolved smoke emissions can greatly enhance simulations compared to daily emissions inventories. Additionally, satellite information has been applied to temporally refine coarse fire emissions data and achieve superior model predictions (Roy et al., 2007).

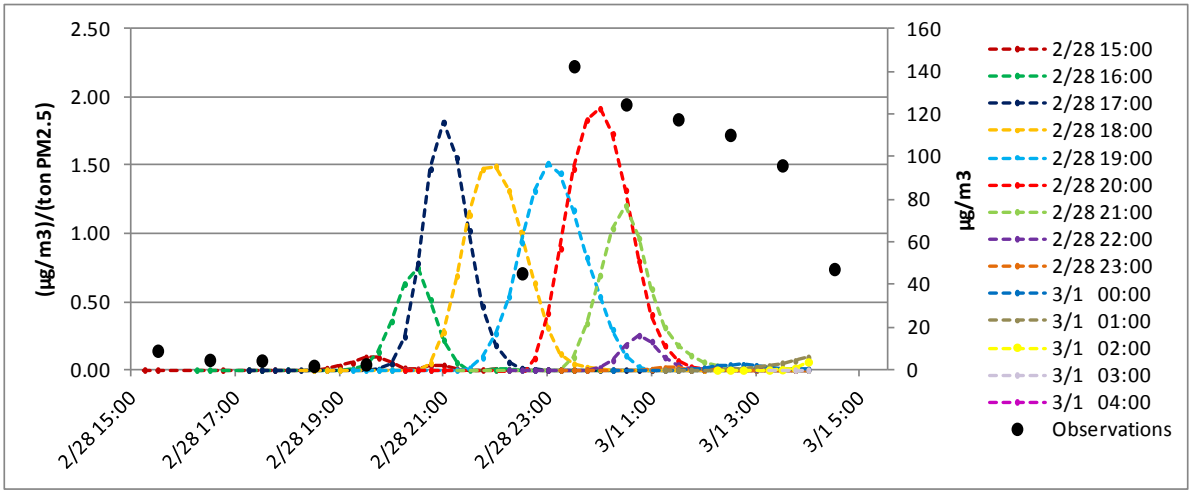

Figure 129. Brute-force sensitivity coefficients for $PM_{2.5}$ concentration response to fire emissions by hour of emissions at South DeKalb for uniform distribution into 10 lowest layers (left axis), and site observations (right axis). Emissions are labeled at the start of the hour. Time is UTC.

4.4.3.3.3.4 Sensitivity to Wind Speed and Direction

Meteorological inputs are an essential component of air quality modeling. In the context of modeling the air quality impact of fires, it is crucial to determine the significance of accurate weather data. Fine carbonaceous particles are mainly a primary pollutant and suspected to be especially sensitive to wind fields. To examine the responsiveness of CMAQ-modeled $PM_{2.5}$ concentrations at specific downwind receptors to changes in the wind field, brute force sensitivities were quantified for different perturbations to wind direction and speed in the 2007 Atlanta Smoke Incident simulation at 4 km grid resolution. Figure 130 shows the effects that 5°, 15°, and 30° clockwise and counterclockwise perturbations to wind direction applied throughout the wind field would have on simulated $PM_{2.5}$ concentrations at the Jefferson St. monitoring station. It is apparent from the analysis that modeled downwind $PM_{2.5}$ concentrations are extremely sensitive to variations in wind direction. Small alterations to the direction of the wind field can lead to major changes in predicted pollutant concentrations at specific downwind locations. At Jefferson St., for instance, a 5° counterclockwise shift in wind inputs increases the maximum simulated $PM_{2.5}$ concentration by 20%. The sensitivities to wind direction at other downwind receptors are similarly large and nonlinear. However, the effects that specific wind direction perturbations (e.g. 15° clockwise) have at each receptor can be very different.

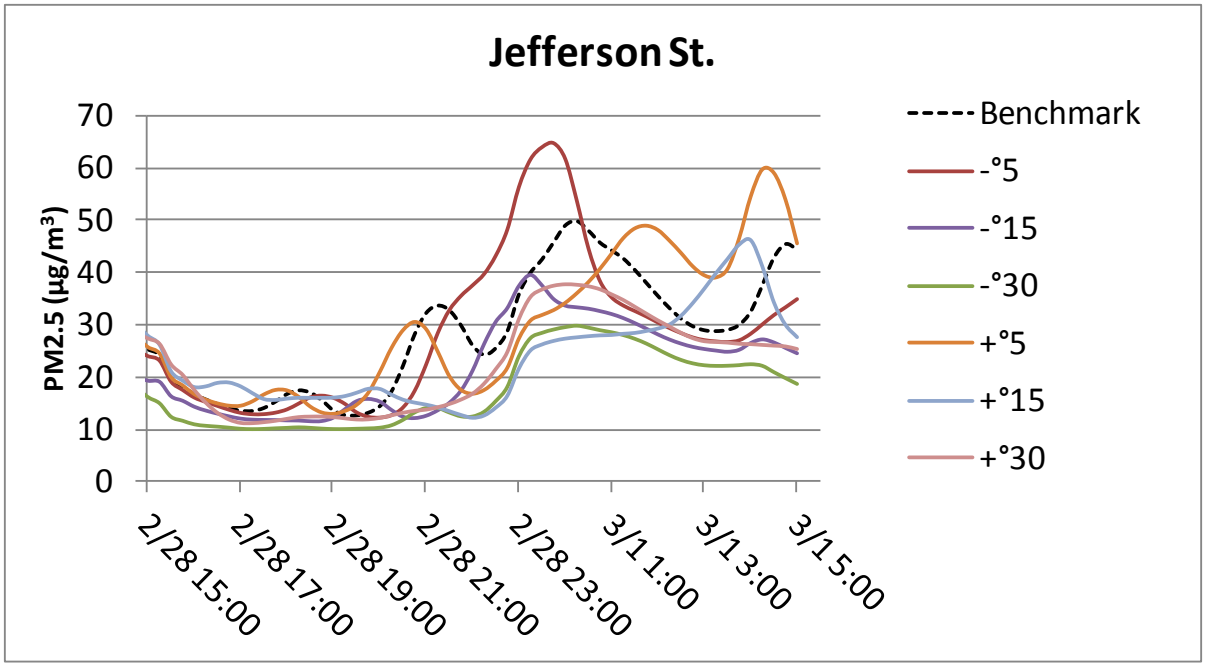

Figure 130. Simulated $PM_{2.5}$ concentrations at the Jefferson St. monitoring site on Feb. 28 and Mar. 1, 2007 under clockwise (+) and counterclockwise (-) perturbations to wind direction. Time is UTC.

The same methodology was applied to explore the sensitivity of modeled $PM_{2.5}$ concentrations to changes in wind speed. In Figure 131 the response of $PM_{2.5}$ concentrations at Jefferson St. to 10, 20, and 30% increases and decreases to wind speed magnitude are presented. Unlike the unpredictable response to perturbations in wind direction, a relatively linear response to wind speed can be observed. However, changes to pollutant concentrations are very large. A 30% decrease to wind speeds nearly doubles the peak $PM_{2.5}$ concentration estimate at the Jefferson St. site. Results at all receptors indicate that $PM_{2.5}$ concentrations significantly increase and experience a growing delay as wind speeds are decreased. Clearly, the sensitivity analyses for wind speed and direction indicate extremely large sensitivities for modeled $PM_{2.5}$ concentrations to perturbations in wind fields.

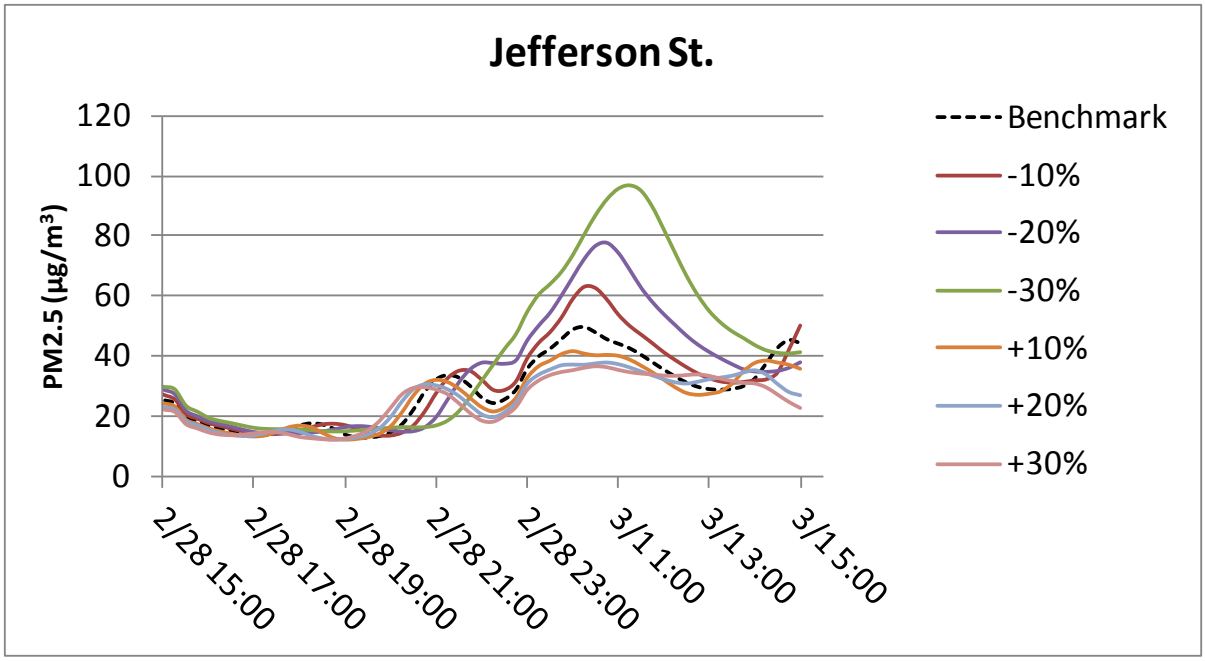

Figure 131. Simulated $PM_{2.5}$ concentrations at the Jefferson St. monitoring site on Feb. 28 and Mar. 1, 2007 under increased (+) and decreased (-) wind magnitude. Time is UTC.

4.4.3.3.3.5 Sensitivity to Planetary Boundary Layer Height

Planetary boundary layer (PBL) height is another meteorological input expected to have a significant effect on model results. To evaluate the sensitivity of CMAQ-predicted pollutant levels to PBL height inputs, heights were increased and decreased by 10, 20, and 30% in our simulation of the Atlanta 2007 smoke episode at 4 km horizontal grid resolution. The $PM_{2.5}$ concentration response at the Jefferson St. monitoring station is shown in Figure 132. Figure 132 also shows the progression of PBL height at Jefferson St. throughout the episode. The results indicate a significant sensitivity to PBL height for certain lapses of the simulation and reduced sensitivities at other instances. As PBL height undergoes its diurnal cycle, sensitivities of $PM_{2.5}$ concentrations to PBL height grows in significance when PBL height increases. When PBL height sharply drops, its relevance to $PM_{2.5}$ concentrations downwind of fires also diminishes. The sensitivities of pollutant concentrations to PBL height in simulations involving fire emissions are also closely linked to plume rise and the vertical distribution of emissions. Emissions distributed above the PBL are injected into the free atmosphere while those distributed into vertical layers within the PBL are subjected to turbulent diffusion and mixing, producing very different impacts to $PM_{2.5}$ concentrations downwind of emissions sources.

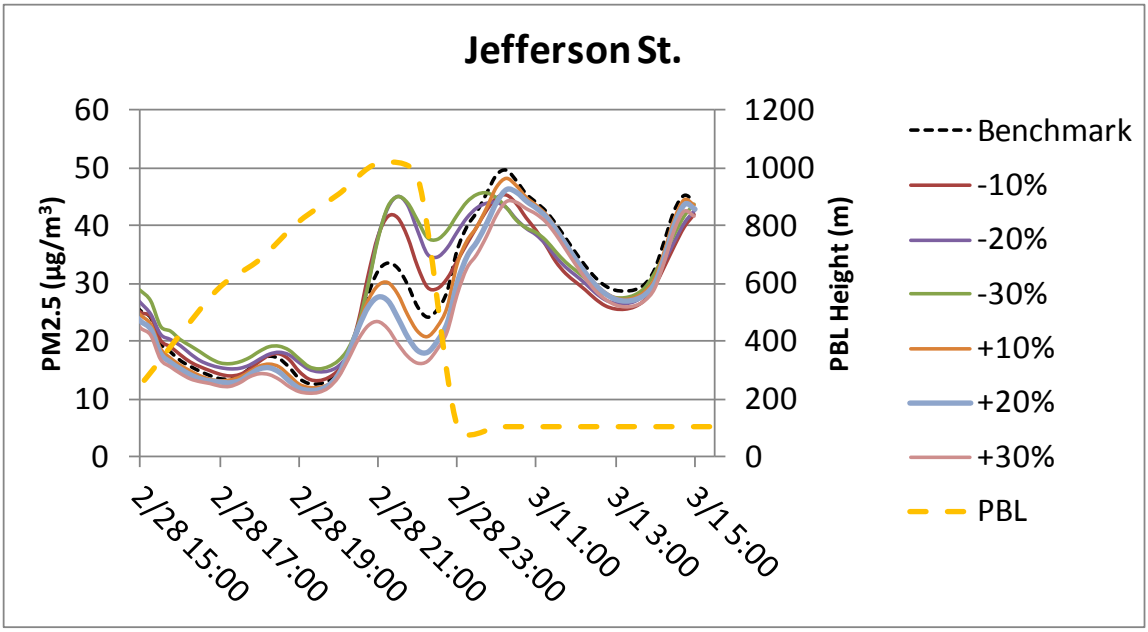

Figure 132. PBL height (right axis) and simulated $PM_{2.5}$ concentrations (left axis) under increased (+) and decreased (-) PBL height at the Jefferson St. monitoring site on Feb. 28 and Mar. 1, 2007. Time is UTC.

4.5 Simulations of Alternative Burning Strategies

Prescribed burning experts consisting mostly of DoD and other land managers in the Southeast were surveyed. The goal of the survey was to identify the most relevant burning scenarios to be simulated with the smoke impact prediction system. Varying the size of burn, ignition method, fuel moisture, season of burn, fuel loads, weather conditions, and time of burn were the most suggested burning options. Considering the priorities assigned to each one of these options, five alternative burning scenarios were simulated to study the effects of the following factors.

1. Frequency of burn: Varying the fire return interval (e.g., from 2 to 5 years) would change the fuel loads and fuel types. Comparing fire suppression conditions with regularly burned healthy forests would illustrate the impacts of fuel accumulation vs. frequent low intensity burning, which is more cost effective. Is it beneficial to bring the fire suppressed parcels into the PB cycle?
2. Season of burn: How would the season (e.g., winter vs. summer) affect the PB impacts? The weather and background atmospheric composition would be different in each season. The fuel moisture, especially for woody fuels may also change from season to season. The contrast of traditional winter/spring burning with summer would illustrate the challenges of conducting PB during poor air quality periods.
3. Size of burn: Varying the size of the burn (e.g., 300 vs. 600 acres) and the proximity of the burn plots (e.g., two 300 acre plots 5 miles away vs. next to each other) would change the smoke plume characteristics. How far apart do parcels have to be from one another such that if subject to PB simultaneously, their impacts will not superimpose upon each other?

4. Ignition type: Hand stripping vs. aerial burning would result in very different plumes. Downwind concentrations of $PM_{2.5}$ would be very different for a 1000 acre burn conducted at a constant rate of spread (representative of hand ignition) than substantially increasing the number of acres burned for the first hour or two and then allowing a constant rate of spread (for example 500 acres consumed in the first two hours; more representative of aerial ignition).
5. Time of burn: The burn can be conducted during different times of the day to make the impact of PB plume different due to varying meteorological conditions.

April 9, 2008 burn at Fort Benning was used to simulate these five scenarios. On that day, 300 acres of compartment F5 was burned. The fuels were 2 years old with an estimated total fuel load of about 5.8 tons per acre. The burn started at 12:30 EDT (16:30 UTC) and ignition was completed by 14:45 EDT. In order to simulate this burn in Daysmoke, it was assumed that ignition started at the top of the hour, 12:00 EDT, and that the plume organized into 4 updraft cores. It was also assumed that 98% of the land burned within the first 2 hours of the burn and the last 6 acres burned in the smoldering phase over another 2 hours. The measured maximums and minimums of temperature and relative humidity near the burn locations were 49 F and 100% RH at 7:00 EDT and 78 F and 50% RH at 15:00 EDT. The winds were calmer, less than 5mph, till 14:00 EDT when the winds speeded up to 12mph.

4.5.1 Frequency of Burn

Two burn frequencies were compared: 2 years, which was the time since last burn in the base case, and 5 years. The typical 5 year old fuels at Fort Benning amount to a total fuel load of 8.5 tons per acre, which is 2.7 tons more than the base case. The hourly emissions estimated by FEPS for the two different fuel loadings are compared in top left panel of Figure 133. When the frequency of burn is 5 years, $PM_{2.5}$ emissions are 37% larger than those emitted by the 2 years old fuels. An assumption was made that since 5 year old fuels would be taller and thicker, the updraft core number would increase to 6 instead of 4. The other three panels in Figure 133 show the Daysmoke predicted (blue and red) and measured (green) $PM_{2.5}$ concentrations downwind at 2 miles (Truck 1), 3.5 miles (Truck 2), and 5 miles (Truck 3). The base case (2 years) in blue compares well with the measurements since the measured values seem to fit within the 63% confidence bars. Daysmoke tends to over predict the peak at 3.5 miles downwind but a slight under prediction is evidenced 5 miles away from the fire. It should be noted that Daysmoke does not account for background concentrations and another burn or $PM_{2.5}$ source in the region may be contributing to the observed values. The downwind $PM_{2.5}$ concentrations with the 5 year old fuels are larger compared to the 2 year old fuels in all three downwind locations (Figure 133).

Fire diameter is an hourly input to Daysmoke along with emissions and it determines the time variation of the heat flux. Increase in fuel load leads to an increase in fire diameters by 21%, which means that the total heat flux will be stronger for the burn with 5 year old fuels and the plume has the potential to be lofted higher. However, since the number of cores also increased by 50% (from 4 to 6) with the older fuels, individual heat fluxes of each plume core has decreased and limited the height of the plume. This along with the increase in emissions led to higher ground-level $PM_{2.5}$ concentrations downwind with the 5 year old fuels (Figure 133).

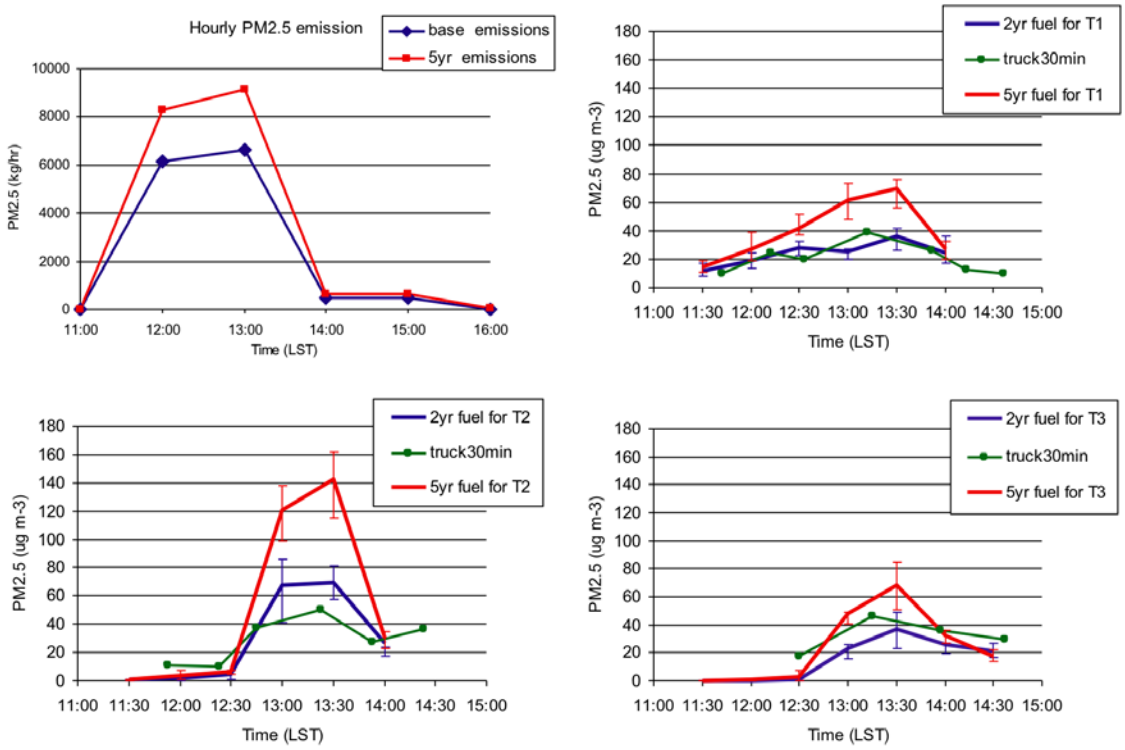

Figure 133. Effects of frequency of burn: 2 year old fuels vs. 5 year old fuels. Comparison of input emissions (top left) and downwind $PM_{2.5}$ concentrations at 2 miles (top right), 3.5 miles (bottom left), and 5 miles (bottom right) from the fire.

4.5.2 Season of burn

Conducting the burn in a different season would change several factors that affect emissions and dispersion of smoke. Even a different day in the same season may present very different meteorological conditions for the burn. Selecting a different day in a different season is obviously more challenging. An attempt has been made to pick days with the same prevailing wind directions, similar wind speeds, and comparable number of days since last rain. The assumption was that the burn could still be conducted as long as these parameters did not deviate too much from their values on the actual burn day. Note, however, that there are other important factors that would lead to a very different burn and a very different plume behavior on the selected days compared to the actual burn day. First, differences in relative humidity would lead to differences in smoldering phase emissions. Then, differences in soil moisture, temperature, and solar intensity would lead to large differences in boundary layer structure. This would affect the rise and dispersion of the smoke plume. Finally, differences in mixing layer height and transport wind speeds would lead to differences in downwind smoke concentrations. The confounding effects of all these differences make it very difficult to predict the implications of conducting the burn in a different season without the help of a simulation system such as the one developed in this project.

The actual burn occurred in early spring (9 April 2008). Here, the same burn was simulated using two different sets of meteorology from winter and summer. Meteorology at the burn location on 11 January 2007 was reported to have wind patterns similar to 9 April 2008, with winds blowing from the southeast, therefore meteorology on that day was used for the winter case. The major difference between the simulated winter and spring days is in the maximum and minimum temperatures. The winter case has temperatures ranging from 28 to 57 F and relative humidity between 32 and 77%. These numbers are lower compared to the base case. The other set of meteorology representing the summer season was from 1 July 2007. The winds were not as consistent on this particular day as they were on 9 April 2008 but during the majority of the burn they were southeasterly. The summer case has temperatures ranging from 70 to 96 F, which are higher than the spring base case, and relative humidity between 41 and 99%. The ambient temperature does not significantly affect the total amount of emissions from the burn. The winter case total $PM_{2.5}$ emissions were 4% lower and the summer case total $PM_{2.5}$ emissions were 6% higher than the spring base case (top left panel in Figure 134). Fire diameters did not vary much amongst the three cases and remained within 4% of each other.

The downwind $PM_{2.5}$ concentrations were higher for the summer case especially when looking at the results at Truck 1 (top right) and Truck 3 (bottom right) locations. This is probably due to higher atmospheric temperature suppressing the plume rise and higher humidity enhancing particle growth. The winter case on the other hand has lower relative humidity, atmospheric temperature, and a slight decrease in emissions. These conditions led to increased fuel consumption and a plume lofting higher from the ground. Therefore one can see a decrease in ground-level $PM_{2.5}$ concentrations at all three truck locations.

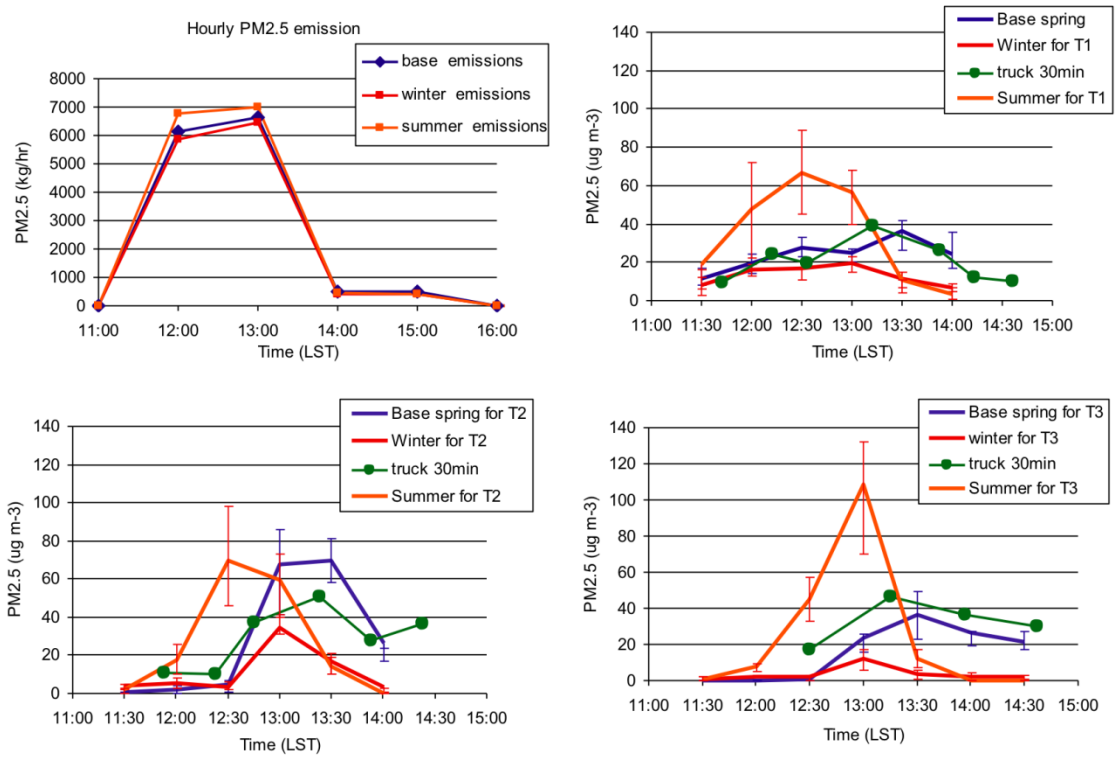

Figure 134. Effects of season of burn: winter and summer vs. spring. Comparison of input emissions (top left) and downwind $PM_{2.5}$ concentration comparison at 2 miles (top right), 3.5 miles (bottom left), and 5 miles (bottom right) from the fire.

4.5.3 Size of burn

On 9 April 2008 a total of 300 acres were burned. Another case where the area of the burn increased to 600 acres was simulated. Doubling the area means that there is twice as much fuel; as a result the emissions of $PM_{2.5}$ increased by 94% (top left panel of Figure 135).

The simulated plumes had similar heights and dispersed similarly for the base case and when the area of the burn was doubled. The major difference was in the maximum concentrations measured at each truck location. Since $PM_{2.5}$ emissions were almost doubled by doubling the size of the burn, ground-level concentrations also increased by almost a factor of two (Figure 135). There is a linear relationship between the area of the burn and the amount of fuel; this results in a quasi-linear increase or decrease in emissions and ground-level concentrations.

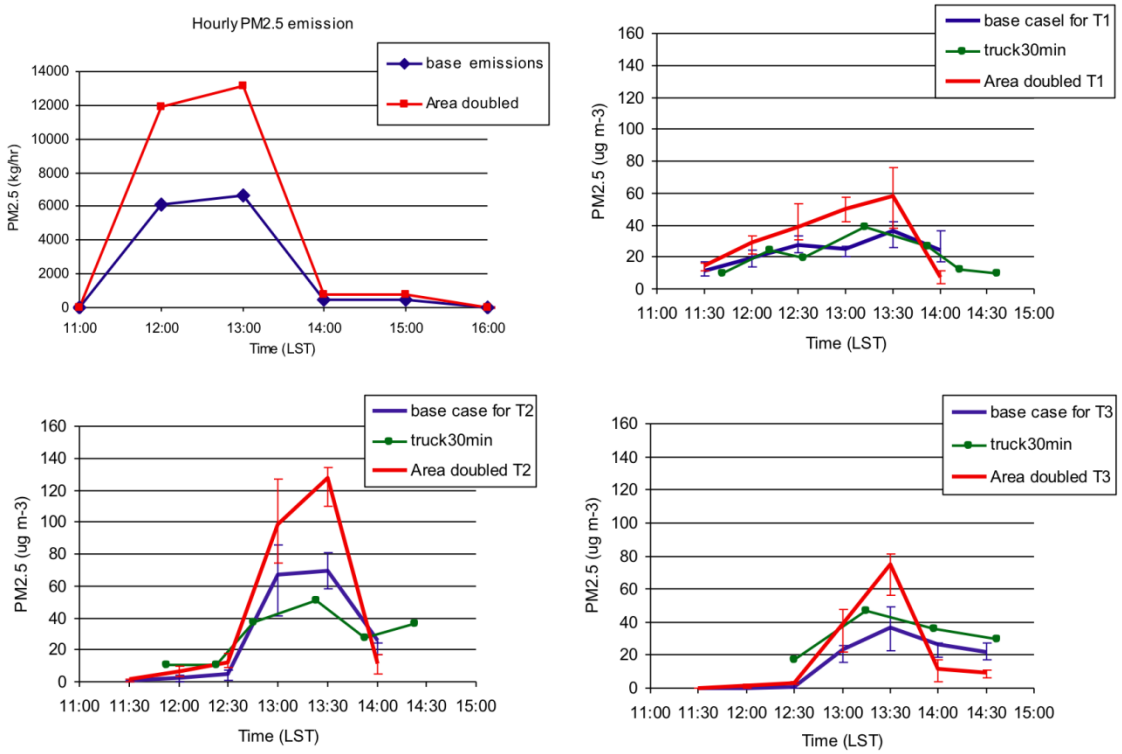

Figure 135. Effects of size of burn original burn: 600 acres vs. 300 acres. Comparison of input emissions (top left) and downwind $PM_{2.5}$ concentrations at 2 miles (top right), 3.5 miles (bottom left), and 5 miles (bottom right) from the fire.

4.5.4 Ignition Type

The base case was hand lit by ground crews riding their ATVs along stripes inside the burn plot and igniting the fuels by flame torch as they drive by. The other common practice that land managers use is aerial ignition. In aerial ignition, a helicopter flies over the burn lot and drops self-igniting fire balls a few meters apart throughout the lot. This method is usually more efficient since it ignites the burn much faster. For the aerial burn case, the burn was assumed to consume 80% of the fuel within the first hour, and the flaming phase ends by the second hour into the burn. Therefore the first hour's emission rate is much larger, twice as much, for the aerial burn compared to the base case and a similar pattern is observed for the fire diameter as well. Over all, aerial burn resulted in 7% less $PM_{2.5}$ emissions than the hand lit base case (top left panel of Figure 136).

Aerial burning plume has sufficient heat flux to create a taller plume than the hand lit base case. Therefore, ground-level $PM_{2.5}$ concentrations remain much lower than the hand lit case at sites 2-5 miles downwind (Figure 136). As the burn goes into the smoldering phase, the $PM_{2.5}$ concentrations due to aerial burn are half of what is expected by hand lit burn.

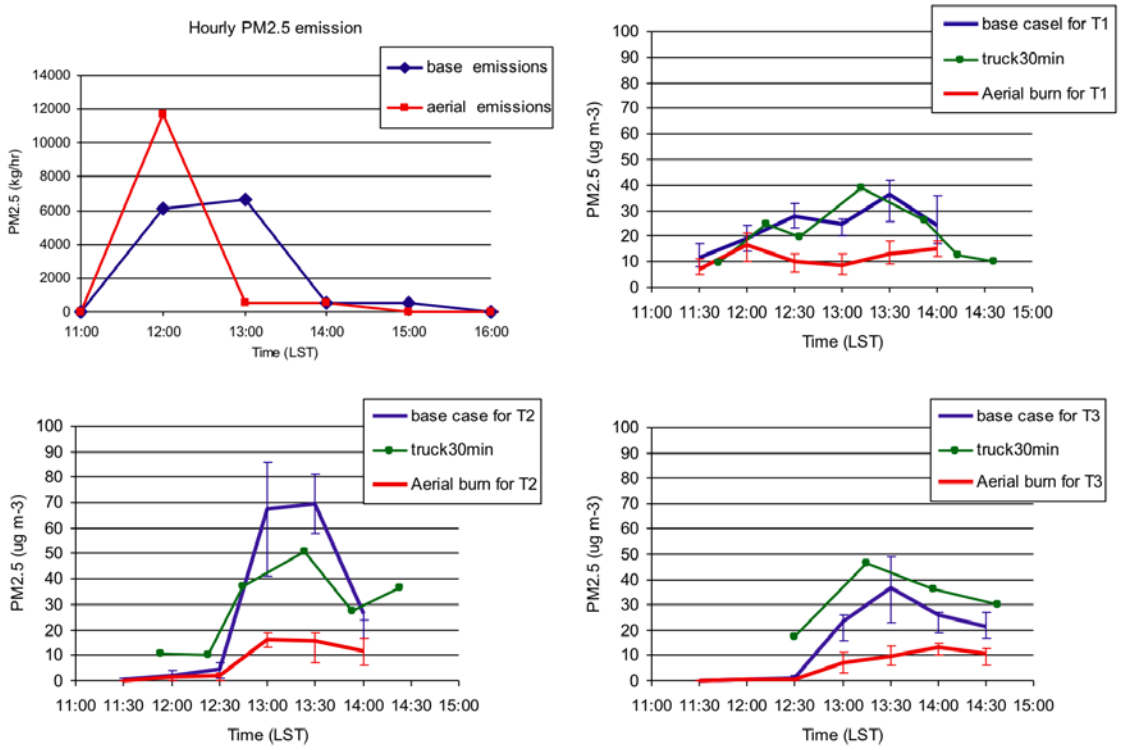

Figure 136. Effects of ignition type: aerial vs. hand lit. Comparison of input emissions (top left) and downwind $PM_{2.5}$ concentrations at 2 miles (top right), 3.5 miles (bottom left), and 5 miles (bottom right) from the fire.

4.5.5 Time of burn

The effect of changing the ignition start time on the same day (9 April 2008) was investigated. Two different ignition times were simulated: one in the morning, 10 am, and another in the afternoon, at 3 pm. Recall that the actual ignition time was 12:30 pm (EDT). $PM_{2.5}$ emissions for the 10 am burn were estimated to be only 78% of total emissions for the base case but the 3 pm burn emitted 39% more $PM_{2.5}$. Fire diameters decreased for both morning and afternoon burn compared to the base case's fire diameters, by 80% and 90% respectively.

Figure 137 compares the $PM_{2.5}$ concentrations at the three truck locations for the morning, noon and afternoon burns. The morning (10am) ignition case results in slightly higher $PM_{2.5}$ concentrations at Truck 1 location due to smaller heat flux, but lower $PM_{2.5}$ concentrations at Truck 2 and Truck 3 locations due to smaller emissions. On the other hand, the afternoon burn (3pm) resulted in higher $PM_{2.5}$ concentrations at all three truck locations due to larger emissions into a collapsing boundary layer.

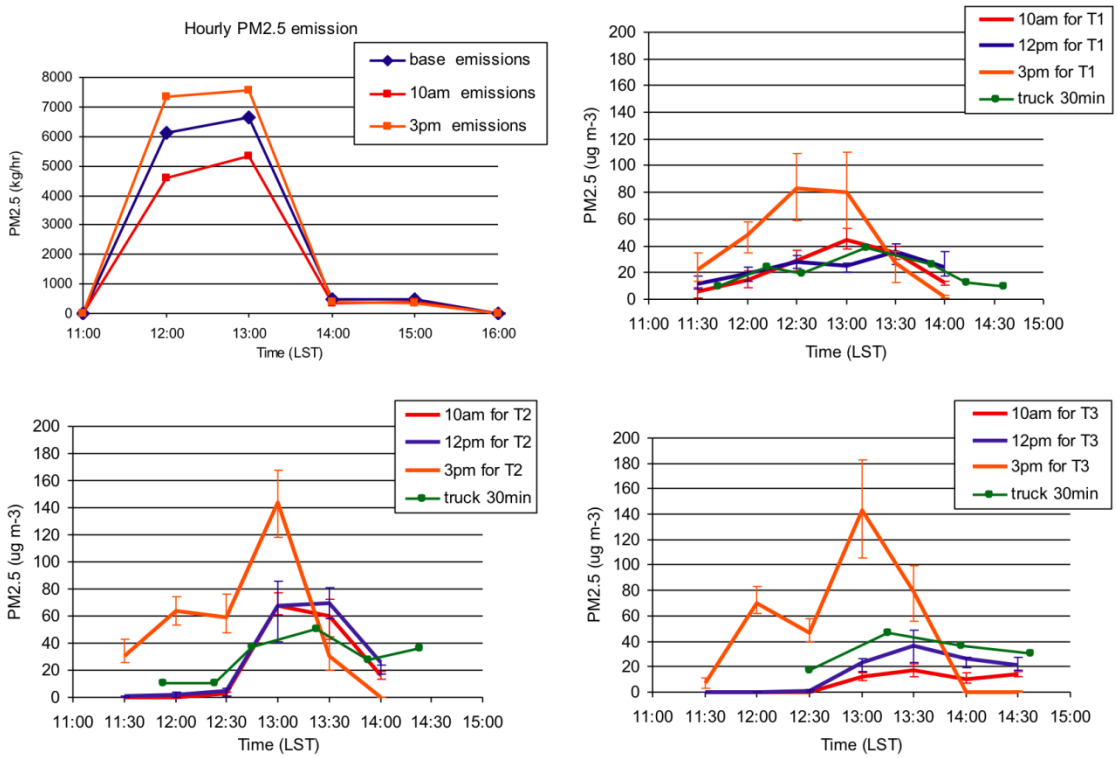

Figure 137. Effects of time of burn: morning and afternoon vs. noon. Comparison of input emissions (top left) and downwind $PM_{2.5}$ concentrations at 2 miles (top right), 3.5 miles (bottom left), and 5 miles (bottom right) from the fire.

4.5.6 Comparison of Strategies

Figure 138 compares the emissions and ground-level $PM_{2.5}$ concentrations of alternative burning scenarios. The scenarios where the amount of $PM_{2.5}$ emission increased the most compared to the base case are: 1) the case where the area (and the updraft plume core number) doubled, and 2) the 5-year-old fuel case. The late afternoon and summer burn scenarios also resulted in increased $PM_{2.5}$ emission compared to the base case but only by a slight margin. The aerial ignition case resulted in significantly larger $PM_{2.5}$ emission early on but total emissions during the course of the burn were smaller. Emissions also decreased in the winter and the morning burn cases.

Among all the alternative burning scenarios the case that would result in the largest $PM_{2.5}$ concentrations 2-5 miles downwind is the late afternoon (3 pm ignition) case since warmer ambient temperatures along with a collapsing boundary layer would severely limit the rise of the smoke plume. The scenarios with 5-year burn frequency instead of 2, twice the acreage, and burn in summer instead of spring all lead to increases in $PM_{2.5}$ concentrations but their ranking varies by distance. For example, the summer burn does not affect Truck 2 location 3.5 miles downwind as much as the other two scenarios. However, it leads to a $PM_{2.5}$ peak comparable to 5-year burn frequency at Truck 1 location 2 miles downwind and the highest $PM_{2.5}$ among the three scenarios at Truck 3 location 5 miles downwind.

The increase in RH and ambient temperature are the main factors for the increase in ground-level $PM_{2.5}$ concentration for the summer case. High humidity gives smoke particles a chance to grow in presence of water droplets. Higher ambient temperature also enhances combustion and results in increased emissions. In the case of 5-year-old fuels, the ground-level $PM_{2.5}$concentrations increased because of the emissions increasing at a higher rate than the fire diameter. Also, a larger number of updraft cores kept the smoke closer to the ground. Doubling the size of the burn essentially increased the emissions without significant change in plume height and resulted in increased ground-level $PM_{2.5}$concentrations.

The scenario that leads to lowest ground-level $PM_{2.5}$ concentrations 2-5 miles downwind from the burn plot is the aerial ignition case. This type of ignition resulted in a much larger fire diameter making the updraft intensity much stronger. The smoke plume penetrated into the free troposphere and left a very small trace in the boundary layer. The second lowest ground-level $PM_{2.5}$ concentrations are obtained with the winter burn scenario. In that case, lower ambient temperatures suppress combustion resulting in lower emissions. In addition, the smoke plume can rise to relatively higher altitudes and smoke particles do not grow as rapidly in dry air as they do in humid air. The early morning burn also leads to lower $PM_{2.5}$ concentrations, especially at Truck 3 location 5 miles downwind.

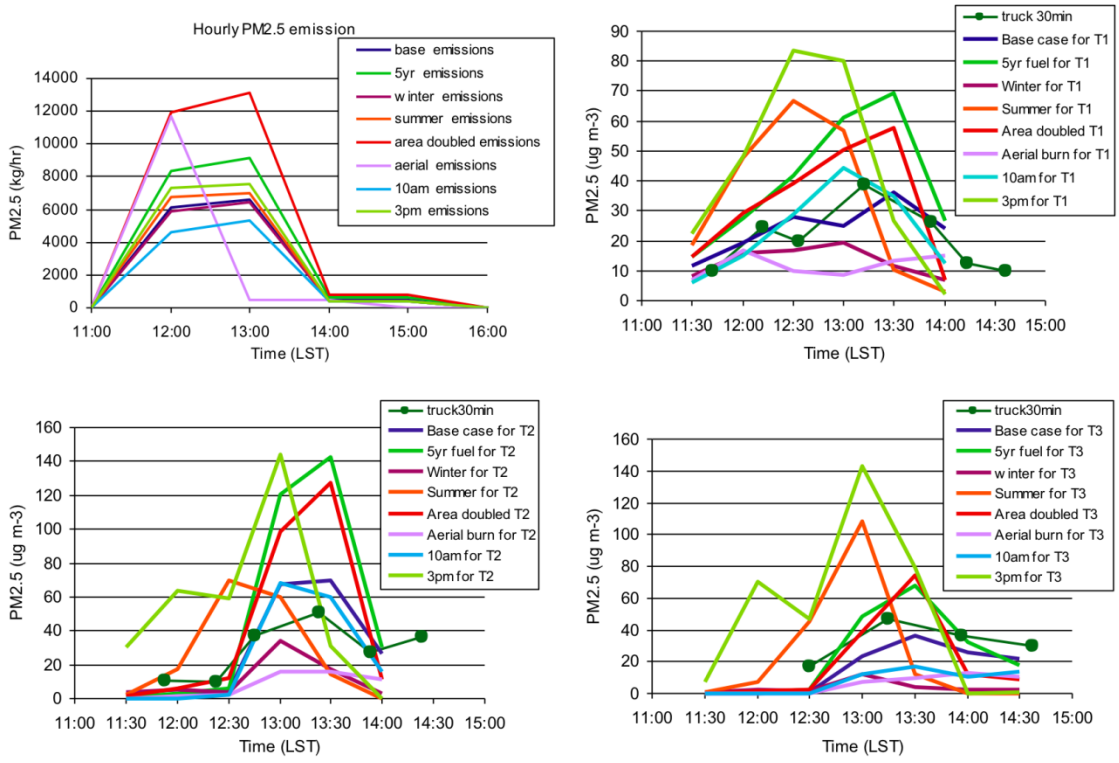

Figure 138. Comparison of the impacts of alternative burning strategies: $PM_{2.5}$ emissions (top left) and downwind $PM_{2.5}$ concentrations at 2 miles (top right), 3.5 miles (bottom left), and 5 miles (bottom right) from the fire.

5 Conclusions and Implications for Future Research/Implementation

Prescribed burning (PB) is an effective and economical land management tool for improving and maintaining an ecosystem, reducing wildfire risk, and improving training realism at Department of Defense (DoD) facilities. However, pollutants emitted from prescribed fires may be transported downwind, mix with emissions from other sources, form other pollutants, and contribute to poor air quality of urban areas in the region. Compliance by those urban areas with ambient air quality standards may require tougher restrictions on DoD's air emissions in the future. Since the alternatives of PB are costly, it is important for DoD to be able to control the emissions from its PB operations and to minimize their air quality impacts. Therefore it is necessary to better characterize PB emissions and to more accurately predict their air quality impacts.

Current estimates of PB emissions are based on studies mostly conducted in the West during 1970s and 1980s. They may not be able to characterize the diverse ecosystem and environmental conditions of the Southeast. For example, some prior studies by the Forest Service (FS) suggest that fine particulate matter ($PM_{2.5}$) emissions from southeastern burns may be much smaller than the current estimates. This is a problem for the fidelity of all air quality simulations. On the other hand, there is no definite answer to how to place these emissions in regional-scale air quality models. Local plume models and regional AQMs have advanced our knowledge of smoke transport and dispersion to a certain level. To increase our understanding, there is now a need for a proper model for prescribed fire plumes in regional scale simulations.

The objectives of this project have been (1) to improve the characterization of PB emissions; (2) develop a modeling system that can accurately predict the impacts of prescribed burns on regional air quality; (3) collect field data most relevant to the modeling of PB plumes; (4) validate the models through evaluations with field data; and (5) assess alternative burning strategies for southeastern DoD facilities. Fort Benning has been selected as the host DoD installation for this project because of the large size of its PB operation and its proximity to a major metropolitan area: Columbus-Phenix City, which is beleaguered with air quality issues.

This project applied various Forest Service tools to the estimation of PB emissions from DoD lands. These tools included the Fuel Characteristic Classification System (FCCS)for the characterization of fuel beds , wildland photo series for the estimation of fuel loads and the model CONSUME for the estimation of fuel consumptions. PB emission factors derived from prior field measurements of particulate matter (PM), carbon monoxide (CO), and volatile organic compounds (VOC) in the Southeast were compared to laboratory and in situ emissions measurements. "Daysmoke," an empirical plume model designed specifically for prescribed burns, and the Community Multiscale Air Quality (CMAQ) model were coupled using the improved grid resolution provided by the Adaptive Grid technology. This enabled adequate representation of plume dynamics and chemistry at local scales as well as accurate prediction of impacts over regional scales. The coupled models were first evaluated using existing data. Additional data needs were identified and fulfilled by monitoring campaigns at Fort Benning AB and Eglin AFB. The models were evaluated by comparing model predictions to measurements. The sources of uncertainty in model predictions were investigated through sensitivity analysis.

Finally, using the evaluated models, various scenarios were simulated to quantify the air quality impacts of alternative PB scenarios, such as changing the burning times, frequencies, and methods.

5.1 Estimation of Fuels and Emissions

The fuels survey conducted at Fort Benning resulted in a model based on photo series for estimating fuel loads on any Fort Benning burn plot. In this model, fuel loads increase rapidly after a burn as shrubs become a significant part of the fuel bed. The increase slows down in time and a plateau is reached after approximately 5 years. This model provides a crosswalk to FCCS fuel classification system. Emissions were estimated for each burn monitored at Fort Benning: there were 3 burns in April 2008, 6 burns in January 2009, and 2 burns in April 2009. The fuel loads were input to CONSUME, which yields total fuel consumption, and then to FEPS for time varying consumption. Emissions are calculated by applying emission factors to the fuel consumptions. Emission factors used here were derived from extensive field studied of prescribed burns conducted by the Forest Service in the Southeastern U.S. in 1990s. To provide input to SERDP project RC-1649, fuel samples were collected at Fort Benning and shipped to the Fire Science Laboratory in Missoula, MT for emission measurements. The emission factors measured in the laboratory were in general agreement with the USFS southeastern fuels emission factors used here.

Emission inputs are critical to dispersion model performance. While comparison to laboratory measurements established a certain level of confidence in emission factors, the uncertainties in fuel loads and fuel consumptions remained unknown. As part of the Prescribed Fire Combustion and Atmospheric Research Experiment (Rx-CADRE) at Eglin Air Force Base (AFB) in February 2011, fuel load and fuel consumption data were collected. Comparison of photo-series based estimates to fuel measurements before the burns revealed that fuel loads were overestimated by 20%. On the other hand, fuel consumptions modeled by CONSUME were underestimated by 7% compared to the difference between pre- and post-burn fuel measurements. Finally, the $PM_{2.5}$ emission factors used for estimating emissions were 25% lower compared to aerostat-based emission measurements per unit mass of fuel consumed. The reasons for this underestimation may be fire induced emissions from the canopy and secondary organic aerosol formation.

The emissions calculated using the fuel load and fuel consumption measurements along with measured emission factors were considered nominal values and input to Daysmoke. Then, these nominal values were perturbed by the amounts of uncertainties attributed to the use of photo series for fuel load, CONSUME 3.0 model for fuel consumption, and emission factors from different sources. Spatial and temporal smoke distributions obtained by perturbing emission inputs were compared to the base distributions that the nominal emissions yielded. The differences were evaluated relative to the measured downwind smoke concentrations. It was found that the uncertainty inherent in atmospheric turbulence modeled by Daysmoke through stochastic terms was typically larger than the uncertainty resulting from perturbing fuel loads and fuel consumptions. Only the uncertainty in emission factors had a greater impact on the variability of downwind smoke concentrations.

A sensitivity analysis was conducted to determine the important parameters of the models used in estimating emissions. Fuel moisture, involvement in flaming phase, duration of ignition, and emission factors are, by far, the most sensitive parameters. The likely ranges of these parameters were tested to determine the level of uncertainty in emission predictions. The uncertainties that are identified in this manner can be used in estimating the uncertainties in downwind concentration predictions by the dispersion models. The sensitivity analysis was extended to the chemistry-transport model where the impact of spatial (both horizontal and vertical) and temporal distribution of emissions on concentrations downwind has been studied (see Section 5.4.3 below).

5.2 Field Measurements

After the preliminary data collection at Fort Benning AB, which resulted in three monitored burns in April 2008, intensive field measurements in 2009 captured eight more burns: six in January and two in April. The burns were monitored by using three trucks equipped with real-time $PM_{2.5}$ and CO monitors covering a 60-degree arc emanating from the burn area and stretching along the predicted wind direction. In response to shifts in wind direction the trucks moved to different locations within their zones, respectively 1-3 km, 3-5 km, and 5-7 km downwind, according to dispatches from the fire tower. The exact locations of the sampler trucks have been tracked by GPS. The trucks remained at any given monitoring location for a minimum of 30 minutes. Each subsequent position was chosen based on a combination of wind shifts, real-time equipment levels, and road availability. All the real-time air samples collected were processed, controlled for quality, and quality assured. The measurements and related information have been posted to a web site[4] for public access.

In 2011, a comprehensive field study was conducted at Eglin AFB where fuels were sampled both before and after the burns for calculating "actual" fuel loading and consumptions. Emissions of CO_2 and $PM_{2.5}$ were measured with a platform mounted on a tethered aerostat. Winds were measured with airborne (mounted on the aerostat) and ground-based sonic anemometers, and pilot balloon soundings. Plume height was measured with a lidar ceilometer as practiced in some of the Fort Benning burns. Ground-level $PM_{2.5}$ data were collected on mobile platforms and calibrated with more accurate $PM_{2.5}$ measurements at a stationary site. All these measurements during the 2011 field study substantially improved the ability to model emissions from prescribed burns and provided more accurate inputs to the Daysmoke plume dispersion model for its evaluation.

The measurement of 3D wind velocities using an aerostat is a novel method. Comparison with the ground compass measurements and balloon position relative to the anchor point showed that the MTi-G's ability (a GPS-aided inertial measurement unit with an attitude heading reference system) to correct for changes in the sonic anemometer orientation relative to the global reference system was about 5°.

[4] http://sipc.ce.gatech.edu/

Aerial determination of $PM_{2.5}$ emission factors using the carbon balance method found good agreement between two days of sampling. Values of 28 and 24 g/kg C burned were determined. These values correspond to 14 and 13 g/kg of biomass burned, respectively, which are only slightly higher than the ground-based and laboratory burn facility measurements, each which agree at about 11 g/kg. More data are necessary to determine whether this difference is statistically significant; if the difference is real, it might be due to fire-induced emissions from the canopy and secondary organic aerosol formation, emissions which are not collected by the ground-based samplers.

5.3 Plume Rise and Dispersion Modeling

This project resulted in several improvements to the capabilities of the plume rise and dispersion model Daysmoke in simulating smoke plumes from PBs. The starting point has been a former version that was subjected to a sensitivity analysis with the Fourier Amplitude Sensitivity Test (FAST). The FAST analysis identified empirical parameters important for plume height prediction (Liu et al., 2008). Therefore, many empirical coefficients have been pre-assigned or expressed in terms of other variables.

A thorough review of the Daysmoke model theory and computer code was performed. Several improvements to the model were implemented and tested. For example, provision for adiabatic expansion allowed for application to a wider range of smoke plume. The new transition from plume to free atmosphere at the plume top resulted in improved modeling of plume depth. The multi-core updraft feature is much more flexible now that it allows for cores of unequal sizes by assigning a stochastic flux component to each updraft core. A bug was discovered that increased plume vertical velocity by 0.5 - 1.0 m/s within the mixing layer. The parameterization of the entrainment coefficient was made a function of plume bent-overness. The detrainment coefficient was removed from being an additional degree of freedom. The free atmosphere horizontal velocity turbulence parameter, which used to be a constant, was made a function of the depth of the boundary layer.

In addition to these improvements, significant effort was spent on building a highly-tilted plume solution through modification of Daysmoke's initial conditions and on developing a method for the determination of the updraft core number. The following summary of Daysmoke model evaluations is intended to describe the improvements made to the model during this project. It also points to modeling issues left for future research.

5.3.1 Evaluation of Daysmoke with Fort Benning Burns

A thorough evaluation of the Daysmoke model was conducted using the field data collected at Fort Benning AB. Daysmoke simulations were compared to observations of $PM_{2.5}$ and plume height for weak plumes from eleven prescribed burns. Daysmoke plume tops were found near the lower end of the range of observed plume tops for six prescribed burns. The plume top heights and the number of updraft cores, which was confirmed by photographic data, are the two most important parameters in the determination of smoke levels by Daysmoke. Comparison of the $PM_{2.5}$ concentrations predicted by Daysmoke with real-time measurements taken from three mobile trucks out to a distance of eight kilometers showed general agreement but there were

several instances of divergence. Uncertainties remained with respect to the precision of the real-time instruments, predicted wind directions, recording of ignition patterns, and the timing of emissions. Investigation of possible contamination by non-smoke PM sources led to the removal of only a small fraction of the data.

The comparison of $PM_{2.5}$ concentrations simulated by Daysmoke to ground-based mobile measurements has shown a relationship between the performance of the model and the gradient of the observed smoke by downwind distance. Daysmoke performance was the best on days when smoke concentration increased with distance downwind from the burn. On days when smoke concentrations decreased with distance, Daysmoke performance was not as good but still acceptable. On days characterized by extremely high smoke gradients, from very high smoke concentrations at 1-3 km downwind to almost no smoke at 5-7 km downwind, Daysmoke performance in predicting $PM_{2.5}$ concentrations was poor.

5.3.2 Highly-tilted Plume Solution

The highly-tilted plume solution was built during this project to deal with extremely high smoke gradients from very high smoke concentrations near the burn to almost no smoke at a short downwind distance. Daysmoke plumes agreed well with Briggs theory for "bent-over" plumes although the two-thirds theory is not explicit in Daysmoke. However, the solutions for "highly-tilted" plumes characterized by weak buoyancy, low initial vertical velocity, and large initial plume diameter do not match Briggs theory.

In the original Daysmoke, the initial plume vertical velocity of 25 ms^{-1} was assumed based on numerical simulations of coupled fire-atmosphere models (Jenkins et al., 2001). The vertical velocity was claimed to be an average over a 20 m grid square and representative of wildfires. However, plume diameters for the burns at Fort Benning, GA, were typically 60 m and the use of 25 ms^{-1} as an average initial vertical velocity for a 60 m diameter prescribed burn plume was problematic. In addition, canopy drag may have further reduced the exit velocity. Forest canopies at Fort Benning ranged from open to partially closed. Anecdotal evidence of trees rocking during plume passage at some prescribed burns suggests significant momentum transfer from the plume to the crown. Furthermore, crown scorch in the aftermath of prescribed burns is suggestive of significant heat transport from plume to trees. Thus the expected impact of canopies on an incipient plume would be to lower the initial vertical velocity and to reduce the initial temperature anomaly below those used in the original Daysmoke.

Meanwhile, the mass flux determined by combustion equations must be conserved. Reducing the initial average vertical velocity through canopy drag must necessarily be accompanied by a commensurate increase in initial plume diameter. That, in addition to reducing initial plume temperature anomaly through heat transfer to the crown, can lead to results that are counterintuitive because of the increased buoyancy efficiency of the larger diameter plume. For example, as shown in Figure 34, reducing initial vertical velocity and initial plume temperature anomaly from, respectively, 25 ms^{-1} and 40 ^{o}C for a 60 m diameter bent-over plume, to 0.5 ms^{-1} and 1.0 ^{o}C resulted in a highly-tilted plume that grew taller through an initial plume diameter seven times larger.

Thus the impact of the forest canopy may be to convert an incipient small diameter, fast-rising bent-over plume into a large diameter slow-rising highly-tilted plume capable of ascending farther than its bent-over counterpart. That Daysmoke plume heights scored slightly low in comparison with observations (refer to the discussion in reference to Figure 101) may in part be explained by the initialization for bent-over plumes. Further research will clarify this issue.

5.3.3 Determining the Number of Updraft Cores

Smoke plumes from prescribed burns are complex in structure; they are typically defined by a number of updraft cores. The multiple-core structure has implications for modeling plume rise as the total mass flux from combustion distributed over many updraft cores, relative to a single updraft core, must be conserved. Multiple-core updraft plumes have larger total surface area to volume ratios than does with a single core, are more exposed to entrainment, and grow to lower heights. This research has shown that specification of updraft core number is the single-most important model parameter for predicting plume rise from prescribed burns.

Simulations of weak plumes by Daysmoke were done initially through subjectively "estimating" updraft core number by taking into consideration factors such as size and shape of the burn area, fuel type, moisture, loadings and heterogeneity, amount and distribution of fire on the landscape, distribution of canopy gaps, transport wind speed, and mixing layer depth. Comparisons between model-simulated $PM_{2.5}$ and high-frequency measurements from real-time samplers revealed a need for an improved emissions production model.

In the final evaluation cycle, Daysmoke was evaluated for a strong plume from a helicopter aerial ignition prescribed burn conducted on 6 February 2011 at Eglin AFB. Because the track of ignition times and locations was fixed by an onboard GPS unit, the cellular automata (CA) fire spread model, Rabbit Rules, could be used to deduce initial conditions required by Daysmoke. The CA fire spread model showed the importance of fire-atmosphere coupling in fire spread rate and fire intensity. Fire-atmosphere coupling increased winds locally from less than 2 ms^{-1} to 10 ms^{-1}. Lines of more intense fire coupled with winds to create low pressure anomaly centers with each center assumed to represent the base of an updraft core.

The numbers of pressure anomaly centers simulated in Rabbit Rules were counted for each minute during the burn. Updraft cores ascending above small, weak centers were assumed to have been absorbed into nearby stronger updraft cores. Furthermore, adjacent strong pressure anomaly centers were assumed to have merged into single updraft cores a short distance aloft as implied by the centers within the large ellipse in Figure 96. This assumption is supported by how the main plume (rightmost updraft core in Figure 97) organized from smoke originating from sources spread out near the ground and the possibility that the two central cores (small arrows) merged into a single core. The final number of updraft cores ranged from one to six with the most frequent number being four. Three/four updraft cores were visible in the photo-image (Figure 97).

In addition to the number of updraft cores, Rabbit Rules supplied initial updraft vertical velocities and relative emissions in percent of total emissions per minute, as initial conditions for Daysmoke. The ability of simulating all these variables with Rabbit Rules provides the means for

performing much more robust model evaluations in the future. The evaluations no longer have to be limited to comparison of Daysmoke-simulated downwind smoke concentrations to measured concentrations; they can include the evaluation of these intermediate variables towards a more complete evaluation of the modeled phenomenon. Rabbit Rules bridges an important gap in the modeling of smoke dispersion by characterizing the fire-atmosphere interaction.

Daysmoke was set with four updraft cores throughout the burn. Initial updraft vertical velocities for the four updraft cores were set to range between 8-12 ms^{-1} stochastically. These and the method for calculating updraft core diameter given in Equation (9) produced the ranges of initial vertical velocity and updraft core diameter shown in Figure 102. The initial temperature anomaly was set to 30 ^{o}C. Simulations with atmospheric soundings from WRF and MM5 produced plume tops that overshot the mixing height from 800 – 1100 m. Plume tops above the mixing height were confirmed by ceilometer measurements. Particulate matter ejected into the free atmosphere above the mixing layer during the active flaming stage ranged from 89 – 93 percent.

The impact of the forest canopy on the simulations needs further explanation. It was argued earlier in Section 5.3.2 that passage of the plume through forest canopies must involve significant momentum and heat transfer from the plume to the crowns. The impact of the forest canopy on Daysmoke may be to convert an incipient small diameter, relatively warm, fast-rising bent-over plume into a large diameter, relatively cool, slow-rising highly-tilted plume capable of ascending higher than its bent-over counterpart. However, this conclusion was based on the assumption of conservation of mass flux. The impact of a closed forest canopy on Rabbit Rules may be to reduce the mass flux. Increased fuels deposition from a dense over-story of a closed canopy relative to an open canopy would be expected to increase fuel loadings and thus increase fire intensity. However, sheltering of the fuel bed from wind and sun may retain higher fuel moisture under closed canopy thus decreasing fire intensity. Furthermore, reduced ambient wind speeds under a closed canopy should contribute to decreased fire intensity through slowing fire spread rates. In extreme conditions, fire confined under a closed canopy may suffer from oxygen deficiency thus further reducing fire intensity.

Canopy characteristics for the block 703C burn mostly ranged from open to partially closed. For Daysmoke, initial updraft vertical velocities were reduced from 25 ms^{-1} to 8-12 ms^{-1} and initial temperature anomaly reduced from 40 ^{o}C to 30 ^{o}C in comparison with Achtemeier et al. (2011) to partially estimate canopy effects. No adjustments were made in Rabbit Rules beyond the fuel designations shown in Table 2. Fire behavior under a closed canopy relative to fire behavior under an open canopy is a subject for further research the outcome of which could be an additional fuel designation vector in Table 2 or a canopy rule for the CA fire model.

In conclusion, the lack of quantitative initialization data, in particular, the number of updraft cores that define the plume has limited the accuracy of Daysmoke simulations. In this project, Daysmoke was successfully coupled with the CA fire spread model, Rabbit Rules, the latter calculating initial conditions for the former. The coupling can be tighter pending an algorithm that calculates updraft core numbers and diameters from mergers of pressure anomaly centers. Then updraft core data coupled with relative emissions data simulated by Rabbit Rules will enable calculation of emissions for each core.

Although Rabbit Rules offers a solution for the updraft core problem posed in Daysmoke, limitations of both models as currently configured should be noted. First, in this project, both Daysmoke and Rabbit Rules have been designed for and tested against prescribed burns – Daysmoke for weak plumes at Fort Benning AB and strong plumes at Eglin AFB and Rabbit Rules for an aerial ignition in pinelands. Most prescribed burning is done within the gently rolling Piedmont and flat coastal plains of the southeastern United States – areas for which the models have been evaluated. Neither model has yet been applied for burns over mountainous terrain. Second, no studies to date have been done for wildfires spread over large landscapes and which can generate extreme conditions of plume rise and fire-atmosphere coupling. Validation under these conditions is a subject for future study.

Furthermore, detailed ignition data are not available from most prescribed burns. Therefore the ranges of initial conditions for Daysmoke will be determined from a slowly growing number of experimental burns. Then, for other burns, Daysmoke will be initialized from these data using methods yet to be determined.

Finally, ongoing simulations with Daysmoke continue to show that when and where heat and particulate matter are released into the atmosphere are complicated by evolving atmospheric conditions during the burn. From earlier studies of weak plumes, nearly 100 percent of smoke was confined to the mixing layer. This is not always the case for strong plumes (as in Eglin AFB burns) which are typically associated with larger-area burns and therefore larger amounts of particulate matter released. For air quality prediction models, both levels and timing of smoke injection may be critical for accurate prediction of local and regional distributions of particulate matter.

5.3.4 Uncertainty of Input Winds

WRF-simulated winds did not always line up the Daysmoke plume with truck locations. Occasionally, potential stability problems in WRF at 1.3-km resolution introduced unexpected oscillations to wind direction. This compromised efforts to match Daysmoke $PM_{2.5}$ with observed $PM_{2.5}$. The disparity was particularly notable for April 15, 2008 when truck positions were located south-southeast (SSE) from the fire but WRF winds blew the Daysmoke plume to the south-southwest (SSW). Therefore, it was suggested that the WRF winds be validated with winds measurements during the next field experiment at Eglin AFB. A Doppler sodar and an airborne sonic anemometer were arranged to study the uncertainty in wind speeds and wind directions.

The Doppler sodar was tasked with remote sensing of the vertical wind profiles that can be directly input to Daysmoke. Unfortunately, the USFS Northern Research Station sodar reserved for this purpose was damaged during shipment to Eglin AFB. If it could be operated, the sodar would be placed upwind from the burn plot and would have provided wind speed and direction between 100 and 500 m altitudes with approximately10 m resolution. This would be sufficient to run Daysmoke directly with no need for MM5 or WRF wind predictions. In the absence of high resolution vertical wind profile data, it is only possible to make adjustments to the weather prediction models' wind predictions. The intent of the adjustments is to minimize the difference between observed and predicted wind speeds and directions.

During the 8 February 2011 burn at Eglin AFB, wind speed and direction data were available from two sonic anemometers, one mounted on the aerostat flying between 100 and 300 m altitude along the downwind edge of the burn plot and another on a 10 m mast near the tether points. Wind data at 2 m height were also available from the weather station operated at the stationary site about 2 km downwind. Using these three wind measurements, and boundary layer theory, wind profiles predicted by WRF (or MM5) can be adjusted to better match the observations. The adjustment described in Section 4.4.3.2.2.2 is somewhat crude and only used the wind measurements from the airborne sonic anemometer. Continuing research will develop a more sophisticated adjustment scheme making use of wind measurements at 2m and 10 m altitudes as well.

After the adjustment, the agreement between ground-level $PM_{2.5}$ observations and Daysmoke predictions greatly improved (Figure 114) over the initial comparison with unadjusted WRF winds (Figure 111). This shows that the wind speed/direction data from the sonic anemometer attached to the aerostat were not only useful in assessing the uncertainty in WRF predictions of WS and WD but by applying an adjustment to correct the wind direction–despite the crudeness of the adjustment– it was possible to evaluate the predictive skill of Daysmoke.

An adaptive grid version of MM5 that can provide more accurate meteorological inputs at the scales targeted for chemistry/transport modeling in this project (~100 m) was tested. This model was originally developed to resolve optical turbulence in the upper troposphere. Here, the model was applied to the simulation of boundary layer meteorology during the 9 April 2008 burn at Fort Benning. In this application, to better resolve the meteorology around the PB plume, the model was dynamically adapting to the externally supplied $PM_{2.5}$ concentrations from an earlier chemistry/transport simulation. Compared to a standard fixed grid MM5 simulation, there were some significant differences in model results, especially in wind speeds, that could not be explained in terms of grid adaptations. Compared to a standard fixed grid MM5 simulation, as well as a WRF simulation, adaptive MM5 produced much more variability in the wind fields and the influence of the terrain was more apparent. These results were encouraging in terms of providing wind field resolution never achieved before, which could translate in much more accurate transport simulation of prescribed burn plumes. However, since resources were not available to continue the development and evaluation of adaptive MM5, meteorological inputs were interpolated from 1.3 km resolution MM5 or WRF simulations.

5.4 Regional Scale Air Quality Modeling

The incorporation of the adaptive grid algorithm into the CMAQ model started with Version 4.5 of CMAQ by keeping all the functionality and features of the host. First the variable time step algorithm (VARTSTEP) was incorporated to improve computational efficiency. Then the Adaptive Grid CMAQ (AG-CMAQ) code was developed. The code was verified by simulating the April 9, 2008 burn and comparing the results to those of an earlier simulation by CMAQ with fixed, uniform grid. AG-CMAQ increased the grid resolution in the regions of highest $PM_{2.5}$ as it should. In a more rigorous verification aiming to match the results of standard CMAQ with a "non-adapting" run of the AG-CMAQ, all the differences in results were reconciled with the exception of very small (less than 0.1 $\mu g\ m^{-3}$) differences in aerosol nitrates and secondary organic aerosols of biogenic origin. The VARTSTEP algorithm and the newly developed AG-

CMAQ model were documented in two journal articles published in Atmospheric Pollution Research (Garcia-Menendez et al., 2010; Odman and Hu, 2010).

During model development, several deeply hidden "bugs" were discovered in the transport modules of the original CMAQ code. The outcomes of these bugs were various, ranging from incomplete advection to excessive diffusion. Considering the large number of CMAQ users around the world, discovering these bugs was a very important contribution that could only result from the kind of meticulous code review and rigorous code verification procedures employed in this project. It was also discovered during this project that the Smagorinsky formulation of horizontal diffusion based on deformation is only applicable to Cartesian coordinates. Since CMAQ uses generalized coordinates, this is an additional source of error in the original code. The appropriate formulation was derived for generalized coordinates and implemented in the adaptive grid CMAQ code.

5.4.1 Adaptive Grid CMAQ

The adaptive grid CMAQ (AG-CMAQ) has been developed by integrating a dynamic, solution-adaptive grid algorithm into CMAQ. The model can efficiently refine the grid in response to any defined simulation variable or parameter. Although adaptive grid air pollution models have been previously explored, AG-CMAQ is unique in its capacity to model particulate matter and the first built onto an existing community model. Adaptive grid modeling could potentially be the best approach to multiscale modeling of air pollution dynamics and chemistry.

The developed model was verified and its capabilities were demonstrated. The model proved to replicate results that were practically the same to those produced by the standard, static grid CMAQ when no grid adaptation was applied and effectively increased grid resolution in response to pollutant concentrations increases when adaptation was applied. AG-CMAQ performance was evaluated by simulating an air pollution incident affecting the Atlanta metropolitan area caused by two prescribed burns. The evaluation showed that AG-CMAQ successfully reduced the artificial diffusion inherent to photochemical models and produced better defined plumes compared to the standard CMAQ. Additionally, AG-CMAQ allowed both prescribed burn plumes to be distinctly observed and impacts at specific locations to be attributed to a particular prescribed burn. AG-CMAQ predicted $PM_{2.5}$ concentrations with less error than CMAQ at most monitoring station locations affected during the incident. The mean fractional error was reduced by 15% on average, indicating significantly better agreement with site measurements.

The results of this study indicate that AG-CMAQ may provide understanding of air quality and atmospheric dynamics beyond that attainable through a static grid model. However, our evaluation indicates that despite the improvement, AG-CMAQ continues to under-predict $PM_{2.5}$ concentrations. It is likely that the error can at least be partially attributed to processes unrelated to grid resolution within the air quality modeling system. Among these, the ability of meteorological models to simulate fine-scale and short-term variability in winds may be of greatest significance.

Adaptive grids are a tool that could prove useful for various applications beyond plume simulation. Grid refinement driven by reactivity may provide insight into atmospheric chemistry. The need for improved fine-scale wind modeling previously mentioned could be addressed by applying an adaptive grid within weather models. Indeed, adaptive mesh modeling is currently being discussed as a tool applicable to climate models to focus on small-scale processes that cannot be resolved in existing models. Some have even suggested that adaptive grid models may provide the only means of resolving these small-scale processes within a single model (Weller et al., 2010). The potential benefits that could be attained through adaptive grid modeling in the field of air pollution photochemical modeling are only briefly explored in this study. However, adaptive grids will likely lead to additional and greater advantages not necessarily restricted to air quality modeling, but encompassing different geophysical models as well.

5.4.2 Coupling of Daysmoke with AG-CMAQ

Significant progress was made in the development of a coupling technique that can inject Daysmoke particles into the CMAQ grid cells without significant loss of accuracy. The technique is based on Fourier analysis. First, the smoke particle concentrations predicted by Daysmoke are represented as spectra of waves with different frequencies. Then, the waves whose frequencies cannot be supported by the CMAQ grid are identified. If the amplitudes of those waves are negligible, then the plume is handed over to CMAQ; otherwise the plume is continued to be followed by Daysmoke. A standalone analysis system was built by borrowing Fast Fourier Transform (FFT) algorithms from MATLAB. Analysis of several Daysmoke plumes showed that the optimal downwind distance for hand over is a function of grid resolution and changes in time as the plumes evolve.

Based on the findings of the Fourier analysis, a coupling algorithm was developed that sets the downwind distance for handover of Daysmoke plume to CMAQ as a function of time. Two conditions must be satisfied for handover: 1) the Daysmoke plume must fully develop and 2) the difference between Daysmoke plume concentrations before handover and CMAQ grid cell concentrations after handover (i.e., the concentration error incurred during handover) must be minimal. The coding of this algorithm was finished and the review and verification of the code has gone through several cycles. The coupled system of the Adaptive Grid CMAQ (AG-CMAQ) with Daysmoke as the sub-grid scale plume model is named Adaptive Grid Daysmoke CMAQ (AGD-CMAQ).

No burn monitored at Fort Benning in 2009 carried smoke in the direction of regional monitors. So far, only the 9 April 2008 burn, under southeasterly winds, may have affected the monitor at Columbus Airport. A slight increase in $PM_{2.5}$ was detected by the monitor few hours after the burn and this is believed to be a consequence of the PB plume. This leaves the historic Atlanta Smoke Incident of 28 February 2007 as the only other PB case for the evaluation of the coupled Daysmoke-CMAQ system. That case is ideal for regional model evaluation as the smoke was fully captured by the dense network of monitors in the metro-Atlanta area. The comparison of the CMAQ and AG-CMAQ results with observations showed improved replication of the plume and decrease in artificial dilution due to adaptive grid refinements of AQ-CMAQ.

The combination of finer grid resolution and sub-grid scale modeling should provide more detailed simulations of the prescribed burn plume transport. In AGD-CMAQ, smoke emissions are first tracked by Daysmoke as parcels then inserted into the grid cells of AG-CMAQ at appropriate times and places using a procedure called "handover". AGD-CMAQ's benefits have been verified in an application to the 28 February 2007 Atlanta Smoke Incident. The results of the simulation with AGD-CMAQ were superior to the results from the initial Daysmoke-CMAQ coupling as well as the AG- CMAQ model. Not only the predicted $PM_{2.5}$ concentrations were in better agreement with observations at downwind regional monitors, some long-range transport characteristics of the plumes were better simulated as well. AGD-CMAQ was also evaluated with the 9 April 2008 burn at Fort Benning but there the benefits were marginal.

The approach used for coupling Daysmoke with AG-CMAQ can be improved in many ways in the future. The interface between Daysmoke and AG-CMAQ can be made dependent on vertical distribution of smoke. Currently, the difference between Daysmoke and AG-CMAQ concentrations are evaluated along horizontal planes only. Also, the grid adaptations can be designed to minimize the error during the handover process. The Fourier analysis technique can be used to determine the right moment to hand over the plume from the sub-grid scale plume model to the air quality model.

5.4.3 Sensitivities to Emissions Parameters

The sensitivity analyses completed in this project demonstrate that successful modeling of PB impacts on air quality with air quality models is dependent on effective spatiotemporal allocation of emissions. Furthermore, the results indicate that shortcomings observed in previously reported simulations cannot be overcome by solely focusing on fire emissions magnitude. The horizontal and vertical distributions of emissions on gridded domains and their timing are key inputs that must also be carefully planned.

Here, analyses exploring the influence of plume rise showed that modeled $PM_{2.5}$ concentrations are mostly sensitive to the fraction of emissions injected into the PBL. The vertical distribution of emissions within the PBL had little effect on downwind concentrations. For the simulations completed, CMAQ-modeled vertical mixing of fire emissions within the PBL was extremely rapid and efficient. While correctly determining plume penetration into the free atmosphere is crucial to model results, only marginal gains in performance should be expected from applying more detailed representations of vertical plume structure.

Sensitivity estimates related to the horizontal allocation of emissions on a gridded domain indicated that model performance could significantly benefit from more accurately positioning emissions. Predicted $PM_{2.5}$ concentrations were sensitive to the horizontal allocation of emissions. Additionally, model results were clearly responsive to whether fire emissions are distributed as point or area sources. Improving the horizontal allocation of fire emissions may be especially important in regard to plume rise approximations. Using downwind ascent approximations but then injecting fire emissions at the initial location of release is clearly an error that may significantly affect model results; the plume should be injected at the right downwind location. The responsiveness of predicted $PM_{2.5}$ concentrations to small variations in the horizontal allocation of fire emissions also reflects a strong influence from meteorological

inputs. Sensitivities may be primarily driven by variability in meteorological fields. If so, it is important to explore the degree to which simulations are constrained by uncertainties in meteorological fields produced by weather forecasting models.

Perhaps the largest potential gains in model accuracy lie in better characterizing the temporal distribution of fire-related emissions. For the smoke episode, simulated sensitivity analysis showed that fire-related $PM_{2.5}$ impacts are primarily attributable to emissions injected within a specific time frame. The analyses also demonstrated that each individual hour's fire emissions produce a response at downwind receptors lasting 2-3 hours. Reducing the uncertainties associated with distributing emissions into discontinuous inputs and better approximating the timing and progression of pollutant releases is a practical approach to improve model performance. Here again ensuring the adequacy of meteorological inputs is essential.

Beyond spatiotemporal allocation of emissions, additional concerns must be considered to successfully simulate the air quality impacts of PBs with comprehensive modeling systems. Fire-related emissions estimates must still be further improved. Realistic estimates of secondary aerosol formation and precursor emissions may also be important. Furthermore, the response of pollutants subject to strong nonlinearities may be different to the dispersion-related response explored in this study. A substantial improvement in the ability of photochemical air quality models to forecast the impacts of PBs would require jointly addressing these research needs.

5.4.4 Sensitivities to Meteorological Parameters

Long-range impacts of PBs were evaluated by simulating the Atlanta Smoke Incident. Predicted peak $PM_{2.5}$ concentrations were about 70 μgm^{-3} lower than the observations. The reasons for this underprediction were investigated through a sensitivity analysis. The model predictions can be raised to the level of observations by increasing the emissions by a factor of 4 to 6. However, based on the evaluation of emission estimates with field measurements, such a level of increase is not acceptable. On the other hand, vertical redistribution of emissions may be justified since the plume height is subject to uncertainties. The sensitivities of $PM_{2.5}$ concentrations to $PM_{2.5}$ emissions injected into different CMAQ layers at different times were calculated. The sensitivity of peak $PM_{2.5}$ concentrations in Atlanta to emissions injected into the PBL was 0.5 μgm^{-3} per ton at 20:00 GMT, the most sensitive time for emissions. Modeled $PM_{2.5}$ peaks would increase if the emissions penetrating into the free troposphere were redistributed into the PBL. However, the maximum increase that can be achieved in this manner is estimated to be less than 5 μgm^{-3}. Allocating a greater fraction of emissions to 20:00 GMT would increase the peak also but its effect would be small for a realistic increment.

WS and WD are the two other parameters that were analyzed for their contribution to $PM_{2.5}$ concentrations. The Atlanta Smoke Incident was dominated by strong and steady southeasterly winds and WD was predicted more accurately than what is typically achievable by meteorological models. However, sensitivity to WD is very large as $\pm 10^{o}$ rotation of the wind field would make the plume totally miss Atlanta. Reducing WD by 5^{o}, in this case making it more easterly, resulted in a 15 μgm^{-3} increase in peak $PM_{2.5}$ concentrations but advanced the time of the peak by 1 hour. WS proved to be the most important parameter for prediction of peak concentrations. Reducing WS by 30% increased the modeled $PM_{2.5}$ peaks by 50 μgm^{-3} in

Atlanta. Also, it delayed the time of the peak by 1 hour. Therefore, combined with −5° adjustment of WD, 30% reduction of WS would make modeled peaks match the magnitude and timing of observed peaks. But, do such adjustments of WS and WD have any basis? When compared to the most proximate sounding at Peachtree City, midway between the burn locations and Atlanta, WRF-predicted WD and WS are respectively 7-12° more southerly and about 30% larger than the observations at the most relevant altitudes; hence, the adjustments are justified.

Estimated sensitivities of modeled $PM_{2.5}$ concentrations to wind field inputs are especially noteworthy. Analyses indicated that small changes or errors in wind direction or speed within the meteorological data used to drive air quality modeling can have major effects on CMAQ-predicted pollutant levels at locations downwind of prescribed fires. Sensitivities indicated that accurate wind fields might be of greater importance than exact fire emissions estimates to successfully model smoke impacts. Additionally, the $PM_{2.5}$ concentration sensitivities to wind speed and direction are high within the uncertainty range typically associated with meteorological inputs. These findings indicate that smoke dispersion simulations with atmospheric chemistry and transport models are significantly constrained by the uncertainty in meteorological fields produced by weather forecasting models. Moreover, as computational capabilities increase and air quality simulations are undertaken at finer resolutions, the sensitivities of predicted pollutant impacts to inaccuracies in weather inputs will hinder modeling results to an even greater degree.

The modeling system developed incorporates new elements for emission, dispersion and transport processes that are critical for accurate prediction of the air quality impacts of PB plumes. These elements were evaluated using field data and their sources of uncertainty were identified. Uncertainties in emission strength and plume injection height are significant but their contributions to the underprediction of long-range $PM_{2.5}$ concentrations are relatively small. Uncertainties in WS and WD remain the limiting factors. With more accurate wind predictions, the system can be a viable tool for dynamic management of PB operations.

5.5 Recommendations for Future Model Evaluation

This section summarizes the lessons learned during this research for the benefit of future model evaluation efforts. It documents the shortfalls of the field data collected and model evaluations performed as part of this project. It also points to field data needs and provides recommendations for improving the design of future field studies.

The analysis of the prescribed burns at Fort Benning and Eglin AFB generally confirmed the strategy used by ground crews in repositioning the mobile sampling units (trucks) to new locations when winds shifted to blow the plume elsewhere. However, the strategy was limited by the availability of a vista point such as a fire tower and communications via cell phone or radio. Conditions such as view angle and signal strength were not always ideal to orchestrate the sampling by mobile units. Also, the trucks were limited in their access to ideal locations by road availability, access restrictions, and safety issues. In the future, a more in depth forecasting component should be added to data collection campaigns. The forecasts should not be limited to meteorology; they should also include plume rise and dispersion. Maps of expected ground concentrations should be generated. Likely uncertainties in forecast WS and WD should be taken

into account when selecting initial positions for the trucks. Also, advance notification of access restrictions should be requested from the base's command center. The initial sampling locations should be determined in view of all this information so that the most useful data for model evaluation can be collected during the burns.

In general, $PM_{2.5}$ concentrations generated by Daysmoke for weak plumes were in agreement with smoke distributions produced by Gaussian smoke models. For weak plumes, maximum smoke concentrations are found immediately downwind from the burn site. However, for stronger plumes, Daysmoke placed maximum concentrations 4 to 10 miles downwind from the burn sites. If this is correct, Daysmoke presents a significant departure from existing concepts and models. To evaluate Daysmoke in such plume cases, data are needed in the 4-10 miles range, where the predictions would be most different from those by Gaussian models. Experimental design should place monitors mostly in this range for moderate to strong plume burns. In fact, when conditions permit, mobile units should be stretched as far downwind as logistical conditions permit. More units may be necessary to cover this range with sufficient resolution.

In several of the monitored burns, the mobile samplers were turned off shortly after firing was complete so that the trucks can be safely escorted out of the bases. This procedure did not always allow sufficient time for smoke to travel downwind from the burn site and past the truck locations. Thus, several of the observed $PM_{2.5}$ records ended with high smoke concentrations still being measured. The data collection should be extended as much as possible after firing is complete to allow for smoke to pass the most distant truck.

Daysmoke represents the burn area as a square equal in size to the actual burn area. When the actual burn area is highly irregular, some discrepancy should be expected when comparing Daysmoke simulated $PM_{2.5}$ concentrations with observed concentrations, especially close in to the burn area. This would also be the case for other smoke dispersion models that operate with the coordinates of a single point for the burn plot. Correcting the problem would require specification of the geometric shape of the burn site in the models. Until then, irregularly shaped burn plots should be avoided in future field campaigns.

Daysmoke discharges smoke uniformly over the square burn area throughout the course of the burn. In reality, ignition may proceed from one side to the opposite side thus giving a progression of the fire and smoke emissions across the landscape. Correcting the problem requires knowledge of how land managers spread fire over the landscape, and knowledge of the distribution of fuel types and fuel loadings. As part of this project, it was shown that Rabbit Rules, a fire spread model under development at USFS, can map fire and emissions over a landscape with heterogeneous distribution of fuels. Rabbit Rules needs to be provided the times and locations of ignitions during the course of the burn. This information was available for the aerial ignition burns at Eglin AFB. Unfortunately, the ignition patterns were not recorded in sufficient detail for the prior hand-lit burns at Fort Benning. This kind of information should be collected regularly in future field campaigns.

Differences between observed wind directions (as determined by observed $PM_{2.5}$ at truck locations) and modeled wind directions (as determined by Daysmoke simulated $PM_{2.5}$ at truck locations) have been found during the analysis of several burns at Fort Benning. These

discrepancies may have been caused by differences between observed and WRF-predicted wind directions and/or failure of Daysmoke to spread the plume properly. To investigate this issue, wind measurements were included in the Eglin study plan. The plan for wind measurements included remote sensing of the vertical wind profile using a Doppler sodar. Unfortunately, the instrument was damaged during shipment to the site; therefore, the wind measurements had to rely on two anemometers: one on a 10 m mast and another mounted on the aerostat flying at 100 to 250 m altitude. The Doppler sodar, if it could be operated, would have provided wind speed and direction from 100 to 500 m altitude with 10 m resolution. If such data becomes available in future campaigns, WRF- or other model-predicted winds can be better evaluated. Also, it might be possible to run Daysmoke purely with measured winds, instead of modeled winds adjusted by measurements as was the case in this project, and evaluate the accuracy of Daysmoke's plume spread more directly.

5.6 Final Remarks

The CA fire model Rabbit Rules results made it apparent that the fire itself can have a significant impact on local wind speeds and directions over the burn plot. Additionally, a thick smoke plume loaded with particulate matter can alter the radiative balance of the boundary layer. Finally, pyrocumulus formed by prescribed fires can further complicate the interaction between particulate matter levels and local meteorology. Recall that one of the findings of this research was that the ability to accurately predict PB impacts largely depends on the accuracy of the meteorological wind fields derived from WRF. Therefore, it may be critical to account for the fire, plume, and cloud induced micrometeorological effects in predicting the winds that will disperse and transport the smoke plume. Currently, there is no mechanism in the current modeling system to account for the feedbacks on meteorology of fire, smoke (direct effects) or their consequences such as pyrocumulus formation (indirect effects). There may be significant benefits in trying to couple the models in such a way that the meteorology provided by WRF knows about the prescribed burn and is sensitive to the direct or indirect effects of the burn. Such a modeling system was described in Section 4.2.3.4, Coupling Ideas for the Future.

The relevance of this research to land and air quality managers is in the information the impact prediction system can produce related to the contribution of prescribed burns to regional air quality problems. To meet the air quality standards a balance has to be found among all of the sources of pollution including industry, transportation, mining, agriculture, forestry and others. From that perspective, the improved fire emission estimates and improved modeling techniques that can discern different emission sources are the most important products of this research. They will improve the ability of regulators to make decisions based on more accurate predictions and eventually lead to more effective local and regional air quality management.

The modeling system developed here can also be used in assessing the air quality impacts of alternative burning options. During this project, a survey was conducted to identify the most relevant burning scenarios for which land managers would be interested in finding out the potential impacts. Changing the frequency of the burn, season of the burn, size of the burn, ignition type, and time of the burn were among the scenarios of most interest. The local smoke impacts of these scenarios were already investigated through simulations with the impact prediction system (Section 4.5). Ongoing work will determine the regional air quality impacts of

these alternative burning scenarios. Follow on research can focus on other questions for achieving the ecological benefits of prescribed burning while also mitigating the air quality impacts. For example, if land managers have options to regenerate forest understory, what species might they choose that have lower air quality impacts when burned?

Prescribed burning is a necessary activity in the Southeastern U.S. but the resulting emissions can contribute to violation of air quality standards. In a dynamic management environment, decisions have to be made to moderate the potential impacts on air quality from PB, and to obviate the air quality constraints that limit PB. Knowing the uncertainties in emissions and how these uncertainties will impact smoke predictions is critical for effective decision making. Presumptively, predictions with known uncertainties should lead to fewer violations of air quality standards and subsequent benefits to human health and welfare, and allow more acreage to be treated by fire and more frequently, thereby improving ecosystem health and wildlife habitat, and decrease the risk of wildfires.

6 Literature Cited

Achtemeier, G.L., 1998. Predicting dispersion and deposition of ash from burning cane. Sugar Cane, 1998(1): 17-22.

Achtemeier, G.L., 2005a. On plume rise - matching Daysmoke with Briggs Equations for industrial stacks, Sixth Symposium on Fire and Forest Meteorology. American Meteorological Society, Boston, MA, Canmore, CA, pp. J3.4.

Achtemeier, G.L., 2005b. Planned Burn-Piedmont. A local operational numerical meteorological model for tracking smoke on the ground at night: model development and sensitivity tests. International Journal of Wildland Fire, 14(1): 85-98.

Achtemeier, G.L., 2012. Field validation of a free-agent cellular automata model of fire spread with fire-atmosphere coupling. . International Journal of Wildland Fire, in press.

Achtemeier, G.L. and Adkins, C.W., 1997. Ash and smoke plumes produced from burning sugar cane. Sugar Cane, 1997(2): 16-21.

Achtemeier, G.L. et al., 2011. Modeling Smoke Plume-Rise and Dispersion from Southern United States Prescribed Burns with Daysmoke. Atmosphere, 2(3): 358-388.

Alessio, G.A., De Lillis, M., Fanelli, M., Pinelli, P. and Loreto, F., 2004. Direct and indirect impacts of fire on isoprenoid emissions from Mediterranean vegetation. Functional Ecology, 18(3): 357-364.

Anderson, G.K., Sandberg, D.V. and Norheim, R.A., 2004. Fire Emission Production Simulator (FEPS) User's Guide, USDA Forest Service, Pacific Northwest Research Station, Corvallis, OR.

Andrews, P.L., 2008. BehavePlus Fire Modeling System Version 4.0: Variables, USDA: Forest Service, Rocky Mountain Research Station: .

Andrews, P.L., Bevins, C.D. and Seli, R.C., 2005. BehavePlus Fire Modeling System, Version 3.0: User's Guide.

Arakawa, A., 2004. The cumulus parameterization problem: Past, present, and future. Journal of Climate, 17(13): 2493-2525.

Aurell, J., Gullett, B., Pressley, C., Tabor, D. and Gribble, R., 2011. Aerostat-lofted instrument and sampling method forr determination of emissions from open area sourrces. Chemosphere, 85: 806-811.

Battye, B.W. and Battye, R., 2002. Development of emissions inventory methods for wildland fire (final report). , U.S. Environmental Protection Agency, Research Triangle Park, NC.

Baumann, K., 2005. Study of air quality impacts resulting from prescribed burning - Focus on sub-regional $PM_{2.5}$ and source apportionment, Georgia Institute of Technology, Atlanta, GA.

Burling, I.R. et al., 2010. Laboratory measurements of trace gas emissions from biomass burning of fuel types from the southeastern and southwestern United States. Atmospheric Chemistry and Physics, 10(22): 11115-11130.

Byram, G.M., 1959. Combustion of forest fuels. In: K.P. Davis (Editor), Forest Fire Control and Use McGraw Hill, New York, NY, pp. 155-182.

Byun, D. and Schere, K.L., 2006. Review of the governing equations, computational algorithms, and other components of the models-3 Community Multiscale Air Quality (CMAQ) modeling system. Applied Mechanics Reviews, 59(1-6): 51-77.

Byun, D.W. and Ching, J., 1999. Science algorithms of the EPA Model-3 community multiscale air quality (CMAQ) modeling system., EPA/600/R-99/030. National Exposure Research Laboratory, Research Triangle Park, NC.

Cheng, L., McDonald, K.M., Angle, R.P. and Sandhu, H.S., 1998. Forest fire enhanced photochemical air pollution. A case study. Atmospheric Environment, 32(4): 673-681.

Clarke, K.C., Brass, J.A. and Riggan, P.J., 1994. A CELLULAR-AUTOMATON MODEL OF WILDFIRE PROPAGATION AND EXTINCTION. Photogrammetric Engineering and Remote Sensing, 60(11): 1355-1367.

Clements, C.B. et al., 2007. Observing the dynamics of wildland grass fires - FireFlux - A field validation experiment. Bulletin of the American Meteorological Society, 88(9): 1369-+.

Cohan, D.S., Hakami, A., Hu, Y.T. and Russell, A.G., 2005. Nonlinear response of ozone to emissions: Source apportionment and sensitivity analysis. Environmental Science & Technology, 39(17): 6739-6748.

Collela, P. and Woodward, P.R., 1984. The piecewise parabolic method (PPM) for gas-dynamical simulations. J. Comput. Phys., 54: 174-201.

EarthTech, 2000. A user's guide for the CALPUFF dispersion model version 5, Earth Tech, Inc., Concord, MA.

EPA, U.S., 1996. Section 13.1: Wildfires and Prescribed Burning AP 42.

EPA, U.S., 2011. Method 3A-Determination of oxygen and carbon dioxide concentrations in emissions from stationary sources (instrumental analyzer procedure).

Flakes, G.W., 2000. The Computational Beauty of Nature: Computer Explorations of Fractals, Chaos, Complex Systems, and Adaptation. MIT Press, 514 pp.

Garcia-Menendez, F., Yano, A., Hu, Y. and Odman, M.T., 2010. An adaptive grid version of CMAQ for improving the resolution of plumes. Atmospheric Pollution Research, 1(4): 239-249.

Gellert, W., Gottwald, S., Hellwich, M., Kästner, H. and Küstner, H., 1989. The VNR Concise Encyclopedia of Mathematics. Van Nostrand Reinhold; New York.

Gillani, N.V. and Godowitch, J.M., 1999. Plume-in-grid treatment of major point source emissions. In: D.W. Byun and J. Ching (Editors), Science algorithms of the EPA Model-3 community multiscale air quality (CMAQ) modeling system. National Exposure Research Laboratory, Research Triangle Park, NC.

Gillani, N.V. and Pleim, J.E., 1996. Sub-grid-scale features of anthropogenic emissions of NOx and VOC in the context of regional Eulerian models. Atmospheric Environment, 30(12): 2043-2059.

Grell, G.A., Dudhia, J. and Stauffer, D.R., 1994. A description of the fifth-generation Penn State/NCAR mesoscale model (MM5), National Center for Atmospheric Research.

Grell, G.A. et al., 2005. Fully coupled "online" chemistry within the WRF model. Atmospheric Environment, 39(37): 6957-6975.

Hakami, A., Odman, M.T. and Russell, A.G., 2004. Nonlinearity in atmospheric response: A direct sensitivity analysis approach. Journal of Geophysical Research-Atmospheres, 109(D15).

Hao, W.M. et al., 2002. Emissions of trace gases and aerosol particles from biomass fires in the southeastern and central United States, USDA Forest Service.

Hargrove, W.W., Gardner, R.H., Turner, M.G., Romme, W.H. and Despain, D.G., 2000. Simulating fire patterns in heterogeneous landscapes. Ecological Modelling, 135(2-3): 243-263.

Hodzic, A. et al., 2007. Wildfire particulate matter in Europe during summer 2003: meso-scale modeling of smoke emissions, transport and radiative effects. Atmospheric Chemistry and Physics, 7(15): 4043-4064.

Hu, Y.T. et al., 2008a. Simulation of air quality impacts from prescribed fires on an urban area. Environmental Science & Technology, 42(10): 3676-3682.

Hu, Y.T. et al., 2008b. Simulation of air quality impacts from prescribed fires on an urban area. Environmental Science & Technology, 42(10): 3676-3682.

Hwang, D., Byun, D.W. and Talat Odman, M., 1997. An automatic differentiation technique for sensitivity analysis of numerical advection schemes in air quality models. Atmospheric Environment, 31(6): 879-888.

Jenkins, M.A., Clark, T. and Coen, J., 2001. Coupling atmospheric and fire models. In: E.A. Johnson and K. Miyanishi (Editors), Forest Fires: Behavior and Ecological Effects. Academic Press, San Diego, CA, pp. 258-301.

Karamchandani, P. et al., 2000. Development and evaluation of a state-of-the-science reactive plume model. Environmental Science & Technology, 34(5): 870-880.

Karamchandani, P., Seigneur, C., Vijayaraghavan, K. and Wu, S.Y., 2002. Development and application of a state-of-the-science plume-in-grid model. Journal of Geophysical Research-Atmospheres, 107(D19).

Khan, M.N., Odman, M.T. and Karimi, H.A., 2005. Evaluation of algorithms developed for adaptive grid air quality modeling using surface elevation data. Computers, Environment and Urban Systems, 29(6): 718-734.

Koo, B., Wilson, G.M., Morris, R.E., Dunker, A.M. and Yarwood, G., 2009. Comparison of Source Apportionment and Sensitivity Analysis in a Particulate Matter Air Quality Model. Environmental Science & Technology, 43(17): 6669-6675.

Kumar, N. and Russell, A.G., 1996. Development of a computationally efficient, reactive subgrid-scale plume model and the impact in the northeastern United States using increasing levels of chemical detail. Journal of Geophysical Research-Atmospheres, 101(D11): 16737-16744.

Liu, Y., Achtemeier, G.L., Goodrick, S.L. and Jackson, W.A., 2010. Important parameters for smoke plume rise simulation with Daysmoke. Atmospheric Pollution Research, 1: 250-259.

Liu, Y.Q., 2004. Variability of wildland fire emissions across the contiguous United States. Atmospheric Environment, 38(21): 3489-3499.

Liu, Y.Q., Achtemeier, G. and Goodrick, S., 2008. Sensitivity of air quality simulation to smoke plume rise. Journal of Applied Remote Sensing, 2: 12.

Liu, Y.Q. et al., 2009. Smoke incursions into urban areas: simulation of a Georgia prescribed burn. International Journal of Wildland Fire, 18(3): 336-348.

Mathur, R. et al., 2011. Overview of the Two-way Coupled WRF-CMAQ Modeling System, 10th Annual CMAS Conference, Chapel Hill, NC.

Mercer, G.N. and Weber, R.O., 2001. Fire Plumes. In: E.A. Johnson and K. Miyanishi (Editors), Forest Fires: Behavioral and Ecological Effects. Academic Press, New York, NY.

Morris, R.E. et al., 2005. Preliminary evaluation of the community multiscale air, quality model for 2002 over the southeastern United States. Journal of the Air & Waste Management Association, 55(11): 1694-1708.

Napelenok, S.L., Cohan, D.S., Hu, Y.T. and Russell, A.G., 2006. Decoupled direct 3D sensitivity analysis for particulate matter (DDM-3D/PM). Atmospheric Environment, 40(32): 6112-6121.

Odman, M.T. and Hu, Y., 2010. A variable time-step algorithm for air quality models. Atmospheric Pollution Research, 1(4): 229-238.

Odman, M.T. and Hu, Y.T., 2007. A variable time-step algorithm for air quality models. Air Pollution Modeling and Its Applications XVII, 17, 411-420 pp.

Odman, M.T. et al., 2010. Predicting the Regional Air Quality Impacts of Prescribed Burns. In: D.G. Steyn and S.T. Rao (Editors), Air Pollution Modeling and Its Application Xx. NATO Science for Peace and Security Series B-Physics and Biophysics, pp. 189-193.

Odman, M.T. and Russell, A.G., 2000. Mass conservative coupling of non-hydrostatic meteorological models with air quality models. Air Pollution Modeling and Its Application Xiii, 13, 651-660 pp.

Ottmar, R.D. and Vihnanek, R.E., 2009. Fuel loading and fuel consumption for the RxCADRE fires, 4th International Fire Ecology Management Congress. Association for Fire Ecology, Savannah, GA.

Ottmar, R.D., Vihnanek, R.E. and Mathey, J.W., 2000. Longleaf pine, pocosin and marshgrass types in the southeast United States, National Wildfire Coordinating Group.

Ottmar, R.D., Vihnanek, R.E. and Mathey, J.W., 2003. Sand hill, sand pine scrub and hardwoods with white pine types in the southeast United States, National Wildfire Coordinating Group.

Prichard, S.J., Ottmar, R.D. and Anderson, G.K., 2005. Consume 3.0 User's Guide, United States Department of Agriculture Forest Service, Pacific Northwest Research Station, Seattle, WA

Roy, B. et al., 2007. Refining fire emissions for air quality modeling with remotely sensed fire counts: A wildfire case study. Atmospheric Environment, 41(3): 655-665.

Scholl, E.R. and Waldrop, T.A., 1999. Photos for estimating fuel loadings before and after prescribed burning in the upper coastal plain of the southeast, United States Dept. Agriculture, Forest Service, Southern Research Station.

Skamarock, W.C. et al., 2005. A description of the advanced research WRF Version 2.

Srivastava, R.K., McRae, D.S. and Odman, M.T., 2000. An adaptive grid algorithm for air-quality modeling. Journal of Computational Physics, 165(2): 437-472.

Stein, A.F., Rolph, G.D., Draxler, R.R., Stunder, B. and Ruminski, M., 2009. Verification of the NOAA Smoke Forecasting System: Model Sensitivity to the Injection Height. Weather and Forecasting, 24(2): 379-394.

Stewart, D.A. and Liu, M.K., 1981. DEVELOPMENT AND APPLICATION OF A REACTIVE PLUME MODEL. Atmospheric Environment, 15(10-1): 2377-2393.

Tsai, P.S., Frasier, S.J., Goodrick, S., Achtemeier, G.L. and Odman, M.T., 2009. Combined Lidar and Radar Observations of Smoke Plumes from Prescribed Burns, Fourth Symposium on Lidar Atmospheric Applications, 89th American Meteorological Society Annual Meeting. , Phoenix, AZ.

Unal, A. and Odman, M.T., 2003. Adaptive grid modeling for predicting the air quality impacts of biomass burning, 5th American Meteorological Society Symposium on Fire and Forest Meteorology, Orlando, Florida.

Urbanski, S.P., Hao, W.M. and Baker, S., 2009. Chemical Composition of Wildland Fire Emissions. In: A. Bytnerowicz, M. Arbaugh, A. Riebau and C. Andersen (Editors), Developments in Environmental Science. Elsevier, pp. 79-107.

US-EPA, 1996. Section 13.1: Wildfires and Prescribed Burning AP 42.

Vijayaraghavan, K., Karamchandani, P. and Seigneur, C., 2006. Plume-in-grid modeling of summer air pollution in Central California. Atmospheric Environment, 40(26): 5097-5109.

Weller, H., Ringler, T., Piggott, M. and Wood, N., 2010. CHALLENGES FACING ADAPTIVE MESH MODELING OF THE ATMOSPHERE AND OCEAN. Bulletin of the American Meteorological Society, 91(1): 105-+.

WRAP, 2002. 1996 Fire Emission Inventory, Western Regional Air Partnership.

Xiao, X., McRae, D.S., Hassan, H.A., Ruggiero, F.H. and Jumper, G.Y., 2006. Modeling Atmospheric Optical Turbulence, 44th AIAA Sciences Meeting and Exhibit Reno, Nevada.

Yang, E.S., Christopher, S.A., Kondragunta, S. and Zhang, X.Y., 2011. Use of hourly Geostationary Operational Environmental Satellite (GOES) fire emissions in a Community Multiscale Air Quality (CMAQ) model for improving surface particulate matter predictions. Journal of Geophysical Research-Atmospheres, 116: 13.

7 Appendix A: Supporting Data

Supporting data is provided as an archive named “RC-1647-SD”. The archive was compressed and submitted as a supplement to this report in a single file named “RC-1647-SD.zip”. The size of the “zipped” file is 113 Megabytes. When uncompressed it expands to 144 Megabytes. The archive consists of 5 folders whose contents are described in Table A-1. A complete list of the 460 files and 143 folders and subfolders in the archive including their creation dates and sizes follows Table A-1.

Table A-1. Description of Supporting Data Archive RC-1647-SD

Folder	Contents
2007-Atlanta-Data	Emissions and meteorology data related to the February 28, 2007 Atlanta Smoke Incident
2008-Fort_Benning-Data	Emissions, meteorology and smoke data related to 3 burns monitored at Fort Benning in 2008
2009-Fort_Benning-Data	Emissions, meteorology and smoke data related to 8 burns monitored at Fort Benning in 2009
2011-Eglin-Data	Fuels, emissions, meteorology and smoke related to 3 burns monitored at Eglin AFB in 2011
Analyses	Meteorological analyses of Eglin burns and plume analyses of Fort Benning burns

```
Directory of \RC-1647-SD

07/05/2012  06:33 PM    <DIR>          .
07/05/2012  06:33 PM    <DIR>          ..
07/05/2012  07:08 PM    <DIR>          2007-Atlanta-Data
07/05/2012  07:23 PM    <DIR>          2008-Fort_Benning-Data
07/05/2012  07:35 PM    <DIR>          2009-Fort_Benning-Data
07/05/2012  07:35 PM    <DIR>          2011-Eglin-Data
07/05/2012  06:33 PM    <DIR>          Analyses
               0 File(s)              0 bytes

 Directory of \RC-1647-SD\2007-Atlanta-Data

07/05/2012  07:08 PM    <DIR>          .
07/05/2012  07:08 PM    <DIR>          ..
07/05/2012  06:32 PM    <DIR>          Emissions (by Bill Jackson of USFS)
07/05/2012  06:32 PM    <DIR>          Soundings
               0 File(s)              0 bytes

 Directory of \RC-1647-SD\2007-Atlanta-Data\Emissions (by Bill Jackson of
USFS)
```

```
07/05/2012  06:32 PM    <DIR>          .
07/05/2012  06:32 PM    <DIR>          ..
07/05/2012  06:32 PM            46,592
Oconee_hourly_bouyancy_022807_new.xls
07/05/2012  06:32 PM            38,912
Oconee_hourly_emission_022807_new.xls
07/05/2012  06:32 PM            46,080
Piedmont_hourly_bouyancy_022807_new.xls
07/05/2012  06:32 PM            38,400
Piedmont_hourly_emission_022807_new.xls
               4 File(s)        169,984 bytes

 Directory of \RC-1647-SD\2007-Atlanta-Data\Soundings

07/05/2012  06:32 PM    <DIR>          .
07/05/2012  06:32 PM    <DIR>          ..
07/05/2012  06:32 PM            15,362
daysmoke_02282007_Oconee_13layers_rotated.txt
07/05/2012  06:32 PM            39,890
daysmoke_02282007_Oconee_34layers_rotated.txt
07/05/2012  06:32 PM            93,618
daysmoke_02282007_Oconee_80layers_rotated.txt
07/05/2012  06:32 PM            13,444
daysmoke_02282007_Piedmont_13layers_rotated.txt
07/05/2012  06:32 PM            34,906
daysmoke_02282007_Piedmont_34layers_rotated.txt
07/05/2012  06:32 PM            81,918
daysmoke_02282007_Piedmont_80layers_rotated.txt
07/05/2012  06:32 PM    <DIR>          Peachtree City
               6 File(s)        279,138 bytes

 Directory of \RC-1647-SD\2007-Atlanta-Data\Soundings\Peachtree City

07/05/2012  06:32 PM    <DIR>          .
07/05/2012  06:32 PM    <DIR>          ..
07/05/2012  06:32 PM            80,961
daysmoke_02282007_PeachtreeCity_34layers.txt.rotated
07/05/2012  06:32 PM            34,359 Peachtree City-Observed.xlsx
07/05/2012  06:32 PM            95,909 Peachtree_City_Predicted.xlsx
               3 File(s)        211,229 bytes

 Directory of \RC-1647-SD\2008-Fort_Benning-Data

07/05/2012  07:23 PM    <DIR>          .
07/05/2012  07:23 PM    <DIR>          ..
07/05/2012  07:23 PM             6,349 burn-info.pdf
07/05/2012  06:32 PM    <DIR>          Emissions-2008
07/05/2012  06:32 PM    <DIR>          MM5 Surface Winds
07/05/2012  06:32 PM    <DIR>          Soundings
07/05/2012  06:32 PM    <DIR>          UGA Measurements-2008
07/05/2012  06:32 PM    <DIR>          Weather
               1 File(s)          6,349 bytes
```

```
 Directory of \RC-1647-SD\2008-Fort_Benning-Data\Emissions-2008

07/05/2012  06:32 PM    <DIR>          .
07/05/2012  06:32 PM    <DIR>          ..
07/05/2012  06:32 PM               493 20080409_C2H2.data
07/05/2012  06:32 PM               493 20080409_C2H4.data
07/05/2012  06:32 PM               493 20080409_C2H6.data
07/05/2012  06:32 PM               493 20080409_C3H4.data
07/05/2012  06:32 PM               493 20080409_C3H6.data
07/05/2012  06:32 PM               493 20080409_C3H8.data
07/05/2012  06:32 PM               495 20080409_CH4.data
07/05/2012  06:32 PM               499 20080409_CO.data
07/05/2012  06:32 PM               504 20080409_CO2.data
07/05/2012  06:32 PM               495 20080409_NMHC.data
07/05/2012  06:32 PM               495 20080409_NOx.data
07/05/2012  06:32 PM               495 20080409_PM2.5.data
07/05/2012  06:32 PM            15,872 20080409_PM2.5.xls
07/05/2012  06:32 PM               493 20080409_SO2.data
07/05/2012  06:32 PM             1,426 20080414_C2H2.data
07/05/2012  06:32 PM             1,426 20080414_C2H4.data
07/05/2012  06:32 PM             1,426 20080414_C2H6.data
07/05/2012  06:32 PM             1,426 20080414_C3H4.data
07/05/2012  06:32 PM             1,426 20080414_C3H6.data
07/05/2012  06:32 PM             1,426 20080414_C3H8.data
07/05/2012  06:32 PM             1,426 20080414_CH4.data
07/05/2012  06:32 PM             1,443 20080414_CO.data
07/05/2012  06:32 PM             1,456 20080414_CO2.data
07/05/2012  06:32 PM             1,426 20080414_NMHC.data
07/05/2012  06:32 PM             1,426 20080414_NOx.data
07/05/2012  06:32 PM             1,432 20080414_PM2.5.data
07/05/2012  06:32 PM             1,426 20080414_SO2.data
07/05/2012  06:32 PM               713 20080415_C2H2.data
07/05/2012  06:32 PM               713 20080415_C2H4.data
07/05/2012  06:32 PM               713 20080415_C2H6.data
07/05/2012  06:32 PM               713 20080415_C3H4.data
07/05/2012  06:32 PM               713 20080415_C3H6.data
07/05/2012  06:32 PM               713 20080415_C3H8.data
07/05/2012  06:32 PM               713 20080415_CH4.data
07/05/2012  06:32 PM               721 20080415_CO.data
07/05/2012  06:32 PM               727 20080415_CO2.data
07/05/2012  06:32 PM               713 20080415_NMHC.data
07/05/2012  06:32 PM               713 20080415_NOx.data
07/05/2012  06:32 PM               716 20080415_PM2.5.data
07/05/2012  06:32 PM               713 20080415_SO2.data
              40 File(s)         50,191 bytes

 Directory of \RC-1647-SD\2008-Fort_Benning-Data\MM5 Surface Winds

07/05/2012  06:32 PM    <DIR>          .
07/05/2012  06:32 PM    <DIR>          ..
07/05/2012  06:32 PM         4,254,462 wind_fields_08apr09_F-5.gif
07/05/2012  06:32 PM         4,478,100 wind_fields_08apr14-N-1.gif
07/05/2012  06:32 PM         5,203,231 wind_fields_08apr15_BB-3.gif
               3 File(s)     13,935,793 bytes
```

```
 Directory of \RC-1647-SD\2008-Fort_Benning-Data\Soundings

07/05/2012  06:32 PM    <DIR>          .
07/05/2012  06:32 PM    <DIR>          ..
07/05/2012  06:32 PM            62,319 daysmoke_08apr09_F-5_rotated.txt
07/05/2012  06:32 PM            77,271 daysmoke_08apr09_F-
5_rotated_10GMT.txt
07/05/2012  06:32 PM            62,319 daysmoke_08apr14_N-1_rotated.txt
07/05/2012  06:32 PM            62,319 daysmoke_08apr15_BB-3_rotated.txt
               4 File(s)        264,228 bytes

 Directory of \RC-1647-SD\2008-Fort_Benning-Data\UGA Measurements-2008

07/05/2012  06:32 PM    <DIR>          .
07/05/2012  06:32 PM    <DIR>          ..
07/05/2012  06:32 PM    <DIR>          CO data
07/05/2012  06:32 PM            28,672 Ft. Benning Data Log Sheet.xls
07/05/2012  06:32 PM    <DIR>          PM 2.5 Data
               1 File(s)         28,672 bytes

 Directory of \RC-1647-SD\2008-Fort_Benning-Data\UGA Measurements-2008\CO
data

07/05/2012  06:32 PM    <DIR>          .
07/05/2012  06:32 PM    <DIR>          ..
07/05/2012  06:32 PM           257,024 Ft Benning CO 04-09-2008.xls
07/05/2012  06:32 PM           446,464 Ft Benning CO 04-14-2008.xls
07/05/2012  06:32 PM           168,448 Ft Benning CO 04-15-2008.xls
               3 File(s)        871,936 bytes

 Directory of \RC-1647-SD\2008-Fort_Benning-Data\UGA Measurements-2008\PM
2.5 Data

07/05/2012  06:32 PM    <DIR>          .
07/05/2012  06:32 PM    <DIR>          ..
07/05/2012  06:32 PM           217,600 Ft Benning PM 2.5 04-09-2008.xls
07/05/2012  06:32 PM           239,616 Ft Benning PM 2.5 04-14-2008.xls
07/05/2012  06:32 PM           186,880 Ft Benning PM 2.5 04-15-2008.xls
               3 File(s)        644,096 bytes

 Directory of \RC-1647-SD\2008-Fort_Benning-Data\Weather

07/05/2012  06:32 PM    <DIR>          .
07/05/2012  06:32 PM    <DIR>          ..
07/05/2012  06:32 PM            47,628 FBGG1_Apr_09_2008.pdf
07/05/2012  06:32 PM            47,785 FBGG1_Apr_14_2008.pdf
07/05/2012  06:32 PM            47,559 FBGG1_Apr_15_2008.pdf
07/05/2012  06:32 PM            18,146 FBGG1_Site_Info.pdf
               4 File(s)        161,118 bytes

 Directory of \RC-1647-SD\2009-Fort_Benning-Data

07/05/2012  07:35 PM    <DIR>          .
```

```
07/05/2012  07:35 PM    <DIR>          ..
07/05/2012  06:32 PM            29,696 Centroids of Burn Units.xls
07/05/2012  07:35 PM            12,499 Days_of_burns_in_2009.pdf
07/05/2012  06:33 PM    <DIR>          Emissions
07/05/2012  06:33 PM    <DIR>          MM5 Surface Winds
07/05/2012  06:33 PM    <DIR>          Pictures
07/05/2012  06:33 PM    <DIR>          Soundings
07/05/2012  06:32 PM             6,144 Thumbs.db
07/05/2012  06:33 PM    <DIR>          training_area_rx_burn_template_fy09
07/05/2012  07:33 PM    <DIR>          Truck Locations
07/05/2012  06:32 PM           520,396 truck_side_view.JPG
07/05/2012  07:34 PM    <DIR>          UGA Measurements
07/05/2012  06:33 PM    <DIR>          Weather
               4 File(s)        568,735 bytes

 Directory of \RC-1647-SD\2009-Fort_Benning-Data\Emissions

07/05/2012  06:33 PM    <DIR>          .
07/05/2012  06:33 PM    <DIR>          ..
07/05/2012  06:33 PM    <DIR>          April Emissions
07/05/2012  07:43 PM    <DIR>          January Emissions
               0 File(s)              0 bytes

 Directory of \RC-1647-SD\2009-Fort_Benning-Data\Emissions\April Emissions

07/05/2012  06:33 PM    <DIR>          .
07/05/2012  06:33 PM    <DIR>          ..
07/05/2012  06:32 PM             1,426 20090408_C2H2.data
07/05/2012  06:32 PM             1,426 20090408_C2H4.data
07/05/2012  06:32 PM             1,426 20090408_C2H6.data
07/05/2012  06:32 PM             1,426 20090408_C3H4.data
07/05/2012  06:32 PM             1,426 20090408_C3H6.data
07/05/2012  06:32 PM             1,426 20090408_C3H8.data
07/05/2012  06:32 PM             1,426 20090408_CH4.data
07/05/2012  06:32 PM             1,442 20090408_CO.data
07/05/2012  06:32 PM             1,454 20090408_CO2.data
07/05/2012  06:32 PM             1,426 20090408_NMHC.data
07/05/2012  06:32 PM             1,426 20090408_NOx.data
07/05/2012  06:32 PM             1,432 20090408_PM2.5.data
07/05/2012  06:32 PM             1,426 20090408_SO2.data
07/05/2012  06:32 PM               713 20090409_C2H2.data
07/05/2012  06:33 PM               713 20090409_C2H4.data
07/05/2012  06:33 PM               713 20090409_C2H6.data
07/05/2012  06:33 PM               713 20090409_C3H4.data
07/05/2012  06:33 PM               713 20090409_C3H6.data
07/05/2012  06:33 PM               713 20090409_C3H8.data
07/05/2012  06:33 PM               716 20090409_CH4.data
07/05/2012  06:33 PM               721 20090409_CO.data
07/05/2012  06:33 PM               728 20090409_CO2.data
07/05/2012  06:33 PM               716 20090409_NMHC.data
07/05/2012  06:33 PM               716 20090409_NOx.data
07/05/2012  06:33 PM               716 20090409_PM2.5.data
07/05/2012  06:33 PM               713 20090409_SO2.data
              26 File(s)         27,892 bytes
```

```
 Directory of \RC-1647-SD\2009-Fort_Benning-Data\Emissions\January
Emissions

07/05/2012  07:43 PM    <DIR>          .
07/05/2012  07:43 PM    <DIR>          ..
07/05/2012  06:33 PM               713 20090113_C2H2.data
07/05/2012  06:33 PM               713 20090113_C2H4.data
07/05/2012  06:33 PM               713 20090113_C2H6.data
07/05/2012  06:33 PM               713 20090113_C3H4.data
07/05/2012  06:33 PM               713 20090113_C3H6.data
07/05/2012  06:33 PM               713 20090113_C3H8.data
07/05/2012  06:33 PM               716 20090113_CH4.data
07/05/2012  06:33 PM               721 20090113_CO.data
07/05/2012  06:33 PM               728 20090113_CO2.data
07/05/2012  06:33 PM               716 20090113_NMHC.data
07/05/2012  06:33 PM               716 20090113_NOx.data
07/05/2012  06:33 PM               716 20090113_PM2.5.data
07/05/2012  06:33 PM               713 20090113_SO2.data
07/05/2012  06:33 PM             2,852 20090114_C2H2.data
07/05/2012  06:33 PM             2,852 20090114_C2H4.data
07/05/2012  06:33 PM             2,852 20090114_C2H6.data
07/05/2012  06:33 PM             2,852 20090114_C3H4.data
07/05/2012  06:33 PM             2,852 20090114_C3H6.data
07/05/2012  06:33 PM             2,852 20090114_C3H8.data
07/05/2012  06:33 PM             2,855 20090114_CH4.data
07/05/2012  06:33 PM             2,884 20090114_CO.data
07/05/2012  06:33 PM             2,908 20090114_CO2.data
07/05/2012  06:33 PM             2,855 20090114_NMHC.data
07/05/2012  06:33 PM             2,852 20090114_NOx.data
07/05/2012  06:33 PM             2,864 20090114_PM2.5.data
07/05/2012  06:33 PM             2,852 20090114_SO2.data
07/05/2012  06:33 PM             1,426 20090115_C2H2.data
07/05/2012  06:33 PM             1,426 20090115_C2H4.data
07/05/2012  06:33 PM             1,426 20090115_C2H6.data
07/05/2012  06:33 PM             1,426 20090115_C3H4.data
07/05/2012  06:33 PM             1,426 20090115_C3H6.data
07/05/2012  06:33 PM             1,426 20090115_C3H8.data
07/05/2012  06:33 PM             1,432 20090115_CH4.data
07/05/2012  06:33 PM             1,442 20090115_CO.data
07/05/2012  06:33 PM             1,455 20090115_CO2.data
07/05/2012  06:33 PM             1,432 20090115_NMHC.data
07/05/2012  06:33 PM             1,427 20090115_NOx.data
07/05/2012  06:33 PM             1,432 20090115_PM2.5.data
07/05/2012  06:33 PM             1,426 20090115_SO2.data
07/05/2012  06:33 PM               493 20090120_C2H2.data
07/05/2012  06:33 PM               495 20090120_C2H4.data
07/05/2012  06:33 PM               493 20090120_C2H6.data
07/05/2012  06:33 PM               493 20090120_C3H4.data
07/05/2012  06:33 PM               493 20090120_C3H6.data
07/05/2012  06:33 PM               493 20090120_C3H8.data
07/05/2012  06:33 PM               495 20090120_CH4.data
07/05/2012  06:33 PM               499 20090120_CO.data
07/05/2012  06:33 PM               506 20090120_CO2.data
```

```
07/05/2012  06:33 PM               495 20090120_NMHC.data
07/05/2012  06:33 PM               495 20090120_NOx.data
07/05/2012  06:33 PM               495 20090120_PM2.5.data
07/05/2012  06:33 PM               493 20090120_SO2.data
07/05/2012  06:33 PM               713 20090121_C2H2.data
07/05/2012  06:33 PM               713 20090121_C2H4.data
07/05/2012  06:33 PM               713 20090121_C2H6.data
07/05/2012  06:33 PM               713 20090121_C3H4.data
07/05/2012  06:33 PM               713 20090121_C3H6.data
07/05/2012  06:33 PM               713 20090121_C3H8.data
07/05/2012  06:33 PM               716 20090121_CH4.data
07/05/2012  06:33 PM               721 20090121_CO.data
07/05/2012  06:33 PM               731 20090121_CO2.data
07/05/2012  06:33 PM               716 20090121_NMHC.data
07/05/2012  06:33 PM               716 20090121_NOx.data
07/05/2012  06:33 PM               716 20090121_PM2.5.data
07/05/2012  06:33 PM               713 20090121_SO2.data
07/05/2012  06:33 PM               713 20090123_C2H2.data
07/05/2012  06:33 PM               716 20090123_C2H4.data
07/05/2012  06:33 PM               713 20090123_C2H6.data
07/05/2012  06:33 PM               713 20090123_C3H4.data
07/05/2012  06:33 PM               713 20090123_C3H6.data
07/05/2012  06:33 PM               713 20090123_C3H8.data
07/05/2012  06:33 PM               716 20090123_CH4.data
07/05/2012  06:33 PM               721 20090123_CO.data
07/05/2012  06:33 PM               732 20090123_CO2.data
07/05/2012  06:33 PM               716 20090123_NMHC.data
07/05/2012  06:33 PM               716 20090123_NOx.data
07/05/2012  06:33 PM               719 20090123_PM2.5.data
07/05/2012  06:33 PM               713 20090123_SO2.data
07/05/2012  07:41 PM            10,641 fuels-feps.pdf
07/05/2012  07:43 PM         3,979,641 SERDP Field Work January 2009.pdf
07/05/2012  06:33 PM             5,120 Thumbs.db
              81 File(s)      4,085,549 bytes

 Directory of \RC-1647-SD\2009-Fort_Benning-Data\MM5 Surface Winds

07/05/2012  06:33 PM    <DIR>          .
07/05/2012  06:33 PM    <DIR>          ..
07/05/2012  06:33 PM         4,248,492 wind_fields_09apr08_E-2_E-3.gif
07/05/2012  06:33 PM         4,566,154 wind_fields_09apr09_J-6.gif
07/05/2012  06:33 PM         4,180,946 wind_fields_09jan13_O-7.gif
07/05/2012  06:33 PM         4,151,000 wind_fields_09jan14_S-1A_S-1B_S-
2_S-3.gif
07/05/2012  06:33 PM         4,540,853 wind_fields_09jan15_A-9A_A-9B.gif
07/05/2012  06:33 PM         4,286,746 wind_fields_09jan20_O-11.gif
07/05/2012  06:33 PM         4,228,689 wind_fields_09jan21_D-15.gif
07/05/2012  06:33 PM         4,420,453 wind_fields_09jan23_I-3.gif
               8 File(s)     34,623,333 bytes

 Directory of \RC-1647-SD\2009-Fort_Benning-Data\Pictures

07/05/2012  06:33 PM    <DIR>          .
07/05/2012  06:33 PM    <DIR>          ..
```

```
07/05/2012  06:33 PM         2,119,312 Jan-14-2009 (FS).JPG
07/05/2012  06:33 PM         2,856,285 Jan-15-2009 (FS).JPG
07/05/2012  06:33 PM    <DIR>          Study Pictures
               2 File(s)      4,975,597 bytes

 Directory of \RC-1647-SD\2009-Fort_Benning-Data\Pictures\Study Pictures

07/05/2012  06:33 PM    <DIR>          .
07/05/2012  06:33 PM    <DIR>          ..
07/05/2012  06:33 PM           144,668 DSCN1381.jpg
07/05/2012  06:33 PM           129,799 DSCN1386.JPG
07/05/2012  06:33 PM           128,886 DSCN1388.JPG
07/05/2012  06:33 PM           113,195 DSCN1389.JPG
07/05/2012  06:33 PM           102,608 DSCN1390.JPG
07/05/2012  06:33 PM           113,274 DSCN1391.JPG
07/05/2012  06:33 PM           125,626 DSCN1393.JPG
07/05/2012  06:33 PM           152,440 DSCN1394.JPG
07/05/2012  06:33 PM           134,376 DSCN1395.JPG
07/05/2012  06:33 PM           139,345 DSCN1396.JPG
07/05/2012  06:33 PM           121,600 DSCN1397.JPG
07/05/2012  06:33 PM           135,702 DSCN1398.JPG
07/05/2012  06:33 PM           147,358 DSCN1421.JPG
07/05/2012  06:33 PM           131,710 DSCN1454.JPG
07/05/2012  06:33 PM           105,695 Jan-15-2009 (UGA).jpg
07/05/2012  06:33 PM            62,976 Thumbs.db
              16 File(s)      1,989,258 bytes

 Directory of \RC-1647-SD\2009-Fort_Benning-Data\Soundings

07/05/2012  06:33 PM    <DIR>          .
07/05/2012  06:33 PM    <DIR>          ..
07/05/2012  06:33 PM            57,335 daysmoke_09apr08_E-2_rotated.txt
07/05/2012  06:33 PM            62,319 daysmoke_09apr08_E-3_rotated.txt
07/05/2012  06:33 PM            62,319 daysmoke_09apr09_J-6_rotated.txt
07/05/2012  06:33 PM            59,827 daysmoke_09jan13_O-7_rotated.txt
07/05/2012  06:33 PM            59,827 daysmoke_09jan14_S-1A_rotated.txt
07/05/2012  06:33 PM            59,827 daysmoke_09jan14_S-1B_rotated.txt
07/05/2012  06:33 PM            59,827 daysmoke_09jan14_S-2_rotated.txt
07/05/2012  06:33 PM            59,827 daysmoke_09jan14_S-3_rotated.txt
07/05/2012  06:33 PM            59,827 daysmoke_09jan15_A-9A_rotated.txt
07/05/2012  06:33 PM            59,827 daysmoke_09jan15_A-9B_rotated.txt
07/05/2012  06:33 PM            59,827 daysmoke_09jan20_O-11_rotated.txt
07/05/2012  06:33 PM            59,827 daysmoke_09jan21_D-15_rotated.txt
07/05/2012  06:33 PM            59,827 daysmoke_09jan23_I-3_rotated.txt
              13 File(s)        780,243 bytes

 Directory of \RC-1647-SD\2009-Fort_Benning-
Data\training_area_rx_burn_template_fy09

07/05/2012  06:33 PM    <DIR>          .
07/05/2012  06:33 PM    <DIR>          ..
07/05/2012  06:33 PM           137,876 benning_units.jpg
07/05/2012  06:33 PM            22,277 fort_benning_burns_042008.gif
07/05/2012  06:33 PM            27,175 fort_benning_units.gif
```

```
07/05/2012  06:33 PM            28,160 Rx Burn List FY09.xls
07/05/2012  06:33 PM            22,528 Site Prep Burn List FY09.xls
07/05/2012  06:33 PM             6,144 Thumbs.db
07/05/2012  06:33 PM           162,917
training_area_rx_burn_template_fy09.dbf
07/05/2012  06:33 PM               402
training_area_rx_burn_template_fy09.prj
07/05/2012  06:33 PM             3,516
training_area_rx_burn_template_fy09.sbn
07/05/2012  06:33 PM               476
training_area_rx_burn_template_fy09.sbx
07/05/2012  06:33 PM           586,976
training_area_rx_burn_template_fy09.shp
07/05/2012  06:33 PM             2,636
training_area_rx_burn_template_fy09.shx
              12 File(s)      1,001,083 bytes

 Directory of \RC-1647-SD\2009-Fort_Benning-Data\Truck Locations

07/05/2012  07:33 PM    <DIR>          .
07/05/2012  07:33 PM    <DIR>          ..
07/05/2012  07:27 PM             6,394 01-13-2009.pdf
07/05/2012  07:28 PM             6,400 01-14-2009.pdf
07/05/2012  07:30 PM             7,022 01-15-2009.pdf
07/05/2012  07:30 PM             7,014 01-20-2009.pdf
07/05/2012  07:31 PM             6,909 01-21-2009.pdf
07/05/2012  07:31 PM             6,932 01-23-2009.pdf
07/05/2012  07:32 PM             6,450 04-08-2009.pdf
07/05/2012  07:33 PM             6,382 04-09-2009.pdf
               8 File(s)         53,503 bytes

 Directory of \RC-1647-SD\2009-Fort_Benning-Data\UGA Measurements

07/05/2012  07:34 PM    <DIR>          .
07/05/2012  07:34 PM    <DIR>          ..
07/05/2012  06:33 PM    <DIR>          CO Data
07/05/2012  06:33 PM    <DIR>          Data Log Sheets
07/05/2012  07:34 PM             9,485 ft benning sampling grid.pdf
07/05/2012  07:34 PM            19,866 Ft_Benning_2009_Burn_Summary_3.pdf
07/05/2012  06:33 PM    <DIR>          PM 2.5 Data
               2 File(s)         29,351 bytes

 Directory of \RC-1647-SD\2009-Fort_Benning-Data\UGA Measurements\CO Data

07/05/2012  06:33 PM    <DIR>          .
07/05/2012  06:33 PM    <DIR>          ..
07/05/2012  06:33 PM           284,672 Ft Benning CO 01-13-2009.xls
07/05/2012  06:33 PM           368,128 Ft Benning CO 01-14-2009.xls
07/05/2012  06:33 PM           196,608 Ft Benning CO 01-15-2009.xls
07/05/2012  06:33 PM         1,978,368 Ft Benning CO 04-08-2009.xls
07/05/2012  06:33 PM           919,040 Ft Benning CO 04-09-2009.xls
07/05/2012  06:33 PM           220,160 Ft Benning CO 1-20-2009.xls
07/05/2012  06:33 PM           459,264 Ft Benning CO 1-21-2009.xls
07/05/2012  06:33 PM           253,440 Ft Benning CO 1-23-2009.xls
```

```
               8 File(s)      4,679,680 bytes

 Directory of \RC-1647-SD\2009-Fort_Benning-Data\UGA Measurements\Data Log
Sheets

07/05/2012  06:33 PM    <DIR>          .
07/05/2012  06:33 PM    <DIR>          ..
07/05/2012  06:33 PM            26,112 Ft. Benning Data Log Sheet 04-08-
2009.xls
07/05/2012  06:33 PM            24,576 Ft. Benning Data Log Sheet 04-09-
2009.xls
07/05/2012  06:33 PM            26,624 Ft. Benning Data Log Sheet 1-13-
2009.xls
07/05/2012  06:33 PM            25,088 Ft. Benning Data Log Sheet 1-14-
2009.xls
07/05/2012  06:33 PM            25,600 Ft. Benning Data Log Sheet 1-15-
2009.xls
07/05/2012  06:33 PM            26,112 Ft. Benning Data Log Sheet 1-20-
2009.xls
07/05/2012  06:33 PM            25,088 Ft. Benning Data Log Sheet 1-21-
2009.xls
07/05/2012  06:33 PM            24,576 Ft. Benning Data Log Sheet 1-23-
2009.xls
               8 File(s)        203,776 bytes

 Directory of \RC-1647-SD\2009-Fort_Benning-Data\UGA Measurements\PM 2.5
Data

07/05/2012  06:33 PM    <DIR>          .
07/05/2012  06:33 PM    <DIR>          ..
07/05/2012  06:33 PM           128,512 Ft Benning PM 2.5 01-13-2009.xls
07/05/2012  06:33 PM            57,344 Ft Benning PM 2.5 01-14-2009.xls
07/05/2012  06:33 PM           130,560 Ft Benning PM 2.5 01-15-2009.xls
07/05/2012  06:33 PM           265,216 Ft Benning PM 2.5 01-20-2009.xls
07/05/2012  06:33 PM           319,488 Ft Benning PM 2.5 01-21-2009.xls
07/05/2012  06:33 PM           299,008 Ft Benning PM 2.5 01-23-2009.xls
07/05/2012  06:33 PM           268,288 Ft Benning PM 2.5 04-08-09.xls
07/05/2012  06:33 PM           339,456 Ft_Benning_PM_2_5_04-09-09.xls
               8 File(s)      1,807,872 bytes

 Directory of \RC-1647-SD\2009-Fort_Benning-Data\Weather

07/05/2012  06:33 PM    <DIR>          .
07/05/2012  06:33 PM    <DIR>          ..
07/05/2012  06:33 PM            47,236 FBGG1_Apr_08_2009.pdf
07/05/2012  06:33 PM            47,664 FBGG1_Apr_09_2009.pdf
07/05/2012  06:33 PM            47,389 FBGG1_Jan_13_2009.pdf
07/05/2012  06:33 PM            47,387 FBGG1_Jan_14_2009.pdf
07/05/2012  06:33 PM            44,084 FBGG1_Jan_15_2009.pdf
07/05/2012  06:33 PM            46,869 FBGG1_Jan_20_2009.pdf
07/05/2012  06:33 PM            47,135 FBGG1_Jan_21_2009.pdf
07/05/2012  06:33 PM            47,165 FBGG1_Jan_23_2009.pdf
07/05/2012  06:33 PM            18,146 FBGG1_Site_Info.pdf
               9 File(s)        393,075 bytes
```

```
 Directory of \RC-1647-SD\2011-Eglin-Data

07/05/2012  07:35 PM    <DIR>          .
07/05/2012  07:35 PM    <DIR>          ..
07/05/2012  06:33 PM         1,533,542 2011_Study_Plan_for_Eglin_Final.pdf
07/05/2012  06:33 PM            46,677 Eglin_2011_Burn_Information.pdf
07/05/2012  06:33 PM    <DIR>          Emissions
07/05/2012  07:36 PM    <DIR>          Emory Rx-CADRE_data
07/05/2012  06:33 PM    <DIR>          Ottmar's Fuel Data
07/05/2012  07:37 PM    <DIR>          Photos_by_Eglin_AFB
07/05/2012  06:33 PM    <DIR>          RAWS
07/05/2012  06:33 PM            22,103 RX-CADRE-2011.htm
07/05/2012  06:33 PM           725,918 RX_CADRE_2011_Maps.pdf
07/05/2012  06:33 PM    <DIR>          Soundings
07/05/2012  06:33 PM    <DIR>          US EPA aerostat Data
               4 File(s)      2,328,240 bytes

 Directory of \RC-1647-SD\2011-Eglin-Data\Emissions

07/05/2012  06:33 PM    <DIR>          .
07/05/2012  06:33 PM    <DIR>          ..
07/05/2012  06:33 PM               643 2011Feb12_704A_AP42kg.txt
07/05/2012  06:33 PM               694 2011Feb12_704A_CONSUMEkg.txt
07/05/2012  06:33 PM               643 2011Feb12_704A_EPAkg.txt
07/05/2012  06:33 PM               641 2011Feb12_704A_SMRFSkg.txt
07/05/2012  06:33 PM               641 2011Feb12_704A_urbanskikg.txt
07/05/2012  06:33 PM               523 2011Feb6_703C_EPAkg.txt
07/05/2012  06:33 PM               551 2011Feb8_608A_AP42kg.txt
07/05/2012  06:33 PM               585 2011Feb8_608A_CONSUMEefkg.txt
07/05/2012  06:33 PM               533 2011Feb8_608A_EPAkg.txt
07/05/2012  06:33 PM               540 2011Feb8_608A_SMRFSkg.txt
07/05/2012  06:33 PM               548 2011Feb8_608A_Urbskikg.txt
07/05/2012  06:33 PM    <DIR>          Emissions_by_FS_SRS(Scott Goodrick)
              11 File(s)          6,542 bytes

 Directory of \RC-1647-SD\2011-Eglin-
Data\Emissions\Emissions_by_FS_SRS(Scott Goodrick)

07/05/2012  06:33 PM    <DIR>          .
07/05/2012  06:33 PM    <DIR>          ..
07/05/2012  06:33 PM               705 20110206_C2H2.csv
07/05/2012  06:33 PM               705 20110206_C2H4.csv
07/05/2012  06:33 PM               703 20110206_C2H6.csv
07/05/2012  06:33 PM               703 20110206_C3H4.csv
07/05/2012  06:33 PM               705 20110206_C3H6.csv
07/05/2012  06:33 PM               703 20110206_C3H8.csv
07/05/2012  06:33 PM               705 20110206_CH4.csv
07/05/2012  06:33 PM               715 20110206_CO.csv
07/05/2012  06:33 PM               721 20110206_CO2.csv
07/05/2012  06:33 PM               705 20110206_NMHC.csv
07/05/2012  06:33 PM               705 20110206_NOx.csv
07/05/2012  06:33 PM               710 20110206_PM2.5.csv
07/05/2012  06:33 PM               703 20110206_SO2.csv
```

```
07/05/2012  06:33 PM               705 20110208_C2H2.csv
07/05/2012  06:33 PM               705 20110208_C2H4.csv
07/05/2012  06:33 PM               703 20110208_C2H6.csv
07/05/2012  06:33 PM               703 20110208_C3H4.csv
07/05/2012  06:33 PM               705 20110208_C3H6.csv
07/05/2012  06:33 PM               703 20110208_C3H8.csv
07/05/2012  06:33 PM               705 20110208_CH4.csv
07/05/2012  06:33 PM               715 20110208_CO.csv
07/05/2012  06:33 PM               721 20110208_CO2.csv
07/05/2012  06:33 PM               705 20110208_NMHC.csv
07/05/2012  06:33 PM               705 20110208_NOx.csv
07/05/2012  06:33 PM               710 20110208_PM2.5.csv
07/05/2012  06:33 PM               703 20110208_SO2.csv
07/05/2012  06:33 PM             1,303 20110212_C2H2.csv
07/05/2012  06:33 PM             1,303 20110212_C2H4.csv
07/05/2012  06:33 PM             1,303 20110212_C2H6.csv
07/05/2012  06:33 PM             1,303 20110212_C3H4.csv
07/05/2012  06:33 PM             1,303 20110212_C3H6.csv
07/05/2012  06:33 PM             1,303 20110212_C3H8.csv
07/05/2012  06:33 PM             1,303 20110212_CH4.csv
07/05/2012  06:33 PM             1,316 20110212_CO.csv
07/05/2012  06:33 PM             1,327 20110212_CO2.csv
07/05/2012  06:33 PM             1,303 20110212_NMHC.csv
07/05/2012  06:33 PM             1,303 20110212_NOx.csv
07/05/2012  06:33 PM             1,307 20110212_PM2.5.csv
07/05/2012  06:33 PM             1,303 20110212_SO2.csv
              39 File(s)         35,356 bytes

 Directory of \RC-1647-SD\2011-Eglin-Data\Emory Rx-CADRE_data

07/05/2012  07:36 PM    <DIR>          .
07/05/2012  07:36 PM    <DIR>          ..
07/05/2012  06:33 PM            51,712 co 6958 burn 1.xls
07/05/2012  06:33 PM            48,640 co 6958 burn 2.xls
07/05/2012  06:33 PM            64,512 co 6958 burn 3.xls
07/05/2012  06:33 PM            60,928 co2 5479 burn 3.xls
07/05/2012  06:33 PM            48,128 co2 54790 burn 1.xls
07/05/2012  06:33 PM            48,128 co2 6959 burn 1.xls
07/05/2012  06:33 PM            45,568 co2 6959 burn 2.xls
07/05/2012  06:33 PM            59,904 co2 6959 burn 3 .xls
07/05/2012  06:33 PM            99,840 EglinAFB_burn1_BC.xls
07/05/2012  06:33 PM           659,968 EglinAFB_burn1_mass.xls
07/05/2012  06:33 PM           102,400 EglinAFB_burn2_BC.xls
07/05/2012  06:33 PM           455,680 EglinAFB_burn2_mass.xls
07/05/2012  06:33 PM           116,224 EglinAFB_burn3_BC.xls
07/05/2012  06:33 PM         1,029,120 EglinAFB_burn3_mass.xls
07/05/2012  06:33 PM         1,821,696 Eglin_AFB_burn1_met.xls
07/05/2012  06:33 PM         1,439,744 Eglin_AFB_burn2_met.xls
07/05/2012  06:33 PM         1,839,104 Eglin_AFB_burn3_met.xls
07/05/2012  07:36 PM            31,178 GPS Coordinates.pdf
07/05/2012  06:33 PM            49,664 Rx-CADRE_EC-OC.xls
07/05/2012  06:33 PM            42,496 Rx-CADRE_filter_weights.xls
              20 File(s)      8,114,634 bytes
```

```
 Directory of \RC-1647-SD\2011-Eglin-Data\Ottmar's Fuel Data

07/05/2012  06:33 PM    <DIR>          .
07/05/2012  06:33 PM    <DIR>          ..
07/05/2012  06:33 PM           172,006
fuel_consumption_summarry_03_29_2011.pdf
07/05/2012  06:33 PM            35,084
fuel_consumption_summarry_03_29_2011.xlsx
               2 File(s)        207,090 bytes

 Directory of \RC-1647-SD\2011-Eglin-Data\Photos_by_Eglin_AFB

07/05/2012  07:37 PM    <DIR>          .
07/05/2012  07:37 PM    <DIR>          ..
07/05/2012  06:33 PM            34,179 608A 007.JPG
07/05/2012  06:33 PM            41,141 608A 009.JPG
07/05/2012  06:33 PM            40,796 608A 010.JPG
07/05/2012  06:33 PM            34,444 608A 012.JPG
07/05/2012  06:33 PM            34,472 608A 015.JPG
07/05/2012  06:33 PM            39,844 608A 017.JPG
07/05/2012  06:33 PM            40,691 608A 019.JPG
07/05/2012  06:33 PM            40,863 608A 021.JPG
07/05/2012  06:33 PM            42,499 test 703C 032.JPG
07/05/2012  06:33 PM            34,596 test 703C 033.JPG
07/05/2012  06:33 PM            32,590 test 703C 034.JPG
07/05/2012  06:33 PM            34,987 test 703C 035.JPG
              12 File(s)        451,102 bytes

 Directory of \RC-1647-SD\2011-Eglin-Data\RAWS

07/05/2012  06:33 PM    <DIR>          .
07/05/2012  06:33 PM    <DIR>          ..
07/05/2012  06:33 PM         1,650,351 IWDS_B75_Feb_2011.txt
07/05/2012  06:33 PM         1,523,633 IWDS_C-72_Feb_2011.txt
07/05/2012  06:33 PM             1,387 RAWS_data.txt
               3 File(s)      3,175,371 bytes

 Directory of \RC-1647-SD\2011-Eglin-Data\Soundings

07/05/2012  06:33 PM    <DIR>          .
07/05/2012  06:33 PM    <DIR>          ..
07/05/2012  07:38 PM    <DIR>          Measured
07/05/2012  06:33 PM    <DIR>          Modeled
               0 File(s)              0 bytes

 Directory of \RC-1647-SD\2011-Eglin-Data\Soundings\Measured

07/05/2012  07:38 PM    <DIR>          .
07/05/2012  07:38 PM    <DIR>          ..
07/05/2012  06:33 PM    <DIR>          Rawinsonde
07/05/2012  06:33 PM    <DIR>          UAV Anemometer
               0 File(s)              0 bytes

 Directory of \RC-1647-SD\2011-Eglin-Data\Soundings\Measured\Rawinsonde
```

```
07/05/2012  06:33 PM    <DIR>          .
07/05/2012  06:33 PM    <DIR>          ..
07/05/2012  06:33 PM            20,688 Saturday_02_12_11_LLS.UAS
07/05/2012  06:33 PM            21,192 Saturday_02_5_11_LLS.UAS
07/05/2012  06:33 PM            19,170 Sunday_02_06_11_LLS.UAS
07/05/2012  06:33 PM            16,384 Tuesday_02_08_11_LLS.UAS
               4 File(s)         77,434 bytes

 Directory of \RC-1647-SD\2011-Eglin-Data\Soundings\Measured\UAV
Anemometer

07/05/2012  06:33 PM    <DIR>          .
07/05/2012  06:33 PM    <DIR>          ..
07/05/2012  06:33 PM         1,895,082 RxCADRE Jackson Gaurd data.xlsx
07/05/2012  06:33 PM         1,857,536 RxCADRE-2-6.xls
               2 File(s)      3,752,618 bytes

 Directory of \RC-1647-SD\2011-Eglin-Data\Soundings\Modeled

07/05/2012  06:33 PM    <DIR>          .
07/05/2012  06:33 PM    <DIR>          ..
07/05/2012  06:33 PM    <DIR>          MM5-by-FS-NRS
07/05/2012  06:33 PM    <DIR>          WRF-by-GaTech
               0 File(s)              0 bytes

 Directory of \RC-1647-SD\2011-Eglin-Data\Soundings\Modeled\MM5-by-FS-NRS

07/05/2012  06:33 PM    <DIR>          .
07/05/2012  06:33 PM    <DIR>          ..
07/05/2012  06:33 PM            80,066 703C_WRF 6FEB2011_Xindi_04km.txt
07/05/2012  06:33 PM            78,302 Sounding.UVTQ.prediction.01km.txt
07/05/2012  06:33 PM            78,302 Sounding.UVTQ.prediction.04km.txt
07/05/2012  06:33 PM            78,302 Sounding.UVTQ.prediction.12km.txt
07/05/2012  06:33 PM            78,302 Sounding.UVTQ.reanalysis.01km.txt
07/05/2012  06:33 PM            78,302 Sounding.UVTQ.reanalysis.04km.txt
07/05/2012  06:33 PM           233,583
Sounding.UVTQ.reanalysis.12km.diff.prediction.txt
07/05/2012  06:33 PM            78,302 Sounding.UVTQ.reanalysis.12km.txt
07/05/2012  06:33 PM            78,302 Sounding.UVTQ.reanalysis.36km.txt
               9 File(s)        861,763 bytes

 Directory of \RC-1647-SD\2011-Eglin-Data\Soundings\Modeled\WRF-by-GaTech

07/05/2012  06:33 PM    <DIR>          .
07/05/2012  06:33 PM    <DIR>          ..
07/05/2012  06:33 PM            73,364 daysmoke_2011feb06_703C.txt.rotated
07/05/2012  06:33 PM            73,364 daysmoke_2011feb08_608A.txt.rotated
07/05/2012  06:33 PM            72,287 daysmoke_2011feb12_704A.txt.rotated
07/05/2012  06:33 PM            73,364 daysmoke_2011feb12_907D.txt.rotated
               4 File(s)        292,379 bytes

 Directory of \RC-1647-SD\2011-Eglin-Data\US EPA aerostat Data
```

```
07/05/2012  06:33 PM    <DIR>          .
07/05/2012  06:33 PM    <DIR>          ..
07/05/2012  06:33 PM           445,721 Anemometer data preliminary US EPA
v1.pptx
07/05/2012  06:33 PM         5,030,113 data to talat-4-09-12.xlsx
07/05/2012  06:33 PM         1,196,204 IPR input EPA Apr 2011 Eglin
results SERDP.pptx
07/05/2012  06:33 PM               618 README (Wind Bearing).txt
07/05/2012  06:33 PM            13,109 [Book14]Output
datasmoothedclipped2.pdf
               5 File(s)      6,685,765 bytes

 Directory of \RC-1647-SD\Analyses

07/05/2012  06:33 PM    <DIR>          .
07/05/2012  06:33 PM    <DIR>          ..
07/05/2012  06:33 PM    <DIR>          Daysmoke-Fort_Benning
07/05/2012  06:33 PM    <DIR>          Meteorology-2011-Eglin
               0 File(s)              0 bytes

 Directory of \RC-1647-SD\Analyses\Daysmoke-Fort_Benning

07/05/2012  06:33 PM    <DIR>          .
07/05/2012  06:33 PM    <DIR>          ..
07/05/2012  06:33 PM           899,176
Analysis_of_08_April_2009_combined.pdf
07/05/2012  06:33 PM           836,078
Analysis_of_09_April_2009_combined.pdf
07/05/2012  06:33 PM           438,937
Analysis_of_13_January_2009_combined.pdf
07/05/2012  06:33 PM           920,253
Analysis_of_14_April_2008_combined_.pdf
07/05/2012  06:33 PM           450,408
Analysis_of_14_January_2009_combined.pdf
07/05/2012  06:33 PM           592,306
Analysis_of_15_April_2008_combined.pdf
07/05/2012  06:33 PM           934,756
Analysis_of_15_January_2009_combined.pdf
07/05/2012  06:33 PM           481,259
Analysis_of_20_January_2009_combined.pdf
07/05/2012  06:33 PM           456,131
Analysis_of_21_January_2009_combined.pdf
07/05/2012  06:33 PM           433,860
Analysis_of_23_January_2009_combined.pdf
07/05/2012  06:33 PM           418,403
Reanalysis_of_9_April_2008_combined.pdf
              11 File(s)      6,861,567 bytes

 Directory of \RC-1647-SD\Analyses\Meteorology-2011-Eglin

07/05/2012  06:33 PM    <DIR>          .
07/05/2012  06:33 PM    <DIR>          ..
07/05/2012  06:33 PM         2,404,670 Feb_12_2011-UAVs.xlsx
07/05/2012  06:33 PM            86,412 Feb_2011-Soundings.xlsx
```

```
07/05/2012  06:33 PM           914,957 Feb_6_2011-UAVs.xlsx
07/05/2012  06:33 PM         4,400,005 IWDS_B75_Feb_2011.xlsx
07/05/2012  06:33 PM         1,587,725 IWDS_C-72_Feb_2011.xlsx
07/05/2012  06:33 PM         9,529,415 Meteorological Evaluation_v2.1.pdf
07/05/2012  06:33 PM    <DIR>          Re Eglin Soundings Extractions
07/05/2012  06:33 PM    <DIR>          Re Eglin WRF performance
07/05/2012  06:33 PM        12,546,560 Stationary_Site_Meteorology.xls
               7 File(s)     31,469,744 bytes

 Directory of \RC-1647-SD\Analyses\Meteorology-2011-Eglin\Re Eglin
Soundings Extractions

07/05/2012  06:33 PM    <DIR>          .
07/05/2012  06:33 PM    <DIR>          ..
07/05/2012  06:33 PM         7,660,794 Aerostat Analysis.xlsx
07/05/2012  06:33 PM            57,335 daysmoke_2011feb06_AS06.txt.rotated
07/05/2012  06:33 PM             7,495 daysmoke_2011feb06_S06.txt.rotated
07/05/2012  06:33 PM             7,714
daysmoke_2011feb06_S06.txt.rotated.mm5
07/05/2012  06:33 PM             9,987 daysmoke_2011feb06_U06-
1.txt.rotated
07/05/2012  06:33 PM             9,987 daysmoke_2011feb06_U06-
10.txt.rotated
07/05/2012  06:33 PM             9,987 daysmoke_2011feb06_U06-
11.txt.rotated
07/05/2012  06:33 PM             9,987 daysmoke_2011feb06_U06-
12.txt.rotated
07/05/2012  06:33 PM             9,987 daysmoke_2011feb06_U06-
2.txt.rotated
07/05/2012  06:33 PM             9,987 daysmoke_2011feb06_U06-
3.txt.rotated
07/05/2012  06:33 PM             9,987 daysmoke_2011feb06_U06-
4.txt.rotated
07/05/2012  06:33 PM             9,987 daysmoke_2011feb06_U06-
5.txt.rotated
07/05/2012  06:33 PM             9,987 daysmoke_2011feb06_U06-
6.txt.rotated
07/05/2012  06:33 PM             9,987 daysmoke_2011feb06_U06-
7.txt.rotated
07/05/2012  06:33 PM             9,987 daysmoke_2011feb06_U06-
8.txt.rotated
07/05/2012  06:33 PM             9,987 daysmoke_2011feb06_U06-
9.txt.rotated
07/05/2012  06:33 PM            59,827 daysmoke_2011feb08_AS08.txt.rotated
07/05/2012  06:33 PM             7,495 daysmoke_2011feb08_S08.txt.rotated
07/05/2012  06:33 PM             7,714
daysmoke_2011feb08_S08.txt.rotated.mm5
07/05/2012  06:33 PM            64,811 daysmoke_2011feb12_AS12.txt.rotated
07/05/2012  06:33 PM             7,495 daysmoke_2011feb12_S12.txt.rotated
07/05/2012  06:33 PM            12,479 daysmoke_2011feb12_U12-
1.txt.rotated
07/05/2012  06:33 PM            12,479 daysmoke_2011feb12_U12-
2.txt.rotated
```

```
07/05/2012  06:33 PM            12,479 daysmoke_2011feb12_U12-
3.txt.rotated
07/05/2012  06:33 PM            12,479 daysmoke_2011feb12_U12-
4.txt.rotated
07/05/2012  06:33 PM             1,079 eglin_soundings.txt
07/05/2012  06:33 PM             1,313 eglin_soundings.txt_final
07/05/2012  06:33 PM           289,883 Eglin_Soundings.xlsx
07/05/2012  06:33 PM         1,785,443 Eglin_UAV_Feb-06.xlsx
07/05/2012  06:33 PM         3,851,576 Eglin_UAV_Feb-12.xlsx
              30 File(s)     13,979,734 bytes

 Directory of \RC-1647-SD\Analyses\Meteorology-2011-Eglin\Re Eglin WRF
performance

07/05/2012  06:33 PM    <DIR>          .
07/05/2012  06:33 PM    <DIR>          ..
07/05/2012  06:33 PM            19,456 eglin_1p3_metlist.xls
07/05/2012  06:33 PM           110,080 metstat.macro.xls
07/05/2012  06:33 PM            13,894 README
07/05/2012  06:33 PM             4,705 stats.daly.feb11.eglin1p3
07/05/2012  06:33 PM             4,705
stats.daly.feb11.eglin1p3.est.3sites
07/05/2012  06:33 PM             2,153 stats.daly.mm5_02052011.eglin1p3
07/05/2012  06:33 PM             2,153 stats.daly.mm5_02082011.eglin1p3
07/05/2012  06:33 PM            66,082 stats.hrly.feb11.eglin1p3
07/05/2012  06:33 PM            64,717
stats.hrly.feb11.eglin1p3.est.3sites
07/05/2012  06:33 PM           104,013 stats.hrly.feb12.3sites.xlsx
07/05/2012  06:33 PM           121,621 stats.hrly.feb12.xlsx
07/05/2012  06:33 PM           140,118 stats.hrly.feb2011.xlsx
07/05/2012  06:33 PM           104,789 stats.hrly.feb6.3sites.xlsx
07/05/2012  06:33 PM           121,608 stats.hrly.feb6.xlsx
07/05/2012  06:33 PM           103,986 stats.hrly.feb8.3sites.xlsx
07/05/2012  06:33 PM           121,600 stats.hrly.feb8.xlsx
07/05/2012  06:33 PM            13,666 stats.hrly.mm5_02052011.eglin1p3
07/05/2012  06:33 PM            60,436 stats.hrly.mm5_02052011.xlsx
07/05/2012  06:33 PM            13,666 stats.hrly.mm5_02082011.eglin1p3
07/05/2012  06:33 PM            59,834 stats.hrly.mm5_02082011.xlsx
              20 File(s)      1,253,282 bytes
```

8 Appendix B: List of Scientific/Technical Publications

The results of this research were published in 7 journal articles, 3 technical reports, 2 conference or symposium proceedings and 24 conference or symposium abstracts.

8.1 Articles or Papers Published in Peer-reviewed Journals

.

Liu, Y., S. Goodrick, G. Achtemeier, W. A. Jackson, J. J. Qu and W. Wang, 2009: Smoke Incursions into Urban Areas and Air Quality Effects: Simulation and Experiment of A Georgia Prescribed Burn. *International Journal of Wildland Fire*, **18**, 336-348.

Odman, M. T. and Y. Hu, 2010: A variable time-step algorithm for air quality models. *Atmospheric Pollution Research*, **1**, 229-238 (doi: 10.5094/APR.2010.030).

Garcia-Menendez, F., A. Yano, Y. Hu, and M. T. Odman, 2010: An adaptive grid version of CMAQ for improving the resolution of plumes. *Atmospheric Pollution Research*, 1, 239-249 (doi: 10.5094/APR.2010.031).

Achtemeier, G. L., S. A. Goodrick, Y. Liu, F. Garcia-Menendez, Y. Hu, and M. T. Odman, 2011: Modeling Smoke from Wildland Fires: Plume-Rise and Smoke Dispersion from Southern United States Prescribed Burns. *Atmosphere*, 2(3), 358-388.

Garcia-Menendez, F. and M. T. Odman, 2011: Adaptive Grid Use in Air Quality Modeling. *Atmosphere*, **2**(3), 484-509.

Achtemeier, G. L., Y. Liu, S. L. Goodrick, 2012: Simulating fire spread and plume rise for an aerial ignition prescribed burn. *Atmosphere*, submitted.

Garcia-Menendez, F., Y. Hu, and M. T. Odman, 2012: Sensitivity of predicted $PM_{2.5}$ concentrations to spatial and temporal fire emissions allocation during a severe urban smoke episode in a regional-scale air quality model. *Journal of Geophysical Research*, submitted.

8.2 Technical Reports

Odman, M. T., G. L. Achtemeier and L. P. Naeher, Characterization of Emissions and Air Quality Modeling for Predicting the Impacts of Prescribed Burns at DoD Lands, SI-1647 Interim Report to SERDP, December 31, 2008.

Odman, M. T., G. L. Achtemeier and L. P. Naeher, Characterization of Emissions and Air Quality Modeling for Predicting the Impacts of Prescribed Burns at DoD Lands, SI-1647 Annual Report to SERDP, December 31, 2009.

Odman, M. T., G. L. Achtemeier and A. G. Russell, Characterization of Emissions and Air Quality Modeling for Predicting the Impacts of Prescribed Burns at DoD Lands, SI-1647 Annual Report to SERDP, December 31, 2010.

8.3 Conference or Symposium Proceedings

Odman, M. T., Y. Hu, D. S. McRae, S. L. Goodrick, Y. Liu, G. L. Achtemeier, and L. P. Naeher, Predicting the Regional Air Quality Impacts of Prescribed Burns, 30th NATO/SPS International Technical Meeting on Air Pollution Modelling and its Application, San Francisco, CA, 18-22 May 2009 (Odman et al., 2010).

Odman, T., A. Yano, F. Garcia-Menendez, Y. Hu, D. S. McRae, S. Goodrick, Y. Liu, G. Achtemeier, Development and evaluation of an air quality model for predicting the impacts of prescribed burns, 32th NATO/SPS International Technical Meeting on Air Pollution Modelling and its Application, Utrecht, Netherlands, 7 - 11 May 2012 (submitted).

8.4 Conference or Symposium Abstracts

Odman, M. T., Y. Hu, D. S. McRae, G. L. Achtemeier, A dynamic adaptive grid method for improved modeling of biomass burning plumes, 7th Annual CMAS Conference, Chapel Hill, NC, October 6, 2008.

Odman, T., Y. Hu, S. Goodrick, Y. Liu, G. Achtemeier, L. Naeher, Preliminary Evaluation of a Modeling System for Predicting the Air Quality Impacts of Prescribed Burns, Partners in Environmental Technology Technical Symposium &Workshop, Washington, DC, December 2, 2008.

Tsai, P.S., S. J. Frasier, S. Goodrick, G. L. Achtemeier, and M. T. Odman, Combined Lidar and Radar Observations of Smoke Plumes from Prescribed Burns, Fourth Symposium on Lidar Atmospheric Applications, 89th American Meteorological Society Annual Meeting, Phoenix, AZ, 13 January 2009.

Achtemeier, G. L., Y. Liu, S. L. Goodrick, L. P. Naeher, and M. T. Odman, Results from Daysmoke for Weak Smoke Plumes, Eighth Symposium on Fire and Forest Meteorology, Kalispell, MT**,** 13-15 October 2009.

Garcia-Menendez, F., Y. Hu, and M. T. Odman, An adaptive grid version of CMAQ for improving the resolution of plumes, 8th Annual CMAS Conference, Chapel Hill, NC, October 20, 2009.

Yano, A., Y. Hu, G. L. Achtemeier, and M. T. Odman, A sub-grid scale model for the treatment of biomass burning plumes in CMAQ, 8th Annual CMAS Conference, Chapel Hill, NC, October 19-21, 2009.

Achtemeier, G. L., Y. Liu, S. L. Goodrick, L. P. Naeher, T. Odman, S. Frasier, and P. Tsai, Results from Daysmoke for Weak Smoke Plumes, 4th International Fire Ecology and Management Congress, Savannah, GA, 30 November - 4 December, 2009.

Odman, T., F. Garcia, A. Yano, Y. Hu, S. Goodrick, Y. Liu, G. Achtemeier, L. Naeher, Evaluation of a Modeling System for Predicting the Air Quality Impacts of Prescribed Burns, Partners in Environmental Technology Technical Symposium &Workshop, Washington, DC, December 2, 2009.

Achtemeier, G. L., Y. Liu, S. L. Goodrick, L. P. Naeher, T. Odman, S Frasier, and P. Tsai, Results from Daysmoke for Weak Smoke Plumes, 16th Joint Conference on the Applications of Air Pollution Meteorology with the A&WMA, 17-21 January 2010 at Atlanta, GA.

Odman, M. T., Y. Hu, A. Yano, F. Garcia-Menendez, G. L. Achtemeier, S. L. Goodrick, Y. Liu, D. S. Mcrae, L. Naeher, Development of a modeling system for prescribed burn emissions and air quality impacts, 16th Joint Conference on the Applications of Air Pollution Meteorology with the A&WMA, 17-21 January 2010 at Atlanta, GA.

Yano, A., F. Garcia-Menendez, Y. Hu, M. T. Odman, D. S. McRae, and G. L. Achtemeier, Modeling biomass burnings by coupling a sub-grid scale plume model with Adaptive Grid CMAQ, 9th Annual CMAS Conference, Chapel Hill, NC, October 11-13, 2010.

Garcia-Menendez, F., Y. Hu, and M. T. Odman, Evaluation of air quality models applied to wildland fire impact simulation, 9th Annual CMAS Conference, Chapel Hill, NC, October 11-13, 2010.

Odman, M. T., F. Garcia-Menendez, A. Yano, Y. Hu, G. L. Achtemeier, and D. S. McRae, A High-Resolution Modeling System for Regional Carbonaceous Aerosols, 29th Annual Conference of the American Association for Aerosol Research, Portland, OR, October 25-29, 2010.

Odman, T., F. Garcia-Menendez, A. Yano, Y. Hu, S. Goodrick, Y. Liu, G. Achtemeier, Predicting the Air Quality Impacts of Prescribed Burns, Partners in Environmental Technology Technical Symposium & Workshop, Washington, DC, December 1, 2010.

Yano A. and M. T. Odman, Modeling biomass burnings by coupling a sub-grid scale plume model with Adaptive Grid CMAQ, American Meteorological Society's 9th Symposium on Fire and Forest Meteorology, Palm Springs, CA, October 18-20 2011,

Yano' A., M. T. Odman, R. D. Ottmar, S. L. Goodrick, Y. Liu, and B.Gullett, Uncertainties in prescribed fire emissions and their impact on smoke dispersion predictions, American Meteorological Society's 9th Symposium on Fire and Forest Meteorology, Palm Springs, CA, October 18-20 2011,

Yano A. and M. T. Odman, Coupling a subgrid scale plume model for biomass burns with the adaptive grid CMAQ model, 10th Annual CMAS Conference, Chapel Hill, NC, October 24-26, 2011.

Garcia-Menendez, F., Y. Hu, and M. T. Odman, Modeling the air quality impacts of wildfires with CMAQ, 10th Annual CMAS Conference, Chapel Hill, NC, October 24-26, 2011.

Garcia-Menendez, F., D. G. Tokgoz, and M. T. Odman, Analysis of vertical fire emissions distribution in CMAQ, 10th Annual CMAS Conference, Chapel Hill, NC, October 24-26, 2011.

Odman, T., F. Garcia-Menendez, A. Yano, Y. Hu, R. Greenwald, S. Goodrick, Y. Liu, G. Achtemeier, B, Gullett, A modeling system for predicting the air quality of prescribed burns: Final evaluation, Partners in Environmental Technology Technical Symposium &Workshop, Washington, DC, November 29, 2011.

Garcia-Menendez, F., D. G. Tokgoz, Y. Hu and M. T. Odman, Sensitivity of air quality to meteorology inputs in forest fire simulations, 14th Conference on Atmospheric Chemistry, New Orleans, LA, January 22-26, 2012.

Garcia-Menendez, F., Y. Hu and M. T. Odman, Improved Modeling of Wildland Fire Plumes with CMAQ, 17th Conference on Air Pollution Meteorology with the A&WMA, New Orleans, LA, January 22-26, 2012.

Garcia-Menendez, F. and M. T. Odman, Sensitivity Analysis of Model-Related Inputs in Wildland Fire Simulations using CMAQ, Paper #440, 105th Annual AWMA Conference, San Antonio, TX, 19-21 June 2012.

Yano, A., Y. Hu and M. T. Odman, Modeling the impacts of alternative burning strategies on local and regional air quality, 11th Annual CMAS Conference, Chapel Hill, NC, 15-17 October 2012.

Garcia-Menendez, F., Y. Hu and M. T. Odman, High resolution three–dimensional plume modeling with CMAQ, 11th Annual CMAS Conference, Chapel Hill, NC, 15-17 October 2012.

Odman, M. T., F. Garcia-Menendez, A. Yano, Y. Hu, G. L. Achtemeier, Y. Liu, S. L. Goodrick, R. Greenwald, B. Gullett, J. Aurell, W. R. Stevens, R. D. Ottmar, R. J. Yokelson and S. K. Akagi, Diagnostic evaluation of a modeling system for predicting the air quality impacts of prescribed burns, 11th Annual CMAS Conference, Chapel Hill, NC, 15-17 October 2012.

9 Appendix C: Other Supporting Materials

9.1 Scientific or Technical Awards or Honors

Mr. Fernando Garcia-Menendez, a PhD candidate at Georgia Institute of Technology, received the following awards for his work related to this project:

• Georgia Chapter of the Air & Waste Management Association Student Scholarship, October 2009

• Air Quality Research and Study Scholarship (Air & Waste Management Association), June 2010

• Southern Section of the Air & Waste Management Association Student Scholarship, August 2010

• M.A.P. Sustainable Energy Fellowship, May 2011

• Second Place Best Student Oral Presentation at the American Meteorological Society Conference on Air Pollution Meteorology, January 2012

• Anne Robinson Clough Conference Grant, January 2012

• Joint Fire Science Program Graduate Research Innovation (GRIN) Award, June 2012